

CARL GUILMETTE

**PETROLOGY, GEOCHEMISTRY AND
GEOCHRONOLOGY OF HIGHLY FOLIATED
AMPHIBOLITES FROM THE OPHIOLITIC
MÉLANGE BENEATH THE YARLUNG ZANGBO
OPHIOLITES, XIGAZE AREA, TIBET.
Geodynamical implications**

Mémoire présenté
à la Faculté des études supérieures de l'Université Laval
dans le cadre du programme de maîtrise en Sciences de la Terre
pour l'obtention du grade de maître ès sciences (M.Sc.)

Département de géologie et de génie géologique
FACULTÉ DES SCIENCES ET DE GÉNIE
UNIVERSITÉ LAVAL
QUÉBEC

2005

Résumé

On retrouve localement des amphibolites fortement foliées dans le mélange ophiolitique sous les massifs ophiolitiques de la Zone de Suture du Yarlung Zangbo (ZSYZ). Ces blocs représentent la partie supérieure d'une semelle métamorphique démembrée. La géochimie des amphibolites ($\text{La/Yb} = 0.65\text{-}0.97$, $\text{Ta/Th} = 0.33\text{-}0.65$) est similaire à celle des roches mafiques provenant de l'ophiolite, suggérant une origine dans le même bassin d'arrière-arc. Le métamorphisme de haut grade ($P=14$ kbars, $T= 800^\circ\text{C}$) subit par les amphibolites suggère un enfouissement pendant la naissance d'une subduction. Les âges voisins des amphibolites et de la croûte ophiolitique (121-130 vs 120 ± 10 et 126 Ma, respectivement) suggèrent que la naissance de la subduction s'est déroulée dans le bassin arrière-arc Néo-Téthysien. Un tel événement n'avait pas encore été rapporté. La présence de dikes et le métasomatisme tardif responsable de la cristallisation de préhnite pourraient indiquer la subduction d'un centre magmatique. La composition en isotopes stables du fluide responsable confirmerait une telle hypothèse.

Abstract

Blocks of highly foliated amphibolites are locally found within the serpentinite matrix mélange underlying the Yarlung Zangbo ophiolites near Bainang and Buma, Xigaze area, Yarlung Zangbo Suture Zone (YZSZ), Tibet. The mélange is thought to be the result of the tectonic dismemberment of the base of the ophiolitic napes during its obduction over the Indian passive margin, circa 50 Ma. Prior to dismemberment, amphibolites were probably parts of a coherent dynamothermal sole, as observed at the base of many ophiolites. Sampled amphibolites can be subdivided in three groups: garnet, banded and common amphibolites. Medium-grained garnet amphibolites contain the assemblage A) Hb+CPX+Gt+Pl±Rt and B) Gt+Hb+Pl (corona assemblage). Fine to medium-grained banded amphibolites contain the assemblage C) Hb+CPX+Pl+Ep±Sp+Qtz+Ap. Fine-grained common amphibolites contain facies D) Hb+Pl±Ep+Ap+Sp. In all assemblages, plagioclase is pseudomorphosed by an albite-prehnite simplectite. Retrograde cataclastic veins contain the assemblage E) Ab+Pr±Ch+Ep. The geochemistry of the garnet, banded and common amphibolites is very similar to the geochemistry of other mafic blocks in the mélange and of mafic igneous rocks within the ophiolitic massifs. When compared to MORBs, light depletion of LREE ($\text{La/Yb} = 0.65\text{-}0.97$) and mild HFSE depletion ($\text{Ta/Th} = 0.33\text{-}0.65$) would suggest a mixing between the IAT and MORB sources, as seen in back-arc basins and nascent intra-oceanic arcs. The amphibolites were buried at the inception of a subduction within the back-arc to peak metamorphism conditions of 11-14 kbars and ~800 °C. Ar/Ar analysis of amphiboles revealed a metamorphic age of 121-130 Ma, which is synchronous with ages obtained from the overlying ophiolites. Overlapping in ophiolite-sole age relationship reveals inception of the subduction near or at the spreading center from which originated the ophiolite. Subduction of a buoyant body could explain heterogeneous coronitization of pyrope-rich (up to 35 %) garnet by Al-Tschermakites (Al_2O_3 up to 21 wt %) at high-pressure. After exhumation, amphibolites were injected by very fine-grained diabasic dykes and were subject to percolation of a prehnite-precipitating fluid. Oxygen stable isotopes suggest that a magmatic fluid is responsible for prehnite precipitation. The magmatic and metamorphic history of the dynamothermal sole and field

relationships with adjacent units seem to indicate that most of Neo-Tethys oceanic domain was subducted along this new Late Cretaceous subduction zone.

Avant-propos

La réalisation de mes travaux de maîtrise s'est déroulée sur près de trois ans. Je voudrais d'emblée remercier mon directeur Réjean Hébert, qui, en Décembre 2001, a accepté ma candidature pour un projet de fin d'études. Ce travail d'une session à la fin de mon baccalauréat en Génie Géologique s'est extensionné en une maîtrise des plus stimulantes pendant laquelle j'ai pu soumettre un article à *Journal of Metamorphic Geology*. Au printemps 2002, j'ai eu la chance de visiter la région de Xigaze, au Tibet, en compagnie d'un excellent guide tant sur le plan scientifique que culturel. Mille fois merci, Réjean. Mon implication dans l'équipe GÉO (Génèse et Évolution des Ophiolites) m'a aussi permis d'acquérir des connaissances hors de mon champ d'étude grâce à d'éclairantes discussions avec Céline Dupuis et Viviane Dubois-Côté, qui sont à mes yeux aujourd'hui plus que des collègues. Pendant ma maîtrise, j'ai eu le plaisir d'être assistant à l'enseignement dans plusieurs cours, d'être éditeur-journaliste pour le Géoscope, d'être membre du comité organisateur pour la Journée des Sciences de la Terre et d'être président de l'association étudiante des gradués (AESTIÉS). Je suis très fier de mon passage sur le département de Géologie et de Génie Géologique, mais je dois avouer que je n'aurais jamais pu en faire autant sans le support et la confiance totale des gens qui m'entourent. Je tiens donc à remercier une dernière fois mon directeur, Réjean Hébert, qui m'a permis non seulement de repousser mes limites mais aussi qui a été à l'écoute de mes intérêts tout au long de notre collaboration. Merci de m'avoir encouragé à travailler en cartographie pendant les étés 2003 et 2004. Je tiens aussi à remercier mes parents, Claude et Chantale, qui ont une confiance aveugle en moi et qui m'ont supporté et me supporteront encore contre vents et marées. Merci à ma sœur, à mes amis (particulièrement Jean-Philippe et Yoan) qui croient en mon succès d'une manière dogmatique. Finalement, merci à Mylène, qui m'inspire et me supporte chaque jour. Merci à tous, ce mémoire est en quelque sorte un travail d'équipe et j'en suis fier.

Pour ce qui est de la langue de rédaction du mémoire, j'aimerais ajouter quelques lignes. Il m'est arrivé souvent au cours de cette maîtrise de me buter sur des références citant des thèses ou des mémoires écrits dans la langue natale de l'auteur. Non seulement est-il

difficile d'avoir accès à ces documents, mais il est souvent impossible de les comprendre, en particulier lorsque l'on travaille en Chine. J'ai donc choisi de rédiger mon mémoire en anglais afin de favoriser sa diffusion à l'échelle internationale.

List of contents

Résumé.....	II
Abstract.....	III
Avant-propos.....	V
Chapter I : Introduction.....	1
1.1. General introduction	1
1.2. Geological Setting.....	7
1.2.1. The active paleomargin.....	8
1.2.2. The oceanic domain	8
1.2.3. The Passive Paleomargin	11
1.2.4. Liuqu Conglomerate	11
1.3. Dynamothermal Soles	12
1.3.1. The Bainang Dynamothermal Sole	16
1.3.2. Buma vs. Bainang	17
1.4. Previous models for the emplacement of the Yarlung Zangbo ophiolites.....	18
Chapter 2 : Submitted Article	22
Introducing the paper	22
Metamorphic history of highly foliated amphibolites from the ophiolitic mélange beneath the Yarlung Zangbo Ophiolites, Xigaze area, Tibet.....	24
Abstract.....	25
2.1. Introduction.....	26
2.2. Geological Setting.....	29
2.3. Petrography	30
2.3.1. Common amphibolites	30
2.3.2. Clinopyroxene amphibolites	31
2.3.3. Garnet amphibolites	32
2.3.4. Fractures and veins	33
2.3.5. Other related rocks	33
2.4. Mineral Chemistry	34
2.4.1. Analytical method	34
2.4.2. Plagioclase	34
2.4.3. Amphiboles	35
2.4.4. Clinopyroxene	36
2.4.5. Garnet.....	36
2.5. Stable Isotope Geochemistry	37
2.5.1. Analytical Method	37
2.5.2. Results.....	37
2.6. Discussion	38
2.6.1. Metamorphic history from the textural record.....	38
2.6.2. P-T calculations	40
2.6.2.1. P-T conditions for the highly foliated amphibolites	41
2.6.2.2. P-T conditions for the cross-cutting intrusive.....	43
2.6.2.3. P-T-t path	44
2.6.3. Fluid composition	45
2.6.4. Geodynamic significance.....	46

2.7. Conclusion	49
Acknowledgement	50
2.8. References.....	51
2.9. Figure captions.....	62
2.10. List of Tables	65
Chapter 3 : Complementary data	86
3.1. Whole rock chemistry	86
3.1.1. Analytical Method	86
3.1.2. Major elements.....	87
3.1.3. Trace elements	90
3.1.4. Classification.....	90
3.1.5. Geochemistry and geological setting.....	91
3.2. Geochronology.....	96
3.2.1. Analytical Method	96
3.2.2. Results.....	97
Chapter 4 : Discussion and conclusions.....	99
4.1. Complete discussion	99
4.1.1. Geodynamic significance.....	99
4.1.2. Geodynamic Model.....	100
Conclusions.....	105
Complete references.....	107
Chapter 5 : Appendices.....	124
Appendix A.....	125
Geological map of the YZSZ and sample locations	125
Appendix B	129
Petrography of highly foliated amphibolite blocks from the mélange beneath the YZSZ ophiolites.....	129
Appendix C	136
Mineral Chemistry of highly foliated amphibolite blocks from the mélange beneath the YZSZ ophiolites	136
Amphibole Mineral Chemistry	137
Clinopyroxene Mineral Chemistry	152
Garnet Mineral Chemistry	162
Plagioclase Mineral Chemistry	169
Appendix D	176
Geochemistry of the highly foliated amphibolite blocks from the mélange beneath the YZSZ ophiolites.....	176

List of tables

Table 2.1 : Representative analyses of amphibole	66
Table 2.2 : Representative analyses of clinopyroxene	67
Table 2.3 : Representative analyses of garnet	68
Table 2.4 : Oxygen stable isotopes geochemistry	69
Table 2.5 : TWEEQU calculations	70
Table B1 : Petrography of amphibolites I	130
Table B2 : Petrography of amphibolites II	131
Table C1 : Amphibole mineral chemistry	138
Table C2 : Clinopyroxene mineral chemistry	153
Table C3 : Garnet mineral chemistry	163
Table C4 : Plagioclase mineral chemistry	170
Table D1 : Geochemistry of the Bainang amphibolites	177
Table D2 : Geochemistry of the Buma amphibolites	178
Table D3 : Standards for major element analyses	179
Table D4 : Standards for trace element analyses	180

List of figures

Figure 1.1 : Schematic cross-section showing differences between A) Tethyan-type ophiolites and B) Cordilleran-type ophiolites	1
Figure 1.2 : Localisation of the YZSZ and of study area.....	4
Figure 1.3 : Possible mechanisms and ophiolite/sole age-relationship implications for the creation of a dynamothermal sole	13
Figure 1.4 : Geodynamic evolution of the Yarlung Zangbo ophiolites as proposed by Girardeau et al. (1985)	19
Figure 1.5 : Geodynamic evolution of the YZSZ ophiolites as proposed by Dubois-Côté (2004)	19
Figure 1.6 : Geodynamic evolution of the YZSZ ophiolites as proposed by Aitchison et al. (2000)	20
Figure 2.1 : Area of study	71
Figure 2.2 : Geological map.....	72
Figure 2.3 : Petrographic observations	74
Figure 2.4 : Classification of amphiboles	75
Figure 2.5 : Mineral chemistry of amphiboles, Ti vs Al ^{IV}	76
Figure 2.6 : Mineral chemistry of amphiboles (Na + K) vs Al ^{IV}	77
Figure 2.7 : Composition of clinopyroxene	78
Figure 2.8 : Mineral chemistry of clinopyroxene	79
Figure 2.9 : Mineral chemistry of garnet	80
Figure 2.10 : Zonation of garnet	81
Figure 2.11 : P-T estimations.....	83
Figure 2.12 : P-T-t paths	84
Figure 2.13 : Geodynamic model.....	85
Figure 3.1 : Mg# vs SiO ₂ /Al ₂ O ₃ diagram showing possible cumulative processes	88

Figure 3.2 : REE patterns normalized to chondrites for the highly foliated amphibolites from the ophiolitic mélange	89
Figure 3.3 : Extended trace-element patterns normalized to primitive mantle for the highly foliated amphibolites from the ophiolitic mélange	90
Figure 3.4 : Discrimination diagram of Winchester and Floyd (1977) modified by Pearce (1996)	91
Figure 3.5 : Ta/Th _(CN) versus La/Sm _(CN) diagram.....	95
Figure 3.6 : Ar/Ar spectrum for amphiboles from Bainang and Buma with Ca/K plot of released gas.....	98
Figure 4.1 : Geodynamic evolution model for the YZSZ ophiolites.....	104
Figure B1 : Examples of amphibole colors	133
Figure B2 : Examples of inclusion density in plagioclase.....	134
Figure B3 : Examples of cataclastic deformation	135

Chapter I : Introduction

1.1. General introduction

Ophiolites are subaerially exposed mafic-ultramafic igneous sequences which are reminiscent of ocean-floor stratigraphy. Classification of ophiolites is still a matter of debate. Subgroups are mostly defined according to their mode of emplacement, a mechanism that has still to be defined as well (Wakabayashi & Dilek, 2003). Nonetheless, two major subgroups subsisted since the very first time subgroups of ophiolites were defined (Penrose Conference, 1972). These are the Cordilleran and Tethyan-type ophiolites. Cordilleran-type ophiolites (figure 1.1a) are oceanic lithospheric segments found on the hanging wall of subduction zones. Best known example would be the Coast Range ophiolites. Tethyan-type ophiolites (figure 1.1b), like the Oman, the Bay of Islands and the Yarlung Zangbo ophiolites, are rather emplaced over passive margins. They are mostly found as belts within major collisional orogens, where they are interpreted as remnants of the oceanic domain that separated the two colliding bodies.

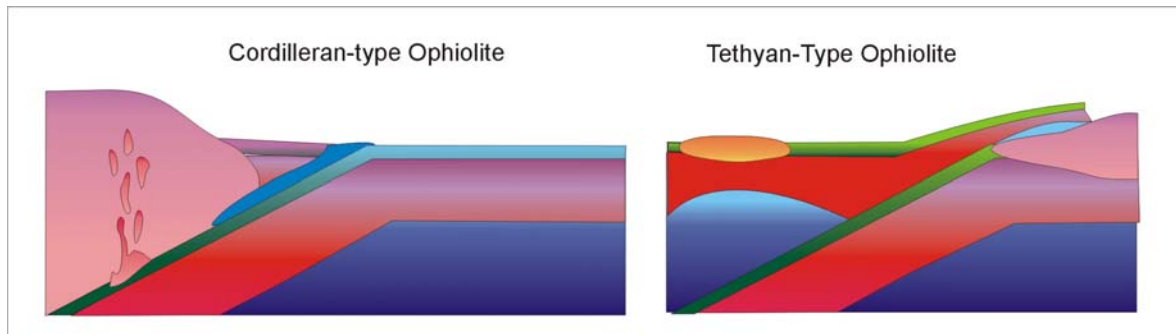


Figure 1.1 : Schematic cross-section showing differences between A) Cordilleran-type ophiolites and B) Tethyan-type ophiolites. A) Cordilleran-type ophiolites are trapped in the fore-arc domain of an active subduction. B) Tethyan-type ophiolites were emplaced over a continental passive-margin after subduction of the edge of the continental plate.

Accordingly, Tethyan-type ophiolites define the location of the suture zone, the very limit between the two converging plates, though this interpretation is currently questioned

(personal communication, R. Hébert, 2004). Suture zones do not only contain ophiolitic massifs but also sedimentary units and tectonic mélanges. As a matter of fact, all episodes of the great Wilson cycle are generally found within suture zones, from intracontinental rift sediments to deep ocean-floor pelites, from ocean island basalts to island arc tholeiites, from highly deformed subduction-related metamorphic rocks to recent fresh collision-related sedimentary basins. Therefore, suture zones are ideal natural laboratories to study pre-collisional settings.

The Yarlung Zangbo Suture Zone (YZSZ, figure 1.2, geological map in Chapter 2 and map A1 in Appendix A) is one of the most interesting suture zones on Earth because it recorded the different stages that led to the uplift of the Tibetan plateau and the Himalayas, usually referred to as the “Roof of the world”. Units along this suture are as old as ~300 Ma and are interpreted as the remnants of the vast Tethys ocean that separated India from Eurasia during Jurassic-Cretaceous times. All tectonic, igneous, metamorphic and sedimentary features found within the orogen are solely related to the India-Eurasia rift and collision, a characteristic that can only be found in some recent orogens. Therefore, studying recent orogens seems critical for North-East American geologists because all of North-East America is made of hardly decipherable ancient superimposed orogens. Another advantage of studying suture zones is that their collisional nature will expose rocks that are generally buried deep below the surface. For instance, the only accessible parts of contemporaneous intraoceanic island arcs are sparse volcanic islands. Scientists have to use indirect methods like geophysics, igneous petrology and isotope geochemistry to model the hidden rock assemblages. In the YZSZ, it is possible for a geologist to literally walk on the MOHO of an arc (Kohistan) or a back-arc (Xigaze) and take pictures of it. Studying ancient oceans is then as much important as studying modern day oceans if we hope to better understand the way our planet works.

Since 1998, the GÉO team (Génèse et Évolution des Ophiolites), supervised by Professor Réjean Hébert, works on the reassessment of the different geodynamical settings under which evolved the Yarlung Zangbo ophiolites. The Yarlung Zangbo ophiolites, outcropping at an altitude of 4000-6000 m, are one of the best preserved ophiolitic segments along the >2000 km long Indus-Yarlung-Zangbo Suture Zone. The study area

(figure 1.2) was centered near Xigaze and was ~250 km long (E-W) by 30 km wide, from Buma to Dazhuqu. Previous mapping and interpretations were mostly made by a Sino-French collaboration during the early ‘80s (Geological map in Appendix A from Wang et al., 1984). Results showed that mafic sections of the different ophiolitic massifs were generated near 120 ± 10 Ma from pre-existing oceanic lithosphere (isotopic evidence, Göpel et al., 1984) over a very slow spreading center (Nicolas et al., 1981; Girardeau et al., 1984; 1985; Girardeau & Mercier, 1988) near the shores of the Tibetan margin (Pozzi et al., 1984). More recent studies by the GÉO team show that the Yarlung Zangbo ophiolites were rather created in back-arc (Xigaze area; Hébert et al., 2000; 2003; Huot et al., 2002; Dubois-Côté et al., 2005; Dupuis et al., 2005a; 2005c) and fore-arc basins (Luobusa area; Zhou et al., 1996; Dubois-Côté et al., 2005) over an intraoceanic subduction. This subduction had to be older than the one responsible for their emplacement over the Indian passive margin (Guilmette et al., 2003; 2005). Inception of the latter subduction induced a quick episode of high-grade metamorphism observable within an underlying dismembered dynamothermal metamorphic sole.

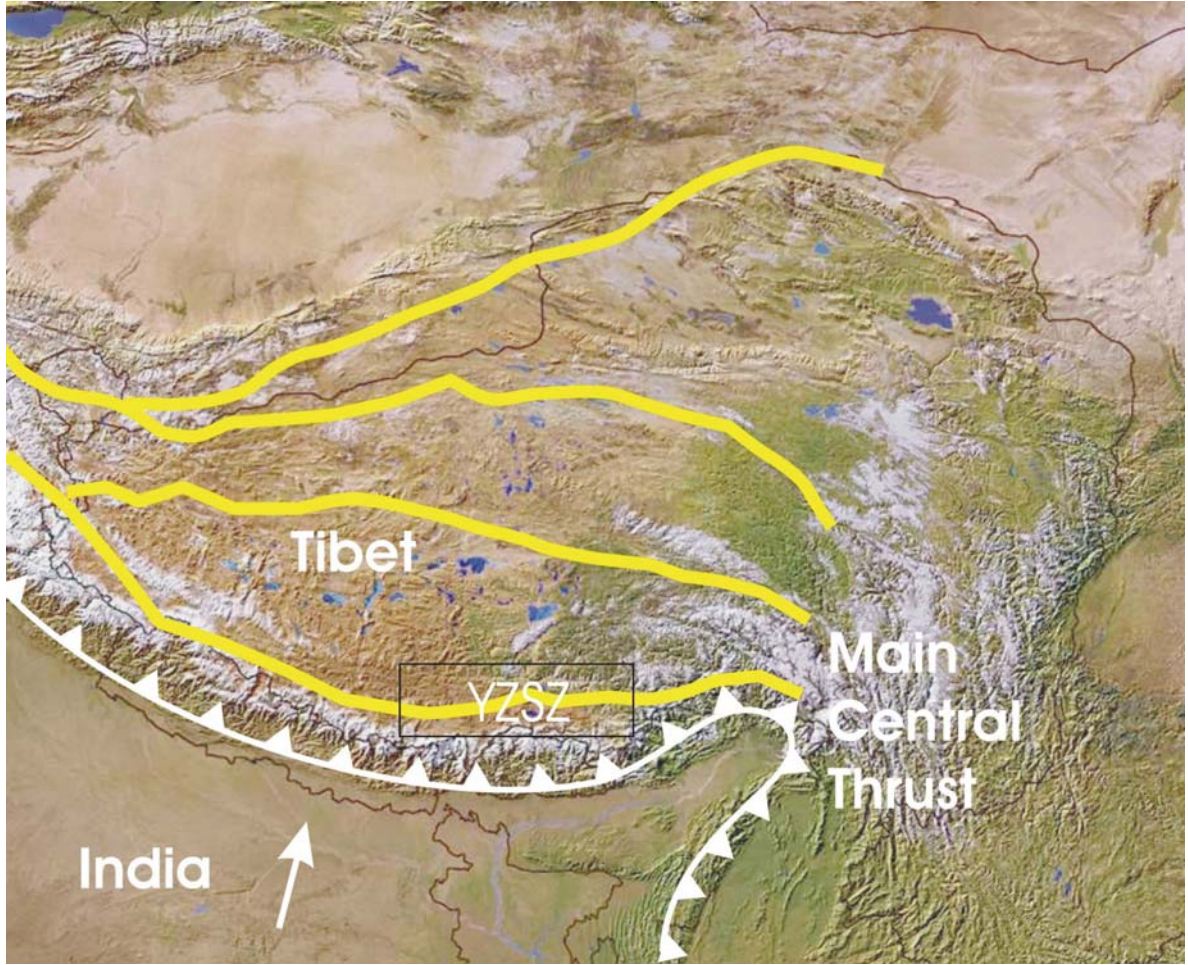


Figure 1.2 : Satellite imagery of the Tibetan plateau, showing the YZSZ and the study area. (modified from Jim Knighton, Clear Light Image Products, Copyright 2000). Refer to figure 2.1 for georeference and scale.

Nicolas et al. (1981) noted the presence of scarce occurrences of garnet-bearing amphibolite blocks underlying the Yarlung Zangbo ophiolites. Those blocks are found within a serpentine-matrix mélange interpreted to have formed by tectonic dismemberment of the base of the ophiolite during its obduction (Huot et al., 2002; Dupuis et al., 2005a; 2005c). They proposed that these highly foliated metamorphic basic rocks might represent a dismembered dynamothermal sole that would have formed soon (about 10 my) after the ophiolites, during the inception of a subduction. However, 70-90 Ma Ar/Ar ages for these rocks were published by the Chinese government in 1987 (Wang et al., 1987). Such a wide age span between ophiolite and sole generation was unexpected and hardly explained. A

second research group worked and are still working in the area since the end of the '90s. Geologists from the University of Hong Kong, in collaboration with the Chinese government, studied sedimentary and volcanic units, mostly around Zedang and Luobusa. They interpreted those Late Cretaceous Ar/Ar metamorphic ages as the time of obduction of the ophiolites over the Indian passive margin. Recent publications confirmed an Ar/Ar age of 88 Ma for «large amphibolite rafts» in the tectonic mélange underlying the Yarlung Zangbo ophiolites near Bainang (Malpas et al., 2003). However, only few mineral chemistry (Burg et al., 1987) and no geochemical data were available yet, even though such informations could confirm or infirm the dynamothermal sole hypothesis. This is the main objective of this M.Sc. Memoir.

Specific objectives were :

1. Describe the structures, textures, mineralogy and mineral chemistry of the different amphibolites.
2. Discriminate the magmatic setting that prevailed during the early history of the meta-basites
3. Estimate P-T conditions of metamorphism for the different metamorphic stages undergone by the amphibolites
4. Find an age for the peak metamorphism of the amphibolites
5. Use previously published and unpublished information together with results from this study to describe the probable settings under which evolved the Yarlung Zangbo ophiolites
6. Extend this interpretation to what is known from the Eastern and Western YZSZ
7. Bring additional knowledge and insight on the ophiolite « emplacement problem » and raise new questions about the obduction mechanism

Thirty-five samples were collected in 2001-2002 from valleys in the ophiolitic mélange near Bainang and Buma. Thin sections were described and a selected representative set was used for mineral analysis using the CAMECA SX-100 at Université Laval. Three samples were crushed and selected minerals were mechanically separated for oxygen extraction and analysis of isotope population at the « Laboratoire d'Isotopes stables de l'Université Laval ». XRD (X-Ray Diffraction) analyses were performed to confirm the quality of the powdered separates at Université Laval as well. Afterwards, 20 samples were sent to Act Labs, Ontario, for ICP-AES analysis of major and trace elements contents. Finally, 3

samples were selected for Ar/Ar step-heating dating at the Geological Survey of Canada, Ottawa. Results (120-130 Ma) will be used to interpret the magmatic and metamorphic history of the highly-foliated amphibolites found beneath the Yarlung Zangbo ophiolites.

This manuscript will be divided into five chapters. The first chapter will provide a complete description of the geological setting, a review of the literature on dynamothermal soles, all available data on the Bainang and Buma amphibolites and a description of previous models proposed for the emplacement of the Yarlung Zangbo ophiolites. The second chapter presents a paper that was submitted to the Journal of Metamorphic Geology. This paper contains most of the work done during the author's masters degree and bears on the metamorphic history of those blocks. The third chapter will present geochemical and geochronological data that will be submitted in a second paper during summer 2005. The fourth Chapter is a broad complementary discussion followed by a final conclusion. Finally, the fifth chapter will contain additional appendices related to this MSc. Memoir.

1.2. Geological Setting

The YZSZ is a major tectonic feature of Southern Tibet (Appendix A). It is the southernmost and the youngest of all sutures found across the Tibetan Plateau (figure 1.2). This suture is widely known to mark the separation between Eurasia and the Indian Plate. Diachronic convergence between the two plates during Jurassic and Cretaceous times forced the destruction of the Tethys and Neo-Tethys oceanic basins. Tethys, is the oceanic basin that formed from the rifting of the Lhasa block (Tibet) and Gondwana during Permo-Triasic times (Gaetani & Garzanti, 1991). During Late Jurassic to Cretaceous times, intra-oceanic subduction zones were active within Tethys. They were likely located near the southern edge of the Lhasa block, already accreted to Eurasia (Pozzi et al., 1984). These subductions induced arc and back-arc ridge accretion (Zhou et al., 1996; Hébert et al., 2000; 2001; 2003; Aitchison et al., 2000; McDermid et al., 2000; 2001; 2002; Huot et al., 2002; Dubois-Côté et al., 2003; 2005; Dupuis et al., 2005a; 2005b; 2005c), giving birth to the Neo-Tethys suprasubduction zone (SSZ) oceanic domain. It is mostly accepted that Cretaceous subduction of Neo-Tethys beneath the Tibetan active margin caused extrusive and intrusive calc-alkaline magmatism (andesites and granodiorites) within the Lhasa block (Allègre et al., 1984; Harrison et al., 1992). Paleocene obduction towards India (Tapponnier et al., 1981a) thrusted portions of the Tethys over passive margin sediments. Eocene collision (Molnar & Tapponnier, 1974) trapped the Tethyan and Neo-Tethyan remnants between the Indian continent to the south and Tibetan calc-alkaline batholiths and volcanic rocks to the north. Late back-thrusting (Tapponnier et al., 1981a), strike-slip (Molnar & Tapponnier, 1974; Allègre et al., 1984) and east-west extension (Tapponnier et al., 1981b) disrupted the belt into heterogeneous ophiolitic massifs overlying an ophiolitic tectonic mélange.

In the study area (figure 1.2), the suture can be subdivided in three major tectonic domains (Burg et al., 1987; Hodges, 2000; Dupuis et al., 2005a). Those are, from north to south : an active paleo-margin, an oceanic domain and a passive paleo-margin.

1.2.1. The active paleomargin

The Lhasa block, northern limit of the suture, contains active margin-derived facies like calc-alkaline batholiths and volcaniclastic assemblages. This intrusive and extrusive magmatism is thought to be the result of a northward andean-type subduction beneath the Lhasa block (Allègre et al., 1984). Emplacement of the Gangdese batholith is constrained between 94 and 41 Ma (Schaerer et al., 1984) though volcanic activity inferred from the Sangri group started as early as 153 ± 6 Ma and lasted up to Late Tertiary (Murphy et al., 1997; Harrison et al., 2000). Also, two main calc-alkaline volcanic belts, the Linzizong volcanics (Coulon et al., 1986), are situated in northern and southern Lhasa block. The northern Linzizong volcanics yield Upper Cretaceous ages (110-80 Ma) while the southern Linzizong volcanics are Paleogene (60-40 Ma) in age (Coulon et al., 1986). The Xigaze group lies south of the batholith and is composed of folded Mid to Late Cretaceous siliciclastic turbiditic deposits that were emplaced in a fore-arc basin (Dürr et al., 1996; Einsele et al., 1994; Wang et al., 2000) during the consumption of tethyan lithosphere of MORB affinity (Wang et al., 2000). Erosion of youngest strata prevents the definition of an upper age for the turbidite deposition. Lower limit is Upper Albian to Coniacian (Wiedmann & Dürr, 1995; Wan et al., 1998) and lies on Tethyan oceanic crust. It is still not quite clear if this is a concordant or faulted contact (Aitchison et al., 2000; Girardeau et al., 1984), though most authors seem to agree on a faulted contact.

1.2.2. The oceanic domain

The oceanic domain in the YSZ occur mainly as a tectonically disrupted ophiolitic belt lying on an ophiolitic mélange that in turn lies on off-scraped ocean-floor sediments and volcanics (Ganser, 1974; Nicolas et al., 1981). In the studied region, most massifs show a correlative stratigraphy. Upper crust consists of sheeted dykes, minor gabbros and pillow basalts (Allègre et al., 1984; Dubois-Côté et al., 2005) overlain by Barremian radiolarites (131-124 Ma, Ziabrev et al., 1999). Mid Cretaceous age for the formation of the ophiolitic crust is confirmed by U/Pb ages of 120 ± 10 Ma from plagiogranites (Göepel et al., 1984)

and Pb/Pb age of 126 ± 1.5 Ma from quartz diorites (Malpas et al., 2003). However, mantle section could be much older (Göepel et al., 1984). Paleo-magnetic data suggest ophiolite genesis occurred at a $10\text{--}20^\circ$ N latitude, near the coast of Tibet (Pozzi et al., 1984). Middle crust and lower crust are mostly missing due to tectonic attenuation, late deformation or very low magmatic regime (Nicolas et al., 1981; Hébert et al., 2003). Harzburgite is the major component of the mantle section, though clinopyroxene harzburgite and lherzolites are observed (Allègre et al., 1984; Dubois-Côté et al., 2005). Although earlier studies claimed these ophiolitic massifs derived from a mid-ocean ridge setting (Nicolas et al., 1981; Girardeau et al., 1985), recent data rather suggest a supra-subduction zone setting (Dubois-Côté et al., 2003; 2005; Hébert et al., 2000; 2001; 2003; Zhou et al., 1996; Huot et al., 2002) with prominent back-arc and arc signatures. This hypothesis fits the lead isotopes systematics indicating a ridge-generated mantle (harzburgite) of older age intruded by arc-related magmas (Göepel et al., 1984). The Bainang and Buma massifs (study area, figure A1), underneath which were found highly deformed amphibolites, show back-arc geochemical signatures (Dubois-Côté et al., 2005).

About 200 km east, near the Zedong area, volcaniclastic assemblages have been described (Aitchison et al., 2000). Preliminary geochemical results would suggest an intra-oceanic arc setting for the genesis of these rocks (McDermid et al., 2001; 2002). Ar/Ar and U/Pb ages constrain arc activity between 161 and 127 Ma (McDermid et al., 2002; Malpas et al., 2003). In this region, strongly depleted mantle has been associated with arc metasomatism (Jinlu massif, Dubois-Côté et al., 2005).

At almost all locations in the studied region, lower contact of the ophiolite is marked by a highly sheared serpentinite mélange containing some sedimentary blocks but mostly rodingitized mafic and ultramafic blocks. This ophiolitic mélange shows a block-in-matrix aspect, with centimetric to kilometric fragments. Geochemical data from fresh mafic and ultramafic blocks suggest a back-arc and even arc setting for their genesis, as seen within ophiolite massifs (Dupuis et al., 2005; Huot et al., 2002; Dubois-Côté et al., 2005). Low to medium grade metamorphism affected these blocks. Geochemical and textural correlations between the mélange and the overlying ophiolite massifs would indicate the mélange formed by tectonical disruption of the ophiolite during obduction over passive margin

(Girardeau et al., 1984; Huot et al., 2002; Dupuis et al., 2005). Near Bainang and Buma, few decametric garnet-bearing amphibolite blocks have been reported. Those have been interpreted as a dismembered dynamothermal sole that would have formed at the inception of the subduction that allowed ophiolite transport towards the Indian passive margin (Nicolas et al., 1981; Guilmette et al., 2005). This study bears on these garnet-bearing blocks but also on nearby highly foliated garnet-free amphibolites. Sample locations are shown in Map A2 in Appendix A.

An imbricate thrust sheet zone can be found south of the ophiolitic sequence, beneath the serpentinite mélange and over Tethyan passive margin sediments. This thrust sheets group, also called the Yamdrok mélange by Searle et al. (1987) and the Bainang terrane by Aitchison et al. (2000), would have preserved an ocean floor stratigraphy (Aitchison et al., 2000). It is composed of red siliceous shales, radiolarian cherts, local basalts and lower fine-grained, thinly bedded deep marine shales (Chang et al., 1984; Aitchison et al., 2000; Ziabrev et al., 2004; Dupuis et al., 2005a; 2005b). The source for these sediments could be a continuous Indian passive margin (Dupuis et al., 2005b). Exotic blocks are decimetric to kilometric and include Permian to Jurassic limestones and seamount-derived Campanian-Maestrichtian micrites and pillow lavas of alkaline affinity (Mercier et al., 1984; Dupuis et al., 2005a). Detailed radiolarian biostratigraphy revealed two subgroups. The northern tract would represent Aptian trench-fill sediments and tuffs. The southern tract would contain older (Triasic-Jurassic) pelagic sediments and intraplate volcanics (Ziabrev et al., 2004; Dupuis et al., 2005a). Structurally, the unit is reminiscent of subduction complexes. These imbricated thrust slices were probably off-scraped from the downgoing tethyan slab (Ziabrev et al., 2001; Chang et al., 1984). Matrix chronology would indicate a Late Cretaceous (Chang et al., 1984; Mercier et al., 1984) to Paleocene (Burg & Chen, 1984) activity for this unit. However, new data (Ziabrev et al., 2004) indicate accretion of the northern tract during Aptian-Albian followed by hanging-wall erosion until post-Campanian accretion of the southern tract.

1.2.3. The Passive Paleomargin

Also called Tethyan series, passive margin units located south of the oceanic domains can be divided in three groups. These are, from north to south, the continental margin turbidites, carbonate flysches and a platform sequence that is Permian to Paleogene in age. These units were thrusted towards the Indian foreland during the Early Paleocene (Burg & Chen, 1984; Burg et al., 1987; Liu & Einsele, 1996; 1999) and now lie as allochthonous units under the oceanic domain and over the Main Central Crystalline Sheet. Geochemistry of sediments confirms a continuous passive margin as a source (Dupuis et al., 2005b). Northern contact is marked by an intensively tectonized zone along which numerous Ordovician granitic intrusions are found. The central section of the suture (study area, figure 1.2) probably represents the least deformed section throughout the whole Himalaya (Searle et al., 1987). Metamorphism range from low to medium-grade with no occurrence of high-grade or high-pressure rocks. Mafic blocks in the flysch show intraplate magmatism affinities and granite crustal assimilation that could be associated with Lhasa block rifting from Pangea (Dupuis et al., 2005a).

1.2.4. Liuqu Conglomerate

Several zones of coarse clastic sediments, derived from rapid deposition, crop out as a series of tectonically disrupted oblique-slip basins, within and at the margin of the intra-oceanic terranes. These sediments, known as the Liuqu Conglomerate, record a Paleogene phase in the tectonic evolution of Tibet (Davis et al., 2002; Aitchison et al., 2000). The sediments were derived from the leading (northern) edge of the Indian margin and an intra-oceanic arc within the Neo-Tethys (Davis et al., 2002). They are interpreted as an evidence of oblique convergence and terrane translation along the YZSZ. The absence of clasts derived from terranes to the north of the YZSZ suggests that basins associated with deposition of the Liuqu Conglomerate developed prior to the final collision between India and Asia, although they are mostly undeformed.

1.3. Dynamothermal Soles

Dynamothermal soles are highly-deformed metamorphic folded slabs (<500 m thick) found structurally beneath the mantle section of many ophiolites (Williams & Smyth, 1973; Jamieson, 1986). Classical examples are found beneath the Bay of Islands (Newfoundland, Canada; Malpas, 1979) and Semail ophiolites (Oman, Gnos et al., 1998; Hacker et al., 1996).

The slab can be coherent (Bay of Islands, Semail) or dismembered (Coast Range, Wakabayashi et al., 1990; Xigaze, this study), depending on the tectonical setting of their genesis, evolution and emplacement. An inverted temperature and pressure gradient has been described in best exposed occurrences (e.g. Semail ophiolite, Gnos et al., 1998). According to previous examples, dynamothermal soles can be divided in two sections : the upper and lower sole (Wakabayashi & Dilek, 2000).

The upper section consists of oceanic mafic material with minor pelagic sediments metamorphosed under high-grade conditions. P-T conditions for peak metamorphism of dynamothermal soles indicate underthrusting (subduction) beneath hot (young) suboceanic mantle. Commonly overlapping age relationship in ophiolite-sole couples indicate inception of subduction at or very near the spreading center where the ophiolite was generated. Such a setting would provide explanation for the high-grade metamorphism that would otherwise not be achieved. Therefore, the upper section of dynamothermal soles can be considered as the very first material accreted to the hangingwall of a subduction zone (Williams & Smyth, 1973; Malpas, 1979; Nicolas & LePichon, 1980; Spray, 1984; Jamieson, 1986; Wakabayashi & Dilek, 2000; 2003). Inverted thermal anomaly responsible for high-grade metamorphism resorbs quickly (<2 my) as the overlying mantle wedge cools down (Peacock, 1988; Hacker, 1990; 1991; Hacker et al. 1996). Accordingly, metamorphic ages of upper dynamothermal soles obtained from commonly applied isotopic systems such as Ar/Ar are thought to be a close approximation of the inception of intraoceanic subduction (Spray, 1984; Peacock, 1988). Present day field relationships (ophiolite structurally overlying sole, compatible deformation in sole and tectonized mantle, sole over passive margin pattern when present) indicate that this subduction is often, if not always,

the same that allowed ophiolite emplacement over a passive margin (Tethyan-type ophiolites) or a subduction complex (Cordilleran-type ophiolites) (figures 1.1 and 1.3).

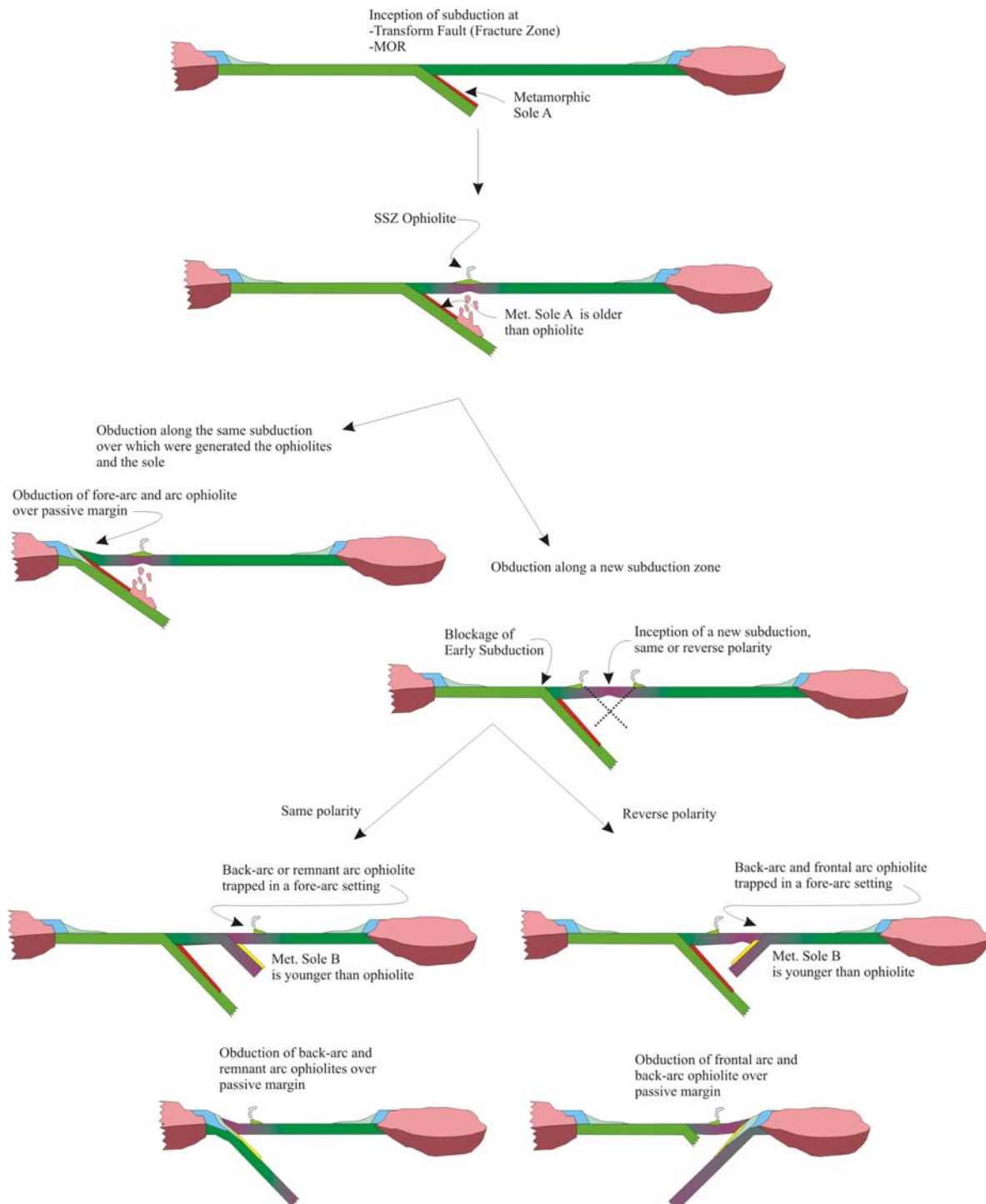


Figure 1.3 : Possible mechanisms and ophiolite/sole age-relationship implications for the creation of a dynamothermal sole (modified from Wakabayashi & Dilek, 2000).

The lower section of a metamorphic sole, as observed in Tethyan-type ophiolites, is made of passive margin sediments metamorphosed under medium to low-grade conditions during obduction of the ophiolitic napes. It can either be an integrant part of the folded slab and show internal inversed metamorphic gradient or occur as a coherent homogeneous metamorphic terrane of much larger size than the upper sole. The lower section of a dynamothermal sole could be defined as : metamorphic passive margin rocks deformed during thrusting of ophiolitic napes.

Detailed studies of the well-exposed Semail Tethyan-type ophiolitic nape and sole lead to general assumptions about emplacement processes that have to be carefully evaluated. One of these hazardous assumptions would be that ophiolites form very near their emplacement site (<500 km) and that their emplacement took place very soon after their generation at a spreading center (<5 my) (Hacker et al. 1996; Wakabayashi & Dilek, 2000). This generalized interpretation caused many geologists to attribute any Ar/Ar age from a metamorphic sole to the time of obduction of the ophiolite. It might be true for the well-studied Semail ophiolite, but extensive geochronological studies have yet to be conducted on other ophiolite-sole couples before it can be generalized. Presence of upper section of a dynamothermal sole (high-grade amphibolites) beneath Cordilleran-type ophiolites (Coast-Range ophiolite, Wakabayashi, 1990; Wakabayashi & Dilek, 2000) proves the limited application of such an assumption for these ophiolites were never obducted. Therefore, it could be possible that a very large time span separates upper and lower sole metamorphism. It might even be possible that the two parts would be separated physically by metamorphic subduction complex material. Another hazardous assumption is that high-grade metamorphism within the sole can only be achieved by inception of a subduction at a spreading center. This generalized assumption is based on the shallow nature of the Semail metamorphic sole. In this particular setting, metamorphic modelisations were made for depths of 18 km (~6 kbars, Hacker, 1990; 1991), which is not true for all dynamothermal soles. For instance, the metamorphic sole beneath the Bay of Islands ophiolite is interpreted to have formed at a depth of 22 to 37 km. Such a difference in extent of burial implies 1) different hanging wall temperatures and 2) different transit time to reach the estimated depth. Therefore, older (but relatively still young) crust could attain high-grade metamorphism if buried at greater depths even though inception of subduction does not

occur at the spreading center. However, overlapping ages for ophiolite-sole couples remains a diagnostic feature for inception at the spreading center.

The current study will show that upper and lower section of metamorphic soles should not always be treated as a whole for there can be major age differences (up to 50 Ma) between their peak metamorphism. It also shows that geochemistry of the sole is an underestimated tool in clarifying the ophiolite emplacement problem because it allows insight in the nature of the geological region where inception of subduction occurred. This study will also address the possibility that Tethyan and Cordilleran-type ophiolites are not different types of ophiolites but rather different stages, Tethyan-type ophiolite being the final stage. Finally, it will test the hypothesis that inception of subduction has to be related to blockage of an early subduction (Mueller & Phillips, 1991; Boutelier et al., 2003) and that it can result in close migration of the subduction plane towards weaker lithosphere with or without polarity switch (figure 1.3).

1.3.1. The Bainang Dynamothermal Sole

The first geologist to emphasize the presence of garnet-bearing amphibolites within the ophiolitic mélange was Nicolas (1981). He suggested a dismembered dynamothermal sole as a probable origin for the amphibolites and their genesis was integrated to the overall geodynamic model (Girardeau et al., 1985b). Garnet-bearing amphibolites were sampled from Bainang for thermobarometric calculations. Burg et al. (1987) presented a very brief overview of those results. Amphibolites from the ophiolitic mélange near the locality of Bainang were subjected to high-grade metamorphism of 800-1250°C constraining pressures of 6-9 kbars. However, methods used for P (sphene-ilmenite reaction) and T (Ganguly, 1979; Powell, 1985) estimations are now obsolete or incomplete. Chinese government published inaccessible Ar/Ar ages for amphibolites in the ophiolitic mélange near Bainang of about 80 Ma (Wang et al., 1987). Those ages are cited in some papers from Aitchison, Ziabrev and Malpas, but no detailed information is available. Malpas et al. (2003) confirmed these 80 Ma ages with a 88 Ma Ar/Ar age from « large amphibolite rafts in the ophiolitic mélange near Bainang ». However, there is no petrographic nor geochemical data available from those rocks. Such incomplete information prove the necessity of the current study and results will confirm that a great confusion exists about the very nature of the garnet-bearing and other highly foliated amphibolites.

1.3.2. Buma vs. Bainang

Highly foliated amphibolites were sampled in two valleys near the localities of Buma and Bainang (see Appendix A for location). Buma is a very small village at the entrance of the valley in which we sampled the amphibolites. It is situated at the western limit of the area of study. Bainang lies about 170 km east of Buma, near the eastern end of the area of study. It is a major town and many geological features were named after it (i.e. Bainang terrane, Bainang massif, Bainang amphibolites). However, Bainang is not the closest agglomeration to the sampling site. The valley from which were sampled the amphibolites lies about 5 km east of Bainang. Luobusang, a small village in the sampled valley, would be the closest locality. Nonetheless, we chose to keep the « Bainang amphibolites » nomenclature to avoid confusion with literature.

The Bainang and Buma amphibolites, 170 km apart one from the other, outcrop as clasts in the ophiolitic mélange. Between the two localities, the mélange often pinches out, becoming very thin or even disappearing. Therefore, it might seem hazardous to regroup the two amphibolite occurrences as one dynamothermal sole. However, the overlying ophiolitic belt is mostly continuous and ages from overlying radiolarite cover are similar (Aitchison et al., 2003). Geochemistry of these ophiolitic massifs is relatively homogeneous when compared with nearby unconnected massifs like Jungbwa to the west or Zedang to the east. Early oceanic deformation styles are however divergent. For instance, high-temperature tectonic foliation and lineation within the mantle in Dazhuqu massif indicate thrusting while they indicate strike-slip motion in Liuqu (Girardeau et al., 1985). Such different features might reflect paleo ridge-transform intersections within the study area. Therefore, we assume that all the massifs in the study area come from one restrained homogeneous domain within a suprasubduction zone and that the amphibolites from both locations can be treated as dynamothermal soles resulting from the same event.

1.4. Previous models for the emplacement of the Yarlung Zangbo ophiolites

Figure 1.4 presents the previous model proposed for the emplacement of the Yarlung Zangbo ophiolites (Girardeau et al., 1985b). This model begins with genesis of the ophiolitic massifs over a slow-spreading ridge. Physical characteristics of the ophiolitic massifs (very thin crustal sequence, abundance of sills relative to dykes, almost total absence of gabbroic lower crust) and some geochemical characteristics (i.e. REE contents) led to the hypothesis of a MOR-generated ophiolitic nape. However, Pb/Pb systematic studies pointed out that mantle and crustal section of the ophiolites possibly underwent different histories and were of different ages (crust and magmatites in mantle are 120 ± 10 Ma, mantle unknown but much older; Göpel et al., 1984). Paleo-magnetic data indicated a genesis near the shores of Tibet ($10\text{--}20^\circ\text{N}$, Pozzi, 1984). At that time, Africa was translating towards east relative to Eurasia (Patriat et al., 1982). Accordingly, authors proposed a ridge-generated ophiolitic nape being created in a trans-tension basin along the shores of the Tibetan margin. Changes in tectonic plate motion near 110 Ma would have caused inception of subduction beneath the ophiolites, generating the dynamothermal sole. Further subduction would have caused disruption of the ophiolites in a fore-arc setting to the Gangdese arc until arrival of India, near 50 Ma. Obduction over the passive margin would have caused dismemberment of the base of the ophiolites into a serpentinite-matrix tectonical mélange containing the amphibolite blocks.

Twenty years later, technologic advances made it possible to measure trace elements that have a very low abundance, like some REEs, HFSEs and LILEs. Ocean drilling programs also allowed sampling of recent arcs, back-arcs and MORs. Reinvestigation of the Yarlung Zangbo ophiolites by the GÉO team and discovery of an intraoceanic arc and fore-arc domain 200 km east near Zedang and Luobusa led to the elaboration of an updated supra-subduction zone (SSZ) model. In this model, the Yarlung Zangbo ophiolites were generated over the same slow-spreading ridge, except that this ridge is now bound to a back-arc basin (figure 1.5).

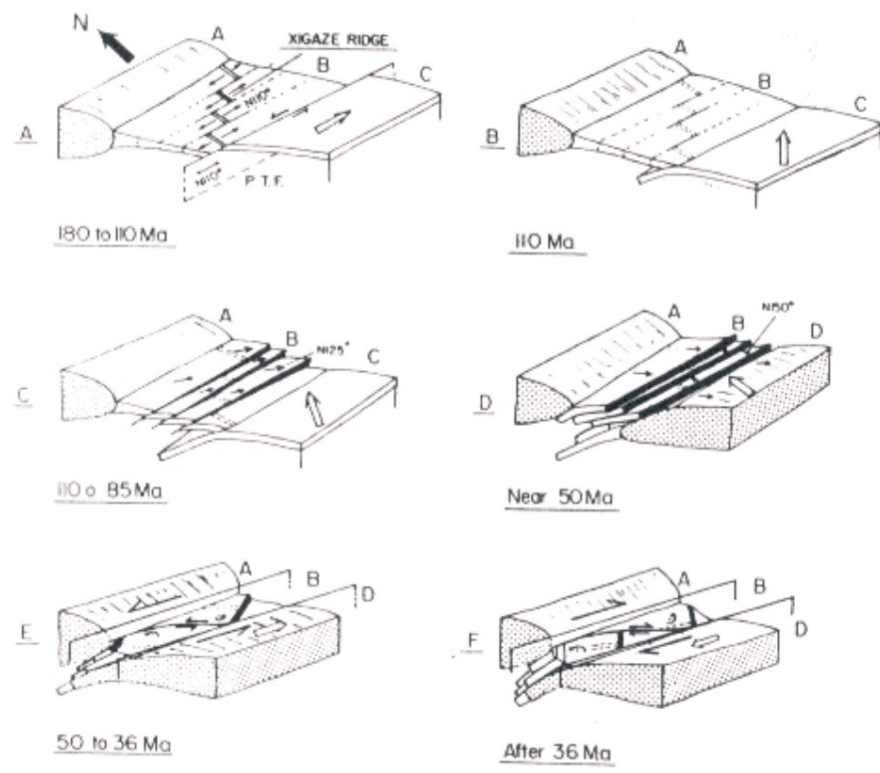


Figure 1.4 : Geodynamic evolution of the Yarlung Zangbo ophiolites as proposed by Girardeau et al. (1985).

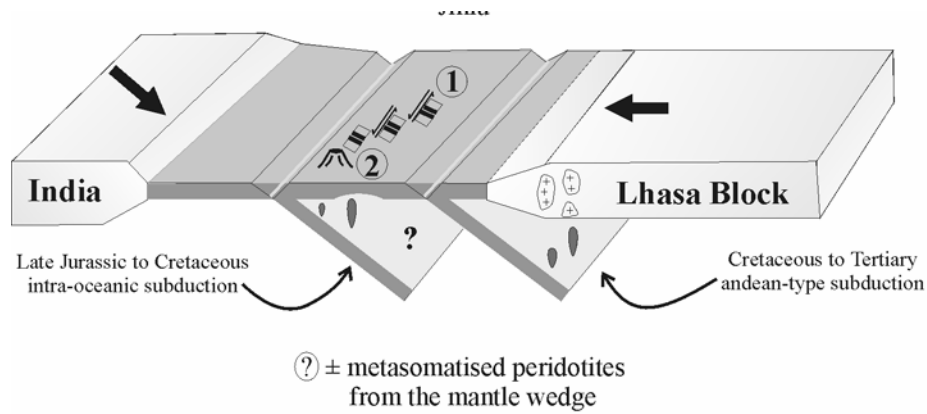


Figure 1.5 : Geodynamic evolution of the YZSZ ophiolites as proposed by Dubois-Côté et al. (2005).

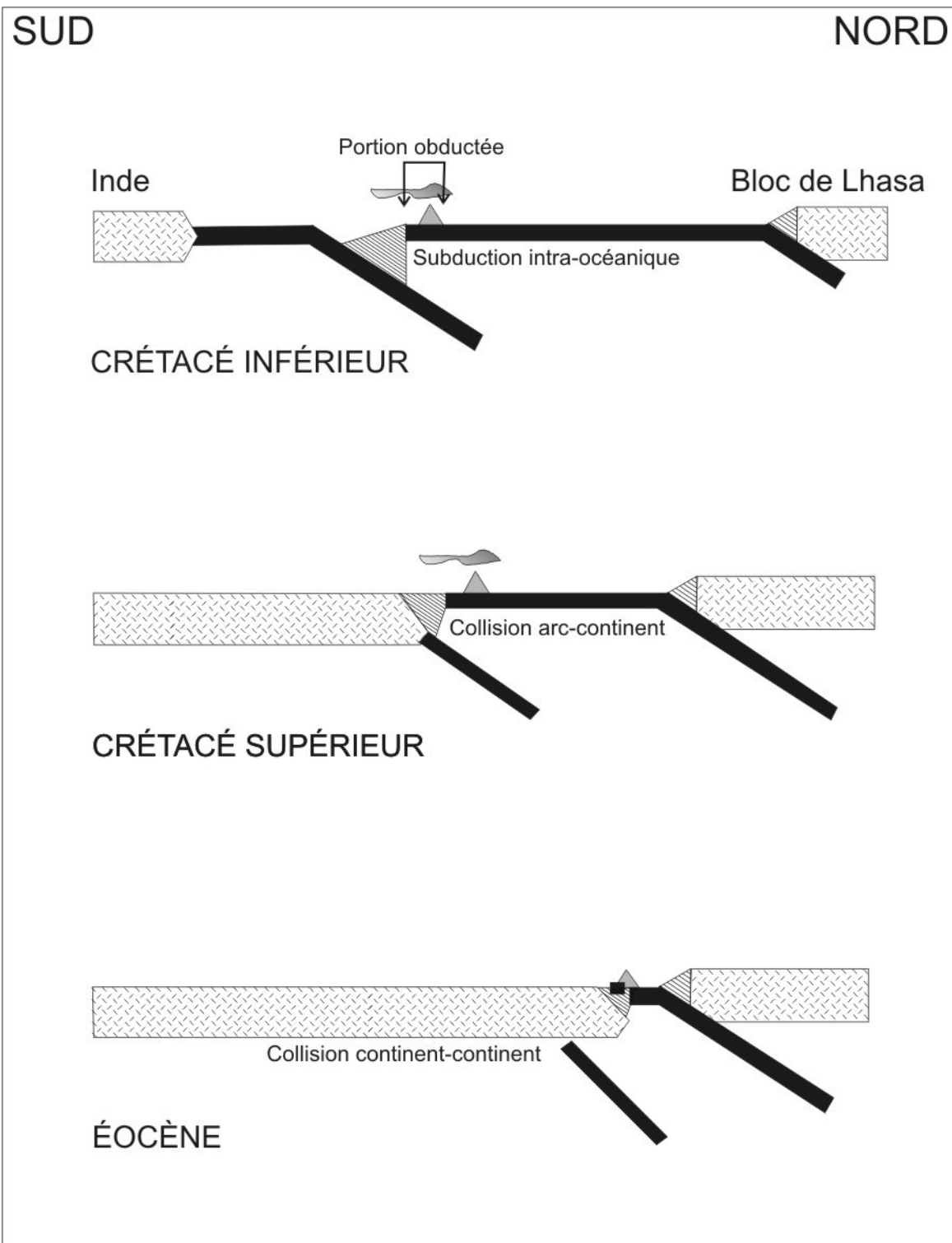


Figure 1.6 : Geodynamic evolution of the YZSZ ophiolites as proposed by Aitchison et al. (2000) (modified from Aitchison et al., 2000).

Divergences between our interpretations and those from other authors (figure 1.6) start here and are mainly based on the nomenclature proposed by Aitchison et al. (2000). This terrane-based nomenclature linked different units of hypothetically similar geodynamic settings all along the 2000 km long YZSZ as coherent terranes. However, this nomenclature did not account for laterally divergent ages and induced confusion in overall models. For instance, the Dazhuqu terrane would contain all mantle sections exposed within the YZSZ. Such a regroupment is fundamentally wrong because the mantle section where these authors mostly worked is of fore-arc origin and cross-cutting dikes are 170 Ma old (Luobusa, Zhou et al., 1996; Dubois-Côté et al., 2005) whereas mantle from Xigaze, 200 km west, is of back-arc affinity and cross-cutting dikes are 126 Ma old (Hébert et al., 2000; Dubois-Côté et al., 2005; Huot et al., 2002; Dupuis et al., 2005; Malpas et al., 2003). The result of this confusion is shown in the overall geodynamic models (figure 1.6) for the evolution of the YZSZ proposed by Malpas (2003), Ziabrev (2004) and Aitchison (2000, 2003). In these models, the Dazhuqu terrane forms in a fore-arc setting and is obducted over India near 80 Ma. Such an evolution cannot be proved by any other rocks than those present in their area of study. Nonetheless, the model was applied to all of the YZSZ, including the Xigaze massifs, because a terrane-based nomenclature does not allow lateral variation in age and setting. We wish not to perpetrate the same mistake and restrict our model to the area of study, between Buma and Dazhuqu, near Xigaze. The new model (see chapters 2 and 4) we propose takes into account all available literature about the concerned units and does not unnecessarily extend to other sections of the YZSZ.

Chapter 2 : Submitted Article

Metamorphic history of highly foliated amphibolites from the ophiolitic mélange beneath the Yarlung Zangbo Ophiolites, Xigaze area, Tibet

Geodynamic significance

Introducing the paper

The following paper was submitted in March 2005 for revision and publication to the Journal of Metamorphic Geology and is now under review. This paper is the first of two companion papers that will contain all the work done by the author for his masters degree. This first paper represents most of the work done by the author and co-authors and includes mineral chemistry, thermobarometric calculations and stable isotope chemistry. The second one will present geochemistry and geochronology of the highly foliated amphibolites together with an elaborated discussion covering all data available for the YZSZ in the study area.

First author is the author of this MSc. Thesis. Second author is professor Réjean Hébert, his supervisor. Third author is Céline Dupuis Ph.D. who did helpful field work and provided samples, analyses and stimulating discussions. Fourth author is Professor Chengshan Wang, who helped us to plan field work in Tibet. Finally, fifth author is Zejung Li who guided us through Tibet and helped for field work.

In the following paper, we first present a brief geological setting followed by petrographic and chemical data for the highly foliated amphibolite blocks from the mélange. We also present restrained oxygen stable isotope chemistry for some mineral separates. These data are then used in thermobarometric calculations that help constrain a P-T-t path. Follow a discussion and conclusions bearing on the geodynamical significance of these amphibolite

blocks in regard of their field-relationships with other units from the suture and their specific metamorphic history.

**Metamorphic history of highly foliated amphibolites from the
ophiolitic mélange beneath the Yarlung Zangbo Ophiolites,
Xigaze area, Tibet**

Geodynamic significance

Guilmette, C.*; Hébert, R.^a; Dupuis, C^a, Wang, C.S.^b; Li, Z.J.^c

^aDépartement de géologie et de génie géologique, Université Laval, Québec, QC, Canada G1K 7P4.

^bSchool of Earth Sciences and Mineral Resources, China University of Geosciences, Xueyuan Road #29, Beijing, People's Republic of China

^cInstitute of Sedimentary Geology, Chengdu University of Technology, Chengdu, Sichuan 610059, People's Republic of China.

*Corresponding author. Tel.: 1-418-656-2131 # 12710; Fax: 1-418-656-7339

E-mail address: carl.guilmette.1@ulaval.ca

Abstract

Blocks of highly foliated amphibolites are locally embedded within a sheared serpentinite matrix mélange underlying the Yarlung Zangbo ophiolites, Xigaze area, South Tibet. In the study area, ophiolites are remnants of an Early Cretaceous back-arc basin that was located in the northern section of the Permo-Cretaceous Tethys ocean, the Neo-Tethys supra-subduction zone (SSZ). Remains of this oceanic basin are now trapped in the Yarlung Zangbo Suture Zone (YZSZ), Southern Tibet. Garnet-bearing amphibolites from the mélange were interpreted as parts of a dismembered dynamothermal sole. Amphibolites sampled are divided in three groups: 1) common amphibolites, 2) clinopyroxene amphibolites and 3) garnet amphibolites. The common amphibolites contain $\text{Hbl}+\text{Pl}\pm\text{Ep}+\text{Ap}+\text{Ttn}$. The clinopyroxene amphibolites contain the assemblage $\text{Hbl}+\text{Cpx}+\text{Pl}+\text{Ep}\pm\text{Ttn}+\text{Qtz}+\text{Ap}$. The garnet amphibolites contain the assemblages $\text{Hbl}+\text{Cpx}+\text{Grt}+\text{Pl}\pm\text{Rt}$ and $\text{Grt}+\text{Hbl}+\text{Pl}$ (corona assemblage). In all assemblages, plagioclase is pseudomorphised by a late albite-prehnite simplectite. Retrograde cataclastic veins containing assemblage $\text{Prh}+\text{Ab}\pm\text{Chl}+\text{Ep}$ are also present. P-T estimates indicate that the amphibolites were buried to peak metamorphic conditions of 13-15 kbars and 750-875 °C. Presence of a metamorphic fluid ($10 \text{ ‰ } \delta^{18}\text{O}$ SMOW) is consistent with oxygen stable isotope geochemistry. Heterogeneous coronitization of pyrope-rich (up to 35 mole %) garnet by Al-Tschermarkite (Al_2O_3 up to 21 wt %) reflect a high-pressure (≈ 18 kbars, 600°C) metamorphic event followed by rapid exhumation. After exhumation, the amphibolites were injected by very fine-grained diabasic dykes and were subject to percolation of a prehnite-precipitating fluid. Field relationships and metamorphic history of the metamorphic sole are in agreement with the following model. The amphibolites were buried during inception of a subduction within the back-arc basin of the Neo-Tethyan SSZ, trapping the Yarlung Zangbo Ophiolites in a fore-arc setting. Subsequent subduction of the arc, fore-arc and trench domains followed by exhumation of the sole would provide explanation for the heterogeneous high-pressure overprint. Injection of dikes and fluid percolation occurred during subduction of a magmatic center prior to obduction over the Indian passive margin.

Keywords : Ophiolite, amphibolite, metamorphic sole, Yarlung Zangbo, subduction, thermobarometry

2.1. Introduction

The Yarlung Zangbo Suture Zone (YZSZ) is a major tectonic feature of Southern Tibet. It is the southernmost and the youngest of all sutures found across the Tibetan Plateau (Fig. 1). This suture is widely known to mark the separation between Eurasia and the Indian Plate. Convergence between the two plates during the Jurassic and Cretaceous forced the destruction of the Tethys oceanic basin. Tethys is the oceanic domain that formed from the rifting of the Lhasa block (Tibet) and Gondwana during Permo-Triassic times (Gaetani & Garzanti, 1991). From the Late Jurassic to the Late Cretaceous, at least one intra-oceanic subduction zone was active within Tethys. This subduction is thought to have been north-dipping and induced arc and back-arc ridge accretion (Zhou et al., 1996; Hébert et al., 2000; 2001; 2003; Aitchison et al., 2000; McDermid et al., 2000; 2001; 2002; Huot et al., 2002; Dubois-Côté et al., 2005; Dupuis et al., 2005a; 2005b, 2005c), giving rise to a Jurassic-Cretaceous intraoceanic supra-subduction zone (SSZ) domain, Neo-Tethys. Cretaceous subduction of Neo-Tethys lithosphere beneath the Andean-type Tibetan active margin (Gangdese arc) also caused extrusive and intrusive calc-alkaline magmatism within the Lhasa block (Allègre et al., 1984; Coulon et al., 1986; Harrison et al., 1992; Murphy et al., 1997). Paleocene obduction towards India (Tapponnier et al., 1981a) thrusted portions of the Tethys and Neo-Tethys over passive margin sedimentary rocks. Eocene collision between the two continents (Molnar & Tapponnier, 1974) trapped the Tethyan remnants between the Indian continent to the south and Tibetan calc-alkaline batholiths and volcanic rocks to the north. Late back-thrusting (Tapponnier et al., 1981a), strike-slip (Molnar & Tapponnier, 1974; Allègre et al., 1984) and east-west extension (Tapponnier et al., 1981b) disrupted the belt into heterogeneous ophiolitic massifs overlying an ophiolitic tectonic mélange (Beimrang mélange, Huot et al., 2002; ophiolitic mélange, Dupuis et al., 2005a; 2005b).

In our study area (Fig. 2), previous mapping identified the presence of garnet-bearing amphibolitic blocks embedded in the ophiolitic mélange, near the Bainang and Buma

localities (Geological Institute of the Chinese Academy of Geoscience, 1982). These blocks are thought to represent the upper section of a dismembered subophiolitic dynamothermal sole (Nicolas et al, 1981; Guilmette & Hébert, 2003, tte et al. 2005). Dynamothermal soles, or metamorphic soles, are found as folded <500m thick slabs that seem welded beneath the mantle section of many ophiolites (e.g. Williams & Smyth, 1973; Jamieson, 1986). These metamorphic soles can generally be divided into an upper and a lower section. The upper section consists of intraoceanic mafic material and can be found beneath Cordilleran-type and Tethyan-type ophiolites (Wakabayashi & Dilek, 2000, see Wakabayashi & Dilek 2003 for a definition of Cordilleran and Tethyan ophiolites). It is characterised by high-grade metamorphism that is thought to occur at the inception of a subduction (e.g. Williams & Smyth 1973; Malpas, 1979, Nicolas & LePichon, 1980; Spray, 1984; Jamieson, 1986, Wakabayashi & Dilek, 2000; 2003). The lower section, only found beneath Tethyan-type ophiolites, is usually made of passive margin sediments metamorphosed at low-grade conditions. This section forms later when an ophiolite is emplaced over a passive continental margin (Hacker et al., 1996).

Little was known about the Buma amphibolites. For the Bainang amphibolites, previous thermobarometric calculations (mostly garnet-clinopyroxene thermometry) constrained unrealistically high temperature peak metamorphic conditions (800-1200°C) at medium pressures (6-9 kbar, Burg et al., 1987). Such high temperatures would indicate subduction of young hot crust beneath a very hot mantle, implying a small age difference between ophiolite and sole formation (<10 Myr). Based on a Pb/Pb age of 120 ± 10 Ma obtained from plagiogranites in the Xigaze ophiolitic massif (Göepel et al., 1984), Burg et al. (1987) proposed an Early Cretaceous metamorphic age (110 Ma) for the amphibolitic sole. However, Wang et al. (1987) published Ar/Ar ages of 87 to 70 Ma for peak metamorphism of amphibolite blocks in the Bainang area. A recent Ar/Ar date of 88 Ma replicated this age (Malpas et al., 2003). Such a large age span between ophiolite and sole formation (about 30-40 Myr) was not expected and is difficult to explain. No petrographic nor geochemical data support those geochronological studies. Sampling locations are not indicated either.

Since 1998, the Université Laval GEO team (Génèse et Évolution des Ophiolites) undertook a reassessment of the different geodynamical settings under which evolved the

Yarlung Zangbo Ophiolites (Hébert et al., 2000; 2001; 2003; Huot et al., 2002; Dupuis et al., 2005a; 2005b; 2005c; Dubois-Côté et al., 2005; Guilmette & Hébert, 2003; Guilmette et al., 2005; Guilmette et al., in prep.). During this project, petrography, mineral chemistry, thermobarometry, major and trace element geochemistry, stable isotope geochemistry and geochronology of the highly foliated amphibolites were addressed (Guilmette & Hébert, 2003; Guilmette et al., 2005; Guilmette et al., in prep.). Preliminary results, exposed in Guilmette et al. (2005), indicate that the highly foliated amphibolites from the mélange have a MORB-like geochemistry, close to BABBs. They have been metamorphosed under medium to high-grade conditions at medium to high pressures around 123.3 ± 3.1 and 127.4 ± 2.4 Ma (Ar/Ar ages on amphiboles).

The aims of the present paper are to describe and interpret the mineral and textural features of the amphibolite blocks found near Buma and Bainang in order to better constrain their metamorphic history and their geodynamic significance. We also present oxygen stable isotopes chemistry of mineral separates from the highly foliated amphibolites to characterize the intervening fluids. Together with these new data, thermobarometric calculations provide a basis to document the P-T-t path for these rocks and help to validate the geodynamic significance of the Buma and Bainang amphibolites. A second paper (Guilmette et al., in prep.) provides major and trace element whole-rock geochemistry as well as new Ar/Ar ages for these rocks.

2.2. Geological Setting

In the study area (Fig. 2), the ophiolitic mélange is discontinuous and ranges from 0 to 1 km in true thickness, with the Buma and Bainang areas being amongst the thickest occurrences. The mélange consists of a sheared serpentinite matrix containing centimetric to hectometric blocks of various natures. Most common blocks are more or less serpentinized harzburgites and dunites and partially rodingitized mafic intrusives and extrusives, with minor occurrences of quartzites, greenschists and local highly foliated amphibolites. The overlying ophiolitic sequence include, from bottom to top, tectonized harzburgites, a partially serpentinized mantle section intruded by mafic magmas, an important crustal sill complex, pillow basalts and a sedimentary cover. Ophiolite occurrences are interpreted as heterogeneous individual massifs sharing back-arc basin geochemical and morphological affinities (Hébert et al., 2003, Dubois-Côté et al., 2005). The ophiolitic belt is Early Cretaceous in age, as shown by the 120 ± 10 Ma U/Pb (Göepel et al., 1984) and 126 ± 1.5 Ma Pb/Pb (Malpas et al., 2003) ages obtained from crustal magmatites and by Barremian-Aptian radiolarian fauna from the overlying sediments (Zyabrev et al., 1999). Upper pillows are encrusted by siliceous oozes. Red cherts containing the radiolarites are in turn overlain by concordant tuffaceous sedimentary rocks up to 300 m thick (Zyabrev et al., 1999). Ophiolites and their Aptian sedimentary cover share their upper contact with Albian volcaniclastic turbidites from the Xigaze group. According to paleo-currents and clasts compositions, the Xigaze group is interpreted as the fore-arc basin of the Gangdese arc (Dürr et al., 1996). The contact between the fore-arc Xigaze group volcaniclastic rocks and the ophiolitic sedimentary cover is considered to be faulted by most authors (Zyabrev et al., 1999; Aitchison et al., 2000). However, outcrops are very few and badly exposed. The lower contact of the ophiolite is strongly tectonized, as seen in the ophiolitic mélange. Shear sense indicates southward thrusting of the ophiolites over Tethyan sediments. The mélange unit underlying the ophiolites is called either the Bainang terrane (Aitchison et al., 2000) or the Yamdrok mélange (Dupuis et al., 2005a; 2005c). It is an imbricate thrust stack containing slices of red chert with volcanic and volcaniclastic lenses that originate from the Tethys ocean. The Yamdrok mélange is reminiscent of a subduction complex

that would have belonged to a north-dipping intraoceanic subduction zone. The ophiolites and the subduction complex lie in turn over distal Indian passive margin sediments (Dupuis et al., 2005a; 2005c) that underwent low grade metamorphism around 50 Ma (Burg et al., 1983).

2.3. Petrography

Amphibolites sampled from the ophiolitic mélange typically show strongly refolded high-temperature foliation overprinted by some retrograde features. Some rocks also show late cataclastic zones. The intense deformation contrasts with the mostly undeformed low-grade metabasites that are also present in the mélange (Huot et al., 2002; Dupuis et al., 2005a; 2005b). The amphibolites are subdivided into three groups: 1) the common amphibolites 2) the clinopyroxene amphibolites and 3) the garnet amphibolites. All amphibolite groups have undergone minor retrograde metamorphism which can be seen as prehnite plus minor albite and chlorite veinlets. Mineral abbreviations are taken from Kretz (1983).

2.3.1. Common amphibolites

Common amphibolites (Fig. 3a) are fine-grained and “salt and pepper” in color. They contain the assemblage A) Hbl+Pl±Ep+Chl+Ttn+Ap. Green fine-grained (0.5-2.0 mm) magnesio-hornblende, tschermakite and pargasite (Fig. 4) define a nematoblastic texture in which plagioclase is interstitial (Fig. 3a). Some common amphibolites from Buma contain brownish tschermakite instead of green magnesio-hornblende. Among all amphibolite groups, common amphibolites contain the highest plagioclase modes (up to 45% of the rock). All plagioclase grains are pseudomorphised by a very fine grained albite-prehnite simplectite. Granular millimetric (0.5-2 mm) epidote is not found in all common amphibolites but can be a major constituent of the rock (up to 10% of the rock). In the Buma amphibolites, low-birefringence tabular zoicite was identified instead of epidote.

Most common amphibolites contain millimetric euhedral titanite (0.5-2 mm) as the titaniferous phase, whereas some epidote-free common amphibolites also show reaction textures where ilmenite forms from titanite. Some common amphibolites have been overprinted by a late low-grade metamorphic assemblage characterized by green magnesio-hornblende rims around prograde amphiboles and by some prehnite+albite±chlorite+epidote-filled brittle fractures. Prehnite can also be found in veins that propagated by dissolution of the rock.

2.3.2. Clinopyroxene amphibolites

Clinopyroxene amphibolites (Fig. 3b) are fine grained and green in color. They contain the assemblage B) Hbl+Pl+Cpx+Ep±Spn+Qtz+Ap. Green magnesio-hornblende and pargasite (0.5-1.5 mm) define the nematoblastic texture in which plagioclase is interstitial. The clinopyroxene amphibolites differ from the common amphibolites by the presence of elongated xenomorphic clinopyroxene crystals and a much higher proportion of fine-grained granular epidote (up to 30% of the rock). Reaction textures at grain boundaries suggest that the main nematoblastic assemblage (magnesio-hornblende and interstitial plagioclase) grew at the expense of early clinopyroxene. Plagioclase is again pseudomorphised by an albite-prehnite simplectite. Very fine-grained granular epidote is ubiquitous. Titaniferous phase is titanite with few occurrences of ilmenite. Clinopyroxene amphibolites from Buma show a similar assemblage made of brownish magnesio-hornblende, clinopyroxene and zoicite. In some clinopyroxene amphibolites, retrograde metamorphism can be seen as pale green rims around magnesio-hornblende and as prehnite-albite-chlorite-epidote veins and fractures identical to those described in common amphibolites.

The banded amphibolites (Fig. 3b) are a subgroup to the clinopyroxene amphibolites. They share the same main assemblage and mineral chemistry but show additional textures. As indicated by their name, the banded amphibolites contain pale green medium-grained bands alternating with dark green fine-grained nematoblastic bands. The latter bands contain the same mineral assemblage than the other non-banded clinopyroxene amphibolites. The pale-

green bands are centimetric in width (1-5 cm), concordant with foliation and represent up to 25% of the rock. They contain coarse (1-2 cm) inclusion-rich clinopyroxene and plagioclase (pseudomorphised) from which grew heterogranular xenomorphic epidote (1-10 mm and up to 50 % of the band). Some bands contain minor interstitial quartz.

2.3.3. Garnet amphibolites

The garnet amphibolites (Fig. 3c) are medium-grained and dark green to black in color. They contain the assemblage C) Hbl+Cpx+Grt+Pl±Rt. Brown to orange tschermakite and pargasite range from 2-10 mm in size and define a nematoblastic texture for the rock. Coarser (5-15 mm) elongated colorless clinopyroxene is partly resorbed to the benefit of tschermakite. Garnet amphibolites contain the lowest modes (around 20% of the rock) of plagioclase, which is interstitial and pseudomorphised by an albite-prehnite simplectite. Xenomorphic garnet porphyroblasts are medium to coarse-grained (up to 20 mm) and are mostly undeformed. They contain plagioclase (pseudomorphised), amphibole, clinopyroxene and rutile inclusions, indicating that they grew at the expense of the main assemblage. Titaniferous phase is rutile with minor ilmenite. Retrograde metamorphism has heterogeneously overprinted the prograde assemblage, as seen in the 0-5 mm wide coronas around garnet, amphibole and clinopyroxene (Fig. 3d) and also in the precipitation of prehnite+albite±chlorite+epidote in fractures and veins. Coronas around garnet are of three types 1) very fine-grained acicular radial dark green alumino-tschermakites with interstitial albite (Fig. 3e) 2) euhedral fine-grained pseudomorphised plagioclase crosscutting dark-green alumino-tschermakites (Fig. 3f) and 3) chlorite, magnesio-hornblende and plagioclase (Fig. 3d). Coronitized garnet is red in color while corona free garnet is colorless to pink. Other types of coronas include green magnesio-hornblende and greenish clinopyroxene rims around clinopyroxene and green magnesio-hornblende rims around brown tschermakites. Coronitization is heterogeneous in type and size, even at the scale of a hand specimen. For the purpose of thermobarometric calculation, we will consider a second assemblage in garnet amphibolites representing the corona assemblage around red garnet: D) Grt+Hbl+Pl±Chl. The garnet amphibolites also contain the prehnite-

albite-chlorite fractures and veins seen in common and clinopyroxene amphibolites. We have found no garnet amphibolite in Buma locality.

2.3.4. Fractures and veins

All three types of amphibolite contain cataclastic retrograde fractures and veins. Retrograde minerals found in those veins are mostly prehnite and pure albite but also chlorite, epidote and green magnesio-hornblende. These veins often developed along pre-existing mylonitized zones (Fig. 3g). Some veins show replacement textures observed in plagioclase and through nematoblastic amphibole grains. Pervasive retrograde metamorphism is also observed in all plagioclase grains where cryptic prehnite occur as inclusions in albite crystals. Prehnite veins appear to have been more brittle than amphibolite itself and possibly closely predate dismemberment of the metamorphic sole. Prehnitization has been observed in most mafic blocks from the mélange as well (Huot et al. 2002, Dupuis et al. 2005). This late event is ascribed to the assemblage E) Prh+Ab±Chl+Ep.

2.3.5. Other related rocks

A late mafic intrusion cross-cutting all structures was observed in the clinopyroxene amphibolite. This intrusive is a very fine grained hypabyssal rock containing 10% clinopyroxene + plagioclase micro-phenocrysts (Fig. 3h). The aphyric matrix is dark and the rock does not seem to have undergone major metamorphic changes but rather metasomatic low-grade alteration. No prehnite is observed in those rocks. The cross-cutting relationship between the intrusion and the foliated amphibolites show that magmatism was ongoing after prograde metamorphism.

2.4. Mineral Chemistry

2.4.1. Analytical method

The mineral chemistry of twenty-six (26) samples (1 mafic dyke, 11 common amphibolites, 7 clinopyroxene amphibolites and 7 garnet amphibolites) was determined using a CAMECA SX-100 five-spectrometer electron microprobe located at the Université Laval. Analytical conditions were 15 kV, 20 nA with a counting time of 20 s on peaks and 10 s on background. Calibration standards used were generally simple oxides (GEO Standard Block of P&H Developments), or minerals where needed (Mineral Standard Mount MINM25-53 of Astimex Scientific Limited; reference samples from Jarosewich et al., 1980). Data were reduced using the PAP model. Representative analysis for amphibole, clinopyroxene and garnet are shown in Tables 2.1, 2.2 and 2.3. Complete data, including detailed petrographic descriptions of amphibolites, are available via electronic supplement.

2.4.2. Plagioclase

Plagioclase compositions fall in the range of An_{0.8} with a maximal orthose mole proportion of 3%. Rare plagioclase inclusions in amphibole and garnet grains will show a maximum An content of 25%. Regardless of amphibolite type and of textural relationships, most plagioclase grains contain micro-inclusions of prehnite, defining an albite-prehnite pseudomorphic simplectite. However, some albite grains are inclusion free. They are associated with fine to medium-grained prehnite crystals found in fractures and veins. Inclusion-free albite-prehnite veins have been observed within pseudomorphised plagioclase grains. This particular texture indicates that plagioclase was replaced prior to the propagation of prehnite-filled veins and fractures.

2.4.3. Amphiboles

As seen in petrographic descriptions, the three types of amphibolites contain four groups of amphiboles. The common and clinopyroxene amphibolites contain 1) nematoblastic green magnesio-hornblende and tschermakite, whereas the garnet amphibolites contain 2) nematoblastic brown tschermakite and 3) coronitic green alumino-tschermakite. The three types of amphibolites also contain 4) coronitic retrograde green magnesio-hornblende. Representative analyses are shown in Table 2.1. All amphibole is Ca-amphibole with $Ti < 0.5$ and $Ca_B > 1.5$ a.p.f.u. All amphibole analyses were plotted in a Ti vs Al^{IV} diagram (Fig. 5). Fields represent amphibole compositions from low-grade metabasites from the ophiolitic mélange (Beimarang mélange, Huot et al., 2002; ophiolitic mélange, Dupuis et al., 2005a). The four amphibole groups were also plotted in a $(Na+K)$ vs Al^{IV} diagram (Fig. 6). In figure 5, first observation is that amphibole from the highly foliated amphibolites follow a different trend than amphibole from other mafic blocks from the mélange, being more enriched in Al^{IV} for a given Ti content. In figure 6, amphibole composition follows a trend between the tremolite and pargasite end-members. In both diagrams, the Al^{IV} -poor part of the trend ($Al^{IV} < 1.25$ a.p.f.u.) is occupied almost exclusively by group 4) amphibole, even though it can also be richer in Al^{IV} (up to 2.1 a.p.f.u.). Ti and $(Na+K)$ contents for group 4) amphibole vary between 0.02-0.2 and 0.2-0.6 a.p.f.u., respectively. This group has the largest composition span, reflecting the various minerals from which it formed (clinopyroxene, groups 1 and 2 amphibole). When compared to these “core” minerals, group 4) amphibole typically shows a decrease in Al^{IV} , Ti and alkali contents. In figure 5, the central section of the trend is occupied by group 1) amphiboles. The green magnesio-hornblende and tschermakite have Al^{IV} contents between 1.25-2.0 for Ti contents between 0.05-0.2 a.p.f.u and alkali contents between 0.3-0.8 a.p.f.u. The group 2) amphibole has a similar Al^{IV} content (between 1.3-2.0 a.p.f.u.) for a richer Ti content ranging from 0.07-0.30. Alkali content is in the same range than group 1) amphibole (0.3-0.8 a.p.f.u.). However, for a given Al^{IV} content, group 1) amphibole will be, on average, richer in alkali content than group 2) (of about 0.1 a.p.f.u.). Group 3) amphibole occupies the Al^{IV} -rich section of the trend, with Al^{IV} contents of 1.7 to 2.7 a.p.f.u. In figure 5, group 3) amphibole follows a different trend than group 1), 2) and 4). While all other groups

show positive correlation between Al^{IV} and Ti, group 3) amphibole undergoes Ti depletion with Al^{IV} enrichment. For group 3), Ti content varies from 0.25 to 0.01 a.p.f.u. whereas alkali content is fixed at an average of 0.8 a.p.f.u.

2.4.4. Clinopyroxene

All clinopyroxene from the amphibolites is a metamorphic diopside with very low Cr and Ni contents. Representative analyses are shown in Table 2.2. All compositions fall into the range $\text{Wo}_{48-54}\text{En}_{33-44}\text{Fs}_{4-13}\text{Jd}_{0-5}$ (Fig. 2.7). The major difference between the colorless and green clinopyroxene is their Al and Ti contents (Fig. 2.8a). The early colorless diopside found in the garnet amphibolites contains up to 7% Al_2O_3 and 1% TiO_2 , while the late greenish diopside found in both garnet and clinopyroxene amphibolites contains a maximum of 4% Al_2O_3 and 0.4% TiO_2 . Also, the greenish diopside from the clinopyroxene amphibolites is richer in Na_2O (0.5-1.5%), as shown in figure 2.8b.

Magmatic clinopyroxene phenocrysts analyzed in the diabasic dyke are augite with a more magnesian composition within the range $\text{Wo}_{32-41}\text{En}_{45-47}\text{Fs}_{13-22}$. When compared with metamorphic clinopyroxene, they are as Ti and Al-rich as the colorless clinopyroxene but are clearly Na-poor.

2.4.5. Garnet

Garnet composition varies in the range $\text{Py}_{14-37}\text{Alm}_{35-57}\text{Sp}_{01-06}\text{Gr}_{13-35}\text{And}_{01-03}$ (Fig. 2.9). Representative compositions are shown in Table 2.3. The garnet without corona shows variation in almandine-grossular molecular content from $\text{Alm}_{35-57}\text{Gr}_{13-35}$ at a constant pyrope content of about 15%. Garnet with corona has a higher pyrope content of 20 to 37%, according to the type of corona. The highest pyrope contents are found in samples where garnet is coronitized by the aluminous tschermakites. The lowest pyrope contents are associated with euhedral plagioclase + hornblende coronas. Intermediate compositions are found in highly retrogressed garnets found within green amphibole+chlorite+plagioclase

coronas. Figure 2.10 a-b shows zonation for samples LUS-07 (euhedral plagioclase + amphibole corona) and LUS-12 (aluminous tschermakite + plagioclase corona). In both cases, garnet rims are depleted in grossular content and enriched in almandine and pyrope by 2-7% mole proportion. Such a small variation indicates crystal homogeneity, which is a criterion for phase stability during garnet growth.

2.5. Stable Isotope Geochemistry

2.5.1. Analytical Method

A set of nine selected representative mineral separates were prepared for oxygen extraction. These separates (about 15 mg) come from three samples (2 common amphibolites, BAI-18 and BAI-20 and 1 clinopyroxene amphibolite, BAI-19, all from Bainang). Plagioclase and amphibole separates were obtained from common and clinopyroxene amphibolites whereas clinopyroxene and prehnite separates were obtained from veins in clinopyroxene amphibolite. Powdered mineral separate contents have been verified with XRD analyses at Laval University (unpublished). Gases were extracted at the “Laboratoire de géochimie isotopique du département de Géologie et de Génie Géologique de l'Université Laval”. Calibration was made from international standard NBS-28 with a standard deviation of 0.1‰ $\delta^{18}\text{O}$ for an average value of 9.7 ‰ $\delta^{18}\text{O}$ SMOW (Standard Mean Ocean Water) over 11 runs. A standard deviation of 0.1 ‰ $\delta^{18}\text{O}$ on a 18.8 ‰ $\delta^{18}\text{O}$ SMOW average value over 21 runs was also obtained from internal standard K1.

2.5.2. Results

Results for the plagioclase, amphibole, clinopyroxene and prehnite mineral separates are shown in table 2.4. XRD spectrums reveal some prehnite in the powder. All three separates from three different samples show high ratios of 15.5-17.9 ‰ $\delta^{18}\text{O}$ SMOW. Amphibole separates were taken from common and clinopyroxene amphibolites as well. XRD analyses

revealed that separates were pure. $\delta^{18}\text{O}$ values are homogeneous regardless of amphibolite type. Values for amphibole composition range from 7.6 to 8.8 ‰ $\delta^{18}\text{O}$ SMOW. One separate was taken from the clinopyroxene-rich bands in the clinopyroxene amphibolites. XRD revealed that the powder was mainly composed of diopside with minor epidote. $\delta^{18}\text{O}$ SMOW value is in the same range as amphiboles with a ratio of 8.3 ‰. One separate has been taken from a pale green-beige vein. XRD analysis confirmed this powder to be almost pure prehnite with minor albite. Result is intermediate with a $\delta^{18}\text{O}$ SMOW of 11.0 ‰.

2.6. Discussion

2.6.1. Metamorphic history from the textural record

The mineral textures preserved in the highly foliated amphibolites allow a tentative reconstitution of the different events that ultimately led to the dismemberment of the subophiolitic metamorphic sole and its emplacement as blocks in the ophiolitic mélange. First, textural relationships observed in some common amphibolites, like euhedral plagioclase pseudomorphosed grains aligned parallel to the foliation and finer grained amphiboles that are interstitial to those plagioclase laths suggest that at least some of the highly foliated amphibolites are issued from metamorphism of a fine-grained diabasic igneous protolith. Fine to medium grain size of other amphibolites are rather reminiscent of gabbroic textures. Banding in some clinopyroxene amphibolites possibly represents metamorphosed and deformed pillow lavas. In all cases, it seems that the protolith for the highly foliated amphibolites from the ophiolitic mélange is the mafic upper crust of an ophiolitic sequence. Elongated clinopyroxene grains that are coarser than the rest of the rock and that are being replaced by nematoblastic amphibole might represent the only preserved primary magmatic minerals. However, the mineral chemistry of these crystals rather indicates metamorphic diopside, perhaps due to reequilibration of the mineral during prograde metamorphism. Metamorphism under high-strain of the protolith induced formation of nematoblastic amphibole in the three amphibolite types. This stage possibly corresponds to peak metamorphic conditions. All minerals whose elongation is parallel to

the main foliation would be issued from this metamorphic event. This includes interstitial xenomorphic plagioclase, nematoblastic amphibole, elongated reequilibrated clinopyroxene, some xenomorphic garnet grains without coronas and tabular zoicite in Buma amphibolites.

In garnet amphibolites, second metamorphic event would be the growth of most hypidiomorphic garnet grains. Indeed, garnet grains do not show helicoidal or elongated textures, suggesting that they are late to post-kinematic. Almost unzoned nematoblastic amphibole and garnet crystals indicate that garnet growth from the nematoblastic assemblage was an equilibrium reaction. Accordingly we suspect that composition of the nematoblastic amphibole grains might not truly represent peak metamorphic conditions. They might have undergone Al-depletion during garnet growth. In clinopyroxene amphibolites, granular epidote growth also seems to have occurred after the main deformational event.

Garnet growth was interrupted by percolation of a hydrous fluid between grain boundaries, causing coronitization of garnet grains. The presence of green amphibole around garnet suggests that the reaction occurred during a retrograde event. Whether this reaction occurred at higher or lower pressures than garnet growth will be addressed by thermobarometric calculations.

All types of amphibolites were affected by the infiltration of a hydrous fluid causing heterogeneous coronitization of nematoblastic amphiboles by green magnesio-hornblende and minor chlorite. Colorless elongated clinopyroxene was partly retrograded to greenish clinopyroxene + green magnesio-hornblende during the same event. It is not clear if this event is the same than the one that caused coronitization of garnet. Different coronitic textures and coronitic amphibole compositions might reflect either a more aluminous environment for corona growth or different P-T conditions.

Once interstitial and coronitic plagioclase had crystallized, all plagioclase grains underwent retrogression, as seen in their strong density of cryptic inclusions (albite-prehnite simplectite) and their homogeneous albitic composition. This event probably occurred after coronitization and prior to prehnitization. Indeed, textural evidences indicate that the

pseudomorphic albite-prehnite simplectite in plagioclase grains was present before fractures and veins allowed massive prehnite crystallisation together with inclusion-free interstitial albite grains. The latter event occurred during brittle deformation of the amphibolites as seen in associated cataclastic corridors, confirming that the rock was already cooled and exhumed during propagation of the prehnite-albite fractures and veins.

2.6.2. P-T calculations

Four methods were used for the purpose of estimating the different pressure and temperature conditions under which evolved the amphibolites. Calculations were made for peak metamorphic assemblages (nematoblastic assemblage in common, clinopyroxene and garnet amphibolites) as well as for retrograde assemblages (coronas around garnet, albite-prehnite simplectite, prehnite-albite fractures and veins). The first method is considered qualitative and involves different reaction curves taken from literature and calibrated for MORB-like protoliths (NCKFMASH or CFMASH system). We are aware that there might be large errors in the estimated P-T conditions related to the geochemistry of the amphibolites, even though their geochemistry is MORB-like (Guilmette et al., 2005). The second method used is the Fe-Mg exchange equilibrium between garnet and clinopyroxene (Ellis & Green, 1979; Pattison & Newton, 1989) or amphibole (Graham & Powell, 1984). For this method, we chose large grains from the peak metamorphic assemblage that were not in contact in order to avoid chemical diffusion. For zoned crystals, we systematically selected core compositions that should better reflect peak metamorphic conditions. The third method was first tested by Ernst and Liu (1998). It consists of a semi-quantitative estimation of P-T conditions during prograde Ca-amphibole crystallisation based on their Al and Ti contents. Limitations include a MORB-like protolith, P-T ranges of less than 22 kbars and 950 °C, and the required presence of an aluminous phase (garnet). To estimate peak metamorphic conditions, only the richest amphiboles must be considered because retrograde metamorphism might induce inter-grain diffusion. In this study, the method was also tested for retrograde amphiboles and for amphiboles not in presence of any aluminous phase. Finally, TWEEQU software was used to estimate P-T conditions for the 2 assemblages containing garnet (C and D). Input mineral compositions (see tables 2.1, 2.2,

2.3 and 2.5) were mainly from the core of large grains that were not in contact, except for assemblage D), the corona assemblage. Correlation between the four sets of results will be considered as a validating criteria for estimation of P-T conditions and building of a P-T-t path.

2.6.2.1. P-T conditions for the highly foliated amphibolites

For assemblage A) Hbl + Pl ± Ep + Ap + Ttn, the common amphibolite assemblage reflects metamorphism in the amphibolite facies. Absence of minerals like garnet or rutile indicates metamorphism at medium or low pressures. Replacement of titanite by ilmenite is observed in epidote-free samples, while titanite is the main Ti-phase in epidote-bearing samples. The petrogenetic grid for basalts is then indicating metamorphic conditions below 10 kbars and between 600-700 °C. This temperature interval corresponds well to the 640-740 °C peak temperatures obtained from the Al-Ti contents of amphiboles. However, high Al content of amphiboles rather indicates pressure conditions of 10-18 kbars. Such high pressures are not supported by the presence of pressure sensitive minerals. Moreover, limitations to the method required the presence of an aluminous phase, a condition which is not respected here. Considered semi-quantitative metamorphic conditions for the common amphibolites are 650-700 °C at pressures of about 10 kbars.

The assemblage B) Hbl+Cpx+Pl+Ep±Spn+Qtz+Ap, is very similar to assemblage A) and should therefore reflect similar P-T conditions. Presence of Cpx and the replacement of titanite by ilmenite indicate metamorphism in the upper amphibolite facies. Al-Ti in Ca-amphiboles method yields medium to high pressure estimates of 8-14 kbars. However, absence of garnet or rutile does not support high pressure metamorphism. At pressures of 8-10 kbars, CPX should be stable from about 700 °C. The Ernst and Liu (1998) method confirms metamorphism in the upper amphibolite facies with temperatures of 610-750 °C. Considered semi-quantitative P-T estimations for the peak metamorphism of the clinopyroxene amphibolites will be 8-10 kbars and 700-750 °C.

Minerals present in assemblage C) Hbl+Cpx+Grt+Pl±Rt (garnet amphibolites) allow a preliminary estimation of P-T conditions. According to Pattison (2003), the assemblage Hbl+Grt+Cpx+Pl without the presence of Opx should reflect metamorphism in the H-P granulite facies. According to reaction curves 3, 4 and 12 in figure 2.11, the presence of pressure sensitive minerals like rutile and garnet in MORB-like rocks indicates a minimum pressure of about 10-12 kbars, regardless of temperature (Green and Ringwood, 1967, Ernst and Liu, 1998). At such pressures, the presence of Cpx and the absence of Opx reflect peak metamorphism temperatures of 750-850 °C. Al and Ti contents of tschermakite support a high-pressure peak metamorphism with pressure estimates up to 15 kbars. Temperatures obtained with the Al-Ti in hornblende method confirm metamorphism near the amphibolite-granulite-eclogite transition with estimates of 700-875 °C. Thermometers using garnet-clinopyroxene Fe-Mg exchanges support high temperature metamorphism. The Pattison-Newton (1989) calibration yields temperatures of 532-769°C for pressures between 10-15 kbars while the Ellis and Green (1979) calibration yields higher temperatures of 686-892 °C for the same pressures. It is important to note that for peak temperature estimations, only the highest part of the interval should be considered. Therefore, peak metamorphic conditions for assemblage C) obtained from the petrogenetic grid, from Al-Ti content of amphiboles and from Fe-Mg exchanges should be comprised in the 750-875°C and 10-15 kbars intervals (garnet appears around 10 kbars in MORBs, Green and Ringwood, 1967). TWEEQU calculations were made from low Py-content garnet with, if possible, no corona, from core nematoblastic amphibole and clinopyroxene compositions and from model plagioclase compositions. Results support amphibolite-granulite-eclogite transition peak metamorphism. For temperatures of 750-875 °C, pressures will range between 13 and 14.5 for hypothetical plagioclase compositions of An₄₀₋₆₀. Such compositions are observed in other natural and synthetic assemblages metamorphosed under the same conditions (Pattison et al. 2003 and reference therein).

For assemblage D) Grt+Hb+Pl, petrographic observations indicate replacement of garnet by amphibole prior to apparition of plagioclase. This could be a clue that coronitisation of garnet occurred during decompression in presence of water and started out of the stability field of plagioclase. This hypothesis is supported by very high Al and low Ti content of

amphiboles yielding pressure and temperature estimates of 14-36 kbars and 580-760 °C. The amphibole-garnet Fe-Mg thermometer of Graham and Powell (1984) confirm those results with overlapping estimates of 450-600 °C. Temperatures of 600 °C will be obtained in TWEEQU calculations for plagioclase compositions of An₀₅ at a pressure of 27-28 kbars. Higher anorthite mole fraction in plagioclase (up to An₂₀) yield higher temperatures and lower pressures in the range of 605-777 °C and 28-21 kbars. However, since the Al-Ti in Ca-amphibole method was not tested for retrograde amphiboles, we will rather consider the Graham and Powell (1984) thermometer that indicates coronitization of garnet at 600 °C. Corresponding pressure would be as high as 27 kbars. Such high pressure estimates are not supported by the mineral assemblages and by mineral chemistry. A metamorphic event occurring at 27 kbars should have caused resorption of plagioclase and jadeite apparition, which is not clearly observed. It has to be noted, though, that plagioclase was already pseudomorphised during prehnite precipitation. Another problem related to this H-P event is the absence of sodic clinopyroxene. However, it is clear that Cpx has been reequilibrated from peak metamorphic composition during a retrograde event. Na mobility during retromorphosis might explain the absence of a Na-cpx. In any case, very few features support a 27 kbars retrograde event. Accordingly, we propose that this event might have occurred at the upper limit of plagioclase stability, which would be about 18 kbars at 600°C.

For assemblage E), Frey et al. (1991) calculated a stability field for the assemblage Prh+Ep+Act+Chl+Ab+Qtz+H₂O in the basaltic system. This stability field extends from 200 to 300°C at pressures of 0-4 kbars.

2.6.2.2. *P-T conditions for the cross-cutting intrusive*

Mineral chemistry of augite micro-phenocrysts allowed estimation of P-T conditions for the emplacement of cross-cutting dyke. Crystallisation temperatures of 900 to 1150 °C were obtained using the Lindsley (1983) Cpx isotherms (Fig. 2.7), whereas the Nimis (1995) Cpx-based barometer for basalts yielded pressures of 0.4 to 0.9 kbars. Such conditions reflect emplacement of mafic magmas through the sole at very shallow depths,

which strongly contrasts with medium to high pressure estimates obtained from the amphibolites. Accordingly, amphibolites had to be already exhumed prior to dike injection.

2.6.2.3. *P-T-t path*

Three hypothetical P-T-t paths for the three types of highly foliated amphibolites from the mélange are shown in figure 2.12. According to thermobarometric calculations, peak metamorphism occurred at 750-875°C and 13-15 kbars, as seen in assemblage C) (garnet amphibolites). Further burial along a cooled thermal gradient followed by rapid exhumation led to coronitization of garnet at about 18 kbars and 600°C (box D' in Fig. 12). The last metamorphic event (assemblage E) occurred in the stability field of prehnite. Such a P-T-t path would have a counter clockwise (pressure axis upward) loop behavior. Rocks containing assemblage A) (common amphibolites) have followed a cooler burial path (Fig. 12), leading to a peak metamorphism of 700-750°C and 8-10 kbars. For facies B) (clinopyroxene amphibolites), pressure-temperature estimates fall in the upper amphibolite facies with 10 kbars and 650-700 °C.

When compared with the P-T path for other blocks in the mélange (curve 3 in Fig. 12, Huot et al. 2002, Dupuis et al. 2005), it is clear that highly foliated amphibolites underwent a more complex metamorphic history. This study shows that the highly foliated metabasites have been buried at oceanic mantle depths conditions (8-18 kbars, i.e. 30-60 km) that can only be reached along a subduction plane. Peacock et al. (1994) modeled different P-T trajectories for an oceanic crust subducted in various settings. Curve 1 in figure 12 is the path followed by a young (0-5 Ma) slow-subducting (1 cm/yr) crust under a hot mantle at constant shear. This path leads to the P-T peak metamorphic conditions evaluated for most dynamothermal soles (Jamieson 1986, Spray 1984, Peacock et al., 1988, Wakabayashi and Dilek, 2000) and for the foliated amphibolite blocks found in the ophiolitic mélange beneath Yarlung Zangbo ophiolites as well. We suggest that amphibolites from the ophiolitic mélange might have followed a path similar to the path defined by curve 1 to achieve peak metamorphism. Then, underplating of the crustal rocks to the hanging wall

might have prevented further burial along this path. Peacock et al. (1994) also showed that aging of a nascent subduction zone rapidly affects the P-T trajectory of the subducted crust by significant cooling, as proposed in curve 2. Steady state is thought to occur after about 30 Ma, but is almost reached after 10 Ma. Thus, during steady state subduction (curve 2), some of the underplated rocks must have been loosened and brought to even greater depths, as seen in assemblage D). Finally, all rocks converge at near surface conditions where they were intruded by basic to intermediate dikes at shallow depth. Intrusion of magmas would have followed percolation of a Ca-rich fluid that induced pervasive and vein prehnitization.

2.6.3. Fluid composition

Table 2.4 shows isotopic composition of fluid in equilibrium with mineral separates from Bainang calculated according to the equations of Zheng (1993 a, b) and to the temperature estimates for the amphibolites. Most of the amphiboles from common and clinopyroxene amphibolites formed at temperatures of 650-750°C. A metamorphic fluid in equilibrium with those amphiboles at these temperatures would then have had an isotopic composition of 9.8-11.1 ‰ $\delta^{18}\text{O}$ SMOW. Clinopyroxene most probably crystallised under the same temperature range. The fluid present during CPX growth would then have a composition of about 10.4 ‰ $\delta^{18}\text{O}$ SMOW. For the late phases, evaluation of an isotopic composition for the equilibrium fluid gets complicated. The partition coefficient for heavy isotopes in plagioclase and prehnite drastically changes within the temperature interval over which prehnite and albite are assumed to have formed (Zheng, 1993a). If we assume that all prehnite and albite formed during one single event, the calculated isotopic ratio of the equilibrium fluid would be 5.3-13.5 ‰ $\delta^{18}\text{O}$ SMOW. Average value would be around 9.4 ‰ $\delta^{18}\text{O}$ SMOW, which will be considered as the composition of the equilibrium fluid.

The different amphibolites from Bainang and Buma have been percolated by at least two fluids during their evolution. We propose that the isotopic composition of the fluid that was present during amphibole and clinopyroxene crystallisation (9.8-11.1 ‰ $\delta^{18}\text{O}$ SMOW) reflects a metamorphic reservoir, possibly created by stepwise dehydration of a subducting

oceanic crust. After cooling and exhumation, a second fluid (about 9.4 ‰ $\delta^{18}\text{O}$ SMOW) partly retrogressed the rocks. This Ca-bearing fluid precipitated prehnite in tension cracks and pervasively reequilibrated plagioclase in a prehnite-albite simplectite. This fluid could have had many origins, resulting either as a mixing between the metamorphic reservoir and sea-water, from a metamorphic reservoir, from a magmatic reservoir or from a mixing between the latter two (Taylor, 1997). A magma-derived reservoir is likely involved since we have observed post-metamorphic prehnite-free diabasic intrusives cross-cutting the amphibolites.

2.6.4. Geodynamic significance

Mineral assemblages and estimated P-T conditions for the Bainang and Buma highly foliated amphibolite blocks found beneath the Yarlung Zangbo ophiolites are similar to those found in coherent or dismembered dynamothermal soles around the world (Jamieson, 1986, Spray, 1984, Peacock 1988, Wakabayashi and Dilek, 2000). The presence of a metamorphic fluid reservoir possibly derived from dehydration of a subducting slab ($\delta^{18}\text{O}$ values of 10 ‰) support a dynamothermal sole nature for the highly foliated amphibolite blocks. Field relationships also suggest a dismembered dynamothermal sole origin for those blocks (Nicolas et al. 1981). Presence of a dismembered dynamothermal sole beneath the supra-subduction zone Yarlung Zangbo ophiolites indicates inception of a second subduction within the SSZ domain. As discussed in Wakabayashi and Dilek (2000), in SSZ ophiolite-sole couples, it is very unlikely that the dynamothermal sole would be linked to the subduction zone that is responsible for the creation of the overlying SSZ ophiolite. Such a setting would require that the sole would be significantly older than the ophiolite, which has never been observed. Moreover, published ages rather suggest that metamorphism occurred 40 Ma after ophiolite generation (Wang et al., 1987; Malpas et al. 2003). However, we obtained contrasting 123.3 ± 3.1 , 127.4 ± 2.4 and 127.7 ± 2.3 Ma Ar/Ar ages (Guilmette et al., 2005). Metamorphic conditions estimated in this study suggest that inception of the subduction responsible for dynamothermal sole metamorphism occurred near a disturbed abnormally hot geothermal gradient. The most likely site for the inception

of subduction would then be the spreading center from which originate the ophiolites (i.e. within the back-arc basin; Fig. 2.13 c). Such a setting would indicate that within our study area, the Yarlung Zangbo Ophiolites were trapped in a fore-arc setting soon after their formation in a back-arc basin. Back-arc lithosphere trapped in a fore-arc setting has also been proposed as a probable evolution for the Coast Range Ophiolites (Wakabayashi and Dilek, 2000). The next event recorded in the dynamothermal sole would be the high-pressure event of the garnet-bearing amphibolites followed by rapid exhumation of the sole. Subduction of the trench, fore-arc and frontal arc (Boutelier et al. 2003) might be a cause for this metamorphic event (Fig. 2.13 d). It would also provide an explanation for the presence of calc-alkaline basalts in the ophiolitic mélange (Dupuis et al., 2005a). Once exhumed, the sole was intruded at shallow depths by a mafic magma inducing percolation of a prehnite-precipitating magmatic fluid. Since no late cross-cutting dikes nor prehnitization have been reported within the Yamdrok terrane, it is likely that intrusion and fluid percolation occurred prior to its accretion as a subduction complex. This relationship would reflect subduction of an active magmatic center during Mid Cretaceous times (Fig. 2.13 e), also proposed by Ziabrev (2004). Shervais (2003) also favored the hypothesis of MOR subduction as an explanation for the « death » of an ophiolite. Further subduction of a large section of the Tethys until Late Cretaceous to Paleocene times led to accretion of gradually shallower ocean-floor sedimentary cover (Fig. 2.13 f) (southern tract, Bainang terrane, Zyabrev et al. 2004, Yamdrok mélange, Dupuis et al., 2005a; 2005c) until obduction over Indian passive margin sediments (Triasic flysch, Dupuis et al., 2005a; 2005c).

Major questions arise about the event(s) that would have caused inception of a subduction within a SSZ (13 c). Boutelier et al. (2003) suggested a trench-India collision followed by trench, fore-arc and arc subduction to explain the absence of an arc in the Xigaze area. This model supports the trapping of the back-arc ophiolites in a fore-arc setting. However, paleo-magnetic data indicate that at the time of ophiolite genesis (and probably of sole metamorphism as well), India and the ophiolites were about 2000-3000 km away one from the other (Pozzi et al. 1984, Abrajevitch et al. 2005). Therefore, another buoyant body, such as an arc, an oceanic plateau, a seamount chain or a continental block, would have been required to block the early subduction and force inception of a new one. For this

paper, we consider the hypothesis proposed by Zyabrev et al. (2004) that a Mid-Ocean Ridge was subducted prior to accretion of Tethyan sea-floor sediments in the subduction complex. Arrival of this MOR possibly slowed the subduction rate and increased tectonic stresses within the SSZ domain (Fig. 2.13 c). Subduction of a MOR provides the magmatic center required to explain injection of dykes and magma-equilibrated fluid percolation (Fig. 2.13 e). As pointed out by Shervais (2003), it would also provide an explanation for the formation of a second generation of subophiolitic amphibolites at 70-80 Ma. Another hypothesis for inception of subduction within a SSZ domain would be a major plate motion reorganisation, as seen in the Pacific around 46 Ma (Emperor-Hawaï bend and initiation of Mariana, Bonin and Tonga subductions). However, this alternate hypothesis does not exclude subduction of a MOR during Mid Cretaceous.

Trapping of the Yarlung-Zangbo back-arc ophiolites in a fore-arc setting addresses important issues on the geometry of the intraoceanic subduction zones active within Tethys. Up to now, Yarlung Zangbo ophiolites were thought to have formed over a Jurassic-Cretaceous north-dipping subduction, as seen in the Yamdrock mélange (subduction complex) structural style (Aitchison et al. 2000, Zyabrev et al. 2004), in the tomographic imaging of the mantle underlying Tibet (Van der Voo 1999) and in the arc-fore-arc Zedang-Luobusa relative positions (Zhou et al. 1996, Aitchison et al. 2000). However, this study rather suggests that the Yamdrock mélange, the main argument for a north-dipping subduction, is rather associated with a younger subduction that was probably active from Early or Mid Cretaceous until the Eocene collision. According to this model, the remaining clues about the orientation of the Jurassic-Cretaceous subduction zone become very light. Tomographic imaging of the mantle reveals three vertical bodies interpreted as sinking oceanic slabs. The slab that was interpreted to originate from subduction beneath the Zedang arc (Aitchison et al. 2000) and the Xigaze back-arc basin is rather vertical. We do not think it really reflects a north or south-directed subduction. For the arc-fore-arc Zedang-Luobusa north-south distribution, it remains to be shown that the Zedang arc was in a frontal or remanant arc setting.

2.7. Conclusion

Highly foliated amphibolites are locally found as blocks embedded in a serpentinite mélange beneath the Yarlung Zangbo ophiolites. Amphibolites found near the Buma and Bainang localities are of three types : 1) common amphibolites, 2) clinopyroxene amphibolites and 3) garnet amphibolites. The common amphibolites contain assemblage A) Hbl+Pl±Ep+Chl+Ttn+Ap. This assemblage is representative of the amphibolite facies and has formed at temperatures of 650-700°C and at pressures of around 10 kbars. The clinopyroxene amphibolites contain assemblage B) Hbl+Pl+Cpx+Ep±Spn+Qtz+Ap. Such an assemblage would reflect metamorphic conditions of 700-750°C and 8-10 kbars. Garnet amphibolites contain assemblage C) Hbl+Cpx+Grt+Pl±Rt and D) Grt+Hbl+Pl±Chl. Assemblage C) would have formed at temperatures of 750-875°C and pressures of 13-15 kbars, which corresponds to the upper granulite facies. Assemblage D) formed after further burrowing of the garnet amphibolites to pressures of about 18 kbars at temperatures of about 600°C. All plagioclase found in assemblages A, B, C and D is pseudomorphised by a cryptic prehnite albite simplectite. The retrograde assemblage E) Prh+Ab±Chl+Ep found in all amphibolites is bound to fractures and veins and is stable at temperatures of 200-300°C and pressures of less than 4 kbars. Oxygen stable isotope ratios from mineral separates reveal that the fluid present during peak metamorphism had a composition around 10 ‰ $\delta^{18}\text{O}$ SMOW, corresponding to a metamorphic reservoir. Isotopic signature of plagioclase pseudomorphs and prehnite veins might reflect a mixing between a magmatic and a metamorphic reservoir. Metamorphic history and oxygen isotopic signature of highly foliated amphibolites are coherent with a dynamothermal sole origin. Medium to high-pressure estimates for peak metamorphism confirm burial of crustal rocks at oceanic mantle depths. High temperature estimates imply subduction of warm crust under a hot mantle. Such conditions can be achieved during inception of a subduction at or near a spreading center. Therefore, the most probable site for inception of a subduction would be the spreading ridge in the Jurassic-Cretaceous back-arc basin from which originate the Yarlung Zangbo Ophiolites. Inception of a subduction plane within the back-arc basin suggests that the ophiolites were trapped in a fore-arc setting soon after their genesis. Accretion of the Yamdrok mélange subduction complex to the hangingwall of this

Cretaceous subduction and following obduction over the Indian passive margin are indicating a north-dipping subduction. Evolution of the north-dipping Cretaceous subduction could include subduction of a magmatic center, as seen in cross-cutting intrusives and concurrent mantle-derived fluid percolation.

Acknowledgement

This work was supported by NSERC/Grant no. 1253 to R.Hébert. We would also like to thank E. Giguère for oxygen isotope analysis and M. Choquette for micro-probe analysis, both at Université Laval, and M. Villeneuve for Ar/Ar dating at the Canadian Geological Survey. We are also grateful to G. Beaudoin, F. Huot, and A. Indares for valuable discussions and to D. Robinson and an anonymous reviewer for constructive comments.

2.8. References

- Abrajevitch, A., Ali J. R., Aitchison, J. C., Badengzhu, Davis, A. D., Liu, J., Ziabrev, S. V., 2005. Neotethys and the India–Asia collision: Insights from a palaeomagnetic study of the Dazhuqu ophiolite, southern Tibet. *Earth and Planetary Science Letters*, **233**, p. 87-102
- Aitchison, J. C., Badengzhu, Davis, A. M., Liu J., Luo H., Malpas, J. G et al. 2000. Remnants of a Cretaceous intra-oceanic subduction system within the Yarlung-Zangbo Suture (southern Tibet). *Earth and Planetary Science Letters*, **183**, p. 231-244
- Allègre, C.J., Courtillot, V., Tapponnier, P., Hirn, A., Mattauer, M., Coulon, et al. 1984. Structure and evolution of the Himalaya-Tibet orogenic belt. *Nature*, **307**, p. 17-22.
- Berman, R. G., 1988. Internally-consistent thermodynamic data for minerals in the system Na (sub 2) O-K (sub 2) O-CaO-MgO-FeO-Fe (sub 2) O (sub 3) -Al (sub 2) O (sub 3) -SiO (sub 2) -TiO (sub 2) -H (sub 2) O-CO (sub 2). *Journal of Petrology*, **29**, p. 445-522
- Berman, R. G., 1990. Mixing properties of Ca-Mg-Fe-Mn garnets. *American Mineralogist*, **75**, p. 328-344
- Berman, R. G., 1991. Thermobarometry using multi-equilibrium calculations; a new technique, with petrological applications. Gordon, T. M. (editor), Martin, R. F. (editor), Quantitative methods in petrology; an issue in honor of Hugh J. Greenwood. *The Canadian Mineralogist*, **29**, Part 4, p. 833-855
- Boutelier, D., Chemenda, A., Burg, J. P., 2003. Subduction versus accretion of intra-oceanic volcanic arcs; insight from thermo-mechanical analogue experiments. *Earth and Planetary Science Letters*, **212**, p. 31-45

Bucher, K., Frey, M., 1994. Petrogenesis of Metamorphic Rocks: Complete revision of Winkler's Textbook, 6th edition. Springer-Verlag, Berlin, 318 p.

Burg, J. P., 1983. Tectogenese comparee de deux segments de chaine de collision; le sud du Tibet (suture du Tsangpo), la chaine hercynienne en Europe (sutures du Massif Central); Compared tectogenesis of two segments of collision chain; southern Tibet (Tsangpo suture zone), European Hercynian Chain; Central Massif suture zones. p. (Pagination mult. [401 p.]),

Burg, J. P., Leyreloup, A., Girardeau, J., Chen, G. M., 1987. Structure and metamorphism of a tectonically thickened continental crust; the Yalu Tsangpo suture zone (Tibet). In : Oxburgh, E. R. (editor), Yardley, B. W. D. (editor), England, Philip C. (editor), Tectonic settings of regional metamorphism, *Philosophical Transactions of the Royal Society of London, Series A: Mathematical and Physical Sciences*, **321**, p. 67-86

Coulon, C., Maluski, H., Bollinger, C., Wang, S., 1986. Mesozoic and Cenozoic volcanic rocks from central and southern Tibet; ^{39}Ar - ^{40}Ar dating, petrological characteristics and geodynamical significance. *Earth and Planetary Science Letters*, **79**, p. 281-302

Dubois-Côté, V., Hébert, R., Wang, C.S., Li, Y.L., and Dostal, J., 2003. Petrology and geochemistry of Yarlung Zangbo Suture Zone (YZSZ) ophiolites, Tibet : Geodynamic implications. [abstract] *GAC-MAC-SEG Joint Annual Meeting (Vancouver)*, **28**, p. 188.

Dubois-Côté, V., 2004. Pétrologie et géochimie des ophiolites de la Zone de Suture du Yarlung Zangbo (ZSYZ), Tibet : Implications géodynamiques. *M.Sc. Thesis*, Université Laval, 231 p.

Dubois-Côté, V., Hébert, R., Wang, C.S., Li, Y.L., and Dostal, J., 2005. Petrological and geochemical evidence for the origin of the Yarlung Zangbo ophiolites, southern Tibet. *Chemical Geology*, **214**, p. 265-286

Dupuis, C., Hébert, R., Dubois-Côté, V. Wang, C. S., Li, Y. L., Li, Z. J., 2005a. Petrology and Geochemistry of Mafic Rocks from Mélange and Flysch Units Adjacent to the Yarlung Zangbo Suture Zone, Southern Tibet. *Chemical Geology*, **214**, p. 287-308

Dupuis, C., Hébert, R., Dubois-Côté, V., Guilmette, C., Wang, C.S., Li, Y.L., Li, Z.J., 2005b. The Yarlung Zangbo Suture Zone ophiolitic mélange (Southern Tibet): New insights from geochemistry of ultramafic rocks. *Journal of Asian Earth Sciences* (in press, corrected proof)

Dupuis, C., Hébert, R., Guilmette, C., Wang, C.S., Li, Z.J., 2005c Geochemistry of sedimentary rocks from mélange and flysch units south of the Yarlung Zangbo Suture Zone, southern Tibet, *Journal of Asian Earth Sciences* (in press, corrected proof)

Dürr, S.B., 1996. Provenance of Xigaze fore-arc basin clastic rocks (Cretaceous South Tibet). *Geological Society of America Bulletin*, **108**, p. 669-684.

Ellis, D. J., Green, D. H., 1979. An experimental study of the effect of Ca upon garnet-clinopyroxene Fe-Mg exchange equilibria. *Contributions to Mineralogy and Petrology*, **71**, p. 13-22

Ernst, W. G., Liu, J., 1998. Experimental phase-equilibrium study of Al- and Ti-contents of calcic amphibole in MORB; a semiquantitative thermobarometer. *American Mineralogist*, **83**, p. 952-969

Fuhrman, M. L., Lindsley, D. H., 1988. Ternary-feldspar modeling and thermometry. *American Mineralogist*, **73**, p. 201-215

Frey, M., DeCapitani, D., Liou, J.G., 1991. A new petrogenetic grid for low-grade metabasites. *Journal of metamorphic petrology*, **9**, p. 497-509

Gaetani, M., Garzanti, E., 1991. Multicyclic history of the northern India continental margin (northwestern Himalaya). *AAPG Bulletin*, **75**, p. 1427-1446

Ganguly, J., 1979. Garnet and clinopyroxene solid solutions, and geothermometry based on Fe-Mg distribution coefficient. *Geochimica et Cosmochimica Acta*, **43**, p. 1021-1030

Göepel, C., Allegre, C. J., Xu R.-H., 1984. Lead isotopic study of the Xigaze ophiolite (Tibet); the problem of the relationship between magmatites (gabbros, dolerites, lavas) and tectonites (harzburgites). *Earth and Planetary Science Letters*, **69**, p. 301-310

Graham, C. M., Powell, R., 1984. A garnet-hornblende geothermometer; calibration, testing, and application to the Pelona Schist, Southern California. *Journal of Metamorphic Geology*, **2**, p. 13-31

Green, D. H., Ringwood, A. E., 1967. The genesis of basaltic magmas. *Contributions to Mineralogy and Petrology*, **15**, p. 103-190

Guilmette, C., Hébert, R., 2003. The Bainang dynamothermal Sole [abstract]. *18th Himalaya-Karakoram-Tibet Workshop, Ascona, Switzerland*, p. 58

Guilmette, C., Hébert, R., Dupuis, C., Dubois-Côté, V., Wang, C.S., Li, Z.J., 2005. Petrology, Geochemistry and Geochronology of highly foliated amphibolites from the ophiolitic mélange underlying the Yarlung Zangbo Suture Zone Ophiolites, Southern Tibet; Geodynamical implications for the dismembered dynamothermal sole. [abstract] *20th Himalaya-Karakoram-Tibet Workshop, Aussois, France, Geologie Alpine Mémoire H.S.* **44**, p. 71

Hacker, B. R., Mosenfelder, J. L., Gnos, E., 1996. Rapid emplacement of the Oman Ophiolite; thermal and geochronologic constraints. *Tectonics*, **15**, p. 1230-1247

Harrison, T.M., Copeland, P., Kidd, W.S.F., and Yin, A., 1992. Rising Tibet. *Science*, **255**, p. 1663-1670.

Hébert, R., Varfalvy, V., Huot, F., Wang, C.S., and Liu, Z.F., 2000. Yarlung Zangbo ophiolites, southern Tibet revisited. [abstract] 15th Himalaya-Karakorum-Tibet workshop. *Earth Science Frontier*, **7**, p. 124-126.

Hébert, R., Wang, C.S., Varfalvy, V., Huot, F., Beaudoin, G., and Dostal, J., 2001. Yarlung Zangbo Suture Ophiolites and their supra-subduction zone setting. [abstract] 16th Himalaya-Karakorum-Tibet workshop. *Journal of Asian Earth Sciences*, **19**, p. 27-28.

Hébert, R., Huot, F., Wang, C.S., Liu, Z.F., 2003. Yarlung Zangbo ophiolites (Southern Tibet) revisited: Geodynamic implications from the mineral record. In: Dylek, Y., Robinson, P.T. (Eds.), *Ophiolites in Earth History*. Geological Society, London, Special Publications, **218**, p. 165-190.

Huot, F., Hébert, R., Varfalvy, V., Beaudoin, G., Wang C.S., Liu Z., et al. 2002. The Beimrang Melange (southern Tibet) brings additional constraints in assessing the origin, metamorphic evolution and obduction processes of the Yarlung Zangbo ophiolite. In: Stuewe, K. (editor), Grasemann, B. (editor), 16th Himalaya-Karakoram-Tibet workshop, *Journal of Asian Earth Sciences*, **21**, p. 307-322

Jamieson, R. A., 1986 P-T paths from high temperature shear zones beneath ophiolites. *Journal of Metamorphic Geology*, **4**, p. 3-22

Jarosewich, E., Nelen, J. A., Norberg, J. A., 1980. Reference samples for electron microprobe analysis, *Geostandards Newsletter*, **4**, p. 43-47

Kempton, P. D., Harmon, R. S., 1992. Oxygen isotope evidence for large-scale hybridization of the lower crust during magmatic underplating. In : McLennan, Scott M. (editor), Rudnick, Roberta L. (editor), The Taylor Colloquium; Origin and evolution of planetary crusts, *Geochimica et Cosmochimica Acta*, **56**, p. 971-986

Klootwijk, C. T., Gee, J. S., Peirce, J. W., Smith, G. M., McFadden, P. L., 1992. An early India-Asia contact; paleomagnetic constraints from Ninetyeast Ridge, ODP Leg 121; with Suppl. Data 92-15, *Geology (Boulder)*, **20**, p. 395-398

Kretz, R., 1983. Symbols for rock-forming minerals. *American Mineralogist*, **68**, p. 277-279

Leake, B. E.; Woolley, A. R.; Birch, W. D.; Burke, E. A. J.; Ferraris, G.; Grice, J. D.; Hawthorne, F. C., Kisch, H. J.; Krivovichev, V. G.; Schumacher, J. C.; Stephenson, N. C N.; Whittaker, E. J W., 2004. Nomenclature of amphiboles; additions and revisions to the International Mineralogical Association's amphibole nomenclature. *American Mineralogist*, **89**, p.883-887

Lindsley, D.H., 1983. Pyroxene thermometry. *American Mineralogist* **68**, p. 477-493.

Liu, J., Bohlen, S.R. and Ernst, W.G. 1996. Stability of hydrous phases in subducting oceanic crust. *Earth and Planetary Science Letters*, **143**, p. 161–171.

Mader, U. K., Percival, J. A., Berman, R. G., 1994. Thermobarometry of garnet-clinopyroxene-hornblende granulites from the Kapuskasing structural zone. In : Percival, J. A. (editor), The Kapuskasing transect of Lithoprobe--Le transect de Kapuskasing du Lithoprobe, *Canadian Journal of Earth Sciences = Journal Canadien des Sciences de la Terre*, **31**, p. 1134-1145

Malpas, J., 1979. The dynamothermal aureole of the Bay of Islands ophiolite suite. *Canadian Journal of Earth Sciences*, **16**, p. 2086-2101

Malpas, J. G., Zhou, M.F., Robinson, P. T., Reynolds, P. H. 2003. Geochemical and geochronological constraints on the origin of the Yarlung Zangbo ophiolites, Southern Tibet. In : Dilek, Y. & Robinson, P. T. (eds) 2003. Ophiolites in Earth History. *Geological Society, London, Special Publications*, **218**, p. 191-206

McDermid, I., Aitchison, J.C., Badengzhu, Davis, A.M., Liu, J.B., Luo, H., et al., 2000. Zedong Terrane, A Mid Cretaceous Intra-Oceanic Arc, South Tibet. [abstract] 15th Himalaya-Karakorum-Tibet workshop. *Earth Science Frontiers*, **7**, p. 265.

McDermid, I.R.C., Aitchison, J.C., Badengzhu, and Davis, A.M., 2001. The Zedong Terrane: An Intra-Oceanic Magmatic Arc Assemblage, Tibet. [abstract] 16th Himalaya-Karakorum-Tibet workshop. *Journal of Asian Earth Sciences*, **19**, p. 44.

McDermid, I.R.C., Aitchison, J.C., Davis, A.M., Harrison, T.M., and Grove, M., 2002. The Zedong Terrane: A Late Jurassic Intra-Oceanic Magmatic Arc within the Yarlung-Tsangpo Suture Zone, Southeastern Tibet. *Chemical Geology*, **187**, p. 267-277.

Molnar, P., and Tapponnier, P., 1975. Cenozoic tectonics of Asia: Effects of a continental collision. *Science*, **189**, p. 419-426.

Mukhopadhyay, B., Bose, M. K., 1994. Transitional granulite-eclogite facies metamorphism of basic supracrustal rocks in a shear zone complex in the Precambrian shield of South India, *Mineralogical Magazine*, **58**, p. 97-118

Murphy, M. A., Yin, A., Harrison, T. M., Duerr, S. B., Chen, Z., Ryerson, F. J., et al. 1997. Did the Indo-Asian collision alone create the Tibetan Plateau ? *Geology (Boulder)*, **25**, p. 719-722

Nicolas, A., Girardeau, J., Marcoux, J., Dupre, B., Wan X.B., Cao Y., et al. 1981. The Xigaze ophiolite (Tibet); a peculiar oceanic lithosphere, *Nature (London)*, **294**, p. 414-417

Nicolas, A., Le Pichon, X., 1980 Thrusting of young lithosphere in subduction zones with special reference to structures in ophiolitic peridotites. *Earth and Planetary Science Letters*, **46**, p. 397-406

Nimis, P., 1995 A clinopyroxene geobarometer for basaltic systems based on crystal-structure modeling. *Contributions to Mineralogy and Petrology*. **121**, p. 115-125

Pattison, D. R. M., Newton, R. C., 1989. Reversed experimental calibration of the garnet-clinopyroxene Fe-Mg exchange thermometer. *Contributions to Mineralogy and Petrology*, **101**, p. 87-103

Pattison, D. R. M., 2003. Petrogenetic significance of orthopyroxene-free garnet + clinopyroxene + plagioclase + or - quartz-bearing metabasites with respect to the amphibolite and granulite facies. *Journal of Metamorphic Geology*, **21**, p. 21-34

Peacock, S. M., Rushmer, T., Thompson, A. B., 1994. Partial melting of subducting oceanic crust. *Earth and Planetary Science Letters*, **121**, p. 227-244

Peacock, S. M., 1988. Inverted metamorphic gradients in the westernmost Cordillera. In : Ernst, Wallace Gary (editor), Metamorphism and crustal evolution of the Western United States, *Rubey Volume*, **7**, p. 953-975

Powell, R., 1985. Regression diagnostics and robust regression in geothermometer/geobarometer calibration; the garnet-clinopyroxene geothermometer revisited. *Journal of Metamorphic Geology*, **3**, p. 231-243.

Pozzi, J. P., Westphal, M., Girardeau, J., Besse, J., Yao X.Z., Xian Y. et al. 1984. Paleomagnetism of the Xigaze ophiolite and flysch (Yarlung Zangbo suture zone, southern Tibet); latitude and direction of spreading. *Earth and Planetary Science Letters*, **70**, p. 383-394

Raase, P., 1974. Al and Ti Contents of Hornblende, Indicators of Pressure and Temperature of Regional Metamorphism. *Contributions to Mineralogy and Petrology*, **45**, p. 231-236

Shervais, J. W., 2001. Birth, death and resurrection; the life cycle of supra-subduction zone ophiolites, *Geochemistry, Geophysics, Geosystems, G3*, **2**, paper no. 2000GC000080

Spray, J. G., 1984. Possible causes of upper mantle decoupling and ophiolite displacement. In : Gass, I. G. (editor), Lippard, S. J. (editor), Shelton, A. W. (editor), Ophiolites and oceanic lithosphere, *Geological Society Special Publications*, **13**, p. 255-268

Sturm, M. E., Klein, E. M., Karsten, J. L., Karson, J. A., 2000. Evidence for subduction-related contamination of the mantle beneath the southern Chile Ridge; implications for ambiguous ophiolite compositionsDilek, Yildirim (editor), Moores, Eldridge M. (editor), Elthon, Don (editor), Nicolas, Adolphe (editor), Ophiolites and oceanic crust; new insights from field studies and the Ocean Drilling Program, *Special Paper - Geological Society of America*, **349**, p. 13-20

Tapponier, P., Mercier, J.L., Proust, F. et al. (27), 1981a. The Tibetan side of the India-Eurasia collision. *Nature*, **294**, p. 405-410.

Tapponier, P., Mercier, J.L., Armijo, R., Han, T., and Zhou, J., 1981b. Field evidence for an active normal faulting in Tibet. *Nature*, **294**, p. 410-414.

Taylor, H., 1997. Oxygen and Hydrogen isotope relationships in hydrothermal mineral deposits. In : Barnes, H.L. (ed.) Ore deposits research section, The Pennsylvania State University; p. 229-302

Van der Voo, R., Spakman, W., Bijwaard, H., 1999. Tethyan subducted slabs under India. *Earth and Planetary Science Letters*, **171**, p. 7-20

Wakabayashi, J., Dilek, Y., 2000. Spatial and temporal relationships between ophiolites and their metamorphic soles; a test of models of forearc ophiolite genesis. In : Dilek, Y., Moores, E. M., Elthon, D., Nicolas, A. (Eds.), Ophiolites and oceanic crust; new insights from field studies and the Ocean Drilling Program, *Special Paper - Geological Society of America*, **349**, p. 53-64

Wakabayashi, J., Dilek, Y., 2003. What constitutes “emplacement” of an ophiolite ? : Mechanisms and relationship to subduction initiation and formation of metamorphic soles. In : Dilek, Y. and Robinson, P. T. (Eds) Ophiolites and Earth history. *Geological Society, London, Special publication*, **218**, p. 427-448

Wang, X.B., Xiao, X.C., Cao, Y.G., Zheng, H.X. 1984. Geological map of the ophiolite zone along the middle Yarlung Zangbo River, Xizang (Tibet). 2nd Geological and Geophysical brigade of geological Bureau of the Tibet Autonomous Region, Publishing House of Surveying and Mapping, Beijing, P.R. China.

Wang, X.B., Bao, P.S., Deng, W.M., Wang, F.G. 1987. Tectonic evolution of the lithosphere of the Himalayas: Xizang (Tibet) ophiolite. In: Chinese Academy of Geological Sciences, (ed.) *People's Republic of China Ministry of Geology and Mineral Resources Geological Memoirs Series 3*. **8**, p. 1-336

Williams, H., Smyth, W. R., 1973. Metamorphic aureoles beneath ophiolite suites and alpine peridotites; tectonic implications with west Newfoundland examples. *American Journal of Science*, **273**, p. 594-621

Zheng, Y.F., 1993a. Calculation of oxygen isotope fractionation in anhydrous silicate minerals. *Geochimica et Cosmochimica Acta*, **57**, p. 1079-1091

Zheng, Y.F., 1993b. Calculation of oxygen isotope fractionation in hydroxyl-bearing silicates. *Earth and Planetary Science Letters*, **120**, p. 247-263

Zhou, M.F., Robinson, P.T., Malpas, J., Li Z., 1996. Podiform chromitites in the Luobusa Ophiolite (southern Tibet); implications for melt-rock interaction and chromite segregation in the upper mantle. *Journal of Petrology*, **37**, p. 3-21

Zyabrev, S.V., Aitchison, J.C., Badengzhu, Davis, A.M., Luo, H., Malpas, J., 1999. Radiolarian biostratigraphy of supra-ophiolite sequences in the Xigaze area, Yarlung Tsangpo suture, Southern Tibet (preliminary report). *Radiolaria* **17**, p. 13-19

Zyabrev, S.V., Aitchison, J.C., Abrajevitch, A.V., Badengzhu, Davis, A.M., Luo, H., 2004. Bainang Terrane, Yarlung-Tsangpo suture, southern Tibet (Xizang, China): a record of intra-Neo-Tethyan subduction-accretion processes preserved on the roof of the world. *Journal of the Geological Society of London* **161**, p. 1-17.

2.9. Figure captions

Figure 2.1 : Schematic tectonic map of the Himalayas, the Tibetan Plateau and surrounding areas showing crustal blocks and suture zones (modified after Huot et al., 2002). MBT = Main Boundary Thrust, MCT = Main Central Thrust, YZSZ = Yarlung Zangbo Suture Zone.

Figure 2.2 : Geological map of the YZSZ showing the sampling regions (modified from the Geological Institute of the Chinese Academy of Geosciences, 1982).

Figure 2.3 : Photomicrographs of different amphibolite types and other rocks (a) Common amphibolite. Note the « cloudy » aspect of pseudomorphised plagioclase (b) Clinopyroxene amphibolite. Upper section is mid to coarse clinopyroxene-plagioclase-epidote±quartz banding. Lower section is clinopyroxene amphibolite (c) Garnet-bearing amphibolite with few retrograde features and deformed colorless clinopyroxene (d) Garnet-bearing amphibolite with chlorite and green amphibole coronas around prograde phases (e) BSE imagery of acicular Al-amphibole around garnet (f) BSE imagery of amphibole and euhedral plagioclase corona around garnet (g) Prehnite vein post-dating cataclastic event (h) Diabasic intrusion with clinopyroxene and plagioclase micro-phenocrysts.

Figure 2.4 : Ca-amphibole nomenclature after Leake et al. (2004).

Figure 2.5 : Ti vs Al^{IV} (apfu) diagram for amphiboles. Fields for « ophiolitic mélange » and « Beimaranng mélange » are from Dupuis et al. (2005a) and Huot et al. (2002). Amphibole nomenclature is from Leake et al. (2004).

Figure 2.6 : $(\text{Na}+\text{K})$ vs Al^{IV} diagram for amphiboles. End-member compositions are indicated (EK = Ekermanite, ED = Edenite, PG = Pargasite, TR = Tremolite, TS = Tschermakite)

Figure 2.7 : Ternary diagram for clinopyroxene nomenclature, with isotherms from Lindsley (1983).

Figure 2.8 : Clinopyroxene composition (a) TiO_2 wt. % vs Al_2O_3 wt. % for all analyzed clinopyroxene (b) Na_2O wt. % vs Al_2O_3 wt. % for all analyzed clinopyroxene.

Figure 2.9 : Ternary diagram for garnet composition. Molecular end-members are grossular, almandine + spessartite and pyrope.

Figure 2.10 : Zonation of garnet from rim to rim for grossular, almandine, spessartite and pyrope mole fraction.

Figure 2.11 : P-T diagram for thermobarometry of amphibolites using the Ti-Al method of Ernst and Liu (1998), the garnet-clinopyroxene Mg-Fe exchange thermometer of Ellis and Green (1979) and Pattison and Newton (1989), the garnet-amphibole Mg-Fe exchange thermometer of Graham and Powell (1984) and TWEEQU calculations. TWEEQU calculations (Berman 1991) were made by using end-member properties from Berman (1988, 1990) and the non-ideal solution properties of : garnet (Berman, 1990), amphibole (Mader et al., 1994) and plagioclase (Furhman & Lindsley, 1988) (a) Results for assemblages A, B and E. (b) results for assemblages C, D and E. Reaction curves 1-2-3 are from Ernst and Liu (1998), 4-5-6 from Green and Ringwood, (1967), 7-8-9 from Mukhopadhyay and Bose, (1994), 10 from Butcher and Frey (1994), 11 and 12 from Liu et al. (1996) and field 13 from Frey et al. (1991) A = amphibolite facies, EA = epidote amphibolite facies, EC = eclogite facies, EG = epidote-glaucophane facies, G = granulite facies, GS = green schist facies, PA = pumpellyite actinolite facies, Z = zeolite facies.

Figure 2.12 : Hypothetical P-T-t paths for highly foliated amphibolites from the mélange. Curve 1 and 2 are from Peacock et al. (1994) Curve 3 is from Huot et al. (2002) and represents P-T path followed by other blocks from the mélange. Upper left corner shows

possible architecture of subduction plane and sole. A-E are referring to the five observed metamorphic assemblages (see text).

Figure 2.13: Geodynamic model for the Yarlung Zangbo ophiolites. See text for explanation.

2.10. List of Tables

Table 2.1 : Representative analyses of amphiboles

Table 2.2 : Representative analyses of clinopyroxene

Table 2.3 : Representative analyses of garnet

Table 2.4 : Stable isotope geochemistry

Table 2.5: Thermobarometric results from TWEEQU. Temperature in °C and Pressure in kbars.

Table 2.1 :

Mineral	Amphiboles										
Facies	garnet amphibolite					clinopyroxene amphibolite			common amphibolite		
Sample Analysis Group	LUS-12		LUS-17			LUS-14	LUS-11	BAI-19	BUM-14	BAI-20	BUM-17
	am4 2	am12 3	am10 2	am3 4	am13 3	am7 2	am13 1	am2 1	am2 1	am4 1	am5 1
SiO ₂	42.54	37.62	41.86	47.36	38.74	44.71	45.26	44.66	40.28	44.14	42.46
Al ₂ O ₃	13.85	21.02	13.29	7.74	15.49	10.84	11.04	11.1	13.17	12.33	12.41
TiO ₂	2.22	0.06	2.38	0.28	0.23	2.22	0.71	0.77	1.22	0.81	1.67
FeO (tot.)	11.37	14.4	14.38	14.69	17.23	13.05	14.12	16.35	19.38	14.04	14.57
MgO	13.41	9.76	10.98	13.12	9.21	13.65	12.41	11.05	8.97	11.64	11.98
MnO	0.15	0.64	0.14	0.27	0.36	0.21	0.28	0.25	0.3	0.25	0.16
CaO	11.35	9.96	11.38	12.62	11.83	11.34	11.87	11.61	11.76	11.78	11.11
Na ₂ O	2.9	2.91	2.51	1.62	2.60	2.46	1.63	1.74	2.41	1.72	2.15
K ₂ O	0.18	0.1	0.33	0.13	0.28	0.12	0.1	0.62	0.81	0.26	0.07
Sum	97.95	96.46	97.24	97.81	95.97	98.24	97.42	98.13	98.3	96.97	96.57
Formula proportions of cations based on 23 O atoms											
Si	6.13	5.46	6.19	6.93	5.88	6.42	6.56	6.55	6.04	6.48	6.23
Aliv	1.87	2.54	1.81	1.07	2.12	1.58	1.44	1.45	1.96	1.52	1.77
Alvi	0.48	1.05	0.51	0.27	0.65	0.25	0.44	0.47	0.37	0.61	0.38
Ti	0.24	0.01	0.26	0.03	0.03	0.24	0.08	0.09	0.14	0.09	0.18
Fe ²⁺	0.82	0.21	1.4	1.51	1.45	0.76	1.09	1.45	1.77	1.23	0.9
Fe ³⁺	0.55	1.54	0.37	0.29	0.74	0.80	0.63	0.56	0.66	0.49	0.89
Mg	2.88	2.11	2.42	2.86	2.09	2.92	2.68	2.41	2.01	2.55	2.62
Mn	0.02	0.08	0.02	0.03	0.05	0.03	0.03	0.03	0.04	0.03	0.02
Ca	1.75	1.55	1.8	1.98	1.92	1.68	1.84	1.82	1.89	1.85	1.75
Na	0.81	0.82	0.72	0.46	0.77	0.68	0.46	0.49	0.7	0.49	0.61
K	0.03	0.02	0.06	0.02	0.05	0.02	0.02	0.11	0.16	0.05	0.01
Sum	15.58	15.37	15.57	15.46	15.75	15.38	15.27	15.43	15.73	15.39	15.37

Table 2.2 :

Mineral	Clinopyroxene							
Facies	garnet amphibolite			clinopyroxene amphibolites				Intrusive
Sample Analysis Type	LUS-12 px2 colorless	LUS-17 px4 green	LUS-14 px6 colorless	LUS-11 px2 green	BAI-19 px4 green	BUM-14 px5 green	BUM-14 px4 green	LUS-02 px1 magmatic
SiO ₂	49.47	52.69	48.32	51.34	52.46	51.36	50.39	52.18
Al ₂ O ₃	6.71	3.15	5.82	3.48	2.75	3.02	3.23	0.94
TiO ₂	0.85	0.23	0.79	0.33	0.11	0.18	0.33	0.05
FeO	5.89	4.52	6.29	5.44	7.35	7.33	6.42	7.32
Fe ₂ O ₃	2.04	2.49	4.6	3.52	1.24	2.69	4.75	3.55
MgO	12.61	13.77	11.36	13.12	12.68	11.76	11.11	12.08
MnO	0.16	0.13	0.19	0.29	0.32	0.27	0.35	0.51
CaO	21.75	24.3	21.04	22.20	22.71	22.31	23.82	23.49
Na ₂ O	0.76	0.62	1.04	0.89	0.74	0.95	0.75	0.64
Sum	100.23	101.9	99.44	100.61	100.36	99.87	101.14	100.76
Formula proportions of cations based on 6 O atoms								
Si	1.83	1.91	1.82	1.90	1.94	1.93	1.88	1.95
Al	0.29	0.14	0.26	0.15	0.12	0.13	0.14	0.04
Ti	0.02	0.01	0.02	0.01	0	0.01	0.01	0
Fe ²⁺	0.18	0.14	0.2	0.17	0.23	0.23	0.2	0.23
Fe ³⁺	0.06	0.07	0.13	0.10	0.04	0.08	0.13	0.1
Mg	0.69	0.75	0.64	0.72	0.7	0.66	0.62	0.67
Mn	0.01	0	0.01	0.01	0.01	0.01	0.01	0.02
Ca	0.86	0.95	0.85	0.88	0.9	0.9	0.95	0.94
Na	0.05	0.04	0.08	0.06	0.05	0.07	0.05	0.05
Sum	4.00	4.00	4.00	3.99	3.99	4.01	4.00	4.00

Table 2.3 :

Mineral Sample Analysis Corona	Garnet					
	LUS-12		LUS-17		LUS07	
	LUS12-gt23 No	LUS12-gt24 yes	LUS17-gt4 Yes	LUS17-gt2 small	LUS07-gt22 yes	LUS07-gt20 no
SiO ₂	39.25	39.86	39.67	38.69	39.34	38.57
Al ₂ O ₃	22.21	22.24	21.30	20.75	21.82	21.49
TiO ₂	0.09	0.08	0.10	0.37	0.13	0.09
FeO	19.98	19.82	20.02	20.59	22.79	21.10
Fe ₂ O ₃	0.52	0.82	1.57	1.72	0.50	0.51
MgO	7.50	10.40	7.22	6.10	5.59	3.60
MnO	0.97	0.53	0.98	0.43	1.78	2.44
CaO	11.06	7.98	10.33	11.92	9.67	12.81
Sum	101.56	101.73	101.19	100.56	101.62	100.60
Formula proportions of cations based on 24 O atoms						
Si	5.92	5.93	6.01	5.95	6.00	5.98
Al	3.95	3.90	3.81	3.76	3.92	3.93
Ti	0.01	0.01	0.01	0.04	0.01	0.01
Fe ²⁺	2.52	2.47	2.54	2.65	2.91	2.74
Fe ³⁺	0.06	0.09	0.18	0.20	0.06	0.06
Mg	1.69	2.31	1.63	1.40	1.27	0.83
Mn	0.12	0.07	0.13	0.06	0.23	0.32
Ca	1.79	1.27	1.68	1.96	1.58	2.13
Sum	16.06	16.04	15.98	16.01	15.98	15.99

Table 2.4

Sample	Mineral	$\delta^{18}\text{O}$ SMOW (mineral)	Temperature (°C)	$\delta^{18}\text{O}$ SMOW (fluid)
Common amphibolite	Albite	17.9	200	9.6
			300	13.5
Clinopyroxene amph.	Albite	15.6	200	7.3
			300	11.1
Common amphibolite	Albite	16.2	200	7.9
			300	11.8
Common amphibolite	Hornblende	7.8	650	10.1
			700	10.1
Common amphibolite	Hornblende	7.5	650	9.8
			700	9.8
Clinopyroxene amph.	Hornblende	8.8	700	11.1
			750	11.0
Common amphibolite	Hornblende	7.5	650	9.8
			700	9.8
Clinopyroxene amph.	Diopsid + épidote	8.3	700	10.4
			750	10.4
Common amphibolite	Prehnite	11.0	200	5.3
			300	8.6

Table 2.4

Method	TWEEQU Berman 1991								
	An#	25		40		50		60	
Assemblage	Sample	P	T	P	T	P	T	P	T
	LUS-12	13	568	14,6	816	16	1000		
Hbl+Cpx+Grt+Pl±Rt	LUS-14	11,64	493	12,3	650	13,1	751	14,1	878
	LUS-17	12	516	12,7	678	13,3	792	14,6	816
	An#	5		10		15		20	
Grt+Hbl+Pl (Coronas)	LUS-12	27,5	605	24,9	679	22,9	728	21,3	768
	LUS-17	27,8	619	25,1	687	23,1	737	21,4	777

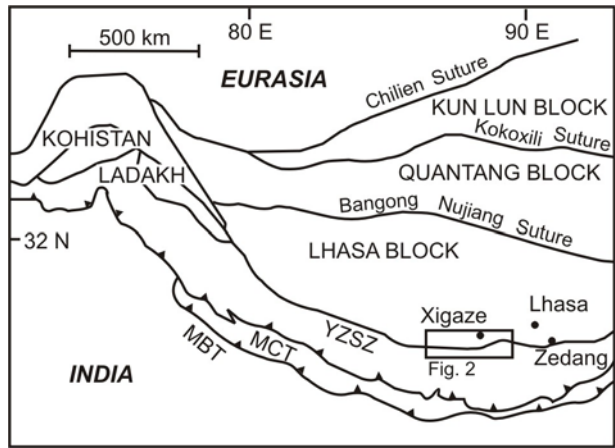


Figure 2.1

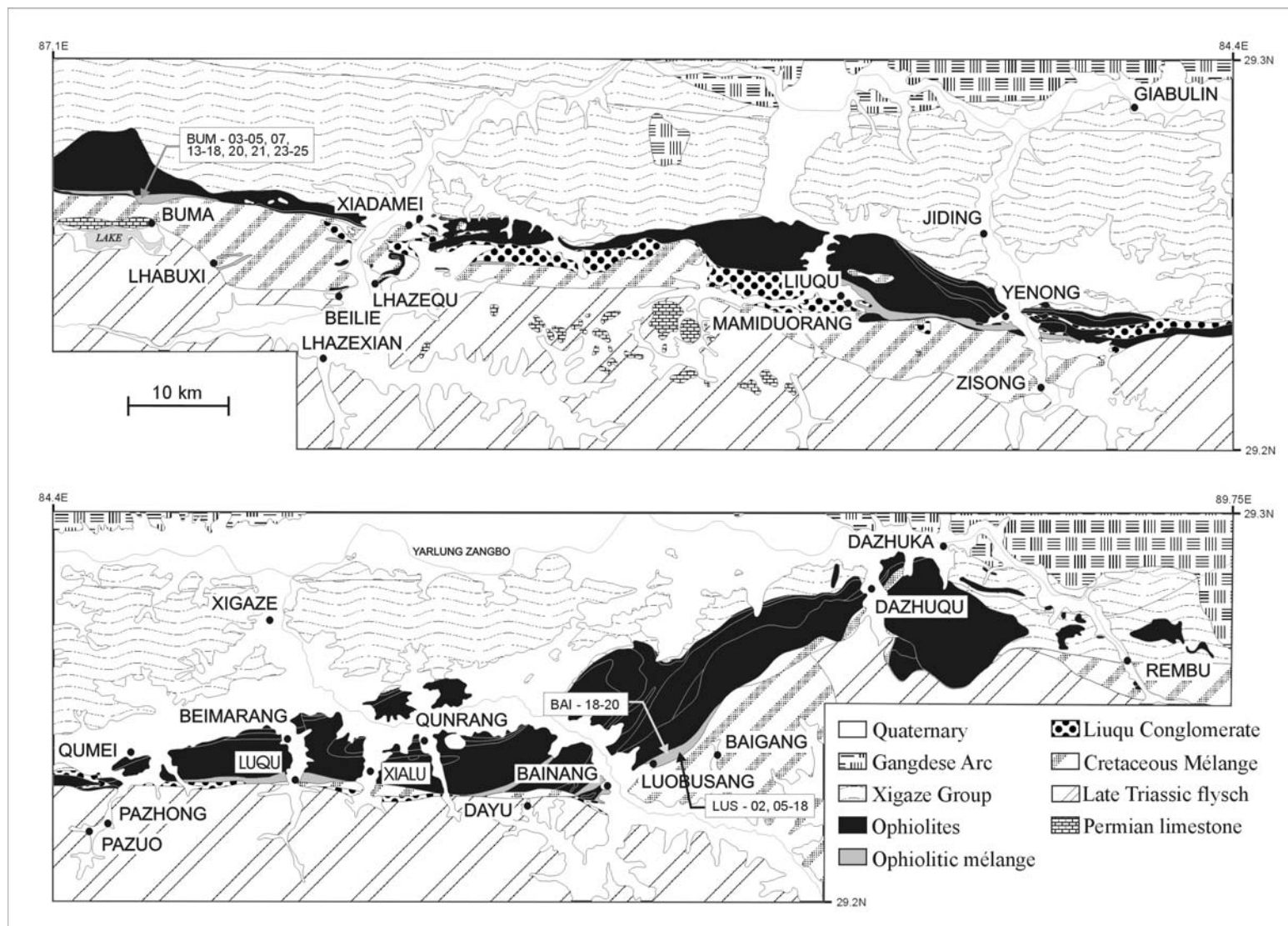
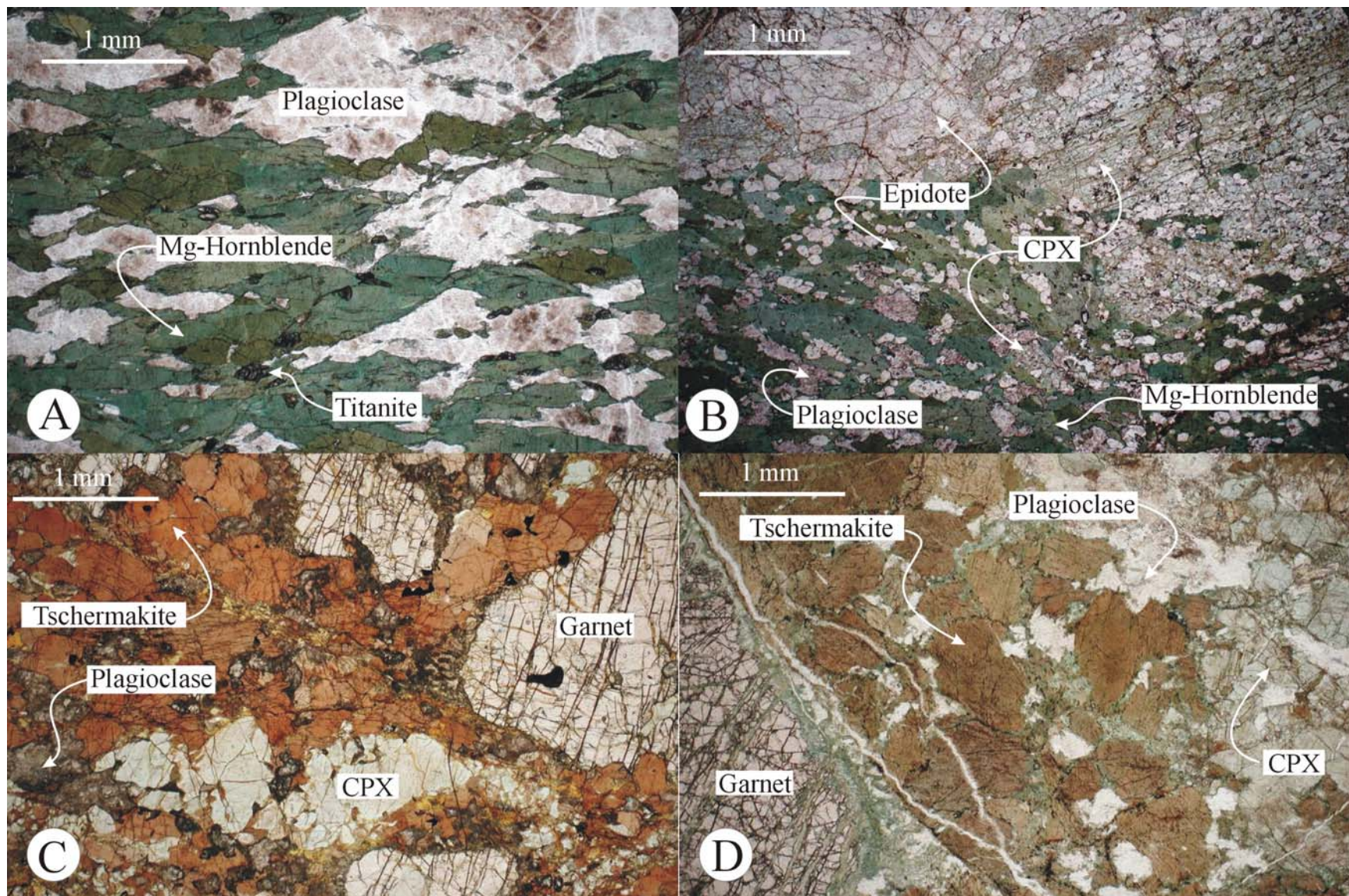


Figure 2.2



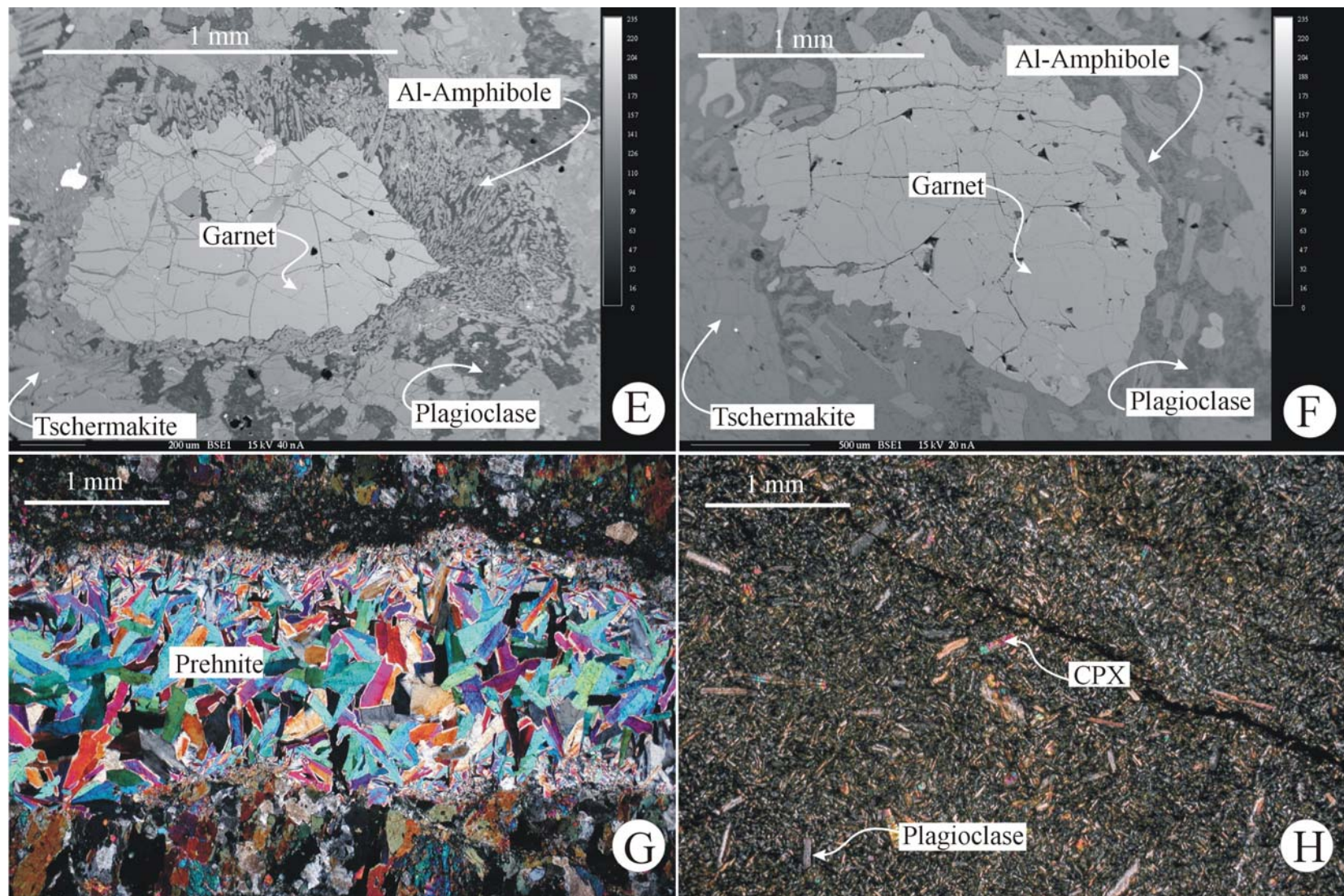


Figure 2.3 :

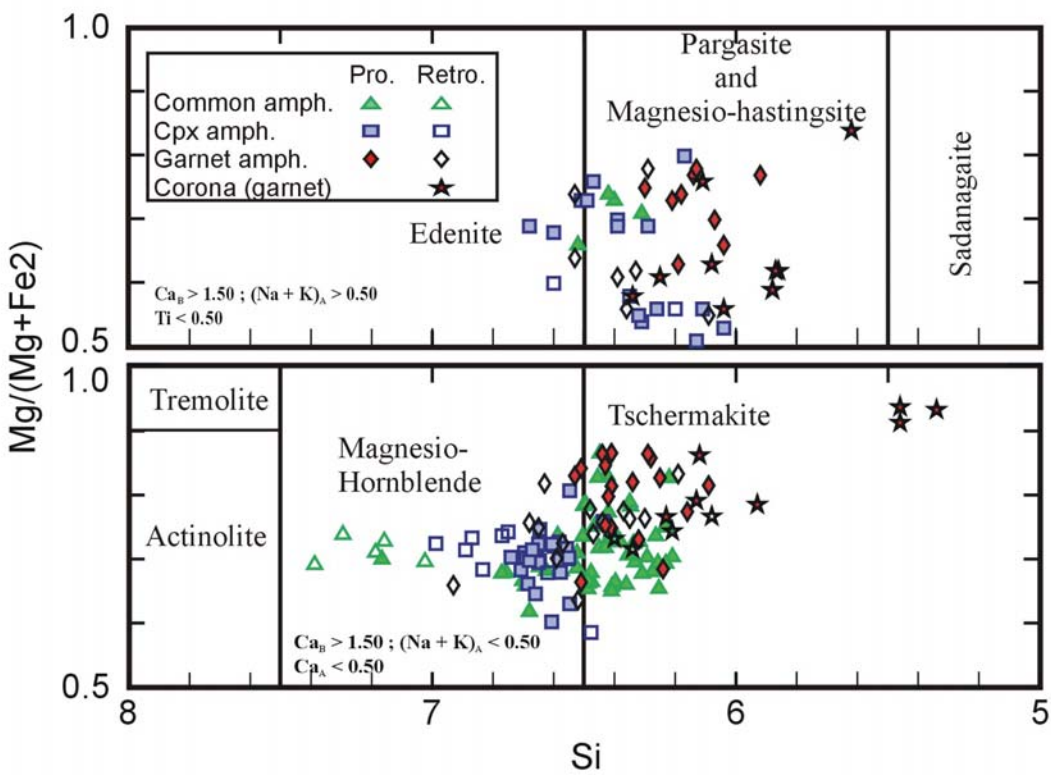


Figure 2.4 :

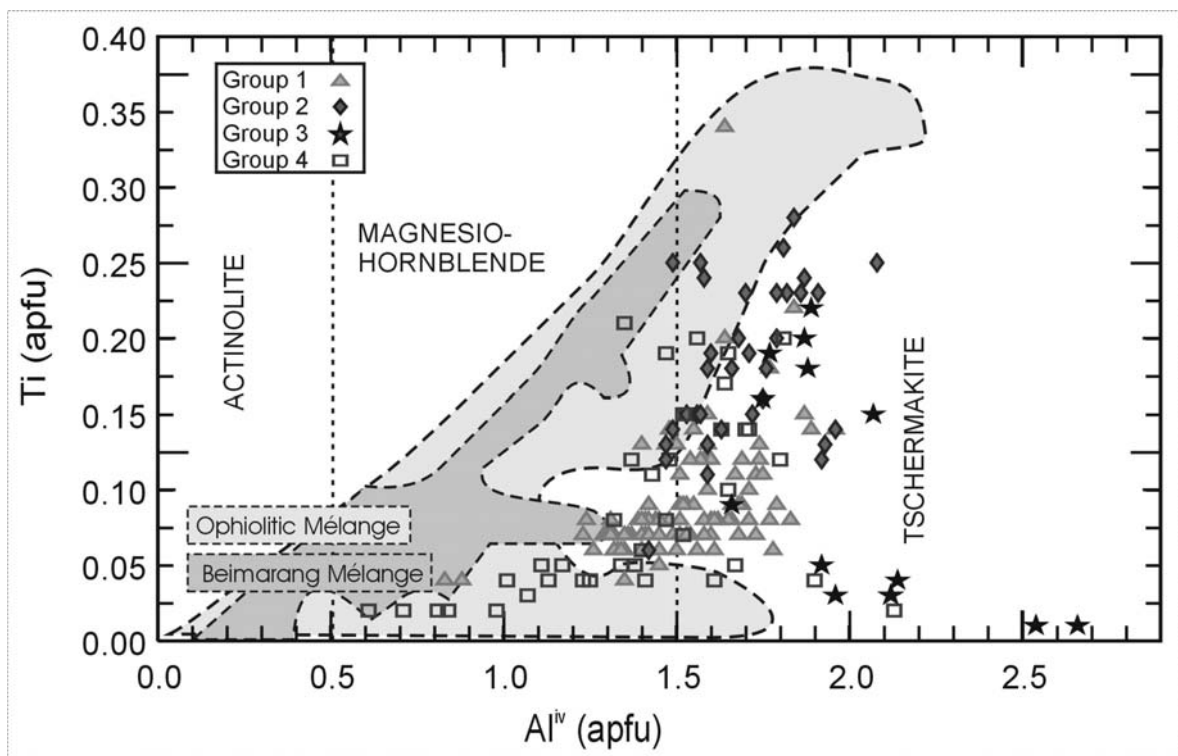


Figure 2.5 :

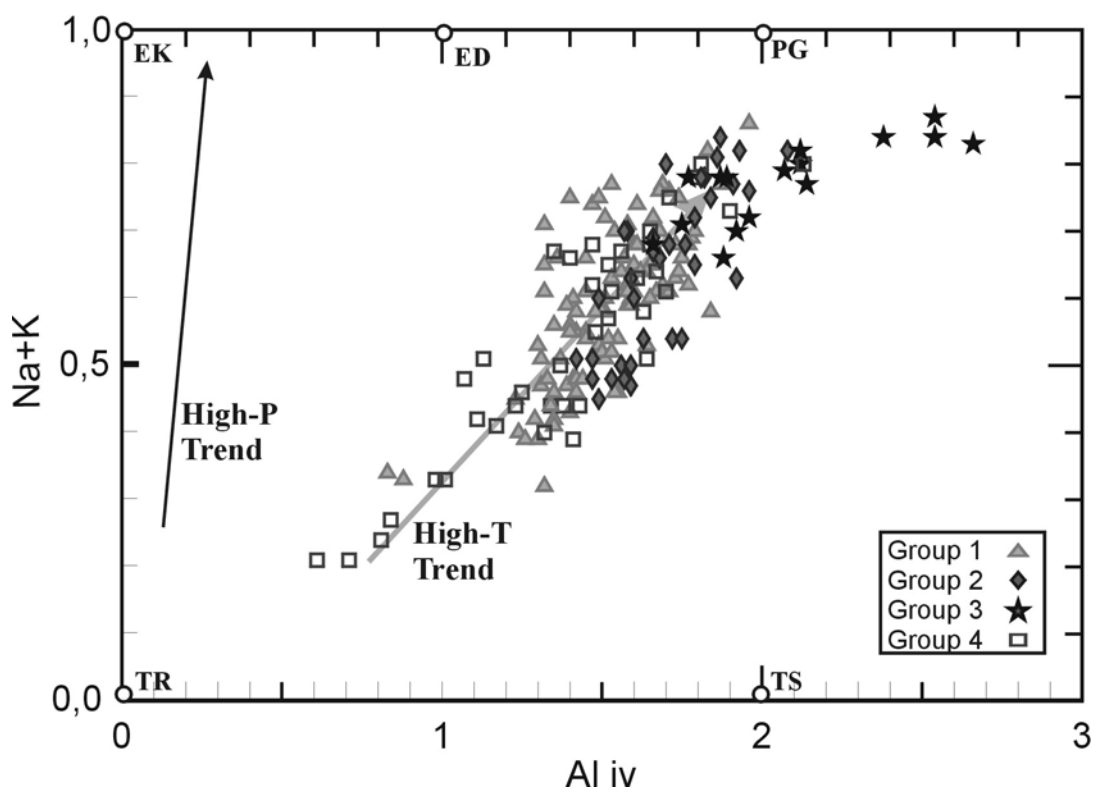


Figure 2.6

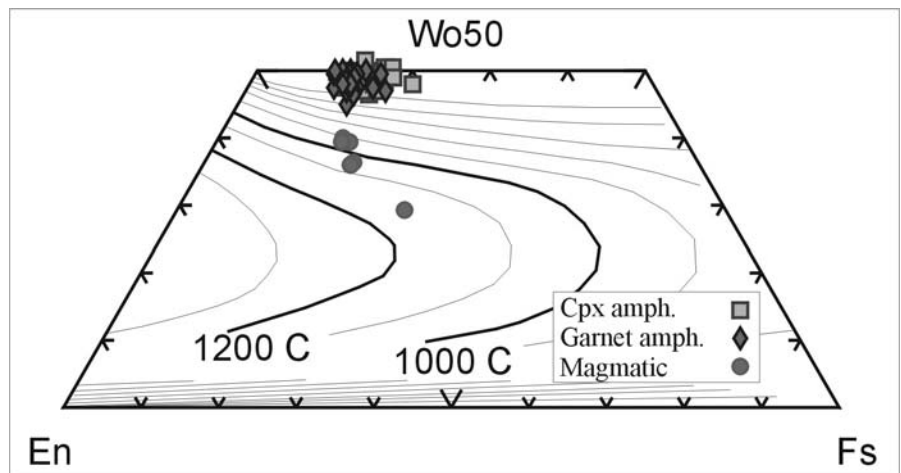


Figure 2.7 :

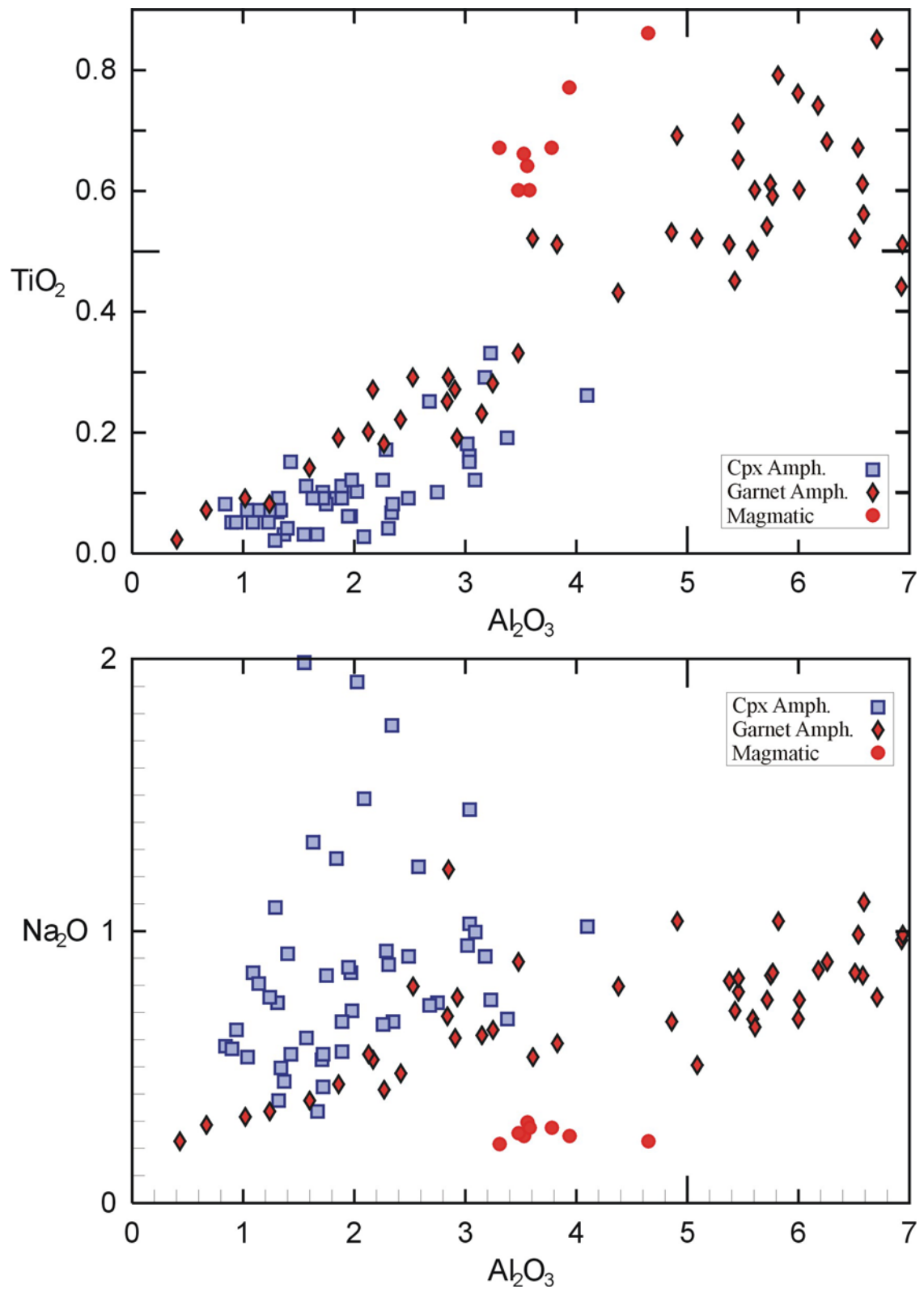


Figure 2.8

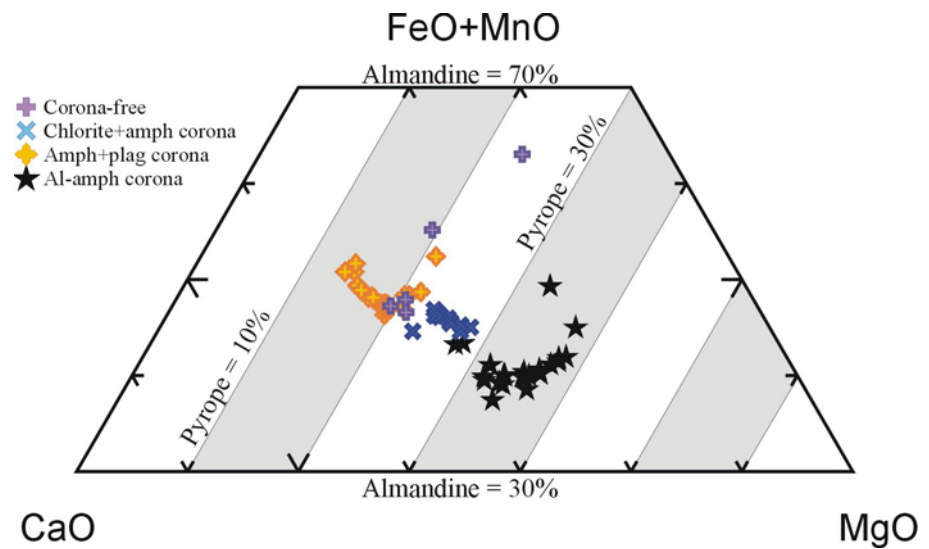


Figure 2.9

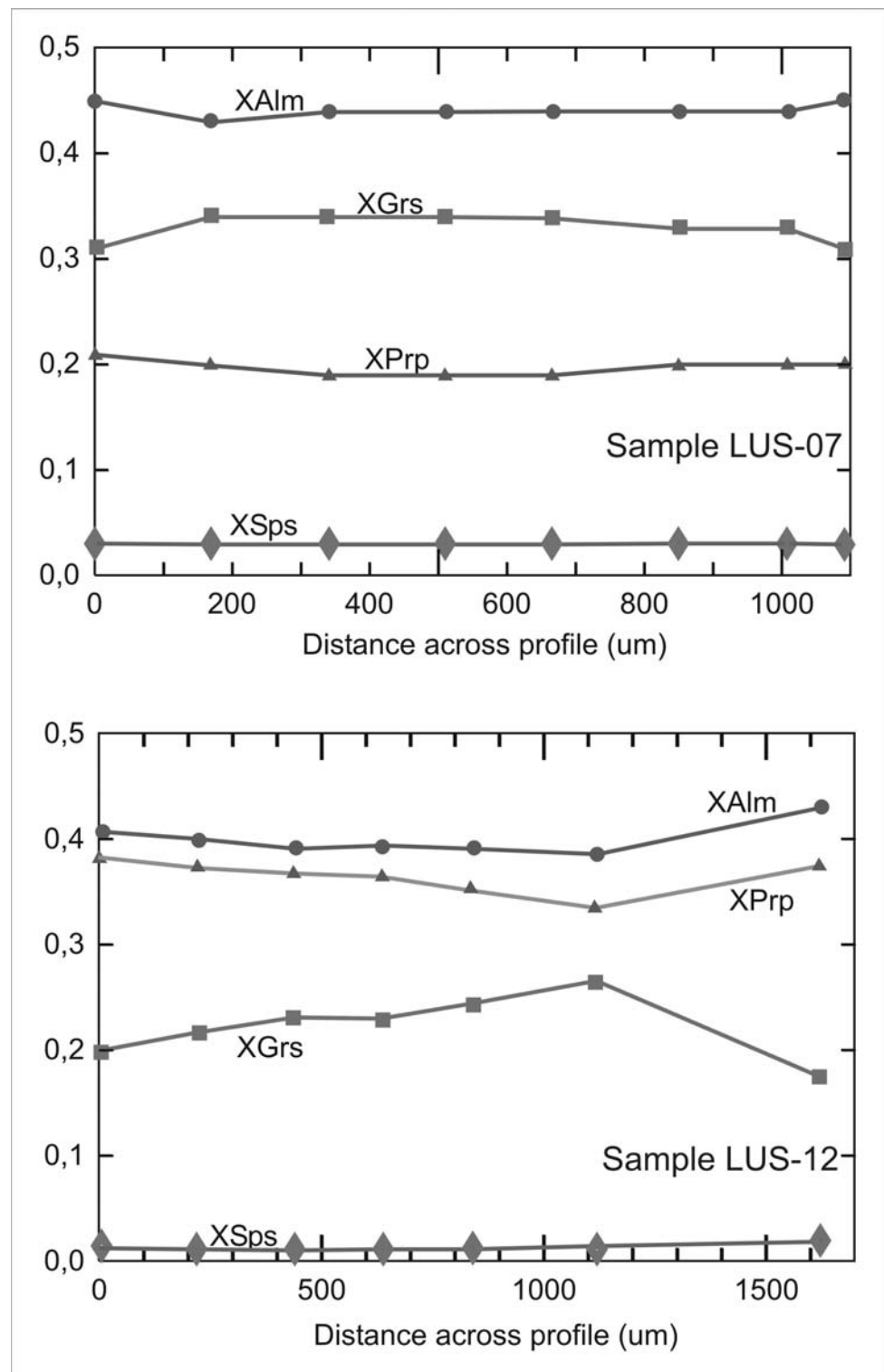
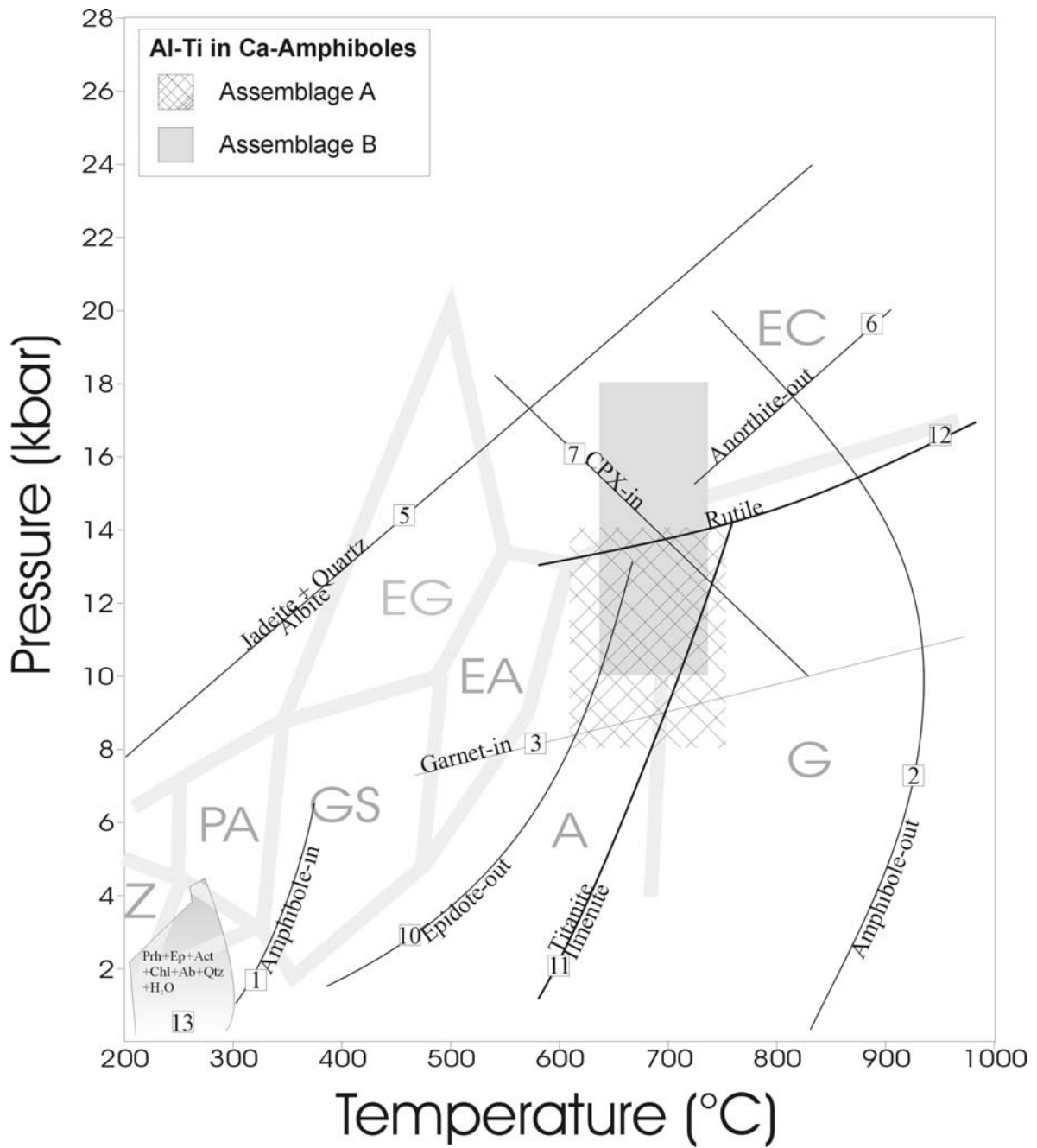


Figure 2.10



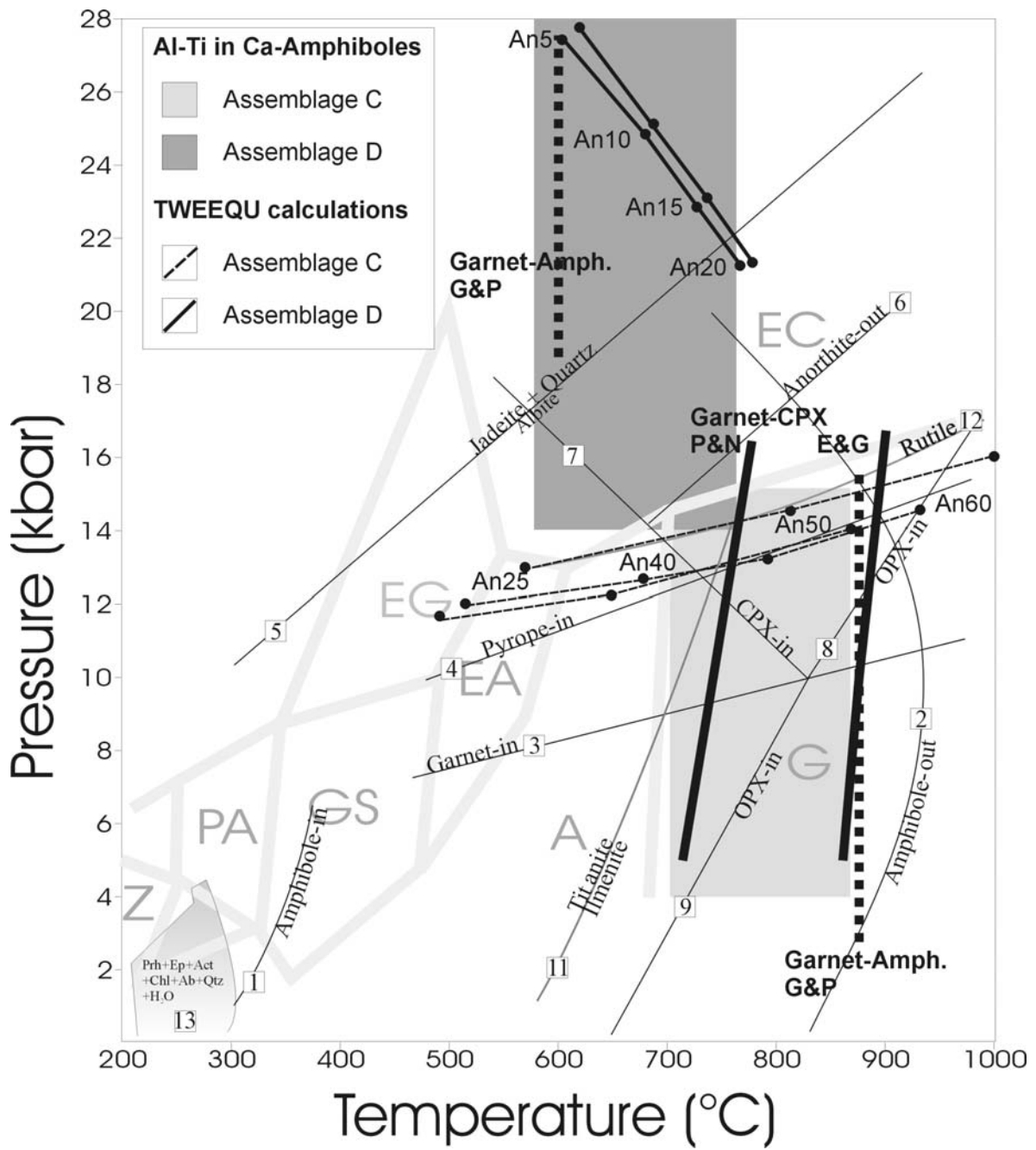


Figure 2.11

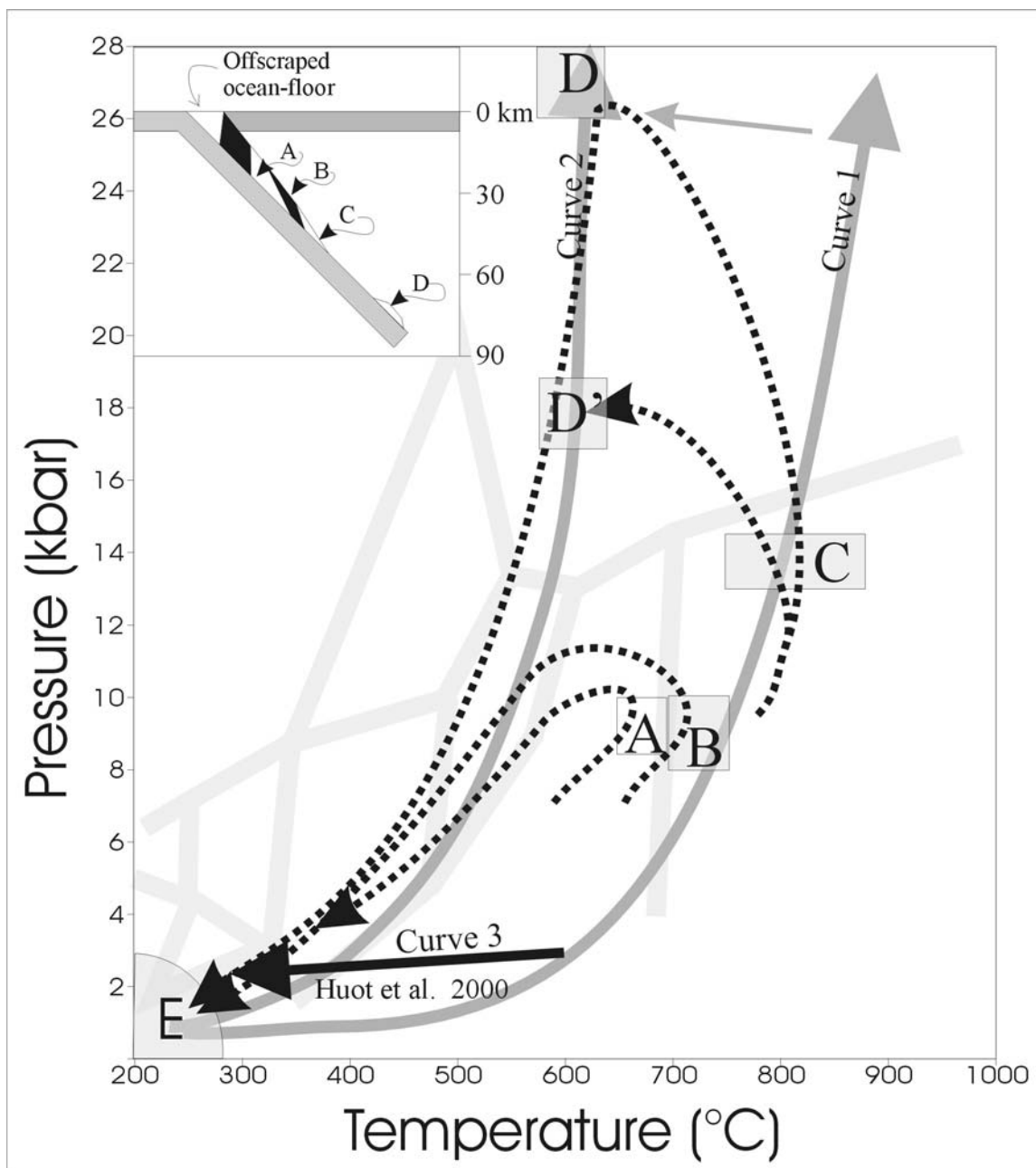
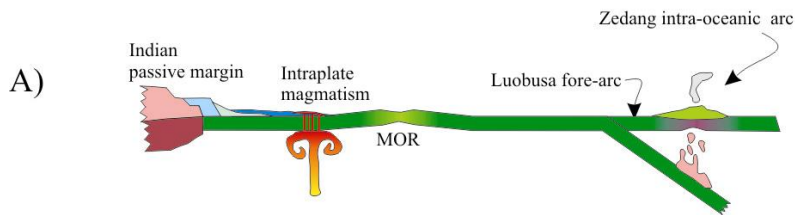
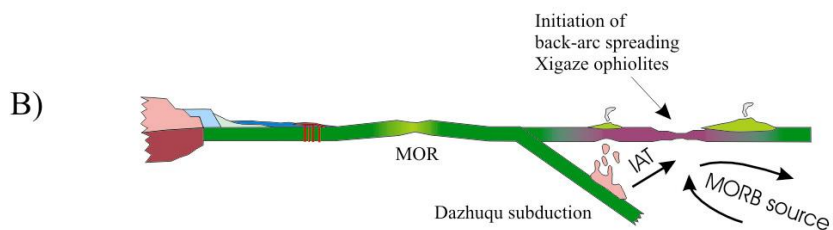


Figure 2.12

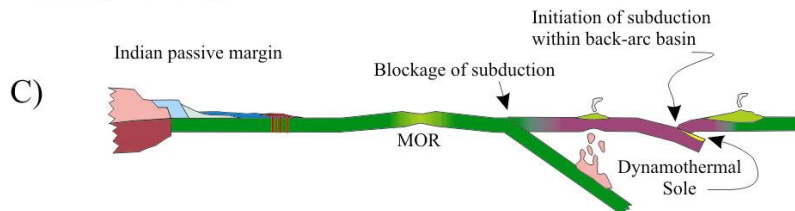
180-150 Ma



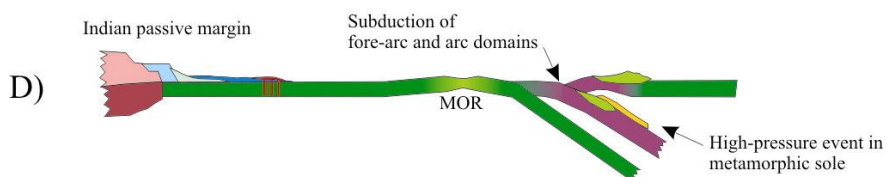
155-130



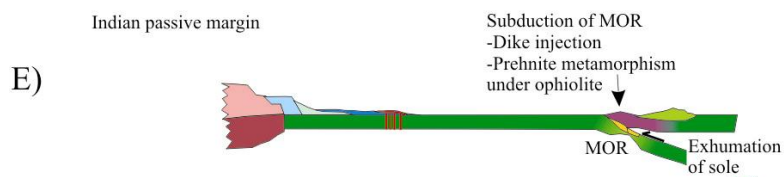
130-115



115-100



100-85



85-60

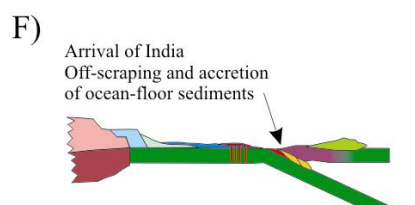


Figure 2.13

Chapter 3 : Complementary data

The following chapter presents data that were obtained from the Bainang and Buma amphibolites but that are not included in Chapter 2. The chapter focuses on geochemistry and geochronology of the amphibolite blocks. Those data will be framework of a companion paper to be submitted during the Summer of 2005.

3.1. Whole rock chemistry

Though they might deserve more attention, geochemical analyses are not fully explored in this manuscript. The reason is that major and trace element geochemistry of the highly foliated amphibolites from the ophiolitic mélange is strongly similar in almost all aspects to that of mafic rocks from the mélange (Huot et al., 2002; Dupuis et al., 2005a) and from the overlying ophiolite (Dubois-Côté et al., 2005). We therefore refer to those papers for a detailed petrological analysis. Major conclusions from these papers also stand for the highly foliated amphibolites. The following sections will provide a description of the results and will highlight the main geochemical features.

3.1.1. Analytical Method

Samples were analysed at Activation Laboratories Ltd in Ancaster, Ontario, Canada. Samples were crushed to -10 (1,7 mm) mesh and approximately 100 g were mechanically split and then pulverized in a mild steel ring and puck pulverizer to 95% -150 (106 microns) mesh. For major elements, a lithium metaborate/tetraborate fusion method was used. Major element contents were determined by ICP-AES. According to replicates and standards results (Appendix D, table D3), precision was typically better than $\pm 1,75\%$. Trace elements contents were determined by ICP-MS. Analytical precision, as determined on replicates and standards (Appendix D, table D4), was better than 10% for most analyses.

3.1.2. Major elements

Tables D1 and D2 from Appendix D show whole rock geochemistry of major and trace elements for 11 mafic rocks from Buma and 9 from Bainang. Among those, we find 4 garnet amphibolites, 5 banded amphibolites, 10 common amphibolites and one late diabasic dyke. Samples are grouped by location and amphibolite type except for sample LUS-02, a diabasic dyke, and sample LUS-16, an Mg-rich banded amphibolite. For classification and plotting purposes, major elements data have been recalculated on an anhydrous basis, with normalizing factor $\text{Fe}^{3+}/\text{FeTot}=0.15$. Relatively high and low values (internal comparison) for major elements are reported in petrographic Tables B1 and B2. Color code indicates which mineral phase would reflect high or low values.

Analyzed amphibolites are characterized by moderate to high Al_2O_3 content (9.73-16.22). High values lie between 15-17 wt. % while low values lie between 9-13 wt. %. All garnet-bearing samples show high Al_2O_3 contents. High values are also thought to reflect high plagioclase or prehnite modes, as observed in thin section (Tables B1-B2). Low Al_2O_3 contents are reflected by low plagioclase modes. SiO_2 contents are constrained between 43.33 and 54.26 wt.%. Low values are between 43 and 46 wt % and high values are between 50 and 55 wt. %. Low SiO_2 abundance would be reflected by low modes of plagioclase (Tables B1-B2). High SiO_2 contents either indicate high plagioclase modes, high clinopyroxene modes, presence of quartz or intense prehnitization (Tables B1-B2). CaO contents are high (7.76-17.34), though highest values can be associated with intense prehnitization, as observed in thin section. TiO_2 and P_2O_5 contents vary in the range of 0.97-1.81 and 0.08-0.25, respectively. For the intrusive sample LUS-02, Al_2O_3 and SiO_2 contents are high with oxide values of 16.2 wt.% and 53.9 wt%, while TiO_2 and P_2O_5 fall in the range of amphibolitic samples. Sample LUS-16 shows low Al_2O_3 composition with 9.54 wt% and a very low P_2O_5 content (0.02 wt%) for a very high MgO content of 14.51 %. High LOI (>2 wt%) are restricted to samples from Buma and to garnet-bearing samples.

As observed in Tables D1 and D2 (Appendix D), most samples have Mg# falling in the range of 70-50. One sample, LUS-16, doesn't fit in this group with a Mg# of 76.81, possibly indicating cumulative processes. The Mg# vs $\text{SiO}_2/\text{Al}_2\text{O}_3$ diagram of Kempton &

Harmond (1992) (figure 3.1) allows to differentiate different cumulative trends with elements that show low to very low mobility during metamorphism. Most of the samples plot in the primitive basalt field with their high Mg#, while some, from Bainang, describe a trend along the tholeiitic differentiation path. Sample LUS-02 , a diabasic dyke, would also result from tholeiitic differentiation. Two samples (BUM-23 and LUS-16, high Mg# common and banded amphibolites, respectively) seem to follow a different trend that could be explained by pyroxene accumulation. These samples, especially LUS-16 which has a very strong SiO₂/Al₂O₃ ratio and Mg#, should be treated with caution because they are metapyroxenites and do not reflect the composition of the initial basaltic liquid.

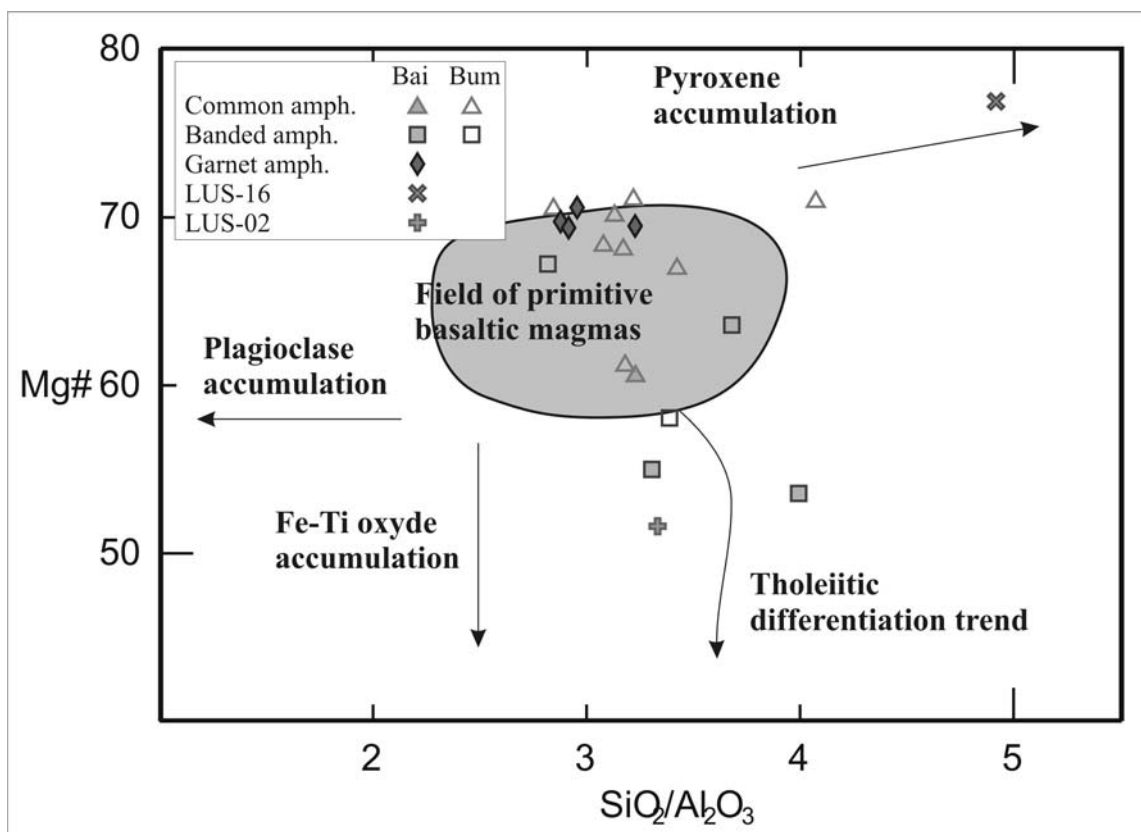


Figure 3.1 : Mg# vs SiO₂/Al₂O₃ diagram showing possible cumulative processes (modified from Kempton and Harmon 1992).

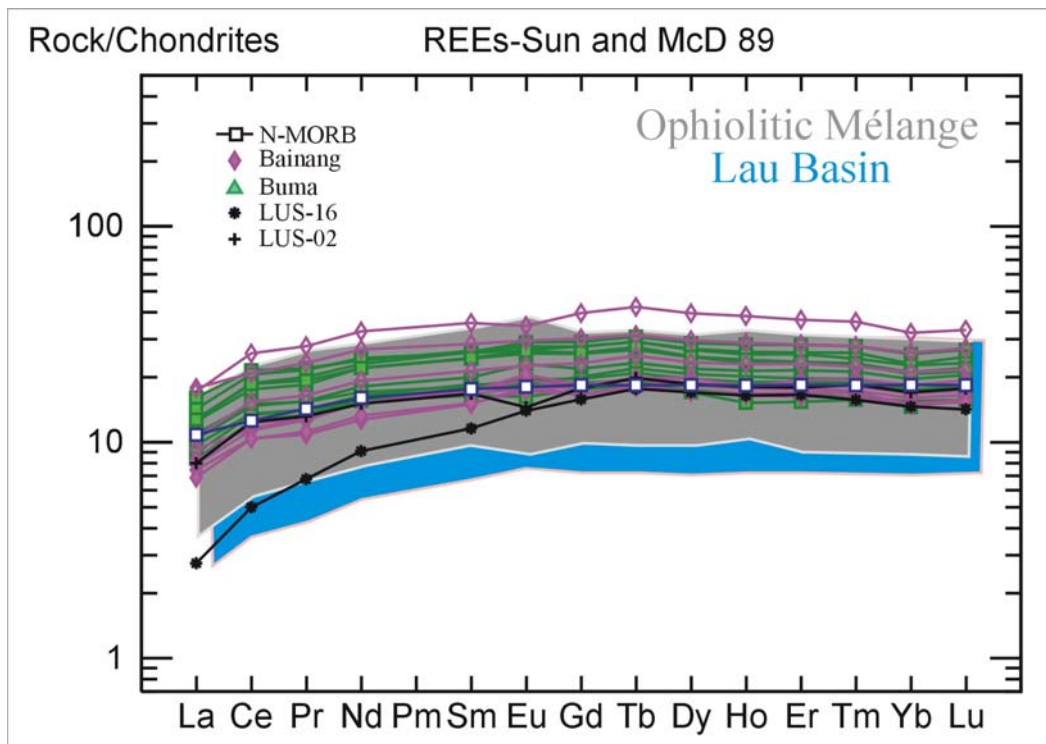


Figure 3.2 : REE patterns normalized to Chondrites for the highly foliated amphibolites from the ophiolitic mélange. LUS-16 is a high-Mg cpx amphibolite and LUS-02 is a dyke.

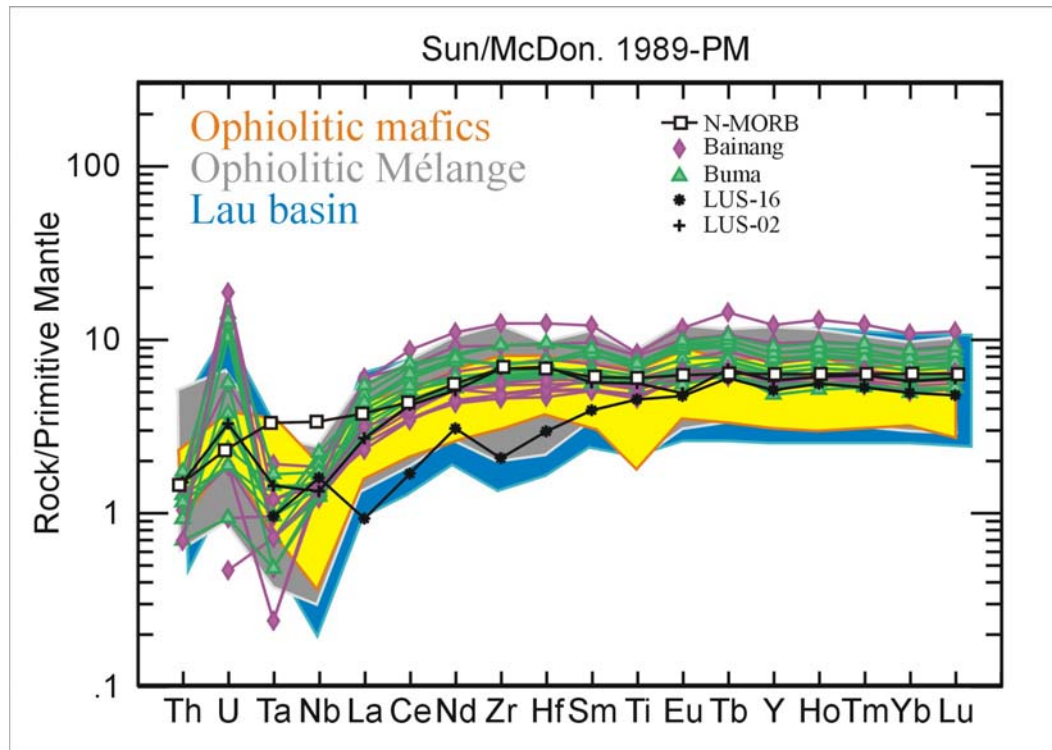


Figure 3.3 : Extended trace-element patterns normalized to primitive mantle for the highly foliated amphibolites from the ophiolitic mélange. LUS-16 is a high-Mg cpx amphibolite and LUS-02 is a dyke.

3.1.3. Trace elements

On chondrite-normalized REE patterns (figure 3.2), all samples (except for LUS-16 which is a cumulate) yielded parallel patterns, suggesting parental magmas. REE diagrams show a flat pattern with a slight depletion in LREE, similar to a typical N-MORB (Sun & McDonough 1989). Highest Mg# correspond to patterns with the lowest REE contents (not shown). We observe no significative Eu anomaly except for sample LUS-02, which is a diabasic dyke with plagioclase micro-phenocrysts. However, on primitive mantle-normalized multi-element patterns (figure 3.3), several anomalies distinguish the meta-basites from typical N-MORBs. We observe slight Ti and moderate Ta-Nb negative anomalies for all samples. Light depletion of LREE ($\text{La/Yb} = 0.65\text{-}0.97$) and mild HFSE decoupling in regard of MORBs ($\text{Ta/Th} = 0.33\text{-}0.65$) would suggest a mixing between IAT and MORB sources, as seen in back-arc basins and nascent intra-oceanic arcs. Geochemistry of highly foliated amphibolites correlates very well with geochemistry of other low-grade meta-basites from the mélange (Huot et al., 2002; Dupuis et al., 2005a), with overlying ophiolitic crust (Dubois-Côté et al., 2005) and with crustal magmatic rocks from the Lau basin (Ewart et al., 1998), an active back-arc basin near the Tonga trench.

3.1.4. Classification

The late metasomatic event that affected all samples and retrogressed all plagioclase prevents us from using traditional discrimination diagrams based on major elements. Na and Ca mobility would induce errors in alkali-based classification. Instead, we show the Zr/Ti vs Nb/Y diagram of Winchester & Floyd (1977) revised by Pearce (1996) which

classifies the rocks according to their alkalinity and stage of differentiation avoiding the use of mobile elements (figure 3.4). All samples, including the diabasic dyke (LUS-02) and excluding the metapyroxenite (LUS-16), plot in the field of basalts or basaltic andesites.

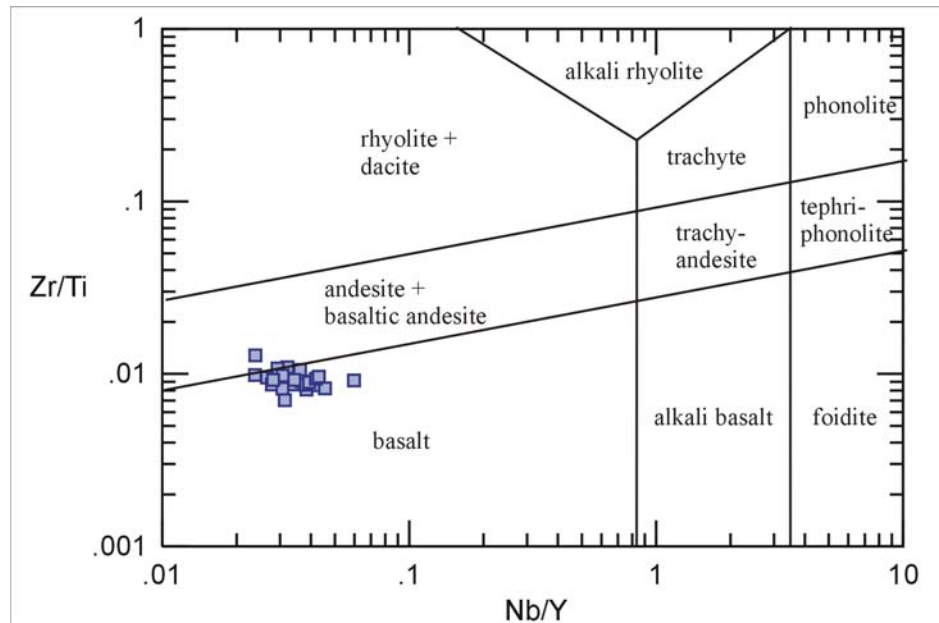


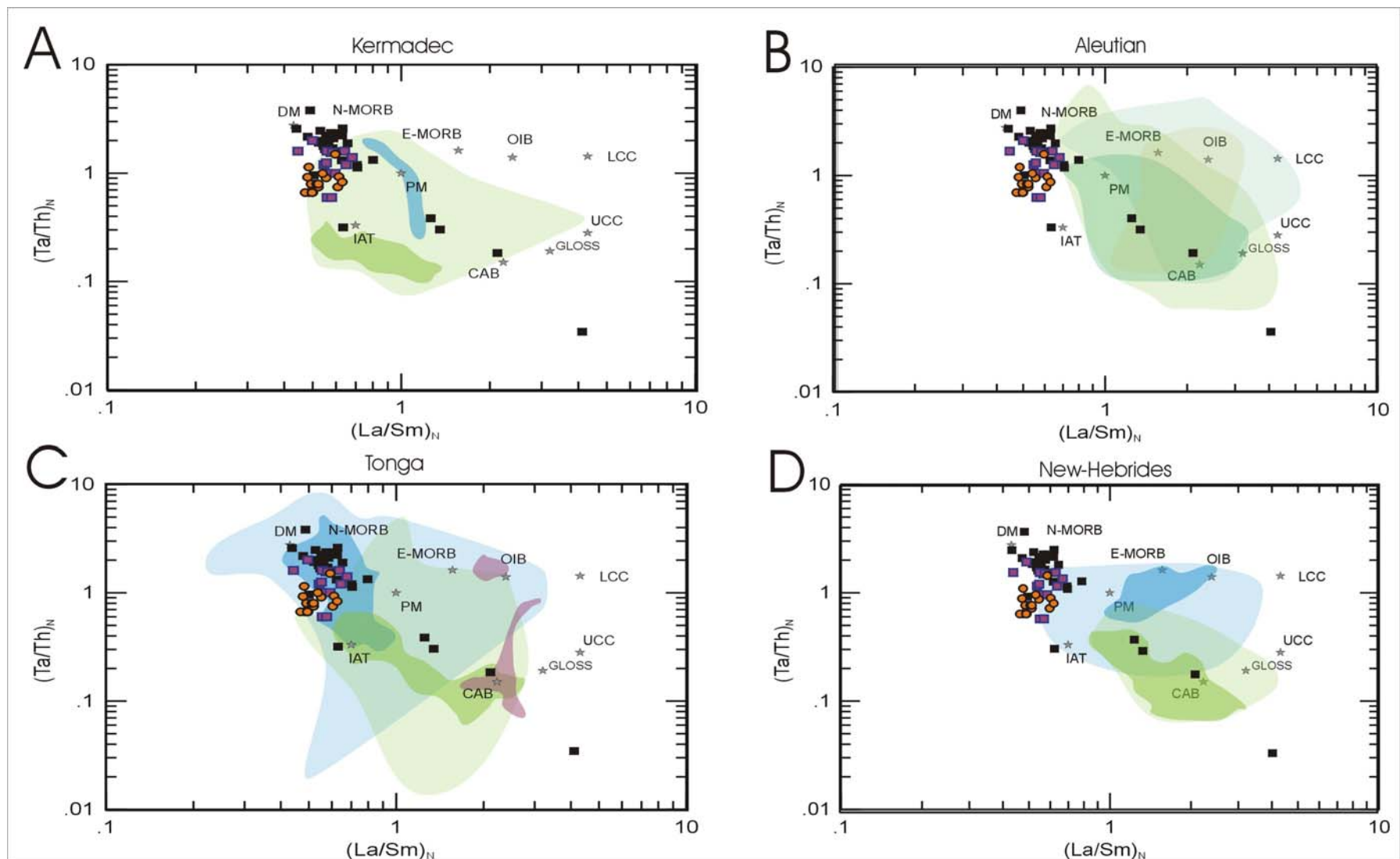
Figure 3.4 : Discrimination diagram of Winchester & Floyd (1977) modified by Pearce (1996). LUS-16 is not plotted.

3.1.5. Geochemistry and geological setting

Figure 3.5 is a very good mean to illustrate the different chemical behaviours related to many tectonic settings, including partial melting, mixing of magmas and assimilation. La and Sm are Light Rare Earth Elements (LREE). These elements are considered as incompatible and will be enriched in the volatiles or in the melt fraction of partially melting rocks. Since La is more incompatible than Sm, a strong ratio should reflect a high degree of partial melting. Ta and Th are High Field Strength Element (HFSE). HFSE are considered as incompatible elements that will be bound to the liquid fraction of the partially melting rocks. Decoupling between Ta and Th occurs when a particular mineral phase forms in the restitic fraction of the melting rock. These minerals (i.e. garnet and rutile) have sites that

allow incorporation of Ta, Nb and some other incompatible elements within the crystal structure. In a suprasubduction zone setting, metamorphic transformations affecting the downgoing slab will cause appearance of such mineral phases. Therefore, magmas issued from partial melting of the subducting plate and of the overlying mantle wedge will be depleted in Ta in regard of Th, which is not retained in the solid fraction. Accordingly, low Ta/Th ratios will reflect proximity to a subduction zone.

On figure 3.5, we also plotted samples from the ophiolitic massifs (Dubois-Côté et al., 2005) and from the ophiolitic mélange (Dupuis et al., 2005a). Most mafic rocks found in the ophiolitic crust, mantle and mélange (including highly foliated amphibolites) plot between the N-MORB pole and the island arc tholeiite end-member. This means all rocks underwent the same LREE enrichment but experienced slight differences lying in the intensity of their Ta negative anomaly. Most mafic blocks from the mélange plot on or very near the N-MORB pole whereas all foliated amphibolites plot halfway from the IAT. Rocks from the ophiolitic crust and mantle are intermediate. As noted by Dupuis et al. (2005a), such a chemical behaviour is reminiscent of back-arc spreading centers.



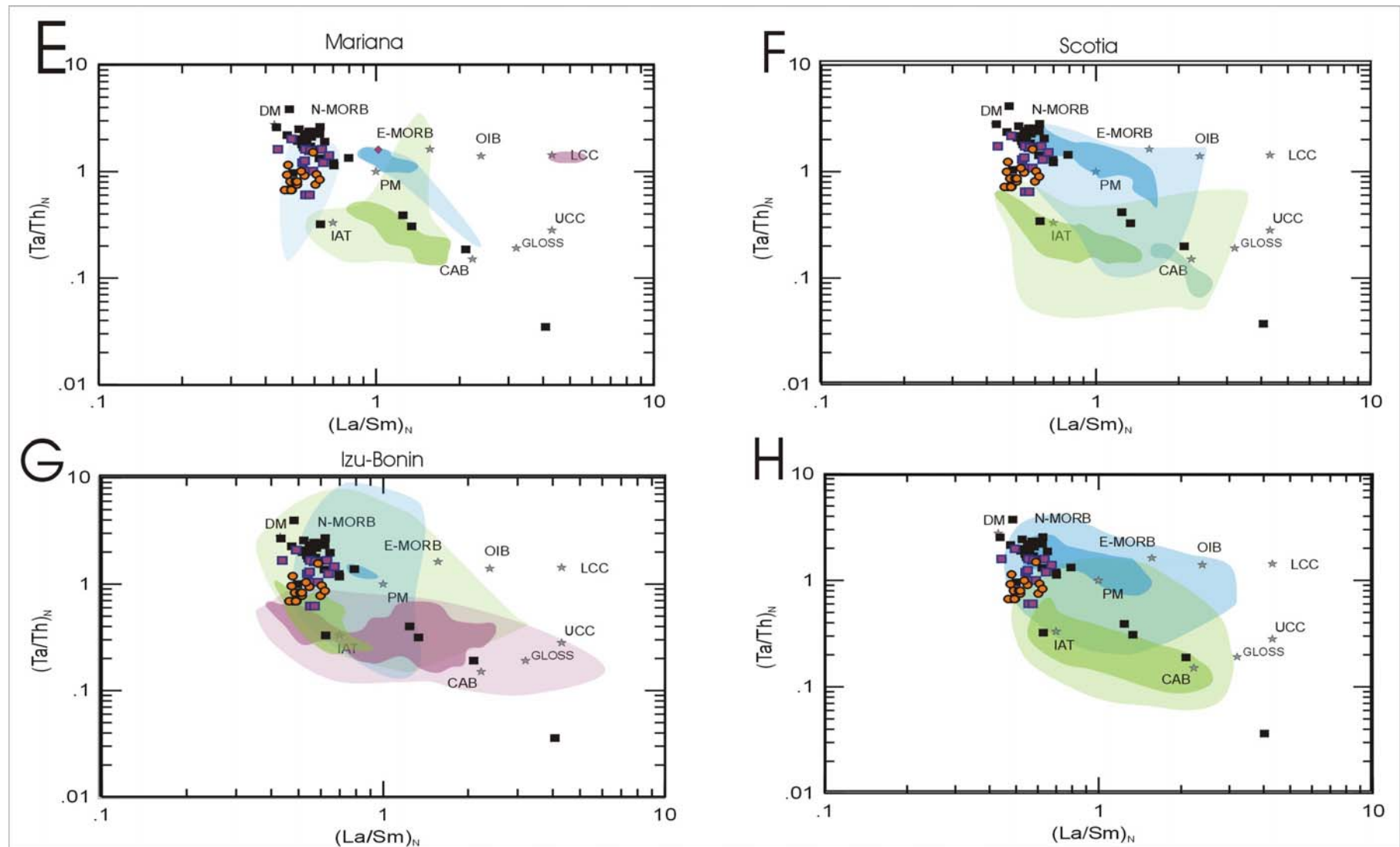


Figure 3.5 : Ta/Th (CN) versus La/Sm (CN) diagram for mafic rocks from the ophiolitic massifs (purple squares, Dubois-Côté et al., 2005), from the ophiolitic mélange (black squares, Dupuis et al., 2005) and for the highly foliated amphibolites from the ophiolitic mélange (orange circles, this study). DM = depleted mantle from Mckenzie & O'Nions (1991) except for Ta and Th from Chauvel et al. (1992). PM (primitive mantle), N-MORB, E-MORB and OIB from Sun & McDonough (1989). IAT (island-arc tholeiite) and CAB (calc-alkaline basalt) from Sun (1980). LCC = lower continental crust from Weaver & Tarney (1984). UCC (upper continental crust) and CC (average continental crust) from Taylor & McLennan (1981). GLOSS (global subducting sediment) from Plank & Langmuir (1998). Data from the YSZSZ ophiolites are plotted against fields compiled for different currently active intraoceanic convergent margins. Geochemical data are from the GEOROC database. Blue fields are for back-arc basins and rifts, green fields are from arc rocks and purple fields are from the fore-arc or trench domains.

When compared with individual arcs, there is a clear match between the geochemistry of the YSZSZ ophiolites and the Lau Basin (Tonga arc). The Lau Basin is the only back-arc from all studied areas that extends towards the IAT pole and not towards the OIB. Such a chemical behaviour can be explained by a peculiar evolution of the basin including an opening in the frontal part of the arc and a following migration of the volcanic front from the remnant arc (Lau Ridge) through the Lau Basin towards the frontal remnant arc (Tonga Ridge) (Hawkins et al., 1995). Therefore, it would suggest that the YSZSZ ophiolites and its metamorphic sole originate from a back-arc basin that opened in the frontal part of a proto-arc. However, when compared to overall back-arc and arc compositions (figure 3.5 H), data from the YSZSZ ophiolites and metamorphic sole rather indicate gradation from a true back-arc spreading center (rocks from the mélange) to rocks from an island arc (metamorphic sole) with rocks from the ophiolite being intermediate. Several workers have proposed that such a zonation might be observed from the spreading center to the margins of a back-arc basin (Hawkins, 1995, and reference therein). However, most agree that the distribution of sampling sites is too scarce to allow such an interpretation. In any case, figure 3.5 suggests that mafic rocks from the ophiolitic massifs, from the ophiolitic mélange and from the metamorphic sole most probably all come from a distinct unique back-arc basin.

3.2. Geochronology

3.2.1. Analytical Method

Selected samples were processed for $^{40}\text{Ar}/^{39}\text{Ar}$ analysis of amphiboles by standard mineral separation techniques, including hand-picking of clear, unaltered crystals in the size range 0.5 to 1 mm. Individual mineral separates were loaded into aluminum foil packets along with a single grain of Fish Canyon Tuff Sanidine (FCT-SAN) to act as flux monitor (apparent age = 28.03 ± 0.28 Ma; Renne et al., 1998). The samples were irradiated for 12 hours at the research reactor of McMaster University in a fast neutron flux of approximately 3×10^{16} neutrons/cm².

Laser $^{40}\text{Ar}/^{39}\text{Ar}$ step-heating analysis was carried out at the Geological Survey of Canada laboratories in Ottawa, Ontario. Upon return from the reactor, samples were split into several aliquots. Heating of individual sample aliquots in steps of increasing temperature was achieved using a Merchantek MIR10 10W CO₂ laser equipped with a 2 mm x 2 mm flat-field lens. The released Ar gas was analyzed with the use of a VG3600 gas source mass spectrometer. Details of data collection protocols can be found in Villeneuve and MacIntyre (1997) and Villeneuve et al. (2000). Error analysis on individual steps follows numerical error analysis routines outlined in Scaillet (2000); error analysis on grouped data follows algebraic methods of Roddick (1988).

Each gas-release spectrum plotted contains step-heating data from two aliquots, alternately shaded and normalized to the total volume of ^{39}Ar released. Such plots provide a visual image of replicated heating profiles, evidence for Ar-loss in the low temperature steps, and the error and apparent age of each step. No evidence for excess ^{40}Ar was observed in any of the samples and, therefore, all regressions are assumed to pass through the $^{40}\text{Ar}/^{36}\text{Ar}$ value for atmospheric air (295.5). All errors are quoted at the 2σ level of uncertainty.

3.2.2. Results

Three samples were chosen for Ar³⁹/Ar⁴⁰ dating. Samples were chosen with respect to their provenance and mineralogy. For Bainang, sample BAI-18 is a common amphibolite with a very simple assemblage (Hb+Pl±Sp+Ap). Amphiboles are tschermakitic-hornblende or tschermakite with a restrained compositional range. Sample LUS-07 is a garnet amphibolite which contains the three types of amphiboles; i.e. Mg-hornblende, tschermakite and Al-tschermakite. Last type is unlikely to be analyzed for Argon for it is bound to garnet grains which were removed during crystal selection. One homogeneous sample was chosen from Buma. Sample BUM-05 is a common amphibolite containing mostly brown tschermakitic hornblende but also some Mg-hornblende. Results are shown in figure 3.6. Ordinate axis shows % of argon released while abscis axis shows both age of released gas and Ca/K ratio of burning amphibole. Large errors on individual steps are the result of low-K content compounded by high Ca. However, reproducible plateaus confirm the ages for all samples. Homogeneous prograde tschermakites from sample BAI-18 yielded a plateau age of 123.6 ± 2.9 Ma. Amphiboles from sample BUM-05 are also homogeneous with a plateau age of 127.7 ± 2.2 Ma. Sample LUS-07 has a relatively heterogeneous amphibole population but yielded a reproducible plateau age of 127.4 ± 2.3 .

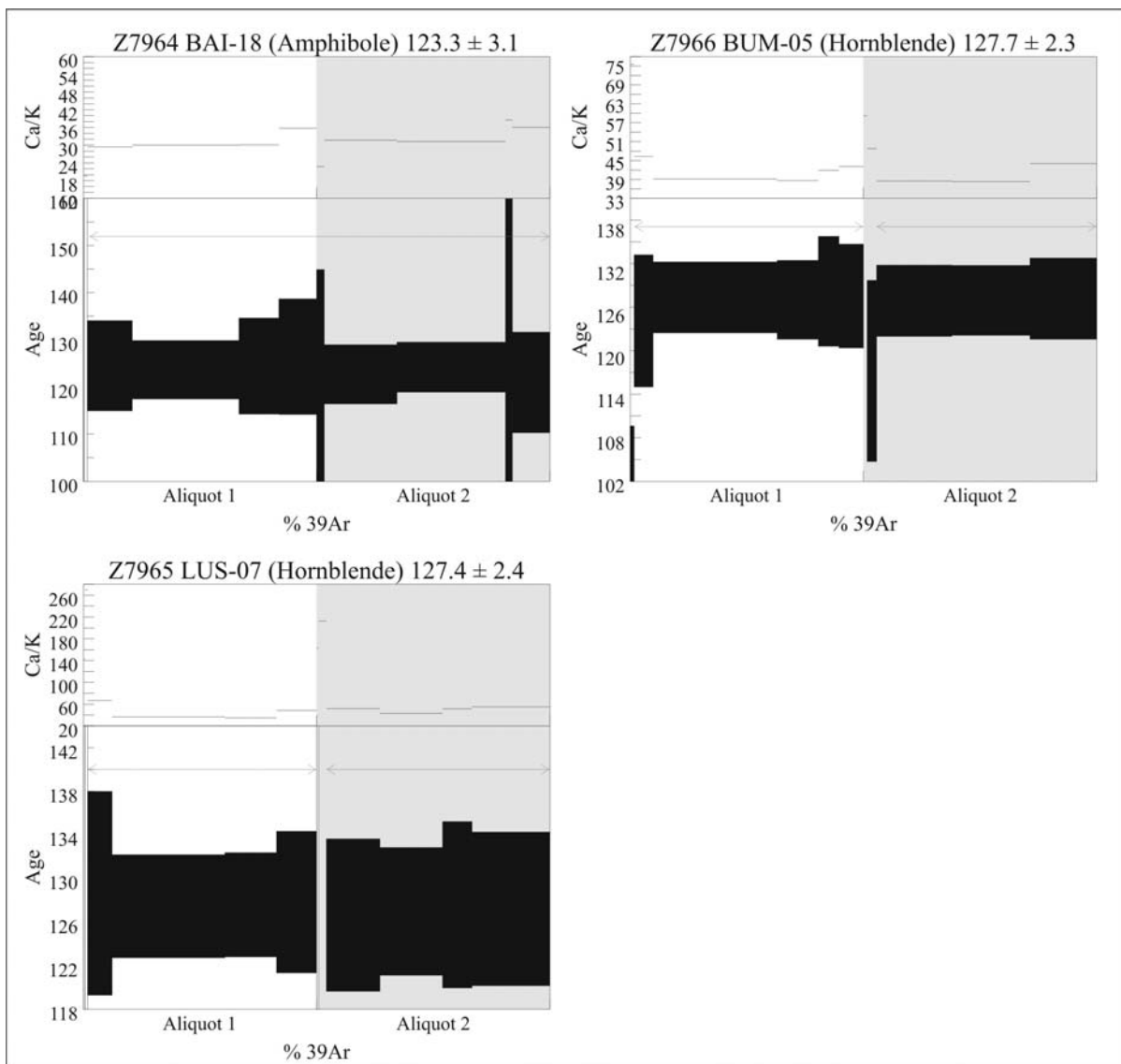


Figure 3.6 : Ar/Ar spectrum for amphiboles from Bainang and Buma with Ca/K plot of released gas.

Chapter 4 : Discussion and conclusions

Chapter 4 includes a complete discussion bearing on all available data for the Buma and Bainang highly foliated amphibolites. These data include those from the Chapter 2 paper together with data presented in Chapter 3.

4.1. Complete discussion

4.1.1. Geodynamic significance

Highly foliated blocks of high-grade amphibolites are found as clasts in the serpentinite matrix mélange underlying the Yarlung Zangbo Ophiolites, Tibet. The mélange is interpreted to result from the tectonical dismemberment of the ophiolite during its obduction. Therefore, rare occurrences of highly foliated amphibolite blocks may represent a dismembered dynamothermal sole. Pressure and temperature estimates for peak metamorphic conditions of those blocks indicate burial of warm mafic crust beneath a very hot hanging wall. Counter-clockwise P-T-t path for the highly foliated amphibolites would fit with metamorphism during the inception of subduction at a spreading center (Guilmette et al. submitted). Undistinguishable ages for the ophiolite and its sole also fits inception of a subduction at a spreading center. Geochemistry of the metamorphic sole and of the ophiolites indicate that they were both created within a back-arc basin. The main geodynamical implication for the highly foliated amphibolites from the ophiolitic mélange beneath the YZSZ ophiolites would then be that there was inception of a subduction within an opening back-arc basin near 127 Ma. Secondary implications would include subduction of a buoyant body to explain high-pressure overprint and subduction of a magmatic center causing dike injection and Ca-metasomatism.

4.1.2. Geodynamic Model

Figure 4.1 is a hypothetic model for the destruction of Meso and Neo-Tethyan domains during Jurassic-Cretaceous times. Continental masses and hypothetic MOR positions are taken from Scotese et al. (1988) for Early Cretaceous to Paleocene. Position of India is from Klootjwick et al. (1992). The geodynamic model proposed here is mostly based on data available from the Central Section of the YZSZ near Xigaze and from the nearby Lhasa block units, though major events for the Ladakh and Zedang areas and from the Bangong-Nujiang Suture Zone are shown as well. Reconstruction of geodynamical evolution starts with the opening of Tethys and the closure of Paleo-Tethys during Triassic times (figure 4.1a). Paleo-Tethys is the oceanic domain that was mostly consumed in one or many Triassic-Jurassic subductions between the Lhasa block and Eurasia (figure 4.1b). Northward motion of Tibet was induced by rifting from Gondwana and then ocean-floor spreading in the Tethys oceanic basin. The arrival of the Lhasa block near the shores of Eurasia caused a slowing in the subduction rate, implying a rearrangement in tectonic plate motions and boundaries. Those changes are mostly observed as the inception of an intra-oceanic subduction zone system within Tethys (figure 4.1b). Accretion of SSZ lithosphere above this subduction can be seen as the Zedang mature arc and the Luobusa fore-arc. In the meanwhile, intra-plate magmatism occurred in the southern part of Tethys, near the edge of the Indian plate, as seen in the OIB found within Jurassic off-scraped radiolarite slices beneath the Yarlung Zangbo ophiolites (Zyabrev et al., 2004; Dupuis et al., 2005a; 2005b). During Latest Jurassic to Early Cretaceous times, tectonic plate motions within Tethys can mostly be attributed to the Tethys Mid Ocean Ridge (MOR) and to the eastward motion of Africa relative to Eurasia (Patriat et al., 1982). Oblique convergence induced back-arc basin opening and intraoceanic arc build-up within Tethys (figure 4.1c), as seen in the Nidar, the Spontang (130-110 Ma arc activity, Mahéo et al., 2003) and the Yarlung Zangbo ophiolites. It is not sure if the subduction responsible for those Early Cretaceous tholeiitic domains is the same that allowed surrection of the Jurassic calc-alkaline and even shoshonitic (Aitchison et al., 2003) volcaniclastic Zedang arc (163-150 Ma, McDermid et al., 2002). Onstart of spreading within the back-arc basin seems to be synchronous with initiation of subduction beneath the Lhasa block (figure 4.1b), as deduced from the Sangri

group volcanics. Development of the intraoceanic SSZ domain is disturbed by a major tectonic event during Early Cretaceous, near 130-125 Ma. Metamorphic sole development beneath the Yarlung Zangbo ophiolites indicates inception of subduction within the back-arc basin near 125 Ma (figure 4.1d). This age correlates very well with Aptian-Albian trench-fill sediments and tuffs accreted directly beneath the Yarlung Zangbo ophiolites in the Bainang subduction complex (Zyabrev et al., 2004). It also correlates with the Barremian-Aptian radiolarite cover and the 120 ± 10 Ma and 126 ± 1.5 Ma Pb-Pb ages from the Yarlung Zangbo ophiolites. Such an overlap in sole-ophiolite age relationship is not unusual and would indicate inception of subduction near or at the back-arc spreading center where the ophiolites were created (Wakabayashi & Dilek, 2000 and reference therein). Mueller & Phillips (1991) showed that inception of a new subduction zone requires blockage of an early subduction by buoyant material (i.e. blockage of the Jurassic subduction, figure 4.1d). Source of blockage within Tethys might have been another intraoceanic arc, a continental fragment or a continental margin. However, no evidence of a continental block within Tethys has ever been described. It is also very unlikely that Indian passive margin might have been present at these latitudes ($10\text{-}20^\circ$ N) during that time. Presence of other older southern intraoceanic arc systems is possible, as seen in the Zedong arc. Thermo-mechanical modeling also required blockage of the early subduction to obtain inception of subduction in the back-arc basin (Boutelier et al., 2003). It also suggested that trapped fore-arc, arc and half of the back-arc domains might be subducted along this new subduction zone (figure 4.1e). Such an event would provide explanation for the relatively stronger IAT geochemical signature in the sole, for the high-pressure overprint observed in some garnet amphibolites and for the presence of some arc-related CAB blocks in the mélange (Dupuis et al., 2005a). Subduction of the arc and of the source of blockage could also explain the major erosional discordance observed from 114 to 74 Ma in the hanging-wall of the Bainang subduction (Ziabrev et al., 2004). However, Ziabrev et al. (2004) rather proposed subduction of the Tethys MOR, a major topographic accident, as an explanation for the erosional discordance. In a geometric point of view, subduction of the Tethys MOR is necessary to stop major spreading within Tethys and allow Indian ocean opening and movement of India towards Tibet at a speed of 10 cm/yr (Patriat et al., 1982). According to paleo-magnetic data, those events occurred during Late Cretaceous times, near 85 Ma

(Scotese et al., 1988; Patriat et al., 1982; Patriat & Achache, 1984). Subduction of the Tethys MOR at that time would then also provide explanation for the 80-90 Ma metamorphic ages (Zyabrev et al., 2004) obtained from amphibole-bearing blocks in the mélange (Wang et al., 1987; Malpas et al., 2003). In our model, we propose, for simplification reasons, that source of blockage was the Tethys MOR (figure 4.1 d-e-f), though we are aware that it could be another unknown buoyant body. In anyways, subduction of the arc and of the Tethys MOR beneath the Yarlung Zangbo ophiolites provide the magmatic center needed to explain the injection of dikes through the sole. However, it seems hazardous to determine which center provided the magma. Present day tectonics show that magmas erupting from a subducting MOR can have SSZ geochemical signatures as well (Taitao peninsula, Sturm et al., 2000). Barometric calculations and the presence of prehnite prior to injection suggest that dikes crystallized at shallow depth, which implies that the sole was already exhumed at that time. Accordingly, it seems more conceivable that subduction of arc caused high-P metamorphism then exhumation (figure 4.1 e) and that subduction of MOR caused intrusion of dikes and circulation of magmatic water with prehnitization.

In this model, asperities present between India and Eurasia are being destroyed along a complex intraoceanic subduction system from about 112 to 80 Ma. It is very likely that subduction rate along this system must have been slowed by augmentation of strain within the subduction plane. Such a slowing would have to be compensated somewhere within the great Tethys oceanic domain. Indeed, tectonic changes from the Albian (about 112 Ma) are observable within the Lhasa block as the onstart of fore-arc basin turbidite deposition (Xigaze group) and extrusion of the Linzizong volcanics (110-80 Ma, Coulon et al., 1986) (figure 4.1 d). We propose that such changes might reflect an acceleration of the subduction rate along the Lhasa subduction. Acceleration of Lhasa subduction and deceleration of Bainang subduction between 112 and about 80 Ma probably resulted in northward traveling of the Yarlung Zangbo ophiolites toward the shores of Tibet. Once the Tethys MOR disappeared (figure 4.1 f), subduction rate within the Bainang subduction accelerated again. Slices of passive margin-derived distal sediments and OIB basalts present in the southern part of Tethys were then accreted to the hangingwall of the Bainang subduction complex (southern tract, Zyabrev et al., 2004; Yamdrock mélange, Dupuis et

al., 2005a; 2005b) (figure 4.1 f). This proves that a large portion of Tethys was destroyed along the Bainang subduction during Late Cretaceous. At that time, it is very likely that Yarlung Zangbo ophiolites and the underlying Bainang subduction complex were now situated near the coasts of Tibet, trapped in a fore-arc setting (figure 4.1 f). Back-arc ophiolites trapped in a fore-arc setting have been observed in the Coast Range area as well (Wakabayashi & Dilek, 2000). Acceleration of the subduction rate within the Bainang subduction and stopping of the spreading within Tethys possibly caused the demise of the Lhasa subduction. This would explain why Late Cretaceous subduction of Tethys lithosphere along the Bainang subduction would be coeval with extrusion and intrusion of SSZ magmas within the Lhasa block (Gangdese batholith, 94-40 Ma, Schaefer et al., 1984; Malpas et al., 2003; Linzizong volcanics, 110-80, 60-40 Ma, Coulon et al., 1986) (figure 4.1 d-e-f). Next stage would be the arrival of India and obduction. Low-grade metamorphism observed within the Indian passive margin units indicate thrusting of the ophiolitic napes over India near 50 Ma (Burg, 1983; Burg & Chen 1984; Burg et al., 1987; Ratschbacher et al., 1994) (figure 4.1 g). This probably corresponds to the dismemberment of ophiolitic napes which created the ophiolitic mélange (Dupuis et al., 2005a; 2005c; Huot et al., 2002; Girardeau et al., 1985) and to the deposition of the Liuqu conglomerate in strikeslip basins (Davis et al., 2002).

However, all of this model is currently under revision for it would seem that the 10-20°N paleo-latitude of the Yarlung Zangbo ophiolite from Pozzi et al. (1984) is wrong. New data would rather indicate equatorial latitudes (Abrajevitch et al., 2005). Such data only affect the « trapping in a fore-arc setting to the Gangdese arc » hypothesis and do not refute or confirm the closure of the back-arc basin near 125 Ma.

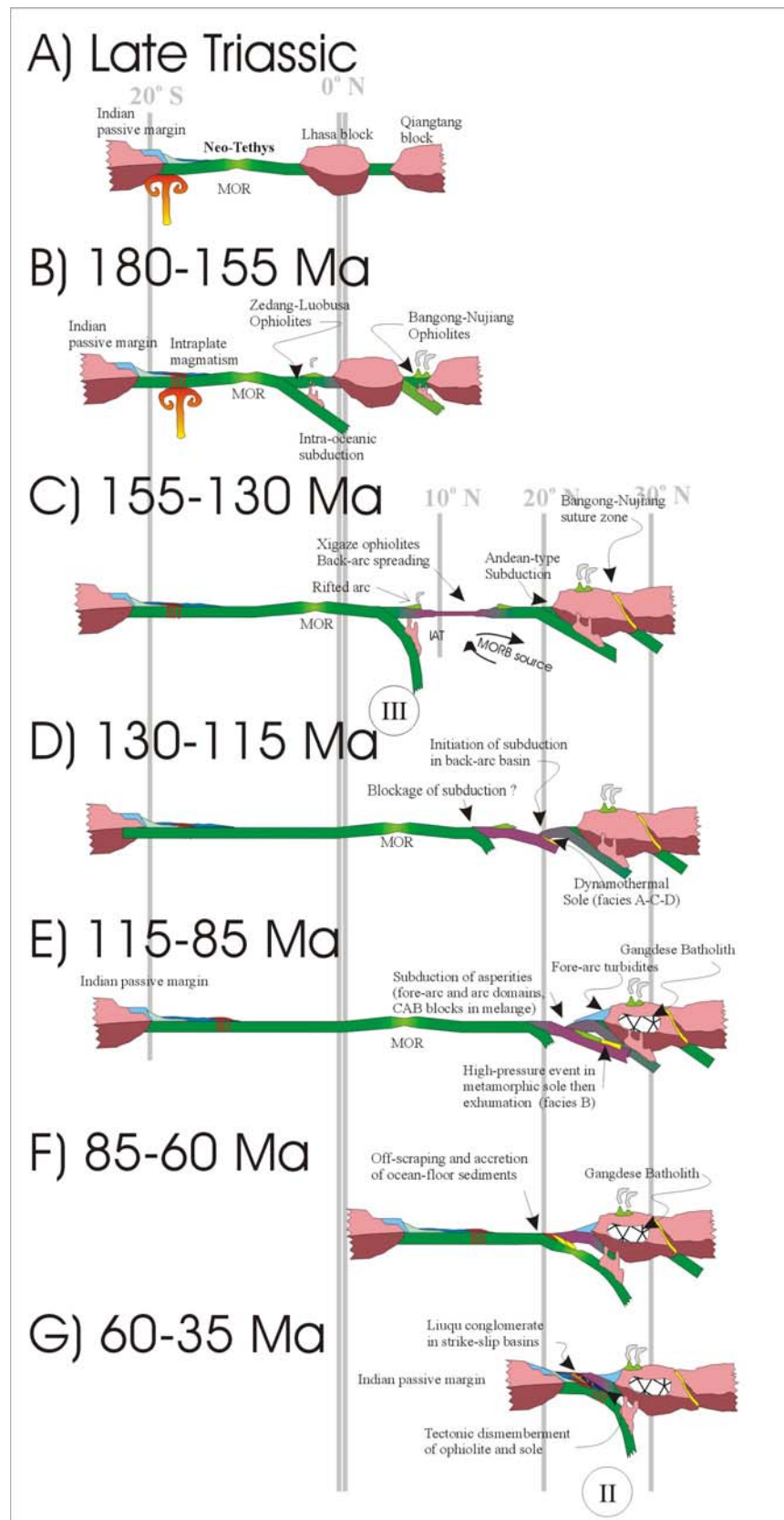


Figure 4.1 : Geodynamic evolution model for the YZSZ ophiolites.

Conclusion

Highly foliated amphibolite blocks are found as clasts in a sheared serpentine ophiolitic mélange. This mélange is found beneath the Yarlung Zangbo ophiolites. It has been formed by tectonic disruption of the lower part of the ophiolite sheets during obduction. Amphibolite blocks were probably part of the upper section of a dismembered dynamothermal sole. Geochemistry shows that this sole is made of tholeiitic oceanic crust created within a SSZ (Back-Arc Basin Basalts; BABBs) similar to the one where the Yarlung Zangbo ophiolites originate from. Metamorphism of the sole suggest inception of a new subduction within the back-arc basin at 127 Ma. Oxygen isotopes reveal the presence of a metamorphic fluid at that time, possibly derived from dehydration of subducted crust. Creation of this new subduction zone within an already existing supra-subduction zone requires blockage of the early subduction. High-pressure retrograde event and switch from accretion to erosion in the hanging wall of the subduction point towards subduction of a thickened oceanic lithosphere from 114 Ma to about 85 Ma. Subduction of an arc domain is supported by the presence of some calc-alkaline blocks in the mélange but remains unclear. The source of blockage must have been subducted too. Hypothesis of the subduction of a MOR near 80 Ma is not rejected for the sole has recorded intrusion of dikes after exhumation. Sole and other blocks in the mélange also recorded a prehnite metamorphic event. This event could be related to the intrusion of the dikes and to the circulation of low-temperature fluids, as shown by oxygen isotopes. Once those obstacles were subducted, accretion in the hanging wall started again. Passive margin sediments were off-scraped until the ophiolite and the passive margin were thrust onto the Indian foreland near 50 Ma. This episode possibly corresponds to dismemberment of the base of the ophiolite as well as its sole.

These new data about the upper section of a now dismembered Tethyan dynamothermal sole show that not all ophiolites developed near the continental margin where they were emplaced. The Yarlung Zangbo ophiolites seem to have developed >4000 km away from the site where they were emplaced (Indian passive margin). However, it could be argued that emplacement occurs at the very inception of an underlying subduction. In such a case,

the Yarlung Zangbo ophiolites have first been emplaced over the Bainang terrane subduction complex. It can then be said that during Early to Late Cretaceous, the Yarlung Zangbo ophiolites evolved mainly as a Cordilleran-type ophiolite. Destruction of Tethys and Neo-Tethys along the many Jurassic-Cretaceous subduction zones led to the collision between India and Eurasia. During this event, Yarlung Zangbo ophiolites underwent the second stage of their emplacement as Tethyan-type ophiolites thrusted over the Indian passive margin. Such a scenario shows 1) that Ar/Ar metamorphic ages of soles must not automatically be associated to obduction, 2) that current ophiolite classification does not refer to the nature of the ophiolite but rather to its evolution, Tethyan-type ophiolites being the final stage. Finally, age and geodynamic differences between the Xigaze and Zedang ophiolites outline the dangers of interpreting the different units along the YZSZ as continuous terranes. Tethys and Neo-Tethys were most likely a very complex oceanic domain and more geochronological constrains are needed to obtain a more realistic geodynamic model.

Complete references

Abrajevitch, A., Ali J. R., Aitchison, J. C., Badengzhu, Davis, A. D., Liu, J., Ziabrev, S. V., 2005. Neotethys and the India–Asia collision: Insights from a palaeomagnetic study of the Dazhuqu ophiolite, southern Tibet. *Earth and Planetary Science Letters*, **233**, p. 87-102

Aitchison, J. C., Badengzhu, Davis, A. M., Liu J., Luo H., Malpas, J. G et al. 2000. Remnants of a Cretaceous intra-oceanic subduction system within the Yarlung-Zangbo Suture (southern Tibet). *Earth and Planetary Science Letters*, **183**, p. 231-244

Aitchison, J. C., Davis, A. M., Abrajevitch, A., Ali, J., Badengzhu, Liu J., Luo H., McDermid, I., Ziabrev, S. 2003. Stratigraphic and Sedimentologic constraints on the age and tectonic evolution of the Neo-tethyan ophiolites along the Yarlung Zangbo suture zone, Tibet. In: Dylek, Y., Robinson, P.T. (Eds.), Ophiolites in Earth History. Geological Society, London, Special Publications **218**, p. 147-164.

Allègre, C.J., Courtillot, V., Tapponnier, P., Hirn, A., Mattauer, M., Coulon, et al. 1984. Structure and evolution of the Himalaya-Tibet orogenic belt. *Nature*, **307**, p. 17-22.

Berman, R. G., 1988. Internally-consistent thermodynamic data for minerals in the system Na (sub 2) O-K (sub 2) O-CaO-MgO-FeO-Fe (sub 2) O (sub 3) -Al (sub 2) O (sub 3) -SiO (sub 2) -TiO (sub 2) -H (sub 2) O-CO (sub 2). *Journal of Petrology*, **29**, p. 445-522

Berman, R. G., 1990. Mixing properties of Ca-Mg-Fe-Mn garnets. *American Mineralogist*, **75**, p. 328-344

Berman, R. G., 1991. Thermobarometry using multi-equilibrium calculations; a new technique, with petrological applications. Gordon, T. M, Martin, R. F. (Eds.) Quantitative methods in petrology; an issue in honor of Hugh J. Greenwood. *The Canadian Mineralogist*, **29**, Part 4, p. 833-855

Boutelier, D., Chemenda, A., Burg, J. P., 2003. Subduction versus accretion of intra-oceanic volcanic arcs; insight from thermo-mechanical analogue experiments. *Earth and Planetary Science Letters*, **212**, p. 31-45

Bucher, K., Frey, M., 1994. Petrogenesis of Metamorphic Rocks: Complete revision of Winkler's Textbook, 6th edition. Springer-Verlag, Berlin, 318 p.

Burg, J. P., 1983. Tectogenese comparee de deux segments de chaine de collision; le sud du Tibet (suture du Tsangpo), la chaine hercynienne en Europe (sutures du Massif Central); Compared tectogenesis of two segments of collision chain; southern Tibet (Tsangpo suture zone), European Hercynian Chain; Central Massif suture zones. p. (Pagination mult. [401 p.]),

Burg, J. P., Leyreloup, A., Girardeau, J., Chen, G. M., 1987. Structure and metamorphism of a tectonically thickened continental crust; the Yalu Tsangpo suture zone (Tibet). In : Oxburgh, E. R., Yardley, B. W. D., England, Philip C. (Eds.), Tectonic settings of regional metamorphism, *Philosophical Transactions of the Royal Society of London, Series A: Mathematical and Physical Sciences*, **321**, p. 67-86

Burg, J.P., Chen, G.M., 1984. Tectonics and structural zonation of southern Tibet, China. *Nature*, **311**, p. 219-223.

Chang, C., 1984. Les caractéristiques tectoniques et l'évolution de la zone de suture du Yarlung-Zangbo. In: Mercier, J.L., Li, G.C. (Eds.), Mission franco-chinoise au Tibet 1980: Étude géologique et géophysique de la croûte terrestre et du manteau supérieur du Tibet et de l'Himalaya. Éditions du Centre National de la Recherche Scientifique, Paris, France, p. 341-350.

Chauvel, C., Hoffmann, A.W., Vidal, P., 1992. HIMU-EM: The French Polynesian connection. *Earth and Planetary Science Letters*, **110**, p. 99-119.

Coulon, C., Maluski, H., Bollinger, C., Wang, S., 1986. Mesozoic and Cenozoic volcanic rocks from central and southern Tibet; ^{39}Ar - ^{40}Ar dating, petrological characteristics and geodynamical significance. *Earth and Planetary Science Letters*, **79**, p. 281-302

Davis, A.M., Aitchison, J.C., Badengzhu, Luo, H., and Zyabrev, S., 2002. Paleogene island arc collision-related conglomerates, Yarlung-Tsangpo suture zone, Tibet. *Sedimentary Geology*, **150**, p. 247-273.

Dubois-Côté, V., Hébert, R., Wang, C.S., Li, Y.L., and Dostal, J., 2003. Petrology and geochemistry of Yarlung Zangbo Suture Zone (YZSZ) ophiolites, Tibet : Geodynamic implications. [abstract] *GAC-MAC-SEG Joint Annual Meeting (Vancouver)*, **28**, p. 188.

Dubois-Côté, V., 2004. Pétrologie et géochimie des ophiolites de la Zone de Suture du Yarlung Zangbo (ZSYZ), Tibet : Implications géodynamiques. *M.Sc. Thesis*, Université Laval, 231 p.

Dubois-Côté, V., Hébert, R., Wang, C.S., Li, Y.L., and Dostal, J., 2005. Petrological and geochemical evidence for the origin of the Yarlung Zangbo ophiolites, southern Tibet. *Chemical Geology*, **214**, p. 265-286

Dupuis, C., Hébert, R., Dubois-Côté, V., Wang, C. S., Li, Y. L., Li, Z. J., 2005a. Petrology and Geochemistry of Mafic Rocks from Mélange and Flysch Units Adjacent to the Yarlung Zangbo Suture Zone, Southern Tibet. *Chemical Geology*, **214**, p. 287-308

Dupuis, C., Hébert, R., Dubois-Côté, V., Guilmette, C., Wang, C.S., Li, Y.L., Li, Z.J., 2005b. The Yarlung Zangbo Suture Zone ophiolitic mélange (Southern Tibet): New insights from geochemistry of ultramafic rocks. *Journal of Asian Earth Sciences* (in press, corrected proof)

Dupuis, C., Hébert, R., Guilmette, C., Wang, C.S., Li, Z.J., 2005c Geochemistry of sedimentary rocks from mélange and flysch units south of the Yarlung Zangbo Suture Zone, southern Tibet, *Journal of Asian Earth Sciences* (in press, corrected proof)

Dürr, S.B., 1996. Provenance of Xigaze fore-arc basin clastic rocks (Cretaceous South Tibet). *Geological Society of America Bulletin*, **108**, p. 669-684.

Einsele, G., Liu, B., Dürr, S., Frisch, W., Liu, G., Luterbacher, H.P et al. 1994. The Xigaze forearc basin; evolution and facies architecture (Cretaceous, Tibet). *Sedimentary Geology*, **90**, p. 1-2.

Ellis, D. J., Green, D. H., 1979. An experimental study of the effect of Ca upon garnet-clinopyroxene Fe-Mg exchange equilibria. *Contributions to Mineralogy and Petrology*, **71**, p. 13-22

Ernst, W. G., Liu, J., 1998. Experimental phase-equilibrium study of Al- and Ti-contents of calcic amphibole in MORB; a semiquantitative thermobarometer. *American Mineralogist*, **83**, p. 952-969

Frey, M., DeCapitani, D., Liou, J.G., 1991. A new petrogenetic grid for low-grade metabasites. *Journal of metamorphic petrology*, **9**, p. 497-509

Fuhrman, M. L., Lindsley, D. H., 1988. Ternary-feldspar modeling and thermometry. *American Mineralogist*, **73**, p. 201-215

Gaetani, M., Garzanti, E., 1991. Multicyclic history of the northern India continental margin (northwestern Himalaya). *AAPG Bulletin*, **75**, p. 1427-1446

Ganguly, J., 1979. Garnet and clinopyroxene solid solutions, and geothermometry based on Fe-Mg distribution coefficient. *Geochimica et Cosmochimica Acta*, **43**, p. 1021-1030

Gansser, A., 1974. The ophiolitic mélange, a world-wide problem on Tethyan examples. *Eclogae Geologicae Helvetiae* **67**, p. 479-507.

Girardeau, J., Mercier, J.-C.C., 1988. Petrology and texture of the ultramafic rocks of the Xigaze ophiolite (Tibet): constraints for mantle structure beneath slow-spreading ridges. *Tectonophysics* **147**, p. 33-58.

Girardeau, J., Nicolas, A., Marcoux, J., Dupre, B., Yougong, Z., Xibin, W., Haixiang, Z., Xucheng, X., 1984. Les ophiolites de Xigaze et la suture du Yarlung Zangbo. In: Mercier, J.L., Li, G.C. (Eds.), Mission Franco-chinoise au Tibet 1980. Éditions du Centre National de la Recherche Scientifique, Paris, p. 189-193.

Girardeau, J., Mercier, J-C.C., Wang, X.B., 1985a. Petrology of the mafic rocks of the Xigaze ophiolite, Tibet: implications for the genesis of the oceanic lithosphere. *Contributions to Mineralogy and Petrology* **90**, p. 309-321.

Girardeau, J., Mercier, J.C.C., et Yougong, Z., 1985b. Origin of the Xigaze ophiolite, Yarlung Zangbo suture zone, southern Tibet. *Tectonophysics* **119**, p. 407-433.

Gnos, E., 1998. Peak metamorphic conditions of garnet amphibolites beneath the Semail Ophiolite; implications for an inverted pressure gradient. *International Geology Review*, **40**, p. 281-304.

Göpel, C., Allegre, C. J., Xu R.-H., 1984. Lead isotopic study of the Xigaze ophiolite (Tibet); the problem of the relationship between magmatites (gabbros, dolerites, lavas) and tectonites (harzburgites). *Earth and Planetary Science Letters*, **69**, p. 301-310

Graham, C. M., Powell, R., 1984. A garnet-hornblende geothermometer; calibration, testing, and application to the Pelona Schist, Southern California. *Journal of Metamorphic Geology*, **2**, p. 13-31

Green, D. H., Ringwood, A. E., 1967. The genesis of basaltic magmas. *Contributions to Mineralogy and Petrology*, **15**, p. 103-190

Guilmette, C., Hébert, R., 2003. The Bainang dynamothermal Sole [abstract]. *18th Himalaya-Karakoram-Tibet Workshop, Ascona, Switzerland*, p. 58

Guilmette, C., Hébert, R., Dupuis, C., Dubois-Côté, V., Wang, C.S., Li, Z.J., 2005. Petrology, Geochemistry and Geochronology of highly foliated amphibolites from the ophiolitic mélange underlying the Yarlung Zangbo Suture Zone Ophiolites, Southern Tibet; Geodynamical implications for the dismembered dynamothermal sole. [abstract] *20th Himalaya-Karakoram-Tibet Workshop, Aussois, France, Géologie Alpine Mémoire H.S. 44*, p. 71

Hacker, B. R., 1990. Simulation of the metamorphic and deformational history of the metamorphic sole of the Oman Ophiolite. *Journal of Geophysical Research, B, Solid Earth and Planets*, **95**, p. 4895-4907.

Hacker, B. R., 1991. The role of deformation in the formation of metamorphic gradients; ridge subduction beneath the Oman Ophiolite. *Tectonics*, **10**, p. 455-473.

Hacker, B. R., Mosenfelder, J. L., Gnos, E., 1996. Rapid emplacement of the Oman Ophiolite; thermal and geochronologic constraints. *Tectonics*, **15**, p. 1230-1247

Harrison, T.M., Yin, A., Grove, M., and Lovera, O.M., 2000. The Zedong window: a record of superposed Tertiary convergence in southeastern Tibet. *Journal Of Geophysical Research*, **105**, p. 19211-19230.

Harrison, T.M., Copeland, P., Kidd, W.S.F., and Yin, A., 1992. Rising Tibet. *Science*, **255**, p. 1663-1670.

Hawkins, J. W., 1995. Evolution of the Lau Basin; insights from ODP Leg 135. In : Taylor, B., Natland, J. (Eds.), Active margins and marginal basins of the western Pacific. *Geophysical Monograph*, **88**, p. 125-173.

Hébert, R., Varfalvy, V., Huot, F., Wang, C.S., and Liu, Z.F., 2000. Yarlung Zangbo ophiolites, southern Tibet revisited. [abstract] 15th Himalaya-Karakorum-Tibet workshop. *Earth Science Frontiers*, **7**, p. 124-126.

Hébert, R., Wang, C.S., Varfalvy, V., Huot, F., Beaudoin, G., and Dostal, J., 2001. Yarlung Zangbo Suture Ophiolites and their supra-subduction zone setting. [abstract] 16th Himalaya-Karakorum-Tibet workshop. *Journal of Asian Earth Sciences*, **19**, p. 27-28.

Hébert, R., Huot, F., Wang, C.S., Liu, Z.F., 2003. Yarlung Zangbo ophiolites (Southern Tibet) revisited: Geodynamic implications from the mineral record. In: Dylek, Y., Robinson, P.T. (Eds.), Ophiolites in Earth History. *Geological Society, London, Special Publications*, **218**, p. 165-190.

Hodges, K.V., 2000. Tectonics of the Himalaya and southern Tibet from two perspectives. *Geological Society of America Bulletin*, **112**, p. 324-350.

Huot, F., Hébert, R., Varfalvy, V., Beaudoin, G., Wang C.S., Liu Z., et al. 2002. The Beimarang Melange (southern Tibet) brings additional constraints in assessing the origin,

metamorphic evolution and obduction processes of the Yarlung Zangbo ophiolite. In: Stuewe, K., Grasemann, B. (Eds), 16th Himalaya-Karakoram-Tibet workshop. *Journal of Asian Earth Sciences*, **21**, p. 307-322.

Jamieson, R. A., 1986. P-T paths from high temperature shear zones beneath ophiolites. *Journal of Metamorphic Geology*, **4**, p. 3-22.

Jarosewich, E., Nelen, J. A., Norberg, J. A., 1980. Reference samples for electron microprobe analysis, *Geostandards Newsletter*, **4**, p. 43-47

Kempton, P. D., Harmon, R. S., 1992. Oxygen isotope evidence for large-scale hybridization of the lower crust during magmatic underplating. In : McLennan, S. M., Rudnick, R. L. (Eds), The Taylor Colloquium; Origin and evolution of planetary crusts. *Geochimica et Cosmochimica Acta*, **56**, p. 971-986.

Klootwijk, C. T., Gee, J. S., Peirce, J. W., Smith, G. M., McFadden, P. L., 1992. An early India-Asia contact; paleomagnetic constraints from Ninetyeast Ridge, ODP Leg 121; with Suppl. Data 92-15, *Geology (Boulder)*, **20**, p. 395-398

Kretz, R., 1983. Symbols for rock-forming minerals. *American Mineralogist*, **68**, p. 277-279

Leake, B. E.; Woolley, A. R.; Birch, W. D.; Burke, E. A. J.; Ferraris, G.; Grice, J. D.; Hawthorne, F. C., Kisch, H. J.; Krivovichev, V. G.; Schumacher, J. C.; Stephenson, N. C N.; Whittaker, E. J W., 2004. Nomenclature of amphiboles; additions and revisions to the International Mineralogical Association's amphibole nomenclature. *American Mineralogist*, **89**, (5-6), p.883-887

Lindsley, D.H., 1983. Pyroxene thermometry. *American Mineralogist* **68**, p. 477-493.

Liu, J., Bohlen, S.R. and Ernst, W.G. 1996. Stability of hydrous phases in subducting oceanic crust. *Earth and Planetary Science Letters*, **143**, p. 161–171.

Liu, G., Einsele, G., 1996. Various types of olistostromes in a closing ocean basin, Tethyan Himalaya (Cretaceous, Tibet). *Sedimentary Geology*, **104**, p. 203-226.

Liu, G., Einsele, G., 1999. Jurassic sedimentary facies and paleogeography of the former Indian passive margin in southern Tibet. *Geological Society of America Special Paper* **328**, p. 75-108.

Liu, J., Bohlen, S.R. and Ernst, W.G. 1996. Stability of hydrous phases in subducting oceanic crust. *Earth and Planetary Science Letters*, **143**, p. 161–171.

Lindsley, D.H., 1983. Pyroxene thermometry. *American Mineralogist* **68**, p. 477-493.

Mader, U. K., Percival, J. A., Berman, R. G., 1994. Thermobarometry of garnet-clinopyroxene-hornblende granulites from the Kapuskasing structural zone. In : Percival, J. A. (editor), The Kapuskasing transect of Lithoprobe--Le transect de Kapuskasing du Lithoprobe, *Canadian Journal of Earth Sciences = Journal Canadien des Sciences de la Terre*, **31** (7), p. 1134-1145

Mahéo, G., Bertrand, H., Guillot, S., Villa, I.M., Keller, F., Capiez, P., 2004. The South Ladakh ophiolites (NW Himalaya, India): an intra-oceanic theoleiitic arc origin with implication for the closure of the Neo-Tethys. *Chemical Geology*, **203**, p. 273-303.

Malpas, J., 1979. The dynamothermal aureole of the Bay of Islands ophiolite suite. *Canadian Journal of Earth Sciences*, **16**, p. 2086-2101

Malpas, J. G., Zhou, M.F., Robinson, P. T., Reynolds, P. H. 2003. Geochemical and geochronological constraints on the origin of the Yarlung Zangbo ophiolites, Southern Tibet. In : Dilek, Y. & Robinson, P. T. (Eds.) 2003. Ophiolites in Earth History. *Geological Society, London, Special Publications*, **218**, p. 191-206

McDermid, I., Aitchison, J.C., Badengzhu, Davis, A.M., Liu, J.B., Luo, H., et al., 2000. Zedong Terrane, A Mid Cretaceous Intra-Oceanic Arc, South Tibet. [abstract] 15th Himalaya-Karakorum-Tibet workshop. *Earth Science Frontiers*, **7**, p. 265.

McDermid, I.R.C., Aitchison, J.C., Badengzhu, and Davis, A.M., 2001. The Zedong Terrane: An Intra-Oceanic Magmatic Arc Assemblage, Tibet. [abstract] 16th Himalaya-Karakorum-Tibet workshop. *Journal of Asian Earth Sciences*, **19**, p. 44.

McDermid, I.R.C., Aitchison, J.C., Davis, A.M., Harrison, T.M., and Grove, M., 2002. The Zedong Terrane: A Late Jurassic Intra-Oceanic Magmatic Arc within the Yarlung-Tsangpo Suture Zone, Southeastern Tibet. *Chemical Geology*, **187**, p. 267-277.

Mckenzie, D. and O'Nions, R.K., 1991. Partial melt distributions from inversion of rare earth element concentrations. *Journal of Petrology*, **32**, p. 1021-1091.

Mercier, J.L. et al. (29), 1984. La collision Inde-Asie côté Tibet. In: Mercier, J.L., Li, G.C. (Eds.), Mission franco-chinoise au Tibet 1980: Étude géologique et géophysique de la croûte terrestre et du manteau supérieur du Tibet et de l'Himalaya. Éditions du Centre National de la Recherche Scientifique, Paris, France, p. 341-350.

Molnar, P., Tapponnier, P., 1975. Cenozoic tectonics of Asia: Effects of a continental collision. *Science*, **189**, p. 419-426.

Mueller, S., Phillips, R. J., 1991. On the initiation of subduction. *Journal of Geophysical Research, B, Solid Earth and Planets*, **96**, p. 651-665.

Mukhopadhyay, B., Bose, M. K., 1994. Transitional granulite-eclogite facies metamorphism of basic supracrustal rocks in a shear zone complex in the Precambrian shield of South India, *Mineralogical Magazine*, **58**, p. 97-118

Murphy, M. A., Yin, A., Harrison, T. M., Duerr, S. B., Chen, Z., Ryerson, F. J., et al. 1997. Did the Indo-Asian collision alone create the Tibetan Plateau ? *Geology (Boulder)*, **25**, p. 719-722

Nicolas, A., Girardeau, J., Marcoux, J., Dupre, B., Wan X.B., Cao Y., et al. 1981. The Xigaze ophiolite (Tibet); a peculiar oceanic lithosphere, *Nature (London)*, **294**, p. 414-417

Nicolas, A., Le Pichon, X., 1980 Thrusting of young lithosphere in subduction zones with special reference to structures in ophiolitic peridotites. *Earth and Planetary Science Letters*, **46**, p. 397-406

Nimis, P., 1995 A clinopyroxene geobarometer for basaltic systems based on crystal-structure modeling. *Contributions to Mineralogy and Petrology*. **121**, p. 115-125

Patriat, P., Segoufin, J., Schlich, R., Goslin, J., Auzende, J.-M., Beuzart, P., et al., 1982. Les mouvements relatifs de l'Inde, de l'Afrique et de l'Eurasie; The relative movements of India, Africa and Eurasia. *Bulletin de la Societe Geologique de France*, **24**, p. 363-373

Pattison, D. R. M., Newton, R. C., 1989. Reversed experimental calibration of the garnet-clinopyroxene Fe-Mg exchange thermometer. *Contributions to Mineralogy and Petrology*, **101**, p. 87-103

Pattison, D. R. M., 2003. Petrogenetic significance of orthopyroxene-free garnet + clinopyroxene + plagioclase + or - quartz-bearing metabasites with respect to the amphibolite and granulite facies. *Journal of Metamorphic Geology*, **21**, p. 21-34

Peacock, S. M., Rushmer, T., Thompson, A. B., 1994. Partial melting of subducting oceanic crust. *Earth and Planetary Science Letters*, **121**, p. 227-244

Peacock, S. M., 1988. Inverted metamorphic gradients in the westernmost Cordillera. In : Ernst, W. G. (ed.), Metamorphism and crustal evolution of the Western United States, *Rubey Volume*, **7**, p. 953-975

Pearce, J. A., 1996. A user's guide to basalt discrimination diagrams. In : Bailes (editor), Trace element geochemistry of volcanic rocks; applications for massive sulphide exploration, *Short Course Notes - Geological Association of Canada*, **12**, p. 79-113.

Plank, T. and Langmuir, C.H., 1998. The geochemical composition of subducting sediment and its consequences for the crust and mantle. *Chemical Geology*, **145**, p. 325-394.

Powell, R., 1985. Regression diagnostics and robust regression in geothermometer/geobarometer calibration; the garnet-clinopyroxene geothermometer revisited. *Journal of Metamorphic Geology*, **3**, p. 231-243.

Pozzi, J. P., Westphal, M., Girardeau, J., Besse, J., Yao X.Z., Xian Y. et al. 1984. Paleomagnetism of the Xigaze ophiolite and flysch (Yarlung Zangbo suture zone, southern Tibet); latitude and direction of spreading. *Earth and Planetary Science Letters*, **70**, p. 383-394

Raase, P., 1974. Al and Ti Contents of Hornblende, Indicators of Pressure and Temperature of Regional Metamorphism. *Contributions to Mineralogy and Petrology*, **45**, p. 231-236

Ratschbacher, L., Frisch, W., Liu, G., Chen, C., 1994. Distributed deformation in southern and western Tibet during and after India-Asia collision. *Journal of Geophysical Research* **99**, p. 19817-19945.

Renne, P. R., Swisher, C. C., Deino, A. L., Karner, D. B., Owens, T. L., DePaolo, D. J., 1998. Intercalibration of standards, absolute ages and uncertainties in (⁴⁰Ar/ ³⁹Ar) dating. *Chemical Geology*, **145**, p. 117-152.

Roddick, J. C., 1988. The assessment of errors in ⁴⁰Ar/ ³⁹Ar dating. in : Mortensen, J. K. (prefacer), Radiogenic age and isotopic studies; Report 2, *Paper - Geological Survey of Canada*, **88-2**, p. 3-8.

Scaillet, S., Numerical error analysis in ⁴⁰Ar/ ³⁹Ar dating. *Chemical Geology*, **162**, p. 269-298, 2000.

Schaerer, U., Xu, R.H., Allegre, C. J., 1984. U-Pb geochronology of Gangdese (Transhimalaya) plutonism in the Lhasa-Xigaze region, Tibet. *Earth and Planetary Science Letters*, **69**, p. 311-320.

Scotese, C. R., Gahagan, L. M., Larson, R. L., 1988. Plate tectonic reconstructions of the Cretaceous and Cenozoic ocean basinsScotese, Christopher R., Sager, William W. (Eds), Mesozoic and Cenozoic plate reconstructions. *Tectonophysics*, **155**, p. 27-48.

Searle, M.P., Windley, B.F., Coward, M.P., Cooper, D.J.W., Rex, A.J., Rex, D., et al., 1987. The closing of Tethys and the tectonics of the Himalaya. *Geological Society of America Bulletin* **98**, p. 678-701.

Shervais, J. W., 2001. Birth, death and resurrection; the life cycle of supra-subduction zone ophiolites, *Geochemistry, Geophysics, Geosystems*, **G3**, 2, paper no. 2000GC000080

Spray, J. G., 1984. Possible causes of upper mantle decoupling and ophiolite displacement. In : Gass, I. G., Lippard, S. J., Shelton, A. W. (Eds), Ophiolites and oceanic lithosphere, *Geological Society Special Publications*, **13**, p. 255-268

Sturm, M. E., Klein, E. M., Karsten, J. L., Karson, J. A., 2000. Evidence for subduction-related contamination of the mantle beneath the southern Chile Ridge; implications for ambiguous ophiolite compositions. In : Dilek, Y., Moores, E. M., Elthon, D., Nicolas, A. (Eds), Ophiolites and oceanic crust; new insights from field studies and the Ocean Drilling Program, *Special Paper - Geological Society of America*, **349**, p. 13-20

Sun, S.S., 1980. Lead isotopic study of young volcanic rocks from mid-ocean ridges, ocean islands and island arcs. *Philosophic Transactions of the Royal Society, London*, **297**, p. 409-445.

Sun, S.-S., et McDonough, W.F., 1989. Chemical and isotopic systematics of oceanic basalts: implications for mantle compositions and processes. In : Saunders, A.D. and Norry, M.J. (Eds), Magmatism in the ocean basins. *The Geological Society of London, Special Publication, London*, **42**. p. 313-345.

Tapponier, P., Mercier, J.L., Proust, F. et al. (27), 1981a. The Tibetan side of the India-Eurasia collision. *Nature*, **294**, p. 405-410.

Tapponier, P., Mercier, J.L., Armijo, R., Han, T., and Zhou, J., 1981b. Field evidence for an active normal faulting in Tibet. *Nature*, **294**, p. 410-414.

Taylor, S.R. and McLennan, S.M., 1981. The composition and evolution of the continental crust: Rare earth element evidence from sedimentary rocks. *Philosophic Transactions of the Royal Society, London*, **A301**, p. 381-399.

Taylor, H., 1997. Oxygen and Hydrogen isotope relationships in hydrothermal mineral deposits. In : Barnes, H.L. (ed.) Ore deposits research section, The Pennsylvania State University; p. 229-302

Van der Voo, R., Spakman, W., Bijwaard, H., 1999. Tethyan subducted slabs under India. *Earth and Planetary Science Letters*, **171**, p. 7-20

Villeneuve, M. E., MacIntyre, D. G., 1997. Laser $^{40}\text{Ar}/^{39}\text{Ar}$ ages of the Babine Porphyries and Newman Volcanics, Fulton Lake map area, west-central British Columbia, Radiogenic age and isotopic studies. *Report 10. Current Research - Geological Survey of Canada*, **1997-F**, p. 131-139.

Villeneuve, M., Sandeman, H. A., Davis, W. J., 2000. A method for intercalibration of U-Th-Pb and $^{40}\text{Ar}/^{39}\text{Ar}$ ages in the Phanerozoic. *Geochimica et Cosmochimica Acta*, **64**, p. 4017-4030.

Wakabayashi, J., 1990. Counterclockwise P-T-t paths from amphibolites, Franciscan Complex, California, relics from the early stages of subduction zone metamorphism. *Journal of Geology*, **98**, p. 657-680.

Wakabayashi, J., Dilek, Y., 2000. Spatial and temporal relationships between ophiolites and their metamorphic soles; a test of models of forearc ophiolite genesis. In : Dilek, Y., Moores, E. M., Elthon, D., Nicolas, A. (Eds.), Ophiolites and oceanic crust; new insights from field studies and the Ocean Drilling Program. *Special Paper - Geological Society of America*, **349**, p. 53-64.

Wakabayashi, J., Dilek, Y., 2003. What constitutes “emplacement” of an ophiolite ? : Mechanisms and relationship to subduction initiation and formation of metamorphic soles. In : Dilek, Y. and Robinson, P. T. (Eds) Ophiolites and Earth history. *Geological Society, London, Special publication*, **218**, p. 427-448

Wan X., Wang L., Wang C.S., Jansa, L., 1998. Discovery and significance of Cretaceous fossils from the Xigaze forearc basin, Tibet. In : Gaetani, M., Windley, B., (Eds.), Papers presented at the 12th international Himalaya-Karakorum-Tibet (HKT) workshop, *Journal of Asian Earth Sciences*, **16**, p. 217-223.

Wang, X.B., Xiao, X.C., Cao, Y.G., Zheng, H.X. 1984. Geological map of the ophiolite zone along the middle Yarlung Zangbo River, Xizang (Tibet). 2nd Geological and Geophysical brigade of geological Bureau of the Tibet Autonomous Region, Publishing House of Surveying and Mapping, Beijing, P.R. China.

Wang, X.B., Bao, P.S., Deng, W.M. & Wang, F.G. 1987. Tectonic evolution of the lithosphere of the Himalayas: Xizang (Tibet) ophiolite. In: Chinese Academy of Geological Sciences, (ed.) *People's Republic of China Ministry of Geology and Mineral Resources Geological Memoirs Series 3. 8*, p. 1-336

Wang, C.S, Liu, Z., Hébert, R., 2000. The Yarlung-Zangbo paleo-ophiolite, southern Tibet: implications for the dynamic evolution of the Yarlung-Zangbo Suture Zone. *Journal of Asian Earth Sciences* **18**, p. 651-661.

Weaver, B.L., Tarney, J., 1984. Empirical approach to estimating the composition of the continental crust. *Nature*, **310**, p. 575-577.

Wiedmann, J., Duerr, S. B., 1995. First ammonites from the Mid-to Upper Cretaceous Xigaze Group, South Tibet, and their significance. *Newsletters on Stratigraphy*, **32**, p. 17-26.

Williams, H., Smyth, W. R., 1973. Metamorphic aureoles beneath ophiolite suites and alpine peridotites; tectonic implications with west Newfoundland examples. *American Journal of Science*, **273**, p. 594-621

Winchester, J. A., Floyd, P. A., 1977. Geochemical discrimination of different magma series and their differentiation products using immobile elements. *Chemical Geology*, **20**, p. 325-343.

Zheng, Y.F., 1993a. Calculation of oxygen isotope fractionation in anhydrous silicate minerals. *Geochimica et Cosmochimica Acta*, **57**, p. 1079-1091

Zheng, Y.F., 1993b. Calculation of oxygen isotope fractionation in hydroxyl-bearing silicates. *Earth and Planetary Science Letters*, **120**, p. 247-263

Zhou, M.F., Robinson, P.T., Malpas, J., Li Z., 1996. Podiform chromitites in the Luobusa Ophiolite (southern Tibet); implications for melt-rock interaction and chromite segregation in the upper mantle. *Journal of Petrology*, **37**, p. 3-21

Zyabrev, S.V., Aitchison, J.C., Badengzhu, Davis, A.M., Luo, H., Malpas, J., 1999. Radiolarian biostratigraphy of supra-ophiolite sequences in the Xigaze area, Yarlung Tsangpo suture, Southern Tibet (preliminary report). *Radiolaria* **17**, p. 13-19

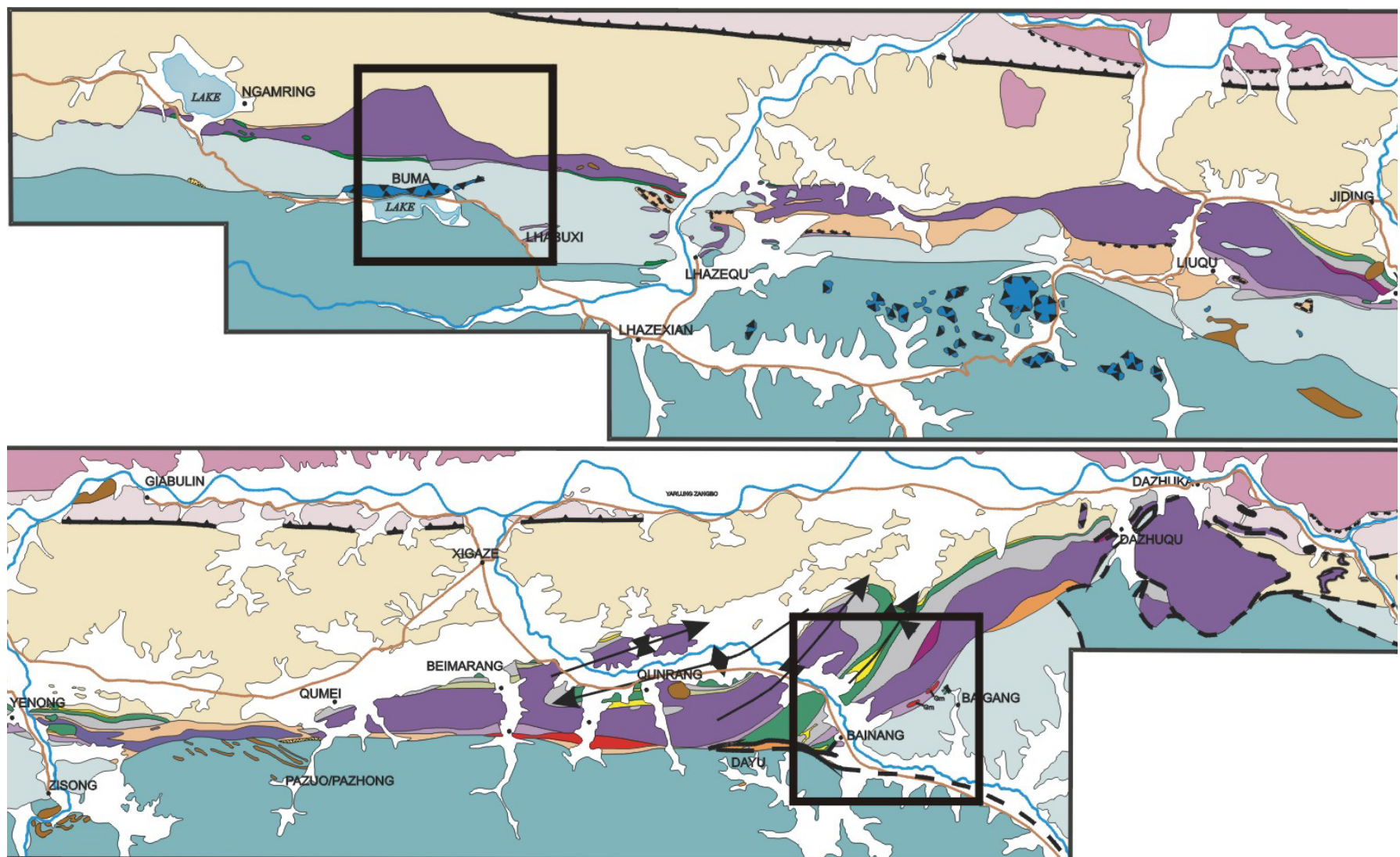
Zyabrev, S.V., Aitchison, J.C., Badengzhu, Davis, A.M., Luo, H., Liu, J.B., 2001. More about the missing Tethys: Bainang terrane Tibet. In: 16th Himalaya-Karakorum-Tibet workshop abstracts, *Journal of Asian Earth Sciences* **19**, p. 82-83.

Zyabrev, S.V., Aitchison, J.C., Abrajevitch, A.V., Badengzhu, Davis, A.M., Luo, H., 2004. Bainang Terrane, Yarlung-Tsangpo suture, southern Tibet (Xizang, China): a record of intra-Neo-Tethyan subduction-accretion processes preserved on the roof of the world. *Journal of the Geological Society of London* **161**, p. 1-17.

Chapter 5 : Appendices

Appendix A

Geological map of the YZSZ and sample locations



Tibetan Active Margin

GANGDESE ARC

XIGAZE GROUP

- Eocene and Neogene systems (undivided)
- Upper Cretaceous Flysch

Tethyan Sediments (India)

RADIOLARIAN CHERT

UPPER TRIASSIC FLYSCH

ABYSSAL SEDIMENTS and BASIC LAVAS

EXOTIC BLOCK and NAPPE

UPPER CRETACEOUS OLISTOSTROME (WILDFLYSCH)

Yarlung Zangbo Ophiolites (Xigaze segment)

Late Cretaceous abyssal sediments

Pillow lavas

Sheeted sills (Diabase)

Gabbro

Cumulates (Dunite and layered gabbro)

Diabase sills and peridotite

Peridotite and Serpentinite

Serpentinite mélange

Garnet amphibolite

LIUQU CONGLOMERATE

QUATERNARY

Figure A1 : Detailed geological map of the Central Segment of the YZSZ, Xigaze area. See figure 2.2 for georeference and scale.

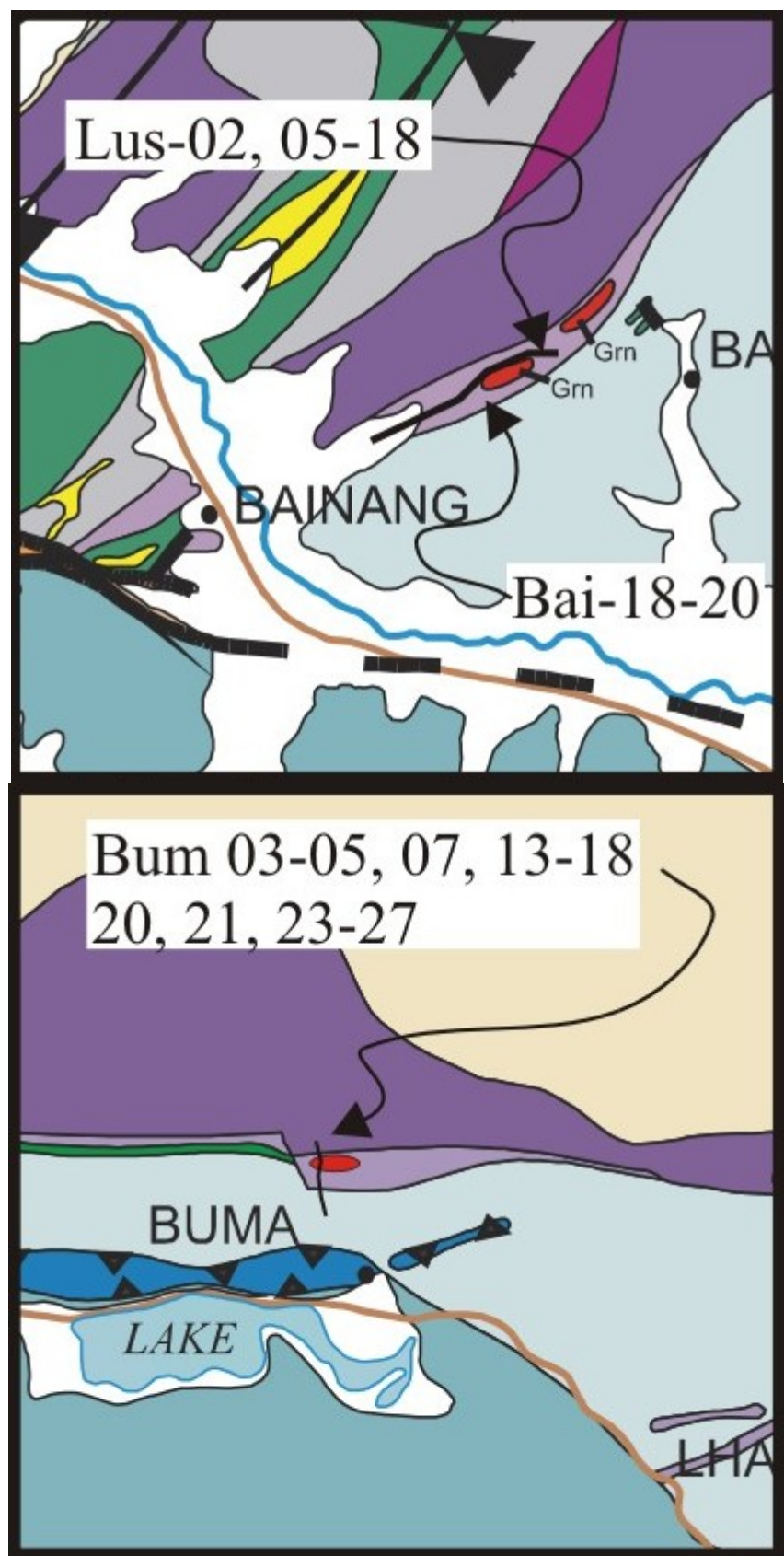


Figure A2 : Sampling Location

Appendix B

Petrography of highly foliated amphibolite blocks from the mélange beneath the YSZ ophiolites

Thin Section	Type	Geochem. (WR)	Prograde minerals						Retrograde minerals				Comments
			Hornblende	Garnet	Cpx	Feldspar	Ti-Phase	Epidote	Others	Corona	Chlorite	Prehnite	
BAI-18	Common	123.3 ± 3.1 Ma Low Si High Ti, Fe	80 % 1 (2)			15 % (2) 2	4 % (1-2) spn+ilm		1% (1-2) Apatite			In plag.	No retrograde except for prehnite Few brittle def.
BAI-19 *	Banded		61 % 1 (1)		6 % (2) gr.	26 % (2) 2	2 % (1) spn	5 % (1) ep.				In plag. And cracks	Moderate to strong cataclastic def.
bands			5 % 1 (2)		30 % (3) gr.	33 % (4) 2		28 % (2-4)				5 % with plag.	
BAI-20 *	Common		65 % 1 (2)			28 % (2-4) 2	1% (1) spn	1 % (1) ep.				5 % in cracks + in plag.	Strong cataclastic def.
BUM-04 *	Banded	Low Si, High Ti, Al, Fe, Mg, Ca	64% 3 (2)		1 % (3) gr. With plag.	20 % (2-4) 3	1 % (1) spn	13 % (2) Zoicite			1 % blue with plag+prehn.	In plag.	Moderate cataclastic def.
BUM-05 *	Common	127.7 ± 2.3 Ma Low Si, High Al, Mg	58 % 4 (2)			30 % (2-4) 4	1 % (1) spn+ilm	10 % (1)ep. 5 % (2) zo.			1 % blue with plag.	In plag.	Strong cataclastic def.
BUM-07 *	Common		63 % 2 (2)			30 % (3) 4	1 % (1) spn	5 % (2) ep+zo.			1 % blue with plag.	In plag.	Strong cataclastic def.
BUM-13	Common		70 % 2 (2)			25 % (3) 2	1 % (1) spn	1 % (1) ep.			1 % blue with plag.	2 % in cracks + in plag.	Moderate cataclastic def.
BUM-14 *	Banded	High Si, Ti, Al Low Mg#	15 % 1 (2)		40 % (3) gr. With plag.	30 % (3) 2	1 % (1) spn					14 % in cracks + in plag	moderate-strong cataclastic def.
BUM-15 *	Common	High Al Low Mg#	55 % 3 (3)			33 % (3) 3	1 % (1-2) spn				1 % blue with plag.	10 % in cracks + in plag.	Weak-moderate cataclastic def.
BUM-16 *	Common	High Ti, Al Low Mg#	40 % 4 (1-2)			48 % (3) 4	1 % (1) spn+ilm				1 % blue with plag.	10 % in cracks + in plag.	Diabasic texture ? Moderate cataclastic def.
BUM-17	Common		50 % 3 (2)			38 % (3) 3	1 % (1) spn				1 % blue with plag.	10 % in cracks + in plag.	Strong cataclastic def.
BUM-18	Common	High Al, Mg#	70 % 2 (2-3)			23 % (3) 3	2 % (1) spn				1 % blue with plag.	4 % in plag.	Weak cataclastic def.
BUM-20 *	Common		54 % 3 (2)			30 % (2) 5	2 % (1) spn+ilm	2 % (1) ep.			10 % grey-yellow with plag.	2 % in plag.	Strong Cataclastic def.
BUM-21 *	Common	High Al	60 % 2 (3)			30 % (3) 3	1 % (1) spn+ilm	5 % (1) ep.				4 % in cracks + in plag.	Moderate cataclastic def.
BUM-23	Common	High Si,Mg# Low Ti, Fe, Ca	45 % 1 (1-2)			42 % (2) 2	2 % (1) spn+ilm	10 % (1-2) ep+zo.			1 % grey in cracks	In plag.	Weak cataclastic def.
BUM-24 *	Banded		48 % 4 (2)		10 % (2) gr. With Plag.	35 % (3) 5	2 % (1) spn	5 % (2) ep+zo.				In plag.	Weak cataclastic def.
BUM-25	Common		52 % 2 (2)			30 % (2) 5	1 % (1) spn+ilm	15 % (2) ep+zo			1 % grey in cracks	1 % in cracks + in plag.	Weak cataclastic def.

Thin Section	Type	Geochem. (WR)	Prograde minerals							Retrograde minerals			Comment
			Hornblende	Garnet	CPX	Feldspar	Ti-Phase	Epidote	Others	Corona	Chlorite	Prehnite	
LUS-05 *	Banded	High Ti, Al, Fe Low Mg#	38 % 2 (1)		2 % (2) gr. With plag.	50 % (2) 2	3 % (1) ilm	5 % (1) ep.			2 % yellow in cracks	In plag.	Moderate cataclastic def.
LUS-06	Banded		41 % 1 (1)		1 % (3) gr.	30 % (2) 2	1 % (1) spn	10 % (1) ep.	5 % quartz in bands		2 % blue with plag.	10 % in cracks + replacement + in plag.	Weak cataclastic def.
LUS-07 *	Garnet	127.4 ± 2.4 Ma High Al, Ca, Mg# Low Ti	30 % 5 (3)	5 % (3)	10 % (4) colorless	40 % (3) 5	2 % (1) rt			Plag+amph 0.3-0.5 mm		13 % in cracks + replacement + in plag.	Strong Cataclastic def.
LUS-08 *	Banded	High Si, Ca Low Ti, Fe, Mg	26 % 2 (1)		10 % (4) gr. With Plag+epido- te	30 % (1) 3	1 % (1) spn	30 % (1) ep. In bands	3 % quartz in bands 1 % apatite			In plag.	Weak cataclastic def.
LUS-09 *	Banded		30 % 2 (1)		15 % (3) gr. With Plag+epido- te	30 % (2) 2	1 % (1) spn	20 % (1) ep. In bands	1 % qtz in bands 1 % apatite			2 % in plag.	Moderate cataclastic def.
LUS-11 *	Banded	High Si, Low Mg	39 % 2 (2)		5 % (2) gr. With Plag	40 % (2) 4	1 % (1) spn					15 % in cracks + replacement + in plag.	Weak cataclastic def.
LUS-12a *	Garnet	High Al, Mg#	47 % 5 (3)	15 % (2)	15 % (3) colorless	20 % (2) 4	2 % (1) rt			Amph+plag. 0.1-0.3 mm		1 % in cracks + in plag.	Weak cataclastic def.
LUS-12b *	Garnet		45 % 5 (2)	15 % (3)	13 % (3) colorless	25 % (2) 5	1 % (1) rt			Amph. 0.1-1 mm		1 % in cracks + in plag.	Weak cataclastic def.
LUS-13 *	Garnet		50 % 4 (3)	4 % (3)		40 % (3) 4	1 % (1) rt			Plag. 0.1-0.3mm		5 % in cracks + in plag.	Weak cataclastic def.
LUS-14 *	Garnet	High Si, Al, Mg# Low Ti, fe	43 % 5 (2)	5 % (2)	10 % (3) colorless	40 % (2) 5	1 % (1) rt			Plag+amph. 0.3-0.5 mm		2 % in cracks + in plag.	Weak cataclastic def.
LUS-15	Common		50 % 2 (3)			44 % (2) 2	1 % (1) spn+ilm					5 % in cracks + in plag.	Moderate cataclastic def.
LUS-16	Common	Low Ti, Al, High Mg, Ca	64 % 4 (3)		10 % (3) gr.	20 % (3-4) 4	1 % (1) spn+ilm	5 % (1- 2) ep.				In Plag.	Strong Cataclastic def.
LUS-17 *	Garnet	Low Si, Ti, Fe High Al, Ca, Mg#	40 % 4 (2)	7 % (2)	5 % (3) colorless	30 % (3) 5	1 % (1) rt			Plag+chl+amp 0.3-0.8 mm	2 % blue with garnet	15 % in cracks + replacement + in plag.	Moderate cataclastic def.
LUS-18 *	Common		45 % 1 (2)			40 % (2) 4	1 % (1) spn	5 % (1- 2) ep.				9 % in cracks + in plag.	Weak cataclastic def.

Tables B1 and B2 : Summary of petrographic data. Abbreviations are taken from Kretz (1983). Thin section name refers to provenance sample. « Type » refers to amphibolite type. « Special » column shows Ar/Ar ages and major elements geochemical particularities. In all columns, number with % refers to mode and bracketed number from 1 to 4 indicates crystal size (1 = <1 mm, 2 = 1-2 mm, 3 = 2-5 mm, 4 = 5-10 mm). In « amphibole » column, number from 1 to 5 indicates color (1=green, 5=orange-brown). In Cpx column, note indicates color (gr. = greenish) and associated minerals. In « Feldspar » column, number from 1 to 5 indicates density of inclusion (degree of recrystallisation) (1=no inclusions, 5 = high density of inclusions). For colored numbers, see « chapter 3 : Major elements » section for explanation. Sample labels with an “*” underwent microprobe analysis.

Figure B1 : Examples of amphibole colors. a) = 1 (green) from BAI-18, b) = 3 (brown-green) from BUM-04 and c) = 5 (orange-brown) from LUS-12 a.

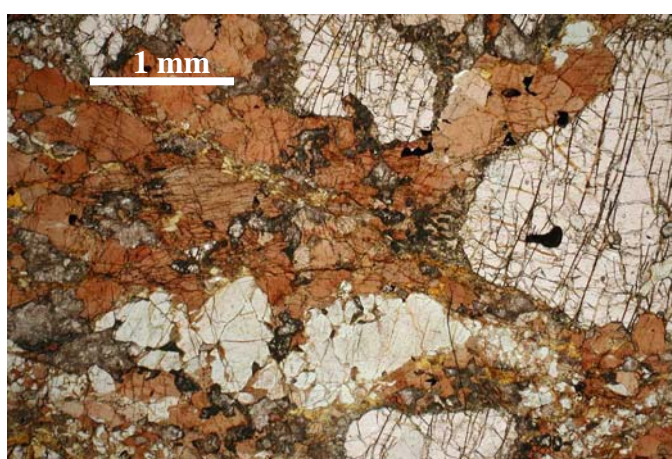
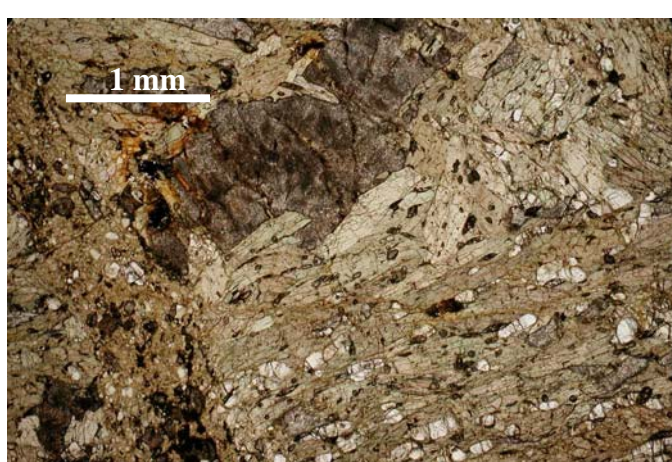


Figure B2 : Examples of inclusion density in plagioclase. A) = 2 from LUS-15, B) = 4 from LUS-16 and C) = 5 from LUS07.

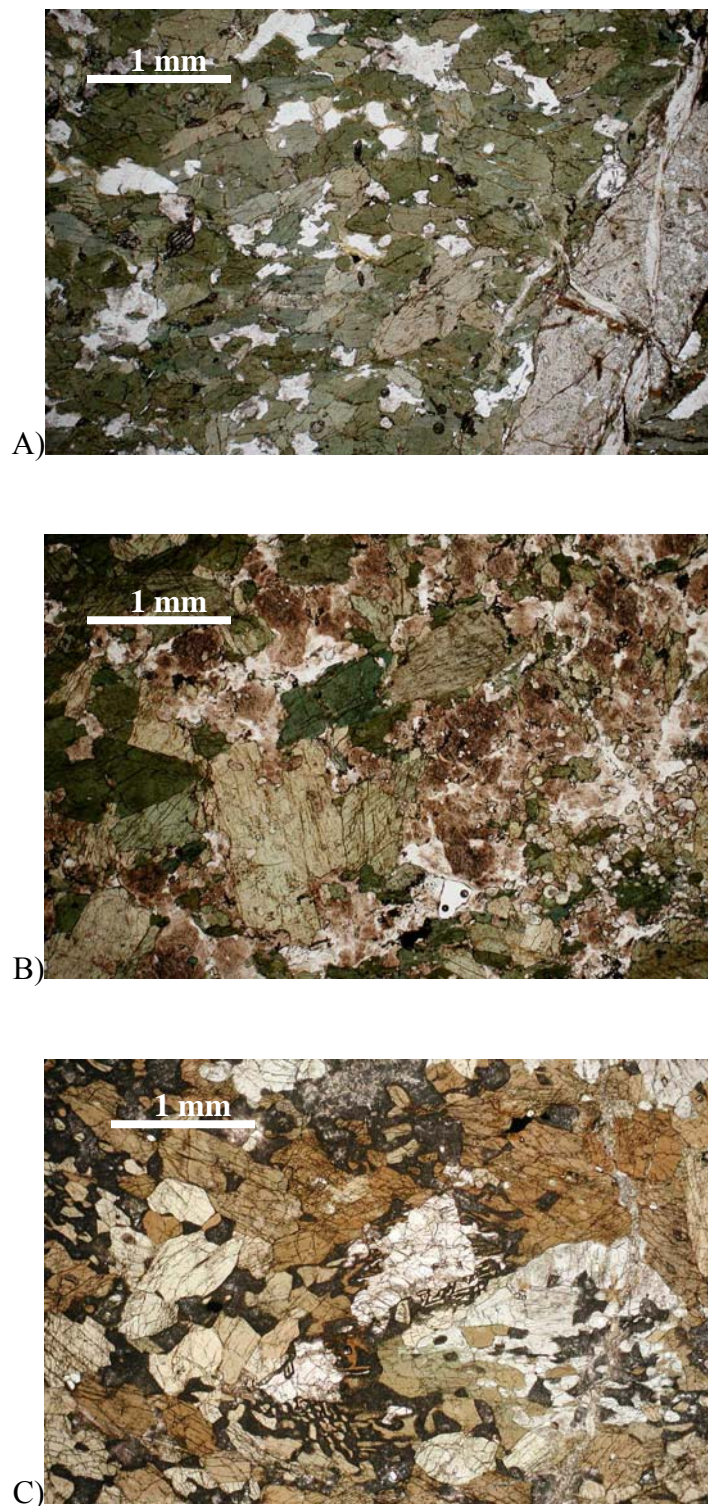
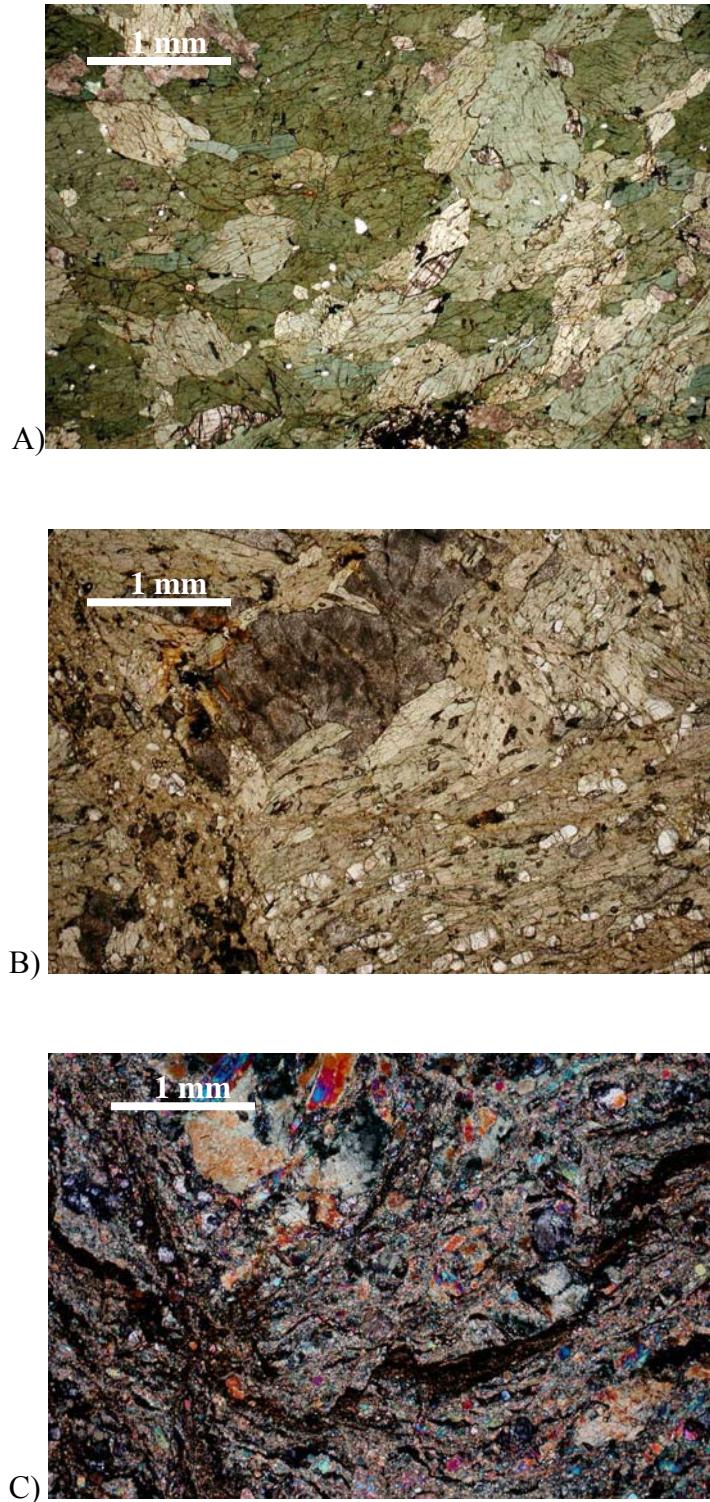


Figure B3 : Examples of cataclastic deformation : A) = weak from BAI-18 B) = moderate from BUM-04 and C) = strong from BUM-07



Appendix C

Mineral Chemistry of highly foliated amphibolite blocks from the mélange beneath the YZSZ ophiolites

Amphibole Mineral Chemistry

Clinopyroxene Mineral Chemistry

Garnet Mineral Chemistry

Plagioclase Mineral Chemistry

Amphibole Mineral Chemistry

Table C1 : Amphibole mineral chemistry

Analysis	BAI18-1	BAI18-2	BAI18-3	BAI18-4	BAI18-5	BAI18-6	BAI18-7	BAI18-8	BAI18-9	BAI18-10	BAI18-11	BAI18-12	BAI18-13	BAI18-14
Amph. Type	prograde													
Color	green													
SiO ₂	44.92	43.10	42.63	44.43	44.44	44.31	42.54	43.04	45.09	43.34	44.95	44.19	44.01	43.81
TiO ₂	0.84	0.91	0.98	0.94	1.11	1.14	1.14	1.00	0.99	1.09	0.86	1.24	0.84	0.97
Al ₂ O ₃	13.50	13.57	13.69	13.65	12.88	13.19	13.40	14.13	12.99	13.61	13.24	13.38	11.86	13.64
Cr ₂ O ₃	0.02	0.05	0.00	0.00	0.00	0.09	0.01	0.07	0.01	0.08	0.06	0.08	0.03	0.09
Fe ₂ O ₃	4.88	7.22	6.15	5.12	7.98	6.15	6.80	6.10	4.59	5.90	4.47	4.35	6.75	6.43
FeO	10.09	8.53	9.29	10.32	7.67	9.95	8.88	10.17	10.74	9.55	10.36	10.70	8.52	8.98
MnO	0.21	0.19	0.25	0.25	0.22	0.24	0.23	0.17	0.21	0.22	0.24	0.21	0.19	0.19
MgO	11.01	11.06	10.87	10.87	11.34	10.81	11.03	10.55	11.12	11.02	11.15	10.91	11.86	11.23
CaO	11.06	11.09	11.24	11.33	10.53	11.07	11.14	11.28	11.44	11.33	11.31	11.27	11.39	11.23
Na ₂ O	2.11	2.01	2.06	2.03	1.97	2.04	2.07	2.18	1.87	2.00	2.02	1.95	1.78	2.05
K ₂ O	0.20	0.21	0.24	0.18	0.22	0.22	0.28	0.28	0.32	0.29	0.19	0.46	0.17	0.20
F	0.09	0.07	0.00	0.11	0.00	0.22	0.09	0.11	0.18	0.00	0.00	0.16	0.00	0.00
Cl	0.01	0.02	0.01	0.01	0.01	0.01	0.00	0.00	0.01	0.00	0.02	0.01	0.01	0.01
H ₂ O	2.03	2.01	2.04	2.03	2.07	1.97	1.99	2.01	2.00	2.06	2.08	1.98	2.04	2.07
Total	100.97	100.05	99.46	101.26	100.41	101.40	99.61	101.07	101.54	100.49	100.93	100.89	99.45	100.89
Si	6.47	6.29	6.27	6.41	6.42	6.40	6.26	6.25	6.49	6.31	6.49	6.41	6.45	6.33
Al ^{iv}	1.53	1.71	1.73	1.59	1.58	1.60	1.74	1.75	1.51	1.69	1.51	1.59	1.55	1.67
Al ^{vi}	0.77	0.63	0.65	0.73	0.62	0.64	0.58	0.68	0.69	0.64	0.74	0.70	0.50	0.66
Ti	0.09	0.10	0.11	0.10	0.12	0.12	0.13	0.11	0.11	0.12	0.09	0.13	0.09	0.11
Cr	0.00	0.01	0.00	0.00	0.00	0.01	0.00	0.01	0.00	0.01	0.01	0.01	0.00	0.01
Fe ³⁺	0.53	0.79	0.68	0.56	0.87	0.67	0.75	0.67	0.50	0.65	0.49	0.47	0.74	0.70
Fe ²⁺	1.22	1.04	1.14	1.24	0.93	1.20	1.09	1.24	1.29	1.16	1.25	1.30	1.04	1.09
Mn	0.03	0.02	0.03	0.03	0.03	0.03	0.02	0.03	0.03	0.03	0.03	0.03	0.02	0.02
Mg	2.37	2.41	2.39	2.34	2.44	2.33	2.42	2.28	2.39	2.39	2.40	2.36	2.59	2.42
Ca	1.71	1.74	1.77	1.75	1.63	1.71	1.76	1.76	1.76	1.77	1.75	1.75	1.79	1.74
Na	0.59	0.57	0.59	0.57	0.55	0.57	0.59	0.61	0.52	0.57	0.57	0.55	0.51	0.57
K	0.04	0.04	0.04	0.03	0.04	0.04	0.05	0.05	0.06	0.05	0.03	0.08	0.03	0.04
F	0.04	0.03	0.00	0.05	0.00	0.10	0.04	0.05	0.08	0.00	0.00	0.07	0.00	0.00
Cl	0.00	0.00	0.00	0.00	0.00	0.00	0.00	0.00	0.00	0.00	0.00	0.00	0.00	0.00
OH	1.96	1.96	2.00	1.95	2.00	1.90	1.95	1.95	1.92	2.00	2.00	1.92	2.00	2.00
Total	17.33	17.34	17.41	17.35	17.22	17.32	17.40	17.42	17.34	17.39	17.35	17.38	17.33	17.35

Table C1 (continued)

Analysis	BAI18-15	BAI20-1	BAI20-2	BAI20-3	BAI20-4	BAI20-5	BAI20-6	BAI20-7	LUS18-1	LUS18-2	LUS18-3	LUS18-4	LUS18-5	BUM05-1
Amph. Type	prograde	core	rim	prograde										
Color	green	green	green	brown										
SiO ₂	46.44	47.61	46.32	50.26	44.14	45.31	45.63	46.34	45.54	44.53	47.09	45.65	45.66	44.09
TiO ₂	0.72	0.74	0.63	0.38	0.81	0.75	0.80	0.61	0.60	0.74	0.62	0.73	0.70	0.70
Al ₂ O ₃	11.17	11.32	11.96	7.96	12.33	11.68	12.07	11.14	10.63	12.11	10.26	11.32	11.21	13.03
Cr ₂ O ₃	0.02	0.07	0.04	0.01	0.00	0.01	0.06	0.08	0.06	0.04	0.08	0.04	0.02	0.06
Fe ₂ O ₃	4.50	4.07	4.67	2.89	4.47	6.31	4.52	3.92	5.30	4.85	3.81	4.82	4.90	3.99
FeO	10.95	10.44	10.12	10.52	10.02	9.07	10.09	10.81	9.97	10.52	10.79	9.76	9.45	8.46
MnO	0.18	0.24	0.28	0.27	0.25	0.25	0.27	0.30	0.25	0.25	0.29	0.24	0.27	0.20
MgO	11.63	12.11	11.91	13.45	11.64	12.14	11.83	11.84	12.04	11.52	12.45	12.37	12.47	12.96
CaO	11.54	11.80	11.68	11.79	11.78	11.67	11.60	11.63	11.93	11.97	12.05	12.00	11.97	11.89
Na ₂ O	1.66	1.35	1.73	1.11	1.72	1.77	1.81	1.74	1.18	1.44	1.42	1.47	1.43	2.26
K ₂ O	0.25	0.19	0.17	0.16	0.26	0.16	0.20	0.19	0.46	0.55	0.29	0.40	0.39	0.27
F	0.14	0.11	0.11	0.00	0.02	0.15	0.22	0.00	0.09	0.03	0.00	0.00	0.00	0.00
Cl	0.02	0.00	0.00	0.01	0.01	0.03	0.01	0.01	0.01	0.01	0.01	0.00	0.00	0.00
H ₂ O	2.01	2.06	2.04	2.10	2.03	2.01	1.97	2.07	2.01	2.04	2.08	2.08	2.07	2.07
Total	101.22	102.11	101.67	100.91	99.48	101.30	101.07	100.69	100.06	100.59	101.25	100.86	100.55	99.98
Si	6.69	6.76	6.63	7.17	6.48	6.52	6.58	6.70	6.65	6.49	6.77	6.59	6.61	6.40
Al ^{iv}	1.31	1.24	1.37	0.83	1.52	1.48	1.42	1.30	1.35	1.51	1.23	1.41	1.39	1.60
Al ^{vi}	0.59	0.65	0.64	0.50	0.61	0.50	0.63	0.60	0.48	0.57	0.51	0.52	0.52	0.63
Ti	0.08	0.08	0.07	0.04	0.09	0.08	0.09	0.07	0.07	0.08	0.07	0.08	0.08	0.08
Cr	0.00	0.01	0.00	0.00	0.00	0.00	0.01	0.01	0.01	0.00	0.01	0.00	0.00	0.01
Fe ³⁺	0.49	0.43	0.50	0.31	0.49	0.68	0.49	0.43	0.58	0.53	0.41	0.52	0.53	0.44
Fe ²⁺	1.32	1.24	1.21	1.25	1.23	1.09	1.22	1.31	1.22	1.28	1.30	1.18	1.14	1.03
Mn	0.02	0.03	0.03	0.03	0.03	0.03	0.03	0.04	0.03	0.03	0.03	0.03	0.03	0.02
Mg	2.50	2.56	2.54	2.86	2.55	2.61	2.54	2.55	2.62	2.50	2.67	2.66	2.69	2.80
Ca	1.78	1.79	1.79	1.80	1.85	1.80	1.79	1.80	1.87	1.87	1.86	1.86	1.86	1.85
Na	0.46	0.37	0.48	0.31	0.49	0.49	0.51	0.49	0.33	0.41	0.40	0.41	0.40	0.63
K	0.05	0.03	0.03	0.03	0.05	0.03	0.04	0.04	0.09	0.10	0.05	0.07	0.07	0.05
F	0.07	0.05	0.05	0.00	0.01	0.07	0.10	0.00	0.04	0.01	0.00	0.00	0.00	0.00
Cl	0.00	0.00	0.00	0.00	0.01	0.00	0.00	0.00	0.00	0.00	0.00	0.00	0.00	0.00
OH	1.93	1.95	1.95	2.00	1.99	1.93	1.90	2.00	1.96	1.99	2.00	2.00	2.00	2.00
Total	17.29	17.20	17.30	17.14	17.39	17.32	17.33	17.33	17.29	17.38	17.31	17.34	17.33	17.53

Table C1 (continued)

Analysis	BUM05-2	BUM05-3	BUM05-4	BUM05-5	core	rim	BUM16-1	BUM16-2	BUM16-3	BUM16-4	BUM16-5	BUM16-6	BUM07-1	BUM07-2
Amph. Type	prograde brown	prograde brown	prograde brown	prograde brown	core brown	rim brown	prograde brown	prograde brown	prograde brown	prograde brown	prograde brown	prograde brown	prograde green	prograde green
Color														
SiO ₂	44.83	43.99	43.74	44.70	43.94	45.53	45.05	45.07	44.93	44.50	44.43	44.83	44.95	43.89
TiO ₂	0.65	0.75	0.72	0.52	0.84	0.66	1.33	1.19	1.15	1.07	1.14	1.23	0.55	0.67
Al ₂ O ₃	12.25	12.46	12.77	11.11	13.22	10.87	10.75	11.28	11.70	12.28	11.72	11.68	12.58	11.98
Cr ₂ O ₃	0.00	0.03	0.00	0.07	0.01	0.05	0.15	0.07	0.05	0.05	0.07	0.12	0.01	0.04
Fe ₂ O ₃	8.00	4.64	5.91	7.14	4.52	3.00	12.18	8.05	2.69	5.16	7.01	3.86	0.00	6.42
FeO	5.12	8.21	6.80	6.73	8.50	9.49	3.72	7.81	11.25	8.95	7.43	10.14	12.29	8.08
MnO	0.21	0.25	0.21	0.24	0.21	0.25	0.39	0.49	0.26	0.22	0.20	0.24	0.25	0.24
MgO	13.73	12.95	13.37	13.37	12.96	13.33	13.00	11.91	12.24	12.47	12.46	12.16	10.92	12.62
CaO	11.27	11.65	11.97	11.58	11.94	11.90	10.46	10.99	11.76	11.59	11.48	11.76	13.04	11.60
Na ₂ O	2.08	2.33	1.95	1.79	2.39	2.15	1.60	1.82	2.53	2.27	1.58	1.95	0.93	2.14
K ₂ O	0.22	0.26	0.24	0.42	0.29	0.25	0.13	0.13	0.14	0.12	0.13	0.14	0.25	0.29
F	0.00	0.00	0.00	0.28	0.06	0.00	2.20	0.00	0.00	1.08	0.00	0.00	1.74	0.00
Cl	0.00	0.01	0.00	0.01	0.00	0.00	0.00	0.01	0.01	0.02	0.00	0.01	0.00	0.01
H ₂ O	2.09	2.05	2.07	1.93	2.05	2.06	1.05	2.08	2.06	1.56	2.06	2.06	1.19	2.05
Total	100.46	99.58	99.73	99.86	100.91	99.53	102.02	100.87	100.74	101.32	99.70	100.17	98.68	100.02
Si	6.42	6.42	6.35	6.50	6.34	6.64	6.45	6.51	6.53	6.43	6.46	6.52	6.68	6.40
Al ^{iv}	1.58	1.58	1.65	1.50	1.66	1.36	1.55	1.49	1.47	1.57	1.54	1.48	1.32	1.60
Al ^{vi}	0.49	0.56	0.53	0.41	0.58	0.51	0.26	0.42	0.53	0.52	0.47	0.53	0.88	0.46
Ti	0.07	0.08	0.08	0.06	0.09	0.07	0.14	0.13	0.13	0.12	0.12	0.14	0.06	0.07
Cr	0.00	0.00	0.00	0.01	0.00	0.01	0.02	0.01	0.01	0.01	0.01	0.01	0.00	0.00
Fe ³⁺	0.86	0.51	0.65	0.78	0.49	0.33	1.31	0.87	0.29	0.56	0.77	0.42	0.00	0.70
Fe ²⁺	0.61	1.00	0.83	0.82	1.02	1.16	0.45	0.94	1.37	1.08	0.90	1.23	1.53	0.99
Mn	0.03	0.03	0.03	0.03	0.03	0.03	0.05	0.06	0.03	0.03	0.02	0.03	0.03	0.03
Mg	2.93	2.81	2.89	2.90	2.79	2.90	2.77	2.56	2.65	2.69	2.70	2.64	2.42	2.74
Ca	1.73	1.82	1.86	1.80	1.84	1.86	1.60	1.70	1.83	1.79	1.79	1.83	2.08	1.81
Na	0.58	0.66	0.55	0.50	0.67	0.61	0.44	0.51	0.71	0.64	0.44	0.55	0.27	0.60
K	0.04	0.05	0.05	0.08	0.05	0.05	0.02	0.02	0.03	0.02	0.02	0.03	0.05	0.05
F	0.00	0.00	0.00	0.13	0.03	0.00	1.00	0.00	0.00	0.49	0.00	0.00	0.82	0.00
Cl	0.00	0.00	0.00	0.00	0.00	0.00	0.00	0.00	0.00	0.00	0.00	0.00	0.00	0.00
OH	2.00	2.00	2.00	1.87	1.97	2.00	1.00	2.00	2.00	1.50	2.00	2.00	1.18	2.00
Total	17.35	17.53	17.45	17.39	17.56	17.51	17.07	17.23	17.57	17.45	17.26	17.41	17.31	17.47

Table C1 (continued)

Analysis	BUM07-3		BUM07-4		BUM15-1		BUM15-2		BUM15-3		BUM15-4		BUM17-1		BUM17-2		BUM17-3		BUM17-4		BUM17-5		BUM17-6		BUM17-7		BUM17-8	
Amph. Type	prograde		prograde		prograde		prograde		rim		core		prograde		retrograde													
Color	green	green	brown	brown	brown	brown	brown	brown	brown	brown	brown	brown	brown	brown	brown	brown	brown	brown	brown	brown	brown	brown	brown	brown	brown	green		
SiO ₂	43.09	43.39	43.30	42.48	46.01	40.81	44.94	44.59	44.05	42.80	42.46	45.35	43.52	48.03														
TiO ₂	0.82	0.74	0.76	0.59	0.64	1.94	1.23	1.34	1.41	3.07	1.67	1.15	1.78	0.18														
Al ₂ O ₃	12.98	13.17	12.45	13.16	9.30	13.10	10.85	11.43	12.02	10.91	12.41	10.45	12.17	7.19														
Cr ₂ O ₃	0.00	0.12	0.04	0.09	0.10	0.16	0.03	0.02	0.14	0.02	0.02	0.00	0.02	0.23														
Fe ₂ O ₃	4.77	5.23	6.34	8.20	7.41	2.26	7.33	6.42	5.25	1.94	8.07	5.34	4.85	3.81														
FeO	8.87	8.48	6.47	5.08	6.54	9.98	6.69	7.74	8.14	11.51	7.31	9.07	9.28	10.65														
MnO	0.19	0.20	0.26	0.27	0.32	0.21	0.17	0.21	0.13	0.14	0.16	0.18	0.09	0.40														
MgO	12.43	12.24	13.19	13.17	13.89	12.10	13.43	12.80	12.80	12.26	11.98	12.74	12.28	13.39														
CaO	11.66	11.67	11.54	11.34	10.87	12.50	11.54	11.57	11.64	12.33	11.11	11.56	11.61	12.45														
Na ₂ O	2.48	2.12	2.09	2.24	2.38	1.89	1.77	1.82	2.04	1.78	2.15	1.90	2.21	1.09														
K ₂ O	0.28	0.29	0.28	0.26	0.21	0.17	0.14	0.07	0.08	0.09	0.07	0.10	0.06	0.10														
F	0.00	1.33	0.00	0.00	0.00	0.00	0.00	0.00	0.02	0.00	0.05	0.00	0.00	0.00														
Cl	0.02	0.02	0.01	0.00	0.01	0.00	0.01	0.01	0.01	0.01	0.00	0.00	0.00	0.00														
H ₂ O*	2.04	1.42	2.04	2.05	2.06	1.98	2.07	2.06	2.05	2.01	2.02	2.06	2.05	2.05														
Total	99.63	100.40	98.77	98.94	99.74	97.11	100.18	100.08	99.77	98.87	99.46	99.89	99.92	99.57														
Si	6.32	6.34	6.35	6.22	6.68	6.16	6.50	6.47	6.41	6.36	6.23	6.60	6.36	7.02														
Al ^{iv}	1.68	1.66	1.65	1.78	1.32	1.84	1.50	1.53	1.59	1.64	1.77	1.40	1.64	0.98														
Al ^{vi}	0.56	0.60	0.50	0.49	0.27	0.49	0.34	0.42	0.47	0.27	0.38	0.40	0.45	0.26														
Ti	0.09	0.08	0.08	0.06	0.07	0.22	0.13	0.15	0.15	0.34	0.18	0.13	0.20	0.02														
Cr	0.00	0.01	0.00	0.01	0.01	0.02	0.00	0.00	0.02	0.00	0.00	0.00	0.00	0.03														
Fe ³⁺	0.53	0.57	0.70	0.90	0.81	0.26	0.80	0.70	0.58	0.22	0.89	0.58	0.53	0.42														
Fe ²⁺	1.09	1.04	0.79	0.62	0.79	1.26	0.81	0.94	0.99	1.43	0.90	1.10	1.13	1.30														
Mn	0.02	0.03	0.03	0.03	0.04	0.03	0.02	0.03	0.02	0.02	0.02	0.02	0.01	0.05														
Mg	2.72	2.67	2.88	2.87	3.01	2.72	2.89	2.77	2.78	2.72	2.62	2.76	2.67	2.92														
Ca	1.83	1.83	1.81	1.78	1.69	2.02	1.79	1.80	1.81	1.96	1.75	1.80	1.82	1.95														
Na	0.71	0.60	0.60	0.64	0.67	0.55	0.49	0.51	0.58	0.51	0.61	0.54	0.63	0.31														
K	0.05	0.05	0.05	0.05	0.04	0.03	0.03	0.01	0.01	0.02	0.01	0.02	0.01	0.02														
F	0.00	0.61	0.00	0.00	0.00	0.00	0.00	0.01	0.01	0.00	0.02	0.00	0.00	0.00														
Cl	0.01	0.00	0.00	0.00	0.00	0.00	0.00	0.00	0.00	0.00	0.00	0.00	0.00	0.00														
OH*	1.99	1.38	2.00	2.00	2.00	2.00	2.00	1.99	1.99	2.00	1.98	2.00	2.00	2.00														
Total	17.59	17.48	17.46	17.47	17.40	17.61	17.31	17.32	17.40	17.50	17.37	17.36	17.45	17.28														

Table C1 (continued)

Analysis	BUM17-9	BUM17-10	BUM17-11	BUM17-12	BUM20-1	BUM20-2	BUM20-3	BUM20-4	BUM20-5	BUM20-6	BUM20-7	BUM20-8	LUS11-1	LUS11-2
	retrograde	retrograde	retrograde	retrograde	prograde	retrograde	retrograde							
	Color	green	green	green	green	green	green	green	green	green	green	green	green	green
SiO ₂	48.73	51.38	49.91	50.30	42.29	43.05	42.59	45.16	43.16	44.31	44.12	44.76	47.13	45.36
TiO ₂	0.16	0.14	0.16	0.16	0.79	0.65	0.75	0.61	0.60	0.62	0.72	0.68	0.42	0.42
Al ₂ O ₃	5.81	5.00	6.67	5.29	13.92	13.37	14.01	11.07	13.16	12.41	12.97	12.18	8.99	10.07
Cr ₂ O ₃	0.00	0.03	0.50	0.00	0.07	0.06	0.00	0.06	0.00	0.01	0.08	0.07	0.40	0.02
Fe ₂ O ₃	3.30	2.60	3.85	3.32	7.80	8.55	7.29	6.90	7.31	8.79	7.44	7.48	4.64	5.25
FeO	10.43	11.50	9.66	9.60	8.32	7.51	8.75	8.01	7.95	6.50	7.98	5.21	10.58	9.73
MnO	0.41	0.35	0.36	0.43	0.24	0.23	0.26	0.24	0.24	0.22	0.25	0.25	0.26	0.27
MgO	14.02	14.19	14.14	14.83	10.84	11.46	10.84	12.29	11.62	12.12	11.66	13.59	12.57	12.56
CaO	12.57	12.53	12.31	12.56	10.88	10.95	11.07	10.95	11.02	10.72	11.00	10.86	12.04	12.19
Na ₂ O	0.76	0.69	0.89	0.70	2.26	2.20	2.19	1.94	2.25	1.96	2.09	2.31	1.40	1.48
K ₂ O	0.13	0.09	0.10	0.06	0.33	0.30	0.32	0.29	0.31	0.35	0.30	0.26	0.11	0.11
F	0.00	0.00	0.08	0.09	0.00	0.04	0.00	0.00	0.00	0.00	0.04	0.01	0.09	0.00
Cl	0.00	0.00	0.00	0.00	0.00	0.01	0.01	0.00	0.00	0.00	0.00	0.00	0.01	0.00
H ₂ O*	2.03	2.09	2.06	2.02	2.04	2.04	2.05	2.06	2.05	2.07	2.06	2.07	2.02	2.04
Total	98.36	100.58	100.68	99.37	99.77	100.41	100.10	99.59	99.67	100.08	100.70	99.74	100.64	99.50
Si	7.19	7.39	7.16	7.29	6.21	6.27	6.23	6.59	6.32	6.42	6.38	6.46	6.83	6.66
Al ^{iv}	0.81	0.61	0.84	0.71	1.79	1.73	1.77	1.41	1.68	1.58	1.62	1.54	1.17	1.34
Al ^{vi}	0.20	0.23	0.29	0.20	0.62	0.56	0.65	0.49	0.59	0.54	0.59	0.53	0.37	0.40
Ti	0.02	0.02	0.02	0.02	0.09	0.07	0.08	0.07	0.07	0.07	0.08	0.07	0.05	0.05
Cr	0.00	0.00	0.06	0.00	0.01	0.01	0.00	0.01	0.00	0.00	0.01	0.01	0.05	0.00
Fe ³⁺	0.37	0.28	0.42	0.36	0.86	0.94	0.80	0.76	0.81	0.96	0.81	0.81	0.51	0.58
Fe ²⁺	1.29	1.38	1.16	1.16	1.02	0.91	1.07	0.98	0.97	0.79	0.97	0.63	1.28	1.19
Mn	0.05	0.04	0.04	0.05	0.03	0.03	0.03	0.03	0.03	0.03	0.03	0.03	0.03	0.03
Mg	3.08	3.04	3.02	3.21	2.37	2.49	2.36	2.67	2.54	2.62	2.51	2.92	2.72	2.75
Ca	1.99	1.93	1.89	1.95	1.71	1.71	1.74	1.71	1.73	1.66	1.71	1.68	1.87	1.92
Na	0.22	0.19	0.25	0.20	0.64	0.62	0.62	0.55	0.64	0.55	0.59	0.65	0.39	0.42
K	0.02	0.02	0.02	0.01	0.06	0.06	0.06	0.05	0.06	0.06	0.05	0.05	0.02	0.02
F	0.00	0.00	0.03	0.04	0.00	0.02	0.00	0.00	0.00	0.00	0.02	0.00	0.04	0.00
Cl	0.00	0.00	0.00	0.00	0.00	0.00	0.00	0.00	0.00	0.00	0.00	0.00	0.00	0.00
OH*	2.00	2.00	1.97	1.96	2.00	1.98	2.00	2.00	2.00	2.00	1.98	2.00	1.96	2.00
Total	17.23	17.14	17.16	17.16	17.42	17.38	17.42	17.31	17.43	17.28	17.35	17.37	17.28	17.36

Table C1 (continued)

Analysis	LUS11-3	LUS11-4	LUS11-5	LUS11-6	LUS11-7	LUS11-8	LUS11-9	LUS11-10	LUS11-11	LUS11-12	LUS11-13	LUS11-14	LUS11-15	LUS05-1
Amph. Type	prograde	retrograde												
Color	green													
SiO ₂	45.40	45.32	46.27	46.12	46.28	45.90	46.23	49.04	46.47	45.58	45.26	44.56	44.77	47.54
TiO ₂	0.58	0.52	0.63	0.60	0.62	0.64	0.38	0.39	0.63	0.52	0.71	0.70	0.56	0.37
Al ₂ O ₃	10.24	10.57	10.49	10.38	10.40	10.17	9.91	7.50	10.21	9.35	11.04	11.03	10.32	8.29
Cr ₂ O ₃	0.02	0.68	0.75	0.63	0.70	0.61	0.00	0.06	0.00	0.69	0.48	0.52	1.15	0.00
Fe ₂ O ₃	4.77	6.14	3.37	3.70	5.21	3.37	8.62	1.26	5.15	3.83	5.73	3.74	5.17	4.73
FeO	9.96	8.61	10.48	9.62	9.91	11.36	7.90	11.98	9.84	9.85	8.96	10.34	8.79	9.26
MnO	0.25	0.25	0.21	0.21	0.25	0.24	0.24	0.24	0.23	0.22	0.28	0.24	0.21	0.37
MgO	12.57	12.59	12.41	12.90	12.41	12.19	12.70	13.49	12.75	12.79	12.41	12.01	12.42	13.93
CaO	12.31	11.85	12.19	12.31	12.03	12.29	11.71	12.54	12.05	12.24	11.87	12.10	11.89	12.08
Na ₂ O	1.40	1.63	1.41	1.32	1.58	1.59	1.38	1.15	1.62	1.28	1.63	1.54	1.42	1.33
K ₂ O	0.11	0.10	0.11	0.11	0.11	0.11	0.10	0.08	0.11	0.11	0.11	0.13	0.10	0.77
F	0.03	0.02	0.00	0.09	0.09	0.10	0.16	0.01	0.10	0.00	0.06	0.00	0.09	0.14
Cl	0.01	0.01	0.00	0.01	0.00	0.00	0.00	0.00	0.02	0.00	0.01	0.00	0.00	0.00
H ₂ O*	2.03	2.05	2.07	2.02	2.04	2.01	2.01	2.06	2.03	2.03	2.04	2.03	1.99	2.01
Total	99.68	100.34	100.39	100.01	101.64	100.57	101.33	99.80	101.21	98.49	100.58	98.92	98.86	100.82
Si	6.65	6.58	6.71	6.70	6.65	6.69	6.65	7.12	6.69	6.74	6.56	6.58	6.60	6.87
Al ^{iv}	1.35	1.42	1.29	1.30	1.35	1.31	1.35	0.88	1.31	1.26	1.44	1.42	1.40	1.13
Al ^{vi}	0.41	0.39	0.50	0.47	0.41	0.43	0.33	0.41	0.42	0.37	0.44	0.50	0.39	0.28
Ti	0.06	0.06	0.07	0.07	0.07	0.07	0.04	0.04	0.07	0.06	0.08	0.08	0.06	0.04
Cr	0.00	0.08	0.09	0.07	0.08	0.07	0.00	0.01	0.00	0.08	0.05	0.06	0.13	0.00
Fe ³⁺	0.53	0.67	0.37	0.40	0.56	0.37	0.93	0.14	0.56	0.43	0.63	0.42	0.57	0.51
Fe ²⁺	1.22	1.05	1.27	1.17	1.19	1.38	0.95	1.46	1.18	1.22	1.09	1.28	1.08	1.12
Mn	0.03	0.03	0.03	0.03	0.03	0.03	0.03	0.03	0.03	0.03	0.03	0.03	0.03	0.05
Mg	2.74	2.73	2.68	2.79	2.66	2.65	2.72	2.92	2.74	2.82	2.68	2.64	2.73	3.00
Ca	1.93	1.84	1.89	1.92	1.85	1.92	1.80	1.95	1.86	1.94	1.84	1.91	1.88	1.87
Na	0.40	0.46	0.40	0.37	0.44	0.45	0.39	0.32	0.45	0.37	0.46	0.44	0.41	0.37
K	0.02	0.02	0.02	0.02	0.02	0.02	0.02	0.01	0.02	0.02	0.02	0.02	0.02	0.14
F	0.01	0.01	0.00	0.04	0.04	0.05	0.07	0.00	0.05	0.00	0.03	0.00	0.04	0.06
Cl	0.00	0.00	0.00	0.00	0.00	0.00	0.00	0.00	0.00	0.00	0.00	0.00	0.00	0.00
OH*	1.99	1.99	2.00	1.96	1.96	1.95	1.93	2.00	1.95	2.00	1.97	2.00	1.96	1.94
Total	17.35	17.32	17.31	17.31	17.31	17.39	17.21	17.29	17.33	17.33	17.32	17.38	17.30	17.38

Table C1 (continued)

Analysis	LUS05-2	LUS05-3	LUS05-4	LUS05-5	LUS08-1	LUS08-2	LUS08-3	LUS08-4	LUS08-5	LUS09-1	LUS09-2	LUS09-3	BAI19-1	BAI19-2
Amph. Type	prograde	retrograde (px)	prograde	prograde	prograde	prograde								
Color	green	green	green	green	green									
SiO ₂	43.55	44.41	43.57	42.98	45.34	41.21	44.54	44.50	44.53	44.66	42.21	42.38	45.39	44.67
TiO ₂	0.76	0.52	0.55	0.73	0.49	0.73	0.68	0.60	0.62	0.53	0.82	0.83	0.78	0.77
Al ₂ O ₃	11.00	10.53	11.40	11.80	9.45	11.11	10.45	10.40	10.80	9.74	11.82	12.12	11.27	11.10
Cr ₂ O ₃	0.00	0.01	0.00	0.02	0.05	0.09	0.00	0.00	0.03	0.01	0.04	0.07	0.01	0.01
Fe ₂ O ₃	6.99	8.25	6.51	7.24	8.83	9.27	6.24	7.11	6.13	5.62	5.44	4.70	3.97	5.07
FeO	9.29	7.61	9.65	9.35	6.22	5.99	8.57	8.53	7.77	12.82	14.23	13.87	12.92	11.78
MnO	0.38	0.43	0.38	0.35	0.25	0.25	0.31	0.27	0.29	0.34	0.32	0.34	0.30	0.25
MgO	12.20	13.10	12.00	11.90	14.14	13.17	13.07	12.87	13.64	10.86	9.32	9.66	10.73	11.05
CaO	11.62	11.85	11.83	11.63	11.49	11.34	11.50	11.50	11.64	11.71	11.61	11.74	11.71	11.62
Na ₂ O	1.78	1.51	1.59	1.76	1.76	1.94	1.81	1.71	1.93	1.56	1.77	1.65	1.70	1.74
K ₂ O	1.21	1.11	1.22	1.41	0.95	1.37	1.27	1.27	1.22	1.10	1.36	1.46	0.61	0.62
F	0.00	0.01	0.10	0.00	0.05	0.09	0.00	0.00	0.00	0.01	0.00	0.15	0.09	0.18
Cl	0.01	0.01	0.01	0.01	0.00	0.01	0.00	0.00	0.01	0.00	0.00	0.00	0.02	0.01
H ₂ O	2.04	2.06	1.99	2.05	2.05	1.96	2.05	2.06	2.06	2.02	2.01	1.94	2.01	1.96
Total	100.83	101.40	100.80	101.22	101.06	98.53	100.48	100.83	100.66	101.00	100.95	100.93	101.50	100.80
Si	6.39	6.44	6.39	6.29	6.55	6.17	6.51	6.49	6.47	6.60	6.31	6.32	6.61	6.55
Al ^{iv}	1.61	1.56	1.61	1.71	1.45	1.83	1.49	1.51	1.53	1.40	1.69	1.68	1.39	1.45
Al ^{vi}	0.29	0.24	0.37	0.33	0.16	0.14	0.31	0.28	0.32	0.30	0.39	0.45	0.54	0.47
Ti	0.08	0.06	0.06	0.08	0.05	0.08	0.07	0.07	0.07	0.06	0.09	0.09	0.08	0.08
Cr	0.00	0.00	0.00	0.00	0.01	0.01	0.00	0.00	0.00	0.00	0.01	0.01	0.00	0.00
Fe ³⁺	0.77	0.90	0.72	0.80	0.96	1.05	0.69	0.78	0.67	0.62	0.61	0.53	0.43	0.56
Fe ²⁺	1.14	0.92	1.18	1.15	0.75	0.75	1.05	1.04	0.94	1.58	1.78	1.73	1.57	1.44
Mn	0.05	0.05	0.05	0.04	0.03	0.03	0.04	0.03	0.04	0.04	0.04	0.04	0.04	0.03
Mg	2.67	2.83	2.62	2.60	3.05	2.94	2.85	2.80	2.95	2.39	2.08	2.15	2.33	2.41
Ca	1.83	1.84	1.86	1.82	1.78	1.82	1.80	1.80	1.81	1.85	1.86	1.88	1.83	1.82
Na	0.51	0.43	0.45	0.50	0.49	0.56	0.51	0.48	0.54	0.45	0.51	0.48	0.48	0.49
K	0.23	0.21	0.23	0.26	0.17	0.26	0.24	0.24	0.23	0.21	0.26	0.28	0.11	0.12
F	0.00	0.00	0.05	0.00	0.02	0.04	0.00	0.00	0.00	0.00	0.00	0.07	0.04	0.08
Cl	0.00	0.00	0.00	0.00	0.00	0.00	0.00	0.00	0.00	0.00	0.00	0.00	0.00	0.00
OH	2.00	1.99	1.95	2.00	1.98	1.95	2.00	2.00	2.00	2.00	2.00	1.93	1.95	1.92
Total	17.56	17.47	17.54	17.59	17.45	17.65	17.55	17.52	17.58	17.51	17.63	17.63	17.42	17.43

Table C1 (continued)

Analysis	BAI19-3	BAI19-4	BUM04-1	BUM04-2	BUM04-3	BUM04-4	BUM04-5	BUM04-6	BUM24-1	BUM24-2	BUM24-3	BUM24-4	BUM24-5	BUM24-6
Amph. Type	retrograde	retrograde	prograde	prograde	prograde	prograde	retrograde	retrograde	retrograde	retrograde	prograde	prograde	prograde	prograde
Color	green	green	brown	brown	brown	brown	green	green	green	green	brown	brown	brown	brown
SiO ₂	47.66	43.66	45.95	45.16	46.23	46.08	45.50	46.96	46.88	47.68	45.48	45.79	45.33	44.83
TiO ₂	0.33	0.64	0.70	0.57	0.59	0.54	0.49	0.39	0.37	0.42	0.67	0.52	0.63	0.63
Al ₂ O ₃	6.60	11.22	11.95	11.64	11.08	11.51	14.27	9.79	10.10	9.28	11.56	11.06	11.33	11.63
Cr ₂ O ₃	0.00	0.00	0.05	0.11	0.00	0.11	0.02	0.04	0.17	0.07	0.04	0.08	0.02	0.16
Fe ₂ O ₃	5.64	4.88	3.71	3.55	2.97	3.47	0.00	4.27	4.47	2.63	1.50	4.04	3.65	3.95
FeO	9.55	13.25	9.03	9.95	10.20	9.11	9.62	9.00	8.63	10.03	11.08	9.28	10.03	9.69
MnO	0.26	0.23	0.24	0.22	0.24	0.24	0.20	0.24	0.22	0.23	0.20	0.24	0.22	0.23
MgO	13.77	10.27	12.94	12.75	12.90	13.10	11.15	13.71	13.67	13.73	13.00	12.76	12.80	12.48
CaO	12.29	12.05	11.86	12.29	11.88	11.91	13.72	12.35	12.19	12.42	12.09	11.96	12.18	12.04
Na ₂ O	0.96	1.55	1.94	1.93	2.14	1.93	1.51	1.53	1.57	1.48	2.63	1.65	2.01	1.88
K ₂ O	0.30	0.62	0.06	0.06	0.08	0.09	0.07	0.06	0.09	0.05	0.05	0.06	0.06	0.06
F	0.00	0.00	0.00	0.00	0.00	0.00	0.00	0.00	0.00	0.00	1.23	0.00	0.00	0.00
Cl	0.01	0.01	0.02	0.00	0.00	0.01	0.01	0.01	0.00	0.00	0.00	0.00	0.01	0.01
H ₂ O	2.04	2.02	2.08	2.07	2.07	2.08	2.06	2.08	2.08	2.08	1.48	2.06	2.06	2.05
Total	99.41	100.39	100.53	100.28	100.38	100.17	98.60	100.41	100.45	100.09	101.00	99.49	100.32	99.63
Si	6.99	6.48	6.60	6.55	6.68	6.65	6.62	6.77	6.75	6.89	6.60	6.67	6.58	6.55
Al ^{iv}	1.01	1.52	1.40	1.45	1.32	1.35	1.38	1.23	1.25	1.11	1.40	1.33	1.42	1.45
Al ^{vi}	0.13	0.44	0.63	0.55	0.57	0.61	1.07	0.43	0.46	0.46	0.58	0.56	0.52	0.55
Ti	0.04	0.07	0.08	0.06	0.06	0.06	0.05	0.04	0.04	0.05	0.07	0.06	0.07	0.07
Cr	0.00	0.00	0.01	0.01	0.00	0.01	0.00	0.00	0.02	0.01	0.00	0.01	0.00	0.02
Fe ³⁺	0.62	0.55	0.40	0.39	0.32	0.38	0.00	0.46	0.48	0.29	0.16	0.44	0.40	0.43
Fe ²⁺	1.17	1.64	1.09	1.21	1.23	1.10	1.17	1.08	1.04	1.21	1.34	1.13	1.22	1.18
Mn	0.03	0.03	0.03	0.03	0.03	0.03	0.02	0.03	0.03	0.03	0.02	0.03	0.03	0.03
Mg	3.01	2.27	2.77	2.76	2.78	2.82	2.42	2.95	2.93	2.96	2.81	2.77	2.77	2.72
Ca	1.93	1.92	1.83	1.91	1.84	1.84	2.14	1.91	1.88	1.92	1.88	1.87	1.89	1.88
Na	0.27	0.45	0.54	0.54	0.60	0.54	0.43	0.43	0.44	0.41	0.74	0.47	0.57	0.53
K	0.06	0.12	0.01	0.01	0.01	0.02	0.01	0.01	0.02	0.01	0.01	0.01	0.01	0.01
F	0.00	0.00	0.00	0.00	0.00	0.00	0.00	0.00	0.00	0.00	0.56	0.00	0.00	0.00
Cl	0.00	0.00	0.00	0.00	0.00	0.00	0.00	0.00	0.00	0.00	0.00	0.00	0.00	0.00
OH	2.00	2.00	2.00	2.00	2.00	2.00	2.00	2.00	2.00	2.00	1.44	2.00	2.00	2.00
Total	17.26	17.48	17.38	17.46	17.46	17.40	17.32	17.34	17.33	17.34	17.63	17.34	17.47	17.43

Table C1 (continued)

Analysis	BUM24-7	BUM24-8	BUM14-1	BUM14-2	BUM14-3	BUM14-4	BUM14-5	BUM14-6	LUS07-1	LUS07-2	LUS07-3	LUS07-4	LUS07-5	LUS07-6
Amph. Type	prograde	prograde	prograde	prograde	prograde	prograde	retrograde	retrograde	corona	corona	corona	retrograde	retrograde	retrograde
Color	brown	brown	brown	brown	brown	brown	green	green	green	green	green	green	green	green
SiO ₂	46.29	44.98	40.37	40.28	40.74	42.08	42.21	41.49	39.69	39.35	40.46	43.30	43.29	44.82
TiO ₂	0.54	0.54	1.21	1.22	1.29	1.11	0.88	1.06	0.27	0.38	0.23	1.25	1.30	1.13
Al ₂ O ₃	10.94	12.32	12.26	13.17	13.83	11.81	10.82	12.31	17.19	17.11	16.15	11.77	12.85	11.28
Cr ₂ O ₃	0.03	0.03	0.09	0.16	0.14	0.10	0.15	0.09	0.08	0.03	0.03	0.07	0.07	0.12
Fe ₂ O ₃	2.61	0.00	6.26	5.84	2.69	5.35	6.29	6.32	6.35	6.90	5.58	6.43	6.46	3.94
FeO	10.56	11.28	13.36	14.12	15.13	13.78	13.01	13.12	11.06	10.00	12.02	6.92	7.18	11.92
MnO	0.22	0.22	0.29	0.30	0.25	0.32	0.30	0.30	0.42	0.46	0.59	0.23	0.19	0.40
MgO	13.08	11.32	9.39	8.97	9.01	9.83	9.94	9.52	8.84	9.11	8.46	13.03	12.67	11.42
CaO	12.03	13.83	11.77	11.76	12.12	11.94	11.68	11.57	11.57	11.48	11.45	11.56	11.55	12.15
Na ₂ O	2.31	1.51	2.16	2.41	2.17	2.10	1.94	2.19	2.68	2.55	2.43	2.01	2.09	1.87
K ₂ O	0.06	0.06	0.76	0.81	0.75	0.74	0.65	0.77	0.14	0.15	0.13	0.07	0.10	0.09
F	0.00	0.00	0.05	0.09	0.07	0.03	0.00	0.00	0.00	0.00	0.05	0.16	0.00	0.23
Cl	0.01	0.00	0.02	0.01	0.01	0.02	0.00	0.01	0.02	0.01	0.05	0.00	0.01	0.01
H ₂ O	2.08	2.03	1.95	1.96	1.96	2.00	1.99	2.01	2.02	2.01	1.97	1.96	2.06	1.95
Total	100.76	98.11	99.93	101.10	100.16	101.22	99.85	100.75	100.33	99.55	99.58	98.77	99.82	101.33
Si	6.68	6.66	6.11	6.04	6.13	6.26	6.35	6.20	5.88	5.86	6.04	6.37	6.30	6.52
Al ^{iv}	1.32	1.34	1.89	1.96	1.87	1.74	1.65	1.80	2.12	2.14	1.96	1.63	1.70	1.48
Al ^{vi}	0.54	0.81	0.29	0.37	0.58	0.33	0.27	0.36	0.88	0.86	0.88	0.41	0.50	0.45
Ti	0.06	0.06	0.14	0.14	0.15	0.12	0.10	0.12	0.03	0.04	0.03	0.14	0.14	0.12
Cr	0.00	0.00	0.01	0.02	0.02	0.01	0.02	0.01	0.01	0.00	0.00	0.01	0.01	0.01
Fe ³⁺	0.28	0.00	0.71	0.66	0.30	0.60	0.71	0.71	0.71	0.77	0.63	0.71	0.71	0.43
Fe ²⁺	1.27	1.40	1.69	1.77	1.90	1.71	1.64	1.64	1.37	1.25	1.50	0.85	0.87	1.45
Mn	0.03	0.03	0.04	0.04	0.03	0.04	0.04	0.04	0.05	0.06	0.07	0.03	0.02	0.05
Mg	2.81	2.50	2.12	2.01	2.02	2.18	2.23	2.12	1.95	2.02	1.88	2.86	2.75	2.48
Ca	1.86	2.19	1.91	1.89	1.95	1.90	1.88	1.85	1.84	1.83	1.83	1.82	1.80	1.89
Na	0.64	0.43	0.63	0.70	0.63	0.61	0.56	0.63	0.77	0.74	0.70	0.57	0.59	0.53
K	0.01	0.01	0.15	0.16	0.14	0.14	0.12	0.15	0.03	0.03	0.02	0.01	0.02	0.02
F	0.00	0.00	0.03	0.04	0.03	0.01	0.00	0.00	0.00	0.00	0.02	0.07	0.00	0.11
Cl	0.00	0.00	0.00	0.00	0.00	0.00	0.00	0.00	0.00	0.00	0.01	0.00	0.00	0.00
OH	2.00	2.00	1.97	1.96	1.96	1.98	2.00	2.00	2.00	2.00	1.97	1.93	2.00	1.89
Total	17.52	17.43	17.69	17.75	17.73	17.65	17.57	17.63	17.63	17.60	17.56	17.41	17.41	17.44

Table C1 (continued)

Analysis	LUS07-7	LUS07-8	LUS07-9	LUS07-10	LUS07-11	LUS07-12	LUS07-13	LUS07-14	LUS07-15	LUS07-16	LUS12-1	LUS12-2	LUS12-3	LUS12-4
Amph. Type	retrograde	retrograde	retrograde	prograde	prograde	prograde	rim (1)	rim (2)	core (3)	core (4)	prograde	prograde	prograde	prograde
Color	green	green	green	brown	brown	brown	green	brown						
SiO ₂	45.49	44.73	44.69	43.06	43.97	44.70	42.07	43.59	44.58	42.92	42.82	43.73	42.50	42.54
TiO ₂	0.69	1.35	1.02	1.63	1.81	1.69	1.14	1.62	1.78	1.82	2.13	2.12	2.14	2.22
Al ₂ O ₃	9.22	12.03	10.48	13.89	12.96	11.96	14.19	12.78	13.13	13.89	12.91	12.74	13.96	13.85
Cr ₂ O ₃	0.04	0.04	0.04	0.12	0.01	0.10	0.11	0.09	0.11	0.12	0.06	0.10	0.11	0.11
Fe ₂ O ₃	5.26	4.51	4.20	5.52	4.65	5.18	8.46	4.37	4.33	5.99	5.00	3.17	4.52	5.08
FeO	8.12	8.37	9.08	9.41	8.54	8.07	6.71	8.97	8.31	7.62	8.33	7.98	7.05	6.80
MnO	0.22	0.18	0.21	0.34	0.19	0.14	0.24	0.27	0.27	0.23	0.10	0.10	0.13	0.15
MgO	13.87	12.96	13.14	11.19	12.73	13.20	12.07	12.39	12.49	12.11	13.14	13.83	13.41	13.41
CaO	12.39	11.60	12.37	11.30	11.69	11.65	11.64	11.65	11.43	11.33	11.82	11.71	11.53	11.35
Na ₂ O	1.38	2.13	1.50	2.35	2.31	2.20	2.18	2.31	2.08	2.24	2.66	2.71	2.80	2.90
K ₂ O	0.08	0.07	0.06	0.10	0.09	0.09	0.11	0.09	0.08	0.09	0.20	0.22	0.17	0.18
F	0.10	0.00	0.06	0.11	0.00	0.00	0.00	0.00	0.09	0.04	0.05	0.00	0.00	0.00
Cl	0.02	0.01	0.01	0.01	0.01	0.00	0.01	0.01	0.01	0.00	0.01	0.02	0.01	0.01
H ₂ O	1.99	2.07	2.01	2.02	2.08	2.09	2.07	2.06	2.05	2.05	2.05	2.08	2.07	2.08
Total	98.87	100.04	98.87	101.05	101.04	101.07	101.00	100.19	100.74	100.42	101.26	100.50	100.41	100.66
Si	6.68	6.47	6.57	6.24	6.32	6.41	6.08	6.34	6.40	6.21	6.18	6.30	6.14	6.13
Al ^{iv}	1.32	1.53	1.43	1.76	1.68	1.59	1.92	1.66	1.60	1.79	1.82	1.70	1.86	1.87
Al ^{vi}	0.28	0.53	0.39	0.61	0.52	0.44	0.50	0.52	0.62	0.58	0.37	0.47	0.51	0.48
Ti	0.08	0.15	0.11	0.18	0.20	0.18	0.12	0.18	0.19	0.20	0.23	0.23	0.23	0.24
Cr	0.00	0.00	0.00	0.01	0.00	0.01	0.01	0.01	0.01	0.01	0.01	0.01	0.01	0.01
Fe ³⁺	0.58	0.49	0.47	0.60	0.50	0.56	0.92	0.48	0.47	0.65	0.54	0.34	0.49	0.55
Fe ²⁺	1.00	1.01	1.12	1.14	1.03	0.97	0.81	1.09	1.00	0.92	1.00	0.96	0.85	0.82
Mn	0.03	0.02	0.03	0.04	0.02	0.02	0.03	0.03	0.03	0.03	0.01	0.01	0.02	0.02
Mg	3.04	2.80	2.88	2.42	2.73	2.82	2.60	2.69	2.67	2.61	2.83	2.97	2.89	2.88
Ca	1.95	1.80	1.95	1.75	1.80	1.79	1.80	1.81	1.76	1.76	1.83	1.81	1.78	1.75
Na	0.39	0.60	0.43	0.66	0.64	0.61	0.61	0.65	0.58	0.63	0.74	0.76	0.78	0.81
K	0.01	0.01	0.01	0.02	0.02	0.02	0.02	0.02	0.02	0.02	0.04	0.04	0.03	0.03
F	0.05	0.00	0.03	0.05	0.00	0.00	0.00	0.00	0.04	0.02	0.02	0.00	0.00	0.00
Cl	0.00	0.00	0.00	0.00	0.00	0.00	0.00	0.00	0.00	0.00	0.00	0.00	0.00	0.00
OH	1.95	2.00	1.97	1.95	2.00	2.00	2.00	2.00	1.96	1.98	1.98	2.00	2.00	2.00
Total	17.36	17.41	17.39	17.43	17.46	17.42	17.43	17.48	17.35	17.40	17.61	17.61	17.60	17.60

Table C1 (continued)

Analysis	LUS12-5	LUS12-6	LUS12-7	LUS12-8	LUS12-9	LUS12-10	LUS12-11	LUS12-12	LUS12-13	LUS12-14	LUS12-15	LUS12-16	LUS13-1	LUS13-2
Amph. Type	prograde brown	prograde brown	prograde brown	prograde brown	retrograde green	retrograde green	corona green	corona brown	corona green	corona green	corona green	corona green	core brown	rim brown
Color														
SiO ₂	42.67	43.06	40.74	42.60	44.99	43.86	36.31	37.62	43.04	41.24	39.26	38.23	44.83	45.80
TiO ₂	2.56	2.16	2.28	2.13	1.76	1.26	0.09	0.06	1.71	1.37	0.05	0.06	1.33	1.08
Al ₂ O ₃	13.32	13.39	15.22	14.26	10.41	12.57	21.23	21.02	14.33	16.08	20.28	21.00	12.60	11.64
Cr ₂ O ₃	0.12	0.12	0.10	0.06	0.09	0.00	0.07	0.11	0.04	0.46	0.11	0.09	0.00	0.04
Fe ₂ O ₃	5.62	4.40	5.60	7.09	3.50	6.31	14.65	14.10	7.63	8.02	10.83	15.21	9.76	8.51
FeO	6.99	8.40	6.85	5.53	8.68	6.85	1.27	1.71	4.10	5.86	3.61	1.27	4.24	5.39
MnO	0.15	0.16	0.13	0.12	0.12	0.11	0.57	0.64	0.10	0.29	0.45	0.63	0.20	0.21
MgO	13.08	12.78	12.66	13.26	14.03	13.75	9.66	9.76	14.00	11.80	10.71	10.01	13.26	13.21
CaO	11.29	11.69	11.56	11.14	11.90	11.72	10.05	9.96	11.51	11.02	10.75	9.88	10.80	10.85
Na ₂ O	2.55	2.47	2.76	2.66	2.30	2.58	2.85	2.91	2.31	2.73	2.97	3.11	1.89	1.82
K ₂ O	0.19	0.17	0.22	0.17	0.16	0.18	0.10	0.10	0.09	0.16	0.12	0.08	0.09	0.06
F	0.00	0.06	0.09	0.00	0.00	0.09	0.22	0.05	0.06	0.00	0.00	0.00	0.10	0.18
Cl	0.02	0.02	0.02	0.01	0.02	0.02	0.00	0.00	0.01	0.01	0.01	0.00	0.02	0.01
H ₂ O	2.07	2.05	2.01	2.09	2.06	2.04	1.94	2.05	2.08	2.08	2.09	2.10	2.06	2.02
Total	100.64	100.90	100.24	101.11	100.02	101.35	99.00	100.07	101.00	101.12	101.23	101.68	101.17	100.80
Si	6.16	6.21	5.92	6.09	6.53	6.29	5.34	5.46	6.12	5.93	5.62	5.46	6.37	6.53
Al ^{iv}	1.84	1.79	2.08	1.91	1.47	1.71	2.66	2.54	1.88	2.07	2.38	2.54	1.63	1.47
Al ^{vi}	0.42	0.49	0.53	0.50	0.31	0.41	1.02	1.05	0.53	0.66	1.04	0.99	0.48	0.49
Ti	0.28	0.23	0.25	0.23	0.19	0.14	0.01	0.01	0.18	0.15	0.00	0.01	0.14	0.12
Cr	0.01	0.01	0.01	0.01	0.01	0.00	0.01	0.01	0.00	0.05	0.01	0.01	0.00	0.00
Fe ³⁺	0.61	0.48	0.61	0.76	0.38	0.68	1.62	1.54	0.82	0.87	1.17	1.63	1.04	0.91
Fe ²⁺	0.84	1.01	0.83	0.66	1.05	0.82	0.16	0.21	0.49	0.71	0.43	0.15	0.50	0.64
Mn	0.02	0.02	0.02	0.01	0.01	0.01	0.07	0.08	0.01	0.04	0.05	0.08	0.02	0.03
Mg	2.81	2.75	2.74	2.83	3.04	2.94	2.12	2.11	2.97	2.53	2.29	2.13	2.81	2.81
Ca	1.75	1.81	1.80	1.71	1.85	1.80	1.58	1.55	1.75	1.70	1.65	1.51	1.64	1.66
Na	0.71	0.69	0.78	0.74	0.65	0.72	0.81	0.82	0.64	0.76	0.82	0.86	0.52	0.50
K	0.04	0.03	0.04	0.03	0.03	0.03	0.02	0.02	0.02	0.03	0.02	0.01	0.02	0.01
F	0.00	0.03	0.04	0.00	0.00	0.04	0.10	0.02	0.03	0.00	0.00	0.00	0.05	0.08
Cl	0.00	0.00	0.00	0.00	0.01	0.00	0.00	0.00	0.00	0.00	0.00	0.00	0.00	0.00
OH	2.00	1.97	1.95	2.00	1.99	1.95	1.90	1.98	1.97	2.00	2.00	2.00	1.95	1.92
Total	17.50	17.53	17.62	17.47	17.53	17.55	17.41	17.38	17.41	17.49	17.49	17.38	17.18	17.17

Table C1 (continued)

Analysis	LUS13-3	LUS13-4	LUS13-5	LUS13-6	LUS13-7	LUS13-8	LUS13-9	LUS13-10	LUS13-11	LUS13-12	LUS14-1	LUS14-2	LUS14-3	LUS14-4
Amph. Type	core	rim	prograde	retrograde	retrograde	retrograde	retrograde							
Color	brown	green	brown	brown	brown	green								
SiO ₂	45.28	46.08	45.39	45.81	45.31	44.96	43.67	45.27	43.90	45.50	44.40	43.65	42.53	46.42
TiO ₂	1.44	0.56	1.24	1.17	1.40	1.39	1.36	1.00	1.50	1.27	1.88	1.69	1.82	1.09
Al ₂ O ₃	11.74	11.46	12.30	11.54	11.89	11.61	12.73	12.89	13.02	11.18	10.76	11.57	11.71	9.47
Cr ₂ O ₃	0.05	0.00	0.00	0.09	0.05	0.10	0.10	0.03	0.00	0.02	0.08	0.05	0.14	0.01
Fe ₂ O ₃	8.39	8.39	10.54	8.62	9.68	9.32	10.06	10.15	10.78	9.74	6.08	6.96	9.51	8.49
FeO	5.12	5.19	3.83	5.04	3.94	4.48	4.02	5.19	4.77	4.59	7.79	7.27	4.94	5.75
MnO	0.20	0.18	0.17	0.18	0.18	0.19	0.20	0.30	0.24	0.25	0.23	0.21	0.23	0.25
MgO	13.36	13.61	13.35	13.42	13.64	13.57	13.12	12.30	12.50	13.31	13.26	12.91	13.42	14.18
CaO	11.01	11.09	10.80	10.92	10.81	11.06	10.87	10.63	10.84	10.85	11.31	11.15	10.76	11.40
Na ₂ O	1.69	1.77	1.68	1.72	1.77	1.69	1.91	1.79	1.87	1.58	2.32	2.41	2.75	1.73
K ₂ O	0.07	0.10	0.06	0.07	0.06	0.07	0.08	0.07	0.09	0.05	0.12	0.09	0.12	0.09
F	0.01	0.10	0.12	0.08	0.03	0.08	0.00	0.02	0.07	0.09	0.06	0.00	0.01	0.00
Cl	0.01	0.02	0.01	0.01	0.01	0.01	0.01	0.01	0.02	0.00	0.01	0.00	0.01	0.01
H ₂ O	2.09	2.05	2.06	2.06	2.09	2.06	2.08	2.11	2.07	2.05	2.04	2.06	2.05	2.10
Total	100.45	100.60	101.55	100.74	100.85	100.58	100.22	101.74	101.67	100.48	100.32	100.02	99.98	100.98
Si	6.47	6.58	6.41	6.53	6.44	6.43	6.28	6.41	6.25	6.51	6.44	6.35	6.19	6.63
Al ^{iv}	1.53	1.42	1.59	1.47	1.56	1.57	1.72	1.59	1.75	1.49	1.56	1.65	1.81	1.37
Al ^{vi}	0.45	0.50	0.46	0.47	0.43	0.39	0.43	0.56	0.44	0.39	0.28	0.34	0.20	0.23
Ti	0.15	0.06	0.13	0.13	0.15	0.15	0.15	0.11	0.16	0.14	0.20	0.19	0.20	0.12
Cr	0.01	0.00	0.00	0.01	0.01	0.01	0.01	0.00	0.00	0.00	0.01	0.01	0.02	0.00
Fe ³⁺	0.90	0.90	1.12	0.92	1.04	1.00	1.09	1.08	1.16	1.05	0.66	0.76	1.04	0.91
Fe ²⁺	0.61	0.62	0.45	0.60	0.47	0.54	0.48	0.61	0.57	0.55	0.94	0.89	0.60	0.69
Mn	0.02	0.02	0.02	0.02	0.02	0.02	0.02	0.04	0.03	0.03	0.03	0.03	0.03	0.03
Mg	2.85	2.90	2.81	2.85	2.89	2.89	2.81	2.60	2.65	2.84	2.87	2.80	2.91	3.02
Ca	1.69	1.70	1.63	1.67	1.65	1.69	1.67	1.61	1.65	1.66	1.76	1.74	1.68	1.75
Na	0.47	0.49	0.46	0.47	0.49	0.47	0.53	0.49	0.52	0.44	0.65	0.68	0.78	0.48
K	0.01	0.02	0.01	0.01	0.01	0.01	0.01	0.01	0.02	0.01	0.02	0.02	0.02	0.02
F	0.00	0.05	0.05	0.04	0.01	0.04	0.00	0.01	0.03	0.04	0.03	0.00	0.00	0.00
Cl	0.00	0.00	0.00	0.00	0.00	0.00	0.00	0.00	0.00	0.00	0.00	0.00	0.00	0.00
OH	1.99	1.95	1.94	1.96	1.98	1.96	2.00	1.99	1.96	1.96	1.97	2.00	1.99	2.00
Total	17.17	17.20	17.11	17.15	17.15	17.18	17.22	17.12	17.18	17.11	17.43	17.43	17.47	17.24

Table C1 (continued)

Analysis	LUS14-5	LUS14-6	LUS14-7	LUS14-8	LUS14-9	LUS14-10	LUS14-11	LUS14-12	LUS14-13	LUS17-1	LUS17-2	LUS17-3	LUS17-4	LUS17-5
Amph. Type	retrograde	retrograde	prograde	prograde	prograde	prograde	corona	corona	corona	retrograde	retrograde	retrograde	retrograde	retrograde
Color	green	brown	brown	brown	brown	brown	brown	brown	brown	green	green	green	green	green
SiO ₂	44.90	46.33	44.71	44.47	43.47	43.99	41.79	43.15	42.35	44.33	44.80	47.36	40.30	42.42
TiO ₂	1.39	1.93	2.22	2.31	1.74	1.66	2.03	1.73	1.87	0.70	0.33	0.28	0.39	0.40
Al ₂ O ₃	10.71	9.53	10.84	11.03	11.32	11.66	13.37	13.14	13.16	10.23	9.81	7.74	13.51	11.22
Cr ₂ O ₃	0.07	0.12	0.00	0.13	0.10	0.07	0.29	0.15	0.07	0.00	1.22	0.03	0.08	0.01
Fe ₂ O ₃	7.35	4.55	7.42	5.31	9.52	8.67	6.73	6.74	8.29	5.10	6.18	2.60	4.23	4.90
FeO	6.99	8.50	6.37	7.96	4.08	5.38	6.96	7.03	6.15	11.57	9.44	12.35	13.99	12.32
MnO	0.21	0.18	0.21	0.19	0.23	0.22	0.23	0.22	0.22	0.28	0.26	0.27	0.25	0.27
MgO	13.31	13.91	13.65	13.30	13.97	13.44	12.42	12.62	12.69	11.79	12.14	13.12	9.58	10.85
CaO	11.12	11.34	10.90	11.21	10.87	10.86	11.11	10.95	10.95	12.08	12.19	12.62	12.64	12.27
Na ₂ O	2.30	2.33	2.46	2.43	2.36	2.41	2.64	2.73	2.69	2.08	1.28	1.62	2.44	2.06
K ₂ O	0.07	0.11	0.12	0.12	0.11	0.12	0.14	0.13	0.13	0.18	0.15	0.13	0.05	0.15
F	0.00	0.56	0.30	0.00	0.00	0.00	0.14	0.00	0.15	0.00	0.00	0.08	0.09	0.00
Cl	0.00	0.01	0.01	0.00	0.01	0.01	0.01	0.01	0.01	0.01	0.01	0.02	0.01	0.01
H ₂ O	2.08	1.82	1.95	2.07	2.07	2.08	1.98	2.07	2.00	2.03	2.04	2.00	1.94	1.99
Total	100.50	101.20	101.14	100.52	99.85	100.57	99.84	100.68	100.73	100.37	99.85	100.21	99.50	98.86
Si	6.48	6.65	6.42	6.43	6.29	6.34	6.11	6.23	6.13	6.53	6.59	6.93	6.10	6.39
Al ^{iv}	1.52	1.35	1.58	1.57	1.71	1.66	1.89	1.77	1.87	1.47	1.41	1.07	1.90	1.61
Al ^{vi}	0.31	0.27	0.25	0.31	0.22	0.31	0.42	0.47	0.38	0.31	0.28	0.27	0.50	0.38
Ti	0.15	0.21	0.24	0.25	0.19	0.18	0.22	0.19	0.20	0.08	0.04	0.03	0.04	0.04
Cr	0.01	0.01	0.00	0.01	0.01	0.01	0.03	0.02	0.01	0.00	0.14	0.00	0.01	0.00
Fe ³⁺	0.80	0.49	0.80	0.58	1.04	0.94	0.74	0.73	0.90	0.57	0.68	0.29	0.48	0.56
Fe ²⁺	0.84	1.02	0.76	0.96	0.49	0.65	0.85	0.85	0.74	1.43	1.16	1.51	1.77	1.55
Mn	0.03	0.02	0.03	0.02	0.03	0.03	0.03	0.03	0.03	0.03	0.03	0.03	0.03	0.03
Mg	2.87	2.98	2.92	2.86	3.02	2.89	2.71	2.72	2.74	2.59	2.66	2.86	2.16	2.44
Ca	1.72	1.74	1.67	1.74	1.69	1.67	1.74	1.69	1.70	1.91	1.92	1.98	2.05	1.98
Na	0.64	0.65	0.68	0.68	0.66	0.67	0.75	0.76	0.76	0.59	0.36	0.46	0.72	0.60
K	0.01	0.02	0.02	0.02	0.02	0.02	0.03	0.02	0.02	0.03	0.03	0.02	0.01	0.03
F	0.00	0.25	0.13	0.00	0.00	0.00	0.06	0.00	0.07	0.00	0.00	0.04	0.04	0.00
Cl	0.00	0.00	0.00	0.00	0.00	0.00	0.00	0.00	0.00	0.00	0.00	0.00	0.00	0.00
OH	2.00	1.74	1.86	2.00	2.00	1.93	2.00	1.93	2.00	2.00	1.96	1.95	2.00	2.00
Total	17.38	17.41	17.38	17.44	17.37	17.37	17.51	17.48	17.48	17.53	17.31	17.46	17.77	17.61

Table C1 (continued)

Analysis	LUS17-6	LUS17-7	LUS17-8	LUS17-9	LUS17-10	LUS17-11	LUS17-12	LUS17-13	LUS17-14	LUS17-15
Amph. Type	retrograde	retrograde	prograde	prograde	prograde	prograde	corona	corona	corona	corona
Color	green	brown	brown	brown	brown	brown	green	green	brown	brown
SiO ₂	42.13	42.80	40.61	44.31	41.86	41.57	40.58	38.74	41.99	42.84
TiO ₂	0.48	1.50	1.29	2.26	2.38	1.21	0.46	0.23	1.40	0.82
Al ₂ O ₃	11.30	14.47	14.13	11.09	13.29	14.29	14.33	15.49	12.88	12.40
Cr ₂ O ₃	0.14	0.01	0.09	0.11	0.10	0.09	0.06	0.01	0.05	0.02
Fe ₂ O ₃	5.69	0.00	6.86	2.49	3.36	6.27	6.77	6.49	3.44	4.28
FeO	11.83	12.48	9.64	11.12	11.35	8.86	10.48	11.39	12.20	13.09
MnO	0.26	0.19	0.38	0.18	0.14	0.25	0.32	0.36	0.30	0.28
MgO	10.83	8.90	10.40	12.09	10.98	11.64	9.92	9.21	10.72	10.28
CaO	12.15	14.73	11.32	11.70	11.38	11.60	11.66	11.83	11.97	12.02
Na ₂ O	2.10	1.58	2.49	1.93	2.51	2.71	2.19	2.60	2.28	2.18
K ₂ O	0.18	0.26	0.20	0.25	0.33	0.28	0.31	0.29	0.26	0.27
F	0.00	0.37	0.00	0.00	0.45	0.00	0.03	0.00	0.12	0.00
Cl	0.00	0.01	0.01	0.01	0.00	0.00	0.02	0.02	0.01	0.01
H ₂ O	1.99	1.84	2.01	2.04	1.81	2.05	1.98	1.97	1.95	2.02
Total	99.08	99.14	99.42	99.57	99.95	100.80	99.11	98.63	99.57	100.50
Si	6.33	6.36	6.04	6.51	6.19	6.07	6.08	5.88	6.25	6.34
Al ^{iv}	1.67	1.64	1.96	1.49	1.81	1.93	1.92	2.12	1.75	1.66
Al ^{vi}	0.34	0.89	0.52	0.43	0.51	0.53	0.61	0.65	0.51	0.51
Ti	0.05	0.17	0.14	0.25	0.26	0.13	0.05	0.03	0.16	0.09
Cr	0.02	0.00	0.01	0.01	0.01	0.01	0.01	0.00	0.01	0.00
Fe ³⁺	0.64	0.00	0.77	0.28	0.37	0.69	0.76	0.74	0.39	0.48
Fe ²⁺	1.49	1.55	1.20	1.37	1.40	1.08	1.31	1.45	1.52	1.62
Mn	0.03	0.02	0.05	0.02	0.02	0.03	0.04	0.05	0.04	0.03
Mg	2.43	1.97	2.31	2.65	2.42	2.53	2.21	2.09	2.38	2.27
Ca	1.96	2.35	1.81	1.84	1.80	1.81	1.87	1.92	1.91	1.91
Na	0.61	0.46	0.72	0.55	0.72	0.77	0.64	0.76	0.66	0.63
K	0.03	0.05	0.04	0.05	0.06	0.05	0.06	0.06	0.05	0.05
F	0.00	0.17	0.00	0.00	0.21	0.00	0.01	0.00	0.06	0.00
Cl	0.00	0.00	0.00	0.00	0.00	0.00	0.00	0.00	0.00	0.00
OH	2.00	1.83	2.00	2.00	1.79	2.00	1.98	2.00	1.94	2.00
Total	17.60	17.46	17.56	17.44	17.59	17.63	17.57	17.75	17.62	17.58

Clinopyroxene Mineral Chemistry

Table C2 : Mineral Chemistry of CPX

Analysis	BAI19-px1	BAI19-px2	BAI19-px3	BAI19-px4	BAI19-px5	BAI19-px6	BAI19-px7	BAI19-px8	BAI19-px9	BUM04-px1	BUM04-px2	BUM04-px3
Rock type	Cpx											
SiO ₂	53,14	51,89	51,63	52,61	52,16	51,04	52,22	51,55	51,36	53,48	53,01	53,29
TiO ₂	0,08	0,09	0,17	0,07	0,06	0,15	0,08	0,12	0,18	0,05	0,09	0,11
Al ₂ O ₃	0,84	2,49	2,29	1,24	1,95	3,04	1,75	3,09	3,02	1,09	1,89	1,57
Cr ₂ O ₃	0,00	0,02	0,01	0,00	0,03	0,00	0,00	0,03	0,01	0,03	0,05	0,01
Fe ₂ O ₃	2,26	4,00	4,28	3,95	3,22	2,49	2,66	2,42	2,69	4,01	1,55	2,10
MgO	12,94	11,87	11,85	12,61	12,05	11,65	12,45	11,75	11,76	14,01	13,09	13,72
CaO	24,11	23,66	23,34	24,03	23,28	22,23	22,82	22,33	22,31	24,55	24,17	24,25
MnO	0,34	0,32	0,29	0,34	0,36	0,27	0,29	0,26	0,27	0,24	0,28	0,25
FeO	6,62	6,11	6,27	5,87	6,74	6,83	6,89	7,28	7,33	3,39	5,79	5,21
Na ₂ O	0,58	0,91	0,93	0,76	0,87	1,03	0,84	1,00	0,95	0,85	0,67	0,61
Total	100,91	101,35	101,04	101,47	100,71	98,72	100,00	99,83	99,88	101,69	100,59	101,13
Si	1,97	1,92	1,92	1,94	1,94	1,93	1,95	1,93	1,92	1,95	1,96	1,96
Al ^{iv}	0,03	0,08	0,08	0,05	0,06	0,07	0,05	0,07	0,08	0,05	0,04	0,04
Al ^{vi}	0,01	0,03	0,02	0,00	0,03	0,07	0,03	0,07	0,06	0,00	0,04	0,02
Fe ²⁺	0,21	0,19	0,20	0,18	0,21	0,22	0,22	0,23	0,23	0,10	0,18	0,16
Mg	0,72	0,66	0,66	0,69	0,67	0,66	0,69	0,66	0,66	0,76	0,72	0,75
Mn	0,01	0,01	0,01	0,01	0,01	0,01	0,01	0,01	0,01	0,01	0,01	0,01
Ti	0,00	0,00	0,01	0,00	0,00	0,00	0,00	0,00	0,00	0,00	0,00	0,00
Cr	0,00	0,00	0,00	0,00	0,00	0,00	0,00	0,00	0,00	0,00	0,00	0,00
Fe ³⁺	0,06	0,11	0,12	0,11	0,09	0,07	0,07	0,07	0,08	0,11	0,04	0,06
Ca	0,96	0,94	0,93	0,95	0,93	0,90	0,91	0,90	0,90	0,96	0,96	0,95
Na	0,04	0,07	0,07	0,05	0,06	0,08	0,06	0,07	0,07	0,06	0,05	0,04
Total	4,00	4,00	4,00	4,00	4,00	4,00	4,00	4,00	4,00	4,00	4,00	4,00
Mg#	0,78	0,78	0,77	0,79	0,76	0,75	0,76	0,74	0,74	0,88	0,80	0,82
Wol. - Ca	0,50	0,51	0,50	0,51	0,50	0,49	0,49	0,48	0,48	0,51	0,50	0,50
Ens. - Mg	0,37	0,35	0,36	0,37	0,36	0,35	0,37	0,35	0,35	0,40	0,38	0,39
Fer. - Fe ²⁺	0,11	0,10	0,11	0,10	0,11	0,12	0,11	0,12	0,12	0,05	0,09	0,08
Jad. - Na	0,02	0,04	0,04	0,03	0,03	0,04	0,03	0,04	0,04	0,03	0,03	0,02

Table C2 (continued)

Analysis	BUM14-px1	BUM14-px2	BUM14-px3	BUM14-px4	BUM14-px5	BUM14-px6	BUM14-px7	BUM14-px8	BUM24-px1	BUM24-px2	BUM24-px3	BUM24-px4
Rock type	Cpx											
SiO ₂	52,24	50,71	50,68	52,18	50,39	50,84	51,58	49,58	52,01	53,23	53,08	53,33
TiO ₂	0,07	0,29	0,19	0,05	0,33	0,25	0,03	0,26	0,09	0,05	0,05	0,07
Al ₂ O ₃	1,04	3,18	3,38	0,94	3,23	2,68	1,67	4,10	1,72	0,90	1,23	1,14
Cr ₂ O ₃	0,03	0,05	0,04	0,08	0,12	0,08	0,03	0,00	0,00	0,03	0,00	0,07
Fe ₂ O ₃	4,91	5,35	3,10	3,55	4,75	4,10	2,86	5,28	2,73	2,97	0,00	3,09
MgO	12,15	11,22	11,10	12,08	11,11	11,27	12,65	10,32	13,70	14,03	13,26	13,75
CaO	24,95	23,59	23,77	23,49	23,82	23,45	22,87	22,17	23,43	24,56	24,53	24,24
MnO	0,37	0,30	0,32	0,51	0,35	0,39	0,36	0,38	0,32	0,28	0,26	0,26
FeO	6,03	6,17	7,08	7,32	6,42	7,11	7,93	7,61	5,53	4,33	7,65	4,27
Na ₂ O	0,54	0,91	0,68	0,64	0,75	0,73	0,34	1,02	0,43	0,57	0,00	0,81
Total	102,32	101,74	100,33	100,84	101,26	100,88	100,31	100,71	99,95	100,93	100,06	101,03
Si	1,93	1,88	1,90	1,95	1,88	1,90	1,93	1,86	1,94	1,96	1,98	1,96
Al ^{iv}	0,05	0,12	0,10	0,04	0,12	0,10	0,07	0,14	0,06	0,04	0,02	0,04
Al ^{vi}	0,00	0,02	0,05	0,00	0,02	0,02	0,01	0,05	0,01	0,00	0,03	0,01
Fe ²⁺	0,19	0,19	0,22	0,23	0,20	0,22	0,25	0,24	0,17	0,13	0,24	0,13
Mg	0,67	0,62	0,62	0,67	0,62	0,63	0,71	0,58	0,76	0,77	0,74	0,75
Mn	0,01	0,01	0,01	0,02	0,01	0,01	0,01	0,01	0,01	0,01	0,01	0,01
Ti	0,00	0,01	0,01	0,00	0,01	0,01	0,00	0,01	0,00	0,00	0,00	0,00
Cr	0,00	0,00	0,00	0,00	0,00	0,00	0,00	0,00	0,00	0,00	0,00	0,00
Fe ³⁺	0,14	0,15	0,09	0,10	0,13	0,12	0,08	0,15	0,08	0,08	0,00	0,09
Ca	0,99	0,94	0,96	0,94	0,95	0,94	0,92	0,89	0,94	0,97	0,98	0,95
Na	0,04	0,07	0,05	0,05	0,05	0,05	0,02	0,07	0,03	0,04	0,00	0,06
Total	4,00	4,00	4,00	4,00	4,00	4,00	4,00	4,00	4,00	4,00	3,99	4,00
Mg#	0,78	0,76	0,74	0,75	0,76	0,74	0,74	0,71	0,82	0,85	0,76	0,85
Wol. - Ca	0,52	0,52	0,52	0,50	0,52	0,51	0,48	0,50	0,49	0,51	0,50	0,50
Ens. - Mg	0,36	0,34	0,34	0,36	0,34	0,34	0,37	0,32	0,40	0,40	0,38	0,40
Fer. - Fe ²⁺	0,10	0,11	0,12	0,12	0,11	0,12	0,13	0,13	0,09	0,07	0,12	0,07
Jad. - Na	0,02	0,04	0,03	0,02	0,03	0,03	0,01	0,04	0,02	0,02	0,00	0,03

Table C2 (continued)

Analysis	BUM24-px5	BUM24-px6	BUM24-px7	LUS02-px1	LUS02-px2	LUS02-px3	LUS02-px4	LUS02-px5	LUS02-px6	LUS02-px7	LUS02-px8	LUS05-px1
Rock type	Cpx	Cpx	Cpx	Dyke	Cpx							
SiO ₂	53,10	53,45	53,84	50,65	50,81	50,65	50,40	50,49	50,41	51,31	47,20	53,37
TiO ₂	0,09	0,04	0,00	0,64	0,67	0,66	0,77	0,60	0,60	0,67	0,86	0,02
Al ₂ O ₃	1,63	1,40	2,58	3,56	3,78	3,53	3,94	3,58	3,48	3,31	4,65	1,29
Cr ₂ O ₃	0,00	0,08	0,02	0,00	0,03	0,00	0,07	0,03	0,01	0,07	0,00	0,04
Fe ₂ O ₃	5,94	3,79	0,00	2,75	2,73	2,43	2,72	2,70	2,56	1,47	5,92	4,07
MgO	13,34	13,64	11,51	15,57	15,35	15,53	15,10	15,46	15,49	15,54	14,13	13,63
CaO	24,13	24,18	22,80	17,35	19,51	17,35	18,93	17,29	17,23	19,18	14,07	23,70
MnO	0,25	0,27	0,37	0,27	0,22	0,29	0,27	0,31	0,30	0,22	0,28	0,46
FeO	2,46	4,10	7,74	9,51	7,49	9,78	8,35	9,57	9,62	8,45	12,63	3,66
Na ₂ O	1,33	0,92	1,24	0,30	0,28	0,25	0,25	0,28	0,26	0,22	0,23	1,09
Total	102,26	101,86	100,10	100,58	100,87	100,47	100,80	100,31	99,97	100,44	99,96	101,33
Si	1,93	1,95	2,00	1,88	1,87	1,88	1,86	1,88	1,88	1,90	1,80	1,95
Al ^{iv}	0,07	0,05	0,00	0,12	0,13	0,12	0,14	0,12	0,12	0,11	0,21	0,05
Al ^{vi}	0,00	0,01	0,11	0,03	0,04	0,03	0,04	0,03	0,03	0,04	0,00	0,01
Fe ²⁺	0,08	0,13	0,24	0,30	0,23	0,30	0,26	0,30	0,30	0,26	0,40	0,11
Mg	0,72	0,74	0,64	0,86	0,84	0,86	0,83	0,86	0,86	0,86	0,80	0,74
Mn	0,01	0,01	0,01	0,01	0,01	0,01	0,01	0,01	0,01	0,01	0,01	0,01
Ti	0,00	0,00	0,00	0,02	0,02	0,02	0,02	0,02	0,02	0,02	0,03	0,00
Cr	0,00	0,00	0,00	0,00	0,00	0,00	0,00	0,00	0,00	0,00	0,00	0,00
Fe ³⁺	0,16	0,10	0,00	0,08	0,08	0,07	0,08	0,08	0,07	0,04	0,17	0,11
Ca	0,94	0,95	0,91	0,69	0,77	0,69	0,75	0,69	0,69	0,76	0,57	0,93
Na	0,09	0,07	0,09	0,02	0,02	0,02	0,02	0,02	0,02	0,02	0,02	0,08
Total	4,00	4,00	3,99	4,00	4,00	4,00	4,00	4,00	4,00	4,00	4,00	4,00
Mg#	0,91	0,86	0,73	0,74	0,78	0,74	0,76	0,74	0,74	0,77	0,67	0,87
Wol. - Ca	0,51	0,50	0,48	0,37	0,41	0,37	0,40	0,37	0,37	0,40	0,32	0,50
Ens. - Mg	0,39	0,39	0,34	0,46	0,45	0,46	0,45	0,46	0,46	0,45	0,45	0,40
Fer. - Fe ²⁺	0,04	0,07	0,13	0,16	0,12	0,16	0,14	0,16	0,16	0,14	0,22	0,06
Jad. - Na	0,05	0,03	0,05	0,01	0,01	0,01	0,01	0,01	0,01	0,01	0,01	0,04

Table C2 (continued)

Analysis	LUS05-px2	LUS07-px1	LUS07-px2	LUS07-px3	LUS07-px4	LUS07-px5	LUS07-px6	LUS07-px7	LUS07-px8	LUS07-px9	LUS07-px10	LUS07-px11
Rock type Cpx		Garnet	Garnet									
SiO ₂	51,78	49,89	51,37	50,50	51,30	51,58	51,30	50,42	50,94	50,79	50,69	53,11
TiO ₂	0,16	0,71	0,53	0,59	0,43	0,52	0,45	0,60	0,60	0,54	0,50	0,19
Al ₂ O ₃	3,04	5,46	4,86	5,77	4,38	3,61	5,43	5,61	6,01	5,72	5,59	1,86
Cr ₂ O ₃	0,00	0,08	0,06	0,09	0,08	0,02	0,10	0,06	0,10	0,01	0,05	0,00
Fe ₂ O ₃	5,40	2,78	1,39	1,39	1,73	2,81	0,56	2,24	0,56	1,65	1,35	2,41
MgO	12,12	11,86	12,64	12,08	12,51	13,34	12,33	12,44	12,53	12,47	12,47	14,36
CaO	22,43	23,04	22,84	22,30	22,99	23,44	22,46	23,01	22,49	22,87	22,59	23,82
MnO	0,41	0,37	0,20	0,31	0,23	0,25	0,23	0,20	0,15	0,16	0,21	0,19
FeO	4,61	5,65	6,79	6,58	6,00	5,59	7,48	5,95	6,70	6,04	6,54	5,33
Na ₂ O	1,45	0,78	0,67	0,85	0,80	0,54	0,71	0,65	0,75	0,75	0,68	0,44
Total	101,39	100,63	101,35	100,47	100,45	101,68	101,04	101,19	100,82	101,00	100,66	101,70
Si	1,91	1,85	1,88	1,87	1,90	1,89	1,89	1,85	1,87	1,87	1,87	1,94
Al ^{iv}	0,09	0,15	0,12	0,13	0,10	0,11	0,11	0,15	0,13	0,14	0,13	0,06
Al ^{vi}	0,04	0,09	0,09	0,12	0,09	0,04	0,12	0,10	0,13	0,11	0,11	0,02
Fe ²⁺	0,14	0,18	0,21	0,20	0,19	0,17	0,23	0,18	0,21	0,19	0,20	0,16
Mg	0,67	0,66	0,69	0,67	0,69	0,73	0,68	0,68	0,69	0,68	0,69	0,78
Mn	0,01	0,01	0,01	0,01	0,01	0,01	0,01	0,01	0,01	0,01	0,01	0,01
Ti	0,01	0,02	0,02	0,02	0,01	0,01	0,01	0,02	0,02	0,02	0,01	0,01
Cr	0,00	0,00	0,00	0,00	0,00	0,00	0,00	0,00	0,00	0,00	0,00	0,00
Fe ³⁺	0,15	0,08	0,04	0,04	0,05	0,08	0,02	0,06	0,02	0,05	0,04	0,07
Ca	0,89	0,92	0,90	0,88	0,91	0,92	0,89	0,91	0,89	0,90	0,89	0,93
Na	0,10	0,06	0,05	0,06	0,06	0,04	0,05	0,05	0,05	0,05	0,05	0,03
Total	4,00	4,00	4,00	4,00	4,00	4,00	4,00	4,00	4,00	4,00	4,00	4,00
Mg#	0,82	0,79	0,77	0,77	0,79	0,81	0,75	0,79	0,77	0,79	0,77	0,83
Wol. - Ca	0,49	0,51	0,49	0,49	0,49	0,50	0,48	0,50	0,48	0,49	0,49	0,49
Ens. - Mg	0,37	0,36	0,37	0,37	0,37	0,39	0,37	0,38	0,37	0,37	0,37	0,41
Fer. - Fe ²⁺	0,08	0,10	0,11	0,11	0,10	0,09	0,12	0,10	0,11	0,10	0,11	0,09
Jad. - Na	0,06	0,03	0,03	0,03	0,03	0,02	0,03	0,03	0,03	0,03	0,03	0,02

Table C2 (continued)

Analysis	LUS07-px12	LUS07-px13	LUS07-px14	LUS07-px15	LUS08-px1	LUS08-px2	LUS08-px3	LUS08-px4	LUS08-px5	LUS09-px1	LUS09-px2	LUS11-px1
Rock type	Garnet	Garnet	Garnet	Garnet	Cpx							
SiO ₂	52,12	53,97	53,60	50,38	53,03	53,01	52,73	53,24	53,25	52,61	52,26	53,02
TiO ₂	0,51	0,09	0,14	0,61	0,10	0,03	0,07	0,03	0,09	0,07	0,04	0,11
Al ₂ O ₃	3,83	1,02	1,60	5,75	2,03	1,55	2,34	2,09	1,84	1,31	2,31	1,89
Cr ₂ O ₃	0,07	0,06	0,05	0,02	0,00	0,09	0,00	0,00	0,00	0,00	0,00	0,07
Fe ₂ O ₃	0,48	0,51	0,22	1,71	6,65	5,85	5,71	4,96	4,12	3,22	3,26	1,62
MgO	13,05	14,29	13,57	12,25	12,67	12,42	12,79	13,66	13,91	12,16	11,78	13,05
CaO	22,96	24,40	24,36	22,06	21,82	21,58	21,95	22,58	22,85	23,90	23,44	23,94
MnO	0,20	0,27	0,28	0,30	0,33	0,28	0,30	0,38	0,33	0,44	0,45	0,31
FeO	7,14	6,14	6,76	6,48	3,74	4,09	3,70	3,08	3,42	6,76	6,92	6,64
Na ₂ O	0,59	0,32	0,38	0,84	1,92	1,99	1,76	1,49	1,27	0,74	0,88	0,56
Total	100,95	101,06	100,95	100,41	102,28	100,89	101,35	101,51	101,08	101,21	101,34	101,19
Si	1,92	1,98	1,97	1,86	1,93	1,95	1,93	1,94	1,94	1,95	1,94	1,95
Al ^{iv}	0,08	0,02	0,03	0,14	0,07	0,05	0,07	0,06	0,06	0,05	0,06	0,05
Al ^{vi}	0,08	0,02	0,04	0,12	0,02	0,02	0,03	0,03	0,02	0,01	0,04	0,04
Fe ²⁺	0,22	0,19	0,21	0,20	0,11	0,13	0,11	0,09	0,10	0,21	0,21	0,21
Mg	0,72	0,78	0,74	0,68	0,69	0,68	0,70	0,74	0,76	0,67	0,65	0,72
Mn	0,01	0,01	0,01	0,01	0,01	0,01	0,01	0,01	0,01	0,01	0,01	0,01
Ti	0,01	0,00	0,00	0,02	0,00	0,00	0,00	0,00	0,00	0,00	0,00	0,00
Cr	0,00	0,00	0,00	0,00	0,00	0,00	0,00	0,00	0,00	0,00	0,00	0,00
Fe ³⁺	0,01	0,01	0,01	0,05	0,18	0,16	0,16	0,14	0,11	0,09	0,09	0,05
Ca	0,91	0,96	0,96	0,87	0,85	0,85	0,86	0,88	0,90	0,95	0,93	0,95
Na	0,04	0,02	0,03	0,06	0,14	0,14	0,13	0,11	0,09	0,05	0,06	0,04
Total	4,00	4,00	4,00	4,00	4,00	4,00	4,00	4,00	3,99	4,00	4,00	4,00
Mg#	0,76	0,81	0,78	0,77	0,86	0,84	0,86	0,89	0,88	0,76	0,75	0,78
Wol. - Ca	0,48	0,49	0,50	0,48	0,48	0,47	0,48	0,48	0,48	0,50	0,50	0,50
Ens. - Mg	0,38	0,40	0,38	0,37	0,38	0,38	0,39	0,41	0,41	0,36	0,35	0,38
Fer. - Fe ²⁺	0,12	0,10	0,11	0,11	0,06	0,07	0,06	0,05	0,06	0,11	0,12	0,11
Jad. - Na	0,02	0,01	0,01	0,03	0,08	0,08	0,07	0,06	0,05	0,03	0,03	0,02

Table C2 (continued)

Analysis	LUS11-px2	LUS11-px3	LUS11-px4	LUS11-px5	LUS11-px6	LUS11-px7	LUS11-px8	LUS11-px9	LUS11-px10	LUS11-px11	LUS11-px12	LUS12-px1
Rock type	Cpx	Cpx	Cpx	Garnet								
SiO ₂	53,17	52,93	52,46	52,73	53,12	52,65	53,67	53,00	52,91	53,12	52,88	49,10
TiO ₂	0,06	0,03	0,10	0,12	0,09	0,12	0,15	0,10	0,07	0,09	0,08	0,52
Al ₂ O ₃	1,97	1,37	2,75	1,98	1,32	2,26	1,43	1,72	1,34	1,71	2,35	5,09
Cr ₂ O ₃	0,54	0,19	0,44	0,28	0,01	0,10	0,04	0,25	0,07	0,01	0,09	0,12
Fe ₂ O ₃	1,41	2,47	1,24	2,50	0,97	2,55	0,93	1,65	1,30	0,75	0,38	4,02
MgO	13,02	13,27	12,68	13,00	13,17	12,80	13,06	13,01	13,03	13,01	12,65	13,39
CaO	23,19	24,30	22,71	23,74	23,91	23,83	23,91	23,90	23,16	23,62	22,65	21,86
MnO	0,29	0,28	0,32	0,27	0,26	0,29	0,30	0,30	0,35	0,28	0,29	0,20
FeO	6,49	6,15	7,35	6,01	7,44	6,36	7,52	6,80	7,75	7,36	8,31	4,74
Na ₂ O	0,85	0,45	0,74	0,71	0,38	0,66	0,55	0,55	0,50	0,53	0,67	0,51
Total	100,99	101,44	100,79	101,33	100,68	101,60	101,56	101,27	100,48	100,48	100,35	99,53
Si	1,96	1,95	1,94	1,94	1,97	1,94	1,97	1,95	1,97	1,97	1,96	1,83
Al ^{iv}	0,04	0,05	0,06	0,06	0,03	0,06	0,03	0,05	0,03	0,03	0,04	0,17
Al ^{vi}	0,05	0,01	0,06	0,03	0,03	0,03	0,03	0,03	0,03	0,04	0,07	0,06
Fe ²⁺	0,20	0,19	0,23	0,19	0,23	0,20	0,23	0,21	0,24	0,23	0,26	0,15
Mg	0,72	0,73	0,70	0,71	0,73	0,70	0,72	0,72	0,72	0,72	0,70	0,75
Mn	0,01	0,01	0,01	0,01	0,01	0,01	0,01	0,01	0,01	0,01	0,01	0,01
Ti	0,00	0,00	0,00	0,00	0,00	0,00	0,00	0,00	0,00	0,00	0,00	0,01
Cr	0,02	0,01	0,01	0,01	0,00	0,00	0,00	0,01	0,00	0,00	0,00	0,00
Fe ³⁺	0,04	0,07	0,04	0,07	0,03	0,07	0,03	0,05	0,04	0,02	0,01	0,11
Ca	0,92	0,96	0,90	0,94	0,95	0,94	0,94	0,94	0,92	0,94	0,90	0,88
Na	0,06	0,03	0,05	0,05	0,03	0,05	0,04	0,04	0,04	0,04	0,05	0,04
Total	4,00	4,00	4,00	4,00	4,00	4,00	4,00	4,00	4,00	4,00	4,00	4,00
Mg#	0,78	0,79	0,75	0,79	0,76	0,78	0,76	0,77	0,75	0,76	0,73	0,83
Wol. - Ca	0,48	0,50	0,48	0,50	0,49	0,50	0,49	0,50	0,48	0,49	0,47	0,48
Ens. - Mg	0,38	0,38	0,37	0,38	0,38	0,37	0,37	0,37	0,38	0,37	0,37	0,41
Fer. - Fe ²⁺	0,11	0,10	0,12	0,10	0,12	0,10	0,12	0,11	0,13	0,12	0,14	0,08
Jad. - Na	0,03	0,02	0,03	0,03	0,01	0,02	0,02	0,02	0,02	0,02	0,03	0,02

Table C2 (continued)

Analysis	LUS12-px2	LUS12-px3	LUS12-px4	LUS12-px5	LUS12-px6	LUS12-px7	LUS12-px8	LUS12-px9	LUS12-px10	LUS12-px11	LUS12-px12	LUS12-px13
Rock type	Garnet	Garnet	Garnet	Garnet								
SiO ₂	49,38	52,47	52,69	49,96	49,61	49,83	49,44	50,01	50,42	50,56	50,24	50,31
TiO ₂	0,61	0,28	0,23	0,44	0,51	0,68	0,76	0,67	0,65	0,51	0,56	0,52
Al ₂ O ₃	6,58	3,25	3,15	6,93	6,94	6,26	6,00	6,54	5,46	5,38	6,59	6,51
Cr ₂ O ₃	0,00	0,04	0,04	0,02	0,01	0,03	0,05	0,06	0,07	0,14	0,08	0,02
Fe ₂ O ₃	4,30	2,33	2,49	3,10	3,10	3,44	3,11	3,44	3,36	3,14	3,53	1,50
MgO	12,88	14,41	13,77	12,46	12,39	12,81	13,17	12,77	13,10	13,27	12,95	12,69
CaO	22,02	22,99	24,30	22,21	22,16	22,16	21,46	22,21	22,69	22,41	21,59	21,53
MnO	0,14	0,10	0,13	0,17	0,10	0,14	0,14	0,11	0,17	0,14	0,12	0,11
FeO	4,41	4,79	4,52	4,81	4,62	4,71	5,52	4,47	4,46	4,59	4,58	6,34
Na ₂ O	0,84	0,64	0,62	0,97	0,99	0,89	0,68	0,99	0,83	0,82	1,11	0,85
Total	101,17	101,29	101,95	101,08	100,42	100,95	100,33	101,28	101,20	100,96	101,33	100,38
Si	1,81	1,91	1,91	1,83	1,83	1,83	1,83	1,83	1,85	1,85	1,83	1,85
Al ^{iv}	0,19	0,09	0,09	0,17	0,17	0,17	0,17	0,17	0,15	0,15	0,17	0,15
Al ^{vi}	0,10	0,05	0,05	0,13	0,13	0,10	0,09	0,11	0,08	0,09	0,12	0,14
Fe ²⁺	0,14	0,15	0,14	0,15	0,14	0,14	0,17	0,14	0,14	0,14	0,14	0,20
Mg	0,70	0,78	0,75	0,68	0,68	0,70	0,73	0,70	0,72	0,73	0,70	0,70
Mn	0,00	0,00	0,00	0,01	0,00	0,00	0,00	0,00	0,01	0,00	0,00	0,00
Ti	0,02	0,01	0,01	0,01	0,01	0,02	0,02	0,02	0,02	0,01	0,02	0,01
Cr	0,00	0,00	0,00	0,00	0,00	0,00	0,00	0,00	0,00	0,00	0,00	0,00
Fe ³⁺	0,12	0,06	0,07	0,09	0,09	0,10	0,09	0,10	0,09	0,09	0,10	0,04
Ca	0,87	0,90	0,95	0,87	0,87	0,87	0,85	0,87	0,89	0,88	0,84	0,85
Na	0,06	0,05	0,04	0,07	0,07	0,06	0,05	0,07	0,06	0,06	0,08	0,06
Total	4,00	4,00	4,00	4,00	4,00	4,00	4,00	4,00	4,00	4,00	4,00	4,00
Mg#	0,84	0,84	0,84	0,82	0,83	0,83	0,81	0,84	0,84	0,84	0,83	0,78
Wol. - Ca	0,49	0,48	0,51	0,49	0,49	0,49	0,47	0,49	0,49	0,49	0,48	0,47
Ens. - Mg	0,40	0,42	0,40	0,38	0,39	0,39	0,40	0,39	0,40	0,40	0,40	0,39
Fer. - Fe ²⁺	0,08	0,08	0,07	0,08	0,08	0,08	0,10	0,08	0,08	0,08	0,08	0,11
Jad. - Na	0,03	0,02	0,02	0,04	0,04	0,04	0,03	0,04	0,03	0,03	0,04	0,03

Table C2 (continued)

Analysis	LUS12-px14	LUS12-px15	LUS12-px16	LUS12-px17	LUS14-px1	LUS14-px2	LUS14-px3	LUS14-px4	LUS14-px5	LUS14-px6	LUS17-px1	LUS17-px2
Rock type	Garnet	Garnet	Garnet	Garnet	Garnet	Garnet	Garnet	Garnet	Garnet	Garnet	Garnet	Garnet
SiO ₂	49,47	52,77	53,20	50,13	51,17	51,97	52,31	52,56	51,34	52,81	49,72	52,50
TiO ₂	0,85	0,22	0,18	0,74	0,25	0,29	0,29	0,20	0,33	0,19	0,69	0,27
Al ₂ O ₃	6,71	2,42	2,27	6,18	2,84	2,85	2,53	2,13	3,48	2,93	4,91	2,17
Cr ₂ O ₃	0,08	0,03	0,01	0,08	0,05	0,05	0,03	0,06	0,00	0,00	0,04	0,09
Fe ₂ O ₃	2,04	1,19	0,56	1,78	3,16	5,59	3,23	1,92	3,52	1,64	5,25	1,47
MgO	12,61	14,10	14,03	13,06	13,15	14,13	13,80	14,09	13,12	13,57	11,60	12,94
CaO	21,75	23,95	24,37	21,68	22,43	21,63	22,55	22,58	22,20	22,38	22,88	23,80
MnO	0,16	0,12	0,12	0,11	0,31	0,26	0,28	0,26	0,29	0,34	0,22	0,27
FeO	5,89	5,13	5,46	5,45	5,72	3,53	5,30	6,17	5,44	6,57	5,02	6,73
Na ₂ O	0,76	0,48	0,42	0,86	0,69	1,23	0,80	0,55	0,89	0,76	1,04	0,53
Total	100,31	100,40	100,62	100,06	99,77	101,52	101,12	100,51	100,61	101,19	101,38	100,77
Si	1,83	1,94	1,95	1,85	1,91	1,90	1,92	1,94	1,90	1,94	1,84	1,94
Al ^{iv}	0,17	0,06	0,05	0,15	0,09	0,10	0,08	0,06	0,10	0,06	0,16	0,06
Al ^{vi}	0,12	0,05	0,05	0,12	0,03	0,02	0,03	0,03	0,05	0,06	0,05	0,04
Fe ²⁺	0,18	0,16	0,17	0,17	0,18	0,11	0,16	0,19	0,17	0,20	0,16	0,21
Mg	0,69	0,77	0,77	0,72	0,73	0,77	0,76	0,78	0,72	0,74	0,64	0,71
Mn	0,01	0,00	0,00	0,00	0,01	0,01	0,01	0,01	0,01	0,01	0,01	0,01
Ti	0,02	0,01	0,01	0,02	0,01	0,01	0,01	0,01	0,01	0,01	0,02	0,01
Cr	0,00	0,00	0,00	0,00	0,00	0,00	0,00	0,00	0,00	0,00	0,00	0,00
Fe ³⁺	0,06	0,03	0,02	0,05	0,09	0,15	0,09	0,05	0,10	0,05	0,15	0,04
Ca	0,86	0,94	0,96	0,86	0,90	0,85	0,89	0,89	0,88	0,88	0,91	0,94
Na	0,05	0,03	0,03	0,06	0,05	0,09	0,06	0,04	0,06	0,05	0,08	0,04
Total	4,00	4,00	4,00	4,00	4,00	4,00	4,00	4,00	4,00	4,00	4,00	4,00
Mg#	0,79	0,83	0,82	0,81	0,80	0,88	0,82	0,80	0,81	0,79	0,80	0,77
Wol. - Ca	0,48	0,49	0,50	0,47	0,48	0,47	0,48	0,47	0,48	0,47	0,51	0,50
Ens. - Mg	0,39	0,41	0,40	0,40	0,39	0,42	0,41	0,41	0,39	0,40	0,36	0,38
Fer. - Fe ²⁺	0,10	0,08	0,09	0,09	0,10	0,06	0,09	0,10	0,09	0,11	0,09	0,11
Jad. - Na	0,03	0,02	0,02	0,03	0,03	0,05	0,03	0,02	0,03	0,03	0,04	0,02

Table C2 (continued)

Analysis	LUS17-px3	LUS17-px4	LUS17-px5	LUS17-px6	LUS17-px7
Rock type	Garnet	Garnet	Garnet	Garnet	Garnet
SiO ₂	48,32	53,76	51,42	52,02	54,21
TiO ₂	0,79	0,07	0,27	0,08	0,02
Al ₂ O ₃	5,82	0,67	2,91	1,24	0,43
Cr ₂ O ₃	0,01	0,00	0,09	0,03	0,00
Fe ₂ O ₃	4,60	0,93	2,80	0,95	0,63
MgO	11,36	13,67	12,44	12,40	13,72
CaO	21,04	24,80	22,76	23,89	24,87
MnO	0,19	0,32	0,41	0,31	0,33
FeO	6,29	6,52	7,17	7,68	7,12
Na ₂ O	1,04	0,29	0,61	0,34	0,23
Total	99,45	101,02	100,86	98,93	101,55
Si	1,82	1,98	1,91	1,97	1,99
Al ^{iv}	0,18	0,02	0,09	0,03	0,01
Al ^{vi}	0,08	0,01	0,04	0,02	0,01
Fe ²⁺	0,20	0,20	0,22	0,24	0,22
Mg	0,64	0,75	0,69	0,70	0,75
Mn	0,01	0,01	0,01	0,01	0,01
Ti	0,02	0,00	0,01	0,00	0,00
Cr	0,00	0,00	0,00	0,00	0,00
Fe ³⁺	0,13	0,03	0,08	0,03	0,02
Ca	0,85	0,98	0,91	0,97	0,98
Na	0,08	0,02	0,04	0,03	0,02
Total	4,00	4,00	4,00	4,00	4,00
Mg#	0,76	0,79	0,76	0,74	0,77
Wol. - Ca	0,48	0,50	0,49	0,50	0,50
Ens. - Mg	0,36	0,38	0,37	0,36	0,38
Fer. - Fe ²⁺	0,11	0,10	0,12	0,13	0,11
Jad. - Na	0,04	0,01	0,02	0,01	0,01

Garnet Mineral Chemistry

Table C3 : Mineral Chemistry of Garnet

Description	LUS07-1 1/8	LUS07-2 2/8	LUS07-3 3/8	LUS07-4 4/8	LUS07-5 5/8	LUS07-6 6/8	LUS07-7 7/8	LUS07-8 8/8	LUS07-9 1/4	LUS07-10 2/4	LUS07-11 3/4	LUS07-12 4/4
SiO ₂	38.98	38.90	38.62	38.90	38.73	38.78	38.77	38.57	38.61	38.22	38.63	38.87
TiO ₂	0.14	0.20	0.21	0.23	0.17	0.15	0.20	0.19	0.18	0.17	0.17	0.11
Al ₂ O ₃	21.89	21.70	21.78	21.67	21.65	21.76	21.96	21.91	21.83	21.80	21.93	22.05
Cr ₂ O ₃	0.07	0.01	0.07	0.06	0.00	0.03	0.06	0.12	0.06	0.00	0.12	0.07
Fe ₂ O ₃	0.25	0.33	0.26	0.43	0.55	0.38	0.05	0.02	0.08	0.06	0.00	0.00
MgO	5.50	5.14	5.00	5.01	5.10	5.17	5.20	5.42	3.86	3.78	4.18	5.53
CaO	11.34	12.42	12.41	12.39	12.38	12.29	12.27	11.55	12.64	12.47	12.87	11.83
MnO	1.54	1.36	1.46	1.38	1.32	1.28	1.26	1.54	2.79	2.74	2.21	1.49
FeO	21.21	20.25	20.90	20.70	20.72	20.80	20.96	21.31	20.98	21.49	20.97	20.66
Na ₂ O	0.02	0.01	0.03	0.05	0.04	0.02	0.02	0.02	0.03	0.02	0.04	0.03
Total	100.95	100.31	100.85	100.85	100.73	100.65	100.78	100.67	101.12	100.76	101.13	100.64
Si	5.97	5.99	5.94	5.97	5.96	5.96	5.95	5.94	5.96	5.93	5.95	5.96
Ti	0.02	0.02	0.02	0.03	0.02	0.02	0.02	0.02	0.02	0.02	0.02	0.01
Al	3.95	3.94	3.95	3.92	3.92	3.94	3.97	3.97	3.97	3.99	3.98	3.99
Cr	0.01	0.00	0.01	0.01	0.00	0.00	0.01	0.01	0.01	0.00	0.01	0.01
Fe ³⁺	0.03	0.04	0.03	0.05	0.06	0.04	0.01	0.00	0.01	0.01	0.00	0.00
Mg	1.26	1.18	1.15	1.15	1.17	1.19	1.19	1.24	0.89	0.88	0.96	1.26
Ca	1.86	2.05	2.05	2.04	2.04	2.03	2.02	1.91	2.09	2.07	2.12	1.94
Mn	0.20	0.18	0.19	0.18	0.17	0.17	0.16	0.20	0.37	0.36	0.29	0.19
Fe ²⁺	2.72	2.61	2.69	2.66	2.67	2.67	2.69	2.74	2.71	2.79	2.70	2.65
Na	0.01	0.00	0.01	0.01	0.01	0.01	0.01	0.01	0.01	0.01	0.01	0.01
Pyr-Mg	0.21	0.19	0.19	0.19	0.19	0.19	0.20	0.20	0.15	0.14	0.16	0.21
Alm-Fe ²⁺	0.45	0.43	0.44	0.44	0.44	0.44	0.44	0.45	0.45	0.46	0.44	0.44
Gross-Ca	0.31	0.34	0.34	0.34	0.33	0.33	0.33	0.31	0.34	0.34	0.35	0.32
And-Fe ³⁺	0.00	0.01	0.00	0.01	0.01	0.01	0.00	0.00	0.00	0.00	0.00	0.00
Spes-Mn	0.03	0.03	0.03	0.03	0.03	0.03	0.03	0.03	0.06	0.06	0.05	0.03

Table C3 (continued)

Description	LUS07-13	LUS07-14	LUS07-15	LUS07-16	LUS07-17	LUS07-18	LUS07-19	LUS07-20	LUS07-21	LUS07-22	LUS07-23
	1/5	2/5	3/5	4/5	5/5	thick cor.					
SiO ₂	38.71	38.58	38.51	38.62	38.46	38.96	38.81	38.57	38.81	39.34	39.05
TiO ₂	0.16	0.08	0.11	0.16	0.17	0.11	0.17	0.09	0.15	0.13	0.14
Al ₂ O ₃	21.95	21.74	21.93	21.80	21.92	21.34	21.55	21.49	21.58	21.82	21.95
Cr ₂ O ₃	0.07	0.08	0.04	0.03	0.04	0.00	0.07	0.06	0.10	0.04	0.07
Fe ₂ O ₃	0.06	0.28	0.00	0.06	0.01	0.81	0.31	0.51	0.70	0.50	0.42
MgO	5.75	4.60	4.68	4.52	4.69	4.04	4.20	3.60	5.08	5.59	5.20
CaO	10.92	12.56	12.47	12.58	12.60	12.55	12.56	12.81	12.34	9.67	12.37
MnO	1.81	1.94	1.87	1.88	1.75	2.42	2.46	2.44	1.42	1.78	1.27
FeO	21.18	20.65	20.47	20.50	20.95	20.28	20.04	21.10	21.03	22.79	21.30
Na ₂ O	0.02	0.02	0.01	0.02	0.03	0.03	0.03	0.03	0.00	0.01	0.04
Total	100.63	100.55	100.10	100.19	100.62	100.56	100.21	100.71	101.26	101.71	101.86
Si	5.95	5.96	5.96	5.98	5.94	6.02	6.01	5.98	5.95	6.00	5.94
Ti	0.02	0.01	0.01	0.02	0.02	0.01	0.02	0.01	0.02	0.01	0.02
Al	3.98	3.96	4.00	3.97	3.99	3.89	3.93	3.93	3.90	3.92	3.94
Cr	0.01	0.01	0.00	0.00	0.01	0.00	0.01	0.01	0.01	0.00	0.01
Fe ³⁺	0.01	0.03	0.00	0.01	0.00	0.09	0.04	0.06	0.08	0.06	0.05
Mg	1.32	1.06	1.08	1.04	1.08	0.93	0.97	0.83	1.16	1.27	1.18
Ca	1.80	2.08	2.07	2.09	2.08	2.08	2.08	2.13	2.03	1.58	2.02
Mn	0.24	0.25	0.25	0.25	0.23	0.32	0.32	0.32	0.18	0.23	0.16
Fe ²⁺	2.72	2.67	2.65	2.65	2.70	2.62	2.60	2.74	2.70	2.91	2.71
Na	0.01	0.01	0.00	0.01	0.01	0.01	0.01	0.01	0.00	0.00	0.01
Pyr-Mg	0.22	0.17	0.18	0.17	0.18	0.15	0.16	0.14	0.19	0.21	0.19
Alm-Fe ²⁺	0.45	0.44	0.44	0.44	0.44	0.43	0.43	0.45	0.44	0.48	0.44
Gross-Ca	0.30	0.34	0.34	0.35	0.34	0.34	0.35	0.35	0.33	0.26	0.33
And-Fe ³⁺	0.00	0.01	0.00	0.00	0.00	0.02	0.01	0.01	0.01	0.01	0.01
Spes-Mn	0.04	0.04	0.04	0.04	0.04	0.05	0.05	0.05	0.03	0.04	0.03

Table C3 (continued)

Description	LUS12-1 thin cor.	LUS12-2 thin cor.	LUS12-3 thin cor.	LUS12-5 1/5	LUS12-6 2/5	LUS12-7 3/5	LUS12-8 4/5	LUS12-9 5/5	LUS12-10 1/7	LUS12-11 2/7	LUS12-12 3/7	LUS12-13 4/7
SiO ₂	39.94	40.34	40.15	39.71	39.51	39.37	39.56	39.41	39.36	39.52	39.69	39.76
TiO ₂	0.13	0.13	0.08	0.15	0.13	0.15	0.13	0.16	0.05	0.08	0.10	0.11
Al ₂ O ₃	21.60	21.61	22.26	22.14	22.03	22.14	21.99	22.08	22.54	22.44	22.05	22.13
Cr ₂ O ₃	0.10	0.11	0.07	0.03	0.13	0.00	0.04	0.11	0.00	0.01	0.19	0.03
Fe ₂ O ₃	1.07	1.53	0.50	0.52	0.45	0.42	0.56	0.50	0.00	0.18	0.61	0.58
MgO	8.92	9.74	9.52	9.63	8.51	8.55	8.55	9.12	10.34	10.07	9.93	9.80
CaO	10.57	9.37	9.19	9.06	10.56	10.17	10.58	9.95	7.50	8.17	8.69	8.59
MnO	0.92	0.74	0.80	0.68	0.82	0.89	0.87	0.75	0.58	0.57	0.50	0.58
FeO	16.69	17.67	18.13	18.46	18.22	18.80	17.94	18.54	19.65	19.28	18.84	18.88
Na ₂ O	0.00	0.02	0.08	0.00	0.02	0.02	0.00	0.01	0.02	0.02	0.02	0.02
Total	99.94	101.34	100.78	100.45	100.38	100.57	100.27	100.63	100.04	100.34	100.61	100.47
Si	6.03	6.01	6.01	5.97	5.97	5.95	5.98	5.94	5.94	5.95	5.96	5.98
Ti	0.02	0.02	0.01	0.02	0.02	0.02	0.02	0.02	0.01	0.01	0.01	0.01
Al	3.84	3.80	3.93	3.92	3.92	3.95	3.92	3.92	4.01	3.98	3.91	3.92
Cr	0.01	0.01	0.01	0.00	0.02	0.00	0.01	0.01	0.00	0.00	0.02	0.00
Fe ³⁺	0.12	0.17	0.06	0.06	0.05	0.05	0.06	0.06	0.00	0.02	0.07	0.07
Mg	2.01	2.16	2.12	2.16	1.92	1.93	1.93	2.05	2.33	2.26	2.22	2.20
Ca	1.71	1.50	1.47	1.46	1.71	1.65	1.71	1.61	1.21	1.32	1.40	1.38
Mn	0.12	0.09	0.10	0.09	0.10	0.11	0.11	0.10	0.07	0.07	0.06	0.07
Fe ²⁺	2.11	2.20	2.27	2.32	2.30	2.38	2.27	2.34	2.48	2.43	2.37	2.38
Na	0.00	0.01	0.02	0.00	0.00	0.01	0.00	0.00	0.01	0.01	0.01	0.01
Pyr-Mg	0.33	0.35	0.35	0.35	0.32	0.32	0.32	0.33	0.38	0.37	0.36	0.36
Alm-Fe ²⁺	0.35	0.36	0.38	0.38	0.38	0.39	0.37	0.38	0.41	0.40	0.39	0.39
Gross-Ca	0.28	0.24	0.24	0.24	0.28	0.27	0.28	0.26	0.20	0.22	0.23	0.23
And-Fe ³⁺	0.02	0.03	0.01	0.01	0.01	0.01	0.01	0.01	0.00	0.00	0.01	0.01
Spes-Mn	0.02	0.02	0.02	0.01	0.02	0.02	0.02	0.02	0.01	0.01	0.01	0.01

Table C3 (continued)

Description	LUS12-14 5/7	LUS12-15 6/7	LUS12-16 7/7	LUS12-17 thin cor.	LUS12-18 thin cor.	LUS12-19 thin cor.	LUS12-20 thin cor.	LUS12-21 acic. cor.	LUS12-22 acic. cor.	LUS12-23 thin cor.	LUS12-24 acic. cor.	LUS12-25 acic. cor.
SiO ₂	39.60	39.31	39.13	39.29	40.04	39.72	39.54	39.60	40.09	39.25	39.86	39.60
TiO ₂	0.11	0.12	0.08	0.11	0.15	0.17	0.15	0.08	0.10	0.09	0.08	0.15
Al ₂ O ₃	22.20	22.28	22.30	21.99	22.19	22.32	22.21	22.18	22.45	22.21	22.24	22.14
Cr ₂ O ₃	0.00	0.04	0.03	0.08	0.10	0.02	0.08	0.00	0.06	0.00	0.13	0.12
Fe ₂ O ₃	0.47	0.03	0.01	0.66	0.97	0.46	0.66	0.78	0.55	0.52	0.82	0.69
MgO	9.48	8.96	10.04	7.63	9.76	9.12	9.30	10.27	10.05	7.50	10.40	9.64
CaO	9.17	9.84	6.52	10.70	9.54	10.34	10.31	7.83	8.81	11.06	7.98	9.45
MnO	0.56	0.66	0.91	1.62	0.53	0.53	0.57	0.63	0.57	0.97	0.53	0.71
FeO	18.81	18.40	20.53	19.27	19.05	18.53	18.51	19.71	19.04	19.98	19.82	18.76
Na ₂ O	0.00	0.00	0.02	0.01	0.01	0.01	0.02	0.01	0.01	0.03	0.02	0.01
Total	100.40	99.67	99.65	101.41	102.35	101.25	101.47	101.15	101.77	101.63	101.87	101.32
Si	5.97	5.97	5.95	5.94	5.94	5.94	5.91	5.93	5.95	5.92	5.93	5.93
Ti	0.01	0.01	0.01	0.01	0.02	0.02	0.02	0.01	0.01	0.01	0.01	0.02
Al	3.94	3.98	4.00	3.92	3.88	3.94	3.92	3.92	3.93	3.95	3.90	3.91
Cr	0.00	0.01	0.00	0.01	0.01	0.00	0.01	0.00	0.01	0.00	0.02	0.01
Fe ³⁺	0.05	0.00	0.00	0.08	0.11	0.05	0.08	0.09	0.06	0.06	0.09	0.08
Mg	2.13	2.03	2.28	1.72	2.16	2.03	2.08	2.29	2.23	1.69	2.31	2.15
Ca	1.48	1.60	1.06	1.73	1.52	1.66	1.65	1.26	1.40	1.79	1.27	1.52
Mn	0.07	0.09	0.12	0.21	0.07	0.07	0.07	0.08	0.07	0.12	0.07	0.09
Fe ²⁺	2.37	2.34	2.61	2.44	2.36	2.32	2.32	2.47	2.36	2.52	2.47	2.35
Na	0.00	0.00	0.01	0.00	0.00	0.00	0.01	0.00	0.00	0.01	0.01	0.00
Pyr-Mg	0.35	0.34	0.38	0.28	0.35	0.33	0.34	0.37	0.36	0.27	0.37	0.35
Alm-Fe ²⁺	0.39	0.39	0.43	0.39	0.38	0.38	0.37	0.40	0.39	0.41	0.40	0.38
Gross-Ca	0.24	0.26	0.18	0.28	0.24	0.27	0.27	0.20	0.23	0.29	0.21	0.25
And-Fe ³⁺	0.01	0.00	0.00	0.01	0.02	0.01	0.01	0.01	0.01	0.01	0.01	0.01
Spes-Mn	0.01	0.01	0.02	0.03	0.01	0.01	0.01	0.01	0.01	0.02	0.01	0.01

Table C3 (continued)

Description	LUS13-1	LUS13-2	LUS14-1	LUS14-2	LUS14-3	LUS17-1	LUS17-2	LUS17-3	LUS17-4	LUS17-5	LUS17-6	LUS17-7		
	hb corona	hb corona	very thin cor.	cor. very thin	cor. very thin	cor. hb-chl	cor. hb corona	1/10	2/10					
SiO ₂	38.59	38.74	38.60	38.57	38.86	39.18	38.69	38.65	39.67	35.68	38.86	38.85		
TiO ₂	0.03	0.12	0.14	0.26	0.18	0.18	0.37	0.07	0.10	0.05	0.16	0.20		
Al ₂ O ₃	21.58	21.57	21.38	21.10	21.24	20.96	20.75	21.19	21.30	19.00	21.55	21.56		
Cr ₂ O ₃	0.10	0.05	0.11	0.07	0.06	0.07	0.06	0.00	0.00	0.04	0.02	0.02		
Fe ₂ O ₃	0.56	0.54	1.02	1.27	1.00	1.91	1.72	1.45	1.57	3.90	0.72	0.85		
MgO	6.23	5.12	5.52	5.70	5.14	6.59	6.10	6.91	7.22	11.64	6.37	6.49		
CaO	4.86	9.24	11.63	11.83	11.99	10.82	11.92	10.56	10.33	6.40	10.85	10.81		
MnO	2.52	2.68	1.90	1.84	2.32	1.27	0.43	0.59	0.98	0.66	1.25	1.21		
FeO	27.01	23.04	20.80	20.20	19.61	20.59	20.59	20.97	20.00	18.56	20.48	20.85		
Na ₂ O	0.03	0.01	0.09	0.00	0.08	0.00	0.00	0.02	0.02	0.05	0.03	0.04		
Total	101.51	101.18	101.21	100.83	100.49	101.69	100.73	100.42	101.19	96.09	100.31	100.90		
Si	5.96	5.98	5.93	5.94	5.99	5.96	5.95	5.94	6.01	5.71	5.97	5.94		
Ti	0.00	0.01	0.02	0.03	0.02	0.02	0.04	0.01	0.01	0.01	0.02	0.02		
Al	3.93	3.92	3.87	3.83	3.86	3.76	3.76	3.84	3.81	3.58	3.90	3.89		
Cr	0.01	0.01	0.01	0.01	0.01	0.01	0.01	0.00	0.00	0.01	0.00	0.00		
Fe ³⁺	0.07	0.06	0.12	0.15	0.12	0.22	0.20	0.17	0.18	0.47	0.08	0.10		
Mg	1.44	1.18	1.26	1.31	1.18	1.49	1.40	1.58	1.63	2.78	1.46	1.48		
Ca	0.81	1.53	1.91	1.95	1.98	1.76	1.96	1.74	1.68	1.10	1.79	1.77		
Mn	0.33	0.35	0.25	0.24	0.30	0.16	0.06	0.08	0.13	0.09	0.16	0.16		
Fe ²⁺	3.49	2.97	2.67	2.60	2.53	2.62	2.65	2.70	2.54	2.48	2.63	2.67		
Na	0.01	0.00	0.03	0.00	0.02	0.00	0.00	0.01	0.01	0.02	0.01	0.01		
Pyr-Mg	0.23	0.19	0.20	0.21	0.19	0.24	0.22	0.25	0.27	0.40	0.24	0.24		
Alm-Fe ²⁺	0.57	0.49	0.43	0.42	0.41	0.42	0.42	0.43	0.41	0.36	0.43	0.43		
Gross-Ca	0.13	0.25	0.31	0.31	0.32	0.28	0.31	0.28	0.27	0.16	0.29	0.29		
And-Fe ³⁺	0.01	0.01	0.02	0.02	0.02	0.03	0.03	0.03	0.03	0.07	0.01	0.02		
Spes-Mn	0.05	0.06	0.04	0.04	0.05	0.03	0.01	0.01	0.02	0.01	0.03	0.03		

Table C3 (continued)

Description	LUS17-8	LUS17-9	LUS17-10	LUS17-11	LUS17-12	LUS17-13	LUS17-14	LUS17-15
	3/10	4/10	5/10	6/10	7/10	8/10	9/10	10/10
SiO ₂	38.91	38.93	38.93	39.11	39.14	38.93	38.95	39.19
TiO ₂	0.18	0.21	0.19	0.22	0.21	0.12	0.12	0.07
Al ₂ O ₃	21.64	21.68	21.59	21.49	21.67	21.69	21.81	21.77
Cr ₂ O ₃	0.04	0.00	0.02	0.02	0.03	0.02	0.00	0.01
Fe ₂ O ₃	0.69	0.74	0.80	1.16	0.77	0.72	0.52	0.74
MgO	6.33	6.47	6.58	6.84	6.90	6.91	7.18	7.44
CaO	10.83	10.96	10.74	10.62	10.56	10.54	10.24	9.95
MnO	1.31	1.26	1.19	1.11	1.07	1.04	0.97	0.88
FeO	20.84	20.69	20.65	20.81	20.58	20.44	20.43	20.40
Na ₂ O	0.03	0.05	0.03	0.06	0.02	0.03	0.02	0.03
Total	100.85	101.05	100.73	101.45	100.96	100.52	100.24	100.49
Si	5.95	5.94	5.96	5.95	5.96	5.95	5.96	5.98
Ti	0.02	0.02	0.02	0.03	0.03	0.01	0.01	0.01
Al	3.90	3.90	3.89	3.85	3.89	3.91	3.93	3.91
Cr	0.01	0.00	0.00	0.00	0.00	0.00	0.00	0.00
Fe ³⁺	0.08	0.09	0.09	0.13	0.09	0.08	0.06	0.09
Mg	1.44	1.47	1.50	1.55	1.57	1.58	1.64	1.69
Ca	1.78	1.79	1.76	1.73	1.72	1.73	1.68	1.63
Mn	0.17	0.16	0.15	0.14	0.14	0.13	0.13	0.11
Fe ²⁺	2.67	2.64	2.64	2.65	2.62	2.61	2.62	2.60
Na	0.01	0.01	0.01	0.02	0.01	0.01	0.01	0.01
Pyr-Mg	0.24	0.24	0.24	0.25	0.26	0.26	0.27	0.28
Alm-Fe ²⁺	0.43	0.43	0.43	0.43	0.43	0.43	0.43	0.43
Gross-Ca	0.29	0.29	0.29	0.28	0.28	0.28	0.27	0.27
And-Fe ³⁺	0.01	0.01	0.01	0.02	0.01	0.01	0.01	0.01
Spes-Mn	0.03	0.03	0.03	0.02	0.02	0.02	0.02	0.02

Plagioclase Mineral Chemistry

Table C4 : Mineral Chemistry of Plagioclase

	BAI20-1	BAI20-2	BAI20-3	BAI20-4	BAI20-5	BAI20-6	BAI20-7	BAI18-1	BAI18-2	BAI18-3	BAI18-4	BAI18-5
SiO ₂	66.84	67.03	64.82	67.18	67.93	67.17	65.61	65.92	64.57	66.89	67.10	66.57
Al ₂ O ₃	21.49	21.72	21.54	20.57	20.56	19.69	21.75	20.91	20.70	20.70	20.96	21.02
CaO	1.44	0.49	0.66	0.16	0.04	0.02	0.42	0.37	1.38	0.66	0.76	0.27
FeO	0.00	0.02	0.02	0.01	0.00	0.03	0.04	0.12	0.20	0.08	0.09	0.01
Na ₂ O	11.51	11.21	11.33	12.07	12.14	12.24	11.39	10.65	11.07	11.64	11.30	11.99
K ₂ O	0.15	0.61	0.49	0.05	0.03	0.03	1.02	0.45	0.05	0.03	0.04	0.15
Total	101.42	101.08	98.86	100.03	100.69	99.17	100.22	98.41	97.98	99.99	100.24	100.01
Si	2.90	2.91	2.89	2.94	2.95	2.97	2.89	2.93	2.90	2.93	2.93	2.92
Al	1.10	1.11	1.13	1.06	1.05	1.03	1.13	1.10	1.10	1.07	1.08	1.09
Ca	0.07	0.02	0.03	0.01	0.00	0.00	0.02	0.02	0.07	0.03	0.04	0.01
Fe	0.00	0.00	0.00	0.00	0.00	0.00	0.00	0.00	0.01	0.00	0.00	0.00
Na	0.97	0.94	0.98	1.03	1.02	1.05	0.97	0.92	0.96	0.99	0.96	1.02
K	0.01	0.03	0.03	0.00	0.00	0.00	0.06	0.03	0.00	0.00	0.00	0.01
Albite	0.93	0.94	0.94	0.99	1.00	1.00	0.93	0.95	0.93	0.97	0.96	0.98
Orthose	0.01	0.03	0.03	0.00	0.00	0.00	0.05	0.03	0.00	0.00	0.00	0.01
Anorthite	0.06	0.02	0.03	0.01	0.00	0.00	0.02	0.02	0.06	0.03	0.04	0.01

Table C4 (continued)

	LUS18-1	LUS18-2	BUM05-1	BUM20-1	BUM16-1	BUM16-2	BUM16-3	BUM07-1	BUM15-1	BUM15-2	BUM15-3	BUM15-4
SiO ₂	68.82	68.57	67.39	68.74	67.44	67.20	66.87	64.45	65.86	65.33	65.54	64.88
Al ₂ O ₃	20.71	20.64	19.98	18.74	18.93	19.51	18.97	19.76	19.08	20.51	20.30	19.34
CaO	0.12	0.52	0.91	0.01	0.26	0.06	0.08	2.34	0.87	1.61	1.60	1.11
FeO	0.04	0.10	0.12	0.03	0.51	0.16	0.11	0.21	0.27	0.41	0.26	0.19
Na ₂ O	11.17	11.03	11.48	11.95	11.91	11.80	11.75	10.78	11.55	10.95	10.83	11.01
K ₂ O	0.05	0.06	0.01	0.01	0.04	0.04	0.03	0.08	0.05	0.43	0.04	0.13
Total	100.92	100.92	99.89	99.48	99.08	98.77	97.80	97.61	97.66	99.24	98.57	96.66
Si	2.97	2.97	2.96	3.02	2.99	2.98	2.99	2.91	2.96	2.91	2.92	2.95
Al	1.05	1.05	1.03	0.97	0.99	1.02	1.00	1.05	1.01	1.08	1.07	1.04
Ca	0.01	0.02	0.04	0.00	0.01	0.00	0.00	0.11	0.04	0.08	0.08	0.05
Fe	0.00	0.00	0.00	0.00	0.02	0.01	0.00	0.01	0.01	0.02	0.01	0.01
Na	0.94	0.93	0.98	1.02	1.02	1.01	1.02	0.94	1.01	0.94	0.94	0.97
K	0.00	0.00	0.00	0.00	0.00	0.00	0.00	0.01	0.00	0.02	0.00	0.01
Albite	0.99	0.97	0.96	1.00	0.99	1.00	1.00	0.89	0.96	0.90	0.92	0.94
Orthose	0.00	0.00	0.00	0.00	0.00	0.00	0.00	0.00	0.00	0.02	0.00	0.01
Anorthite	0.01	0.03	0.04	0.00	0.01	0.00	0.00	0.11	0.04	0.07	0.07	0.05

Table C4 (continued)

	LUS08-1	LUS08-2	LUS08-3	LUS09-1	LUS11-1	LUS11-2	LUS11-3	LUS11-4	LUS11-5
SiO ₂	68.05	66.29	68.40	68.70	68.18	67.18	67.52	67.59	67.12
Al ₂ O ₃	20.70	19.06	19.69	19.77	21.09	20.29	21.33	20.40	20.56
CaO	0.76	0.34	0.18	0.37	1.00	1.23	1.13	0.83	1.18
FeO	0.12	0.03	0.06	0.03	0.09	0.10	0.02	0.02	0.09
Na ₂ O	11.34	11.73	11.89	11.83	10.76	11.08	11.04	10.91	11.16
K ₂ O	0.30	0.11	0.05	0.07	0.15	0.05	0.16	0.22	0.08
Total	101.32	97.57	100.27	100.76	101.27	99.92	101.19	99.96	100.19
Si	2.95	2.97	2.98	2.98	2.94	2.95	2.92	2.96	2.94
Al	1.05	1.00	1.01	1.01	1.07	1.05	1.09	1.05	1.06
Ca	0.04	0.02	0.01	0.02	0.05	0.06	0.05	0.04	0.06
Fe	0.01	0.00	0.00	0.00	0.00	0.00	0.00	0.00	0.00
Na	0.95	1.02	1.01	1.00	0.90	0.94	0.93	0.93	0.95
K	0.02	0.01	0.00	0.00	0.01	0.00	0.01	0.01	0.00
Albite	0.95	0.98	0.99	0.98	0.94	0.94	0.94	0.95	0.94
Orthose	0.02	0.01	0.00	0.00	0.01	0.00	0.01	0.01	0.00
Anorthite	0.03	0.02	0.01	0.02	0.05	0.06	0.05	0.04	0.05

Table C4 (continued)

	LUS05-1	LUS05-2	LUS05-3	LUS05-4	BUM04-1	BUM04-2	BUM24-1	BUM24-2	BUM24-3
SiO ₂	66.03	69.33	67.87	62.26	65.94	67.48	67.87	67.88	67.77
Al ₂ O ₃	22.05	20.06	21.75	23.50	20.70	19.77	19.94	19.62	19.15
CaO	1.29	0.20	1.05	5.46	1.26	0.74	0.38	0.28	0.30
FeO	0.31	0.08	0.09	0.52	0.12	0.00	0.14	0.08	0.09
Na ₂ O	9.91	11.77	11.12	8.75	10.67	11.57	11.54	11.82	11.95
K ₂ O	0.54	0.07	0.19	0.20	0.56	0.08	0.02	0.04	0.03
Total	100.14	101.50	102.06	100.68	99.25	99.63	99.88	99.71	99.29
Si	2.89	2.98	2.92	2.75	2.92	2.97	2.97	2.98	2.99
Al	1.14	1.02	1.10	1.23	1.08	1.02	1.03	1.02	1.00
Ca	0.06	0.01	0.05	0.26	0.06	0.04	0.02	0.01	0.01
Fe	0.01	0.00	0.00	0.02	0.00	0.00	0.01	0.00	0.00
Na	0.84	0.98	0.93	0.75	0.92	0.99	0.98	1.01	1.02
K	0.03	0.00	0.01	0.01	0.03	0.00	0.00	0.00	0.00
Albite	0.90	0.99	0.94	0.74	0.91	0.96	0.98	0.99	0.98
Orthose	0.03	0.00	0.01	0.01	0.03	0.00	0.00	0.00	0.00
Anorthite	0.07	0.01	0.05	0.25	0.06	0.03	0.02	0.01	0.01

Table C4 (continued)

	BUM14-1	BAI19-1	LUS07-1	LUS07-2	LUS12-1	LUS12-2	LUS12-3	LUS12-4	LUS12-5	LUS12-6	LUS12-7	LUS12-8
SiO ₂	67.42	68.25	68.84	68.54	67.84	65.69	68.58	68.51	69.18	68.12	68.16	68.16
Al ₂ O ₃	19.52	20.80	20.28	20.64	21.41	20.76	19.79	20.61	20.16	19.93	19.86	19.81
CaO	0.47	0.07	0.51	0.58	1.14	1.69	0.24	0.50	0.10	0.24	0.53	0.30
FeO	0.07	0.11	0.39	0.02	0.39	0.67	0.23	0.22	0.11	0.40	0.54	0.54
Na ₂ O	11.84	11.05	11.51	11.61	10.92	11.06	11.95	11.48	11.96	10.99	11.96	11.92
K ₂ O	0.08	0.57	0.03	0.04	0.03	0.02	0.02	0.05	0.03	0.04	0.03	0.03
Total	99.39	100.84	101.55	101.43	101.73	99.90	100.80	101.37	101.53	99.72	101.09	100.75
Si	2.97	2.96	2.97	2.96	2.92	2.90	2.98	2.96	2.98	2.98	2.96	2.97
Al	1.01	1.06	1.03	1.05	1.09	1.08	1.01	1.05	1.02	1.03	1.02	1.02
Ca	0.02	0.00	0.02	0.03	0.05	0.08	0.01	0.02	0.00	0.01	0.03	0.01
Fe	0.00	0.00	0.01	0.00	0.01	0.03	0.01	0.01	0.00	0.02	0.02	0.02
Na	1.01	0.93	0.96	0.97	0.91	0.95	1.01	0.96	1.00	0.93	1.01	1.01
K	0.00	0.03	0.00	0.00	0.00	0.00	0.00	0.00	0.00	0.00	0.00	0.00
Albite	0.97	0.96	0.98	0.97	0.94	0.92	0.99	0.97	0.99	0.99	0.97	0.99
Orthose	0.00	0.03	0.00	0.00	0.00	0.00	0.00	0.00	0.00	0.00	0.00	0.00
Anorthite	0.02	0.00	0.02	0.03	0.05	0.08	0.01	0.02	0.00	0.01	0.02	0.01

Table C4 (continued)

	LUS13-1	LUS13-2	LUS13-3	LUS13-4	LUS13-5	LUS13-6	LUS13-7	LUS14-1	LUS14-2	LUS14-3
SiO ₂	67.81	62.75	68.14	67.39	65.88	68.47	66.26	68.32	67.71	67.94
Al ₂ O ₃	19.50	22.73	19.81	19.76	20.50	20.18	20.14	19.77	19.18	18.81
CaO	0.27	4.51	0.18	1.10	1.74	0.90	1.29	0.24	0.42	0.43
FeO	0.08	0.17	0.07	0.23	0.34	0.53	0.46	0.03	0.24	0.09
Na ₂ O	11.80	9.54	11.58	11.54	10.94	11.57	11.04	11.59	11.19	11.86
K ₂ O	0.06	0.05	0.14	0.05	0.06	0.06	0.04	0.15	0.05	0.02
Total	99.51	99.75	99.91	100.07	99.45	101.70	99.23	100.10	98.80	99.15
Si	2.98	2.79	2.98	2.96	2.92	2.96	2.94	2.98	3.00	3.00
Al	1.01	1.19	1.02	1.02	1.07	1.03	1.05	1.02	1.00	0.98
Ca	0.01	0.22	0.01	0.05	0.08	0.04	0.06	0.01	0.02	0.02
Fe	0.00	0.01	0.00	0.01	0.01	0.02	0.02	0.00	0.01	0.00
Na	1.01	0.82	0.98	0.98	0.94	0.97	0.95	0.98	0.96	1.02
K	0.00	0.00	0.01	0.00	0.00	0.00	0.00	0.01	0.00	0.00
Albite	0.98	0.79	0.98	0.95	0.92	0.96	0.94	0.98	0.98	0.98
Orthose	0.00	0.00	0.01	0.00	0.00	0.00	0.00	0.01	0.00	0.00
Anorthite	0.01	0.21	0.01	0.05	0.08	0.04	0.06	0.01	0.02	0.02

Appendix D

Geochemistry of the highly foliated amphibolite blocks from the mélange beneath the YSZ ophiolites

Table D1 : Geochemistry of the Bainang amphibolites

Type Sample	Bainang									
	intrusion LUS-02	common BAI-18	banded				garnet-bearing			
			LUS-05	LUS-08	LUS-11	LUS-16	LUS-07	LUS-12	LUS-14	LUS-17
Oxides (wt%)*										
SiO ₂	55.09	43.33	49.61	54.26	52.27	47.78	46.54	46.26	50.06	45.63
TiO ₂	1.24	1.84	1.78	1.18	1.43	1.00	1.01	1.32	1.13	1.06
Al ₂ O ₃	16.58	13.46	15.05	13.62	14.24	9.74	16.23	15.71	15.56	15.70
Fe ₂ O ₃	11.27	16.11	12.33	8.24	10.12	10.31	10.20	10.65	9.49	9.26
MnO	0.14	0.22	0.20	0.15	0.17	0.21	0.17	0.17	0.16	0.17
MgO	5.09	10.46	6.38	4.03	7.48	14.51	9.95	10.81	9.14	8.88
CaO	3.85	12.06	9.55	15.43	9.91	14.90	13.32	12.19	10.27	17.87
Na ₂ O	6.39	1.92	3.78	2.64	4.06	1.51	2.35	2.66	3.89	1.28
K ₂ O	0.27	0.34	1.12	0.31	0.19	0.05	0.16	0.14	0.14	0.06
P ₂ O ₅	0.11	0.25	0.18	0.14	0.12	0.02	0.09	0.10	0.12	0.08
Total	100.02	100.00	100.00	100.01	100.00	100.02	100.02	100.01	99.98	99.99
Mg#**	51.51	60.44	54.90	53.47	63.49	76.81	69.65	70.48	69.39	69.29
LOI***	2.30	1.62	1.35	1.17	1.30	1.42	2.68	2.36	2.19	2.53
REE (ppm)										
La	1.89	4.06	4.22	2.20	2.50	0.65	1.76	1.87	1.94	1.62
Ce	7.58	15.74	12.74	7.04	9.41	3.05	6.36	6.93	7.43	6.34
Pr	1.25	2.64	2.21	1.23	1.56	0.64	1.03	1.20	1.24	1.06
Nd	7.03	15.19	12.54	7.08	8.98	4.24	5.92	7.11	7.06	6.18
Sm	2.56	5.45	4.36	2.65	3.27	1.77	2.29	2.64	2.55	2.32
Eu	0.84	2.00	1.71	1.12	1.31	0.81	1.04	1.19	1.04	1.00
Gd	3.65	8.13	6.21	3.74	4.76	3.24	3.42	3.77	3.67	3.40
Tb	0.74	1.58	1.17	0.74	0.94	0.66	0.68	0.74	0.73	0.67
Dy	4.71	10.03	7.52	5.04	5.94	4.32	4.34	4.79	4.64	4.35
Ho	1.02	2.17	1.63	1.02	1.30	0.93	0.95	1.01	1.00	0.93
Er	2.96	6.10	4.68	3.20	3.81	2.74	2.81	3.05	2.92	2.69
Tm	0.47	0.92	0.71	0.50	0.57	0.40	0.43	0.46	0.44	0.41
Yb	2.89	5.45	4.41	3.12	3.58	2.48	2.56	2.85	2.72	2.52
Lu	0.45	0.84	0.69	0.49	0.55	0.36	0.40	0.44	0.42	0.39
HFSE										
V	332.39	371.59	298.04	225.30	285.19	363.70	260.31	250.29	255.97	237.58
Y	26.87	56.26	44.20	26.95	33.87	23.68	26.02	28.28	26.53	24.65
Zr	77.39	141.51	105.23	64.04	81.44	23.64	52.32	55.74	62.21	52.09
Hf	2.19	3.90	2.96	1.84	2.42	0.93	1.47	1.64	1.74	1.58
Nb	0.97	1.34	1.05	0.99	0.90	1.16	0.88	0.89	1.59	1.12
Ta	0.06	0.08	0.05	0.03	0.03	0.04	0.02	0.03	0.04	0.01
LILE (ppm)										
Rb	6.19	2.30	13.08	3.05	4.99	N/A	4.83	N/A	1.49	N/A
Ba	34.41	7.08	30.75	8.07	30.09	5.00	6.72	10.84	12.04	3.20
Pb	N/A	N/A	N/A	N/A	N/A	N/A	N/A	N/A	N/A	N/A
Th	0.13	0.14	0.12	0.06	0.09	N/A	0.06	N/A	N/A	N/A
U	0.07	0.12	0.40	0.40	0.04	N/A	0.02	0.01	0.02	0.04
Sr	48.73	24.44	108.21	173.17	101.81	29.32	70.41	79.13	104.97	20.31

*Oxide (wt%) on an anhydrous basis

** Mg# =
Mg²⁺/(Fe²⁺⁺+Mg²⁺),
Fe³⁺/FeTot=0.15

***LOI = Loss
on ignition

Table D2 : Geochemistry of the Buma amphibolites

		Buma									
Type	Sample	common (clinopyroxene and garnet-free)								Banded	
		BUM-05	BUM-07	BUM-15	BUM-16	BUM-17	BUM-18	BUM-21	BUM-23	BUM-04	BUM-14
Oxides (wt%)*											
SiO ₂		44.30	46.14	47.92	49.82	49.29	48.80	46.72	53.31	43.50	50.77
TiO ₂		1.36	1.56	1.26	1.64	1.33	1.26	1.50	1.17	1.60	1.64
Al ₂ O ₃		15.63	14.59	15.35	15.71	14.44	15.21	15.22	13.12	15.49	15.03
Fe ₂ O ₃		11.86	11.75	11.05	10.48	10.41	10.18	11.47	9.50	12.72	10.35
MnO		0.19	0.18	0.19	0.20	0.18	0.17	0.19	0.20	0.19	0.17
MgO		11.99	10.60	10.95	6.99	8.92	10.57	10.46	9.80	11.04	6.06
CaO		12.65	12.72	9.61	11.44	11.76	10.34	11.31	7.99	13.77	11.70
Na ₂ O		1.74	2.21	3.30	3.46	3.40	3.36	2.88	4.37	1.47	3.98
K ₂ O		0.17	0.11	0.28	0.07	0.18	0.05	0.11	0.35	0.07	0.17
P ₂ O ₅		0.11	0.13	0.08	0.17	0.10	0.08	0.11	0.17	0.13	0.16
Total		100.00	100.00	100.00	99.99	100.02	100.02	99.98	99.98	100.00	100.03
Mg#**		70.39	67.98	70.00	61.07	66.84	70.96	68.21	70.82	67.13	57.96
LOI***		3.18	2.94	2.87	2.70	3.83	2.88	2.84	2.78	2.63	2.28
REE (ppm)											
La		2.45	2.95	2.30	3.37	2.11	2.59	3.01	1.98	3.03	3.81
Ce		8.97	10.74	8.29	12.58	8.16	9.20	11.35	7.59	11.44	13.15
Pr		1.47	1.75	1.34	2.05	1.34	1.46	1.83	1.28	1.90	2.09
Nd		8.44	10.29	7.23	11.43	7.65	7.96	10.28	7.30	10.75	11.15
Sm		3.05	3.72	2.51	3.95	2.83	2.77	3.75	2.73	3.99	4.04
Eu		1.33	1.49	0.94	1.55	1.07	1.13	1.53	1.09	1.68	1.61
Gd		4.49	5.27	3.59	5.69	4.12	4.04	5.33	3.87	5.98	5.68
Tb		0.87	1.00	0.69	1.09	0.82	0.78	1.03	0.72	1.15	1.09
Dy		5.55	6.29	4.42	6.79	5.24	4.99	6.32	4.32	7.29	6.87
Ho		1.21	1.32	0.95	1.44	1.14	1.07	1.36	0.86	1.60	1.48
Er		3.56	3.81	2.76	4.23	3.26	3.15	3.89	2.54	4.66	4.30
Tm		0.54	0.58	0.41	0.62	0.50	0.48	0.59	0.40	0.71	0.66
Yb		3.33	3.51	2.63	3.85	2.97	2.92	3.58	2.47	4.34	3.92
Lu		0.52	0.54	0.40	0.59	0.46	0.45	0.56	0.40	0.68	0.63
HFSE											
V		270.53	319.35	254.39	265.76	254.50	246.79	319.76	226.46	345.79	271.60
Y		31.64	35.33	25.06	38.79	29.32	28.31	35.93	22.29	42.14	38.75
Zr		70.69	83.56	70.78	105.90	65.34	69.62	82.74	67.89	81.20	105.79
Hf		2.07	2.33	1.96	2.96	1.92	2.00	2.33	1.97	2.36	3.00
Nb		1.21	1.39	1.05	1.14	0.90	0.97	1.01	0.96	1.62	1.25
Ta		0.03	0.04	0.06	0.05	0.02	0.03	0.04	0.02	0.04	0.07
LILE (ppm)											
Rb		1.58	2.85	3.30	1.57	9.22	1.08	2.17	8.24	N/A	3.99
Ba		21.39	40.77	140.53	42.28	650.73	60.21	35.56	117.61	12.23	33.76
Pb		N/A	N/A	N/A	N/A	N/A	N/A	N/A	N/A	N/A	N/A
Th		0.08	0.10	0.08	0.11	0.06	0.08	0.10	0.06	0.10	0.15
U		0.30	0.08	0.05	0.04	0.02	0.22	0.07	0.12	0.04	0.28
Sr		117.67	94.09	151.92	167.17	604.37	80.43	82.69	283.98	129.67	315.56

*Oxide (wt%) on an anhydrous basis

** Mg# = $\text{Mg}^{2+}/(\text{Fe}^{2+} + \text{Mg}^{2+})$, Fe3+/FeTot = 0.15

***LOI = Loss on ignition

Table D3 : Standards for major elements analysis

SAMPLE	SY3 CERT 3/139	SY- CERT	NIST 694 CERT	NIST 694/8	W-2 CERT	W-2/B314	DNC-1 CERT	DNC-1/34	BIR-1 CERT	BIR-1/B313	GBW 07113 CERT	GBW 07113/C	NBS 1633b CERT	NBS 1633B/C	STM-1 CERT	STM-1/C
Rock Type	syenite	western phosphate rock	diabase		dolerite		basalt		rhyolite		fly ash				syenite	
Element																
SiO ₂	59,62	59,63	11,20	10,89	52,44	52,58	47,04	46,97	47,77	47,83	72,78	72,69	49,24	49,24	59,64	59,70
Al ₂ O ₃	11,75	11,65	1,80	1,88	15,35	15,25	18,30	18,39	15,35	15,51	12,96	12,86	28,43	28,42	18,39	18,24
Fe ₂ O ₃	6,49	6,43	0,79	0,72	10,74	10,55	9,93	9,77	11,26	11,25	3,21	3,11	11,13	11,15	5,22	5,15
MnO	0,32	0,325	0,01	0,011	0,163	0,162	0,149	0,144	0,171	0,169	0,140	0,137	0,020	0,017	0,22	0,218
MgO	2,67	2,63	0,33	0,32	6,37	6,34	10,05	10,20	9,68	9,64	0,16	0,16	0,799	0,78	0,101	0,10
CaO	8,26	8,34	43,60	44,00	10,87	10,85	11,27	11,25	13,24	13,21	0,59	0,60	2,11	2,12	1,09	1,14
Na ₂ O	4,12	4,13	0,86	0,85	2,14	2,22	1,87	1,95	1,75	1,83	2,57	2,55	0,271	0,28	8,94	8,80
K ₂ O	4,23	4,23	0,51	0,48	0,627	0,56	0,229	0,17	0,027	0,07	5,43	5,41	2,26	2,35	4,28	4,07
TiO ₂	0,15	0,147	0,11	0,117	1,06	1,078	0,48	0,484	0,96	0,976	0,30	0,282	1,32	1,300	0,135	0,134
P ₂ O ₅	0,54	0,54	30,20	28,38	0,131	0,14	0,085	0,08	0,05	0,03	0,05	0,05	0,53	0,53	0,158	0,16
LOI	1,16				0,60		0,60									

Table D4 : Standards for analysis of trace elements

Sample ID:	HFSE						LILE					REE														
	V	Y	Zr	Hf	Nb	Ta	Rb	Ba	Pb	Th	U	Sr	La	Ce	Pr	Nd	Sm	Eu	Gd	Tb	Dy	Ho	Er	Tm	Yb	Lu
Control Material W2	269	22,4	97	2,5	7,8	0,53	21	181	8	2,44	0,58	193	11,2	26,1	3,04	13,1	3,23	1,19	3,81	0,69	3,98	0,80	2,29	0,364	2,13	0,323
Certified W2	262*	24*	94*	2,56*	7,9	0,5	20*	182*	9	2,2*	0,53	194*	11,4*	24*	(5,9)	14,0	3,25*	1,1*	3,6*	0,63	3,8*	0,76*	2,5	0,4	2,05*	0,33*
Control Material WMG-1	161	14,3	55	1,4	5,1	0,34	5	114	18	1,29	0,72	39	8,28	18,1	2,14	9,33	2,28	0,780	2,57	0,45	2,47	0,49	1,41	0,218	1,30	0,202
Certified WMG-1	(149)	(12)	(43)	(1,3)	(6)	(0,5)	(4)	(114)	(15)	(1,1)	(0,65)	(41)	(8,2)	(16)		(9)	(2,3)	(0,8)		(0,4)	(2,8)	(0,5)		(0,2)	(1,3)	(0,21)
Blank	-5	-0,5	-1	-0,1	-0,2	-0,01	-1	-3	-5	-0,05	-0,01	-2	-0,05	-0,05	-0,01	-0,05	-0,01	-0,005	-0,01	-0,01	-0,01	-0,01	-0,01	-0,005	-0,01	-0,002
Calibration Standard MAG1	125	26,6	115	3,3	13,7	1,18	147	505	8	12,6	3,09	132	42,6	93,5	9,81	36,8	6,99	1,51	6,18	0,97	5,19	0,98	2,78	0,426	2,61	0,388
Certified MAG1	140*	28*	126*	3,7*	12	1,1	149*	479*	24*	11,9*	2,7*	146*	43*	88*	9,3	38*	7,5*	1,55*	5,8*	0,96*	5,2*	1,02*	3	0,43*	2,6*	0,40*
Calibration Standard BIR1	314	16,3	15	0,6	0,5	0,03	-1	7	-5	0,05	0,02	108	0,72	2,27	0,40	2,43	1,08	0,565	1,93	0,42	2,66	0,58	1,76	0,289	1,70	0,261
Certified BIR1	313*	16*	15,5	0,6*	0,6	0,04	0,25*	7	3	0,03	0,01	108*	0,62*	1,95*	0,38*	2,5*	1,1*	0,54*	1,85*	0,36*	2,5*	0,57*	1,7*	0,26*	1,65	0,26*
Calibration Standard DNC1	141	17,8	36	1,0	1,3	0,08	4	105	-5	0,27	0,07	139	3,86	9,24	1,11	4,96	1,41	0,633	2,11	0,45	2,87	0,64	1,96	0,328	1,99	0,314
Certified DNC1	148*	18*	41*	1,01*	3	0,098*	(4,5)	114*	6,3	(0,2)	(0,1)	145*	3,8*	10,6	1,3	4,9*	1,38*	0,59*	2	0,41*	2,7	0,62	2*	(0,33)	2,01*	0,32*
Calibration Standard GXR-2	52	18,9	262	6,6	10,6	0,86	83	2 230	119	9,54	3,36	155	27,2	58,8	5,67	20,5	3,72	0,830	3,31	0,54	3,04	0,62	1,85	0,304	1,91	0,297
Certified GXR-2	52	17	269	8,3	11	0,9	78	2 240	690	8,8	2,9	160	25,6	51,4		(19)	3,5	0,81	(3,3)	0,48	3,3		(0,3)	2,04	(0,27)	
Calibration Standard LKSD-3	72	30,3	173	4,3	8,4	0,66	74	698	-5	11,6	4,90	242	50,6	101,2	11,9	44,2	7,98	1,53	6,63	0,95	5,06	1,00	2,93	0,460	2,78	0,433
Certified LKSD-3	82	30	178	4,8	8	0,7	78	680	29	11,4	4,6	240	52	90		44	8,0	1,50		1,0	4,9			2,7	0,4	
Calibration Standard MICA Fe	110	46,5	872	26,4	282	34,3	2 040	155	12	178	95,6	4	200	421	50,4	180	33,1	0,648	22,7	2,68	10,8	1,50	3,79	0,565	3,50	0,502
Certified MICA Fe	135*	48*	800*	26*	270*	35*	2200*	150*	13*	150*	80*	5*	200*	420*	49*	180*	33*	0,7*	21*	2,7*	11*	1,6*	3,8*	0,48*	3,5*	0,5*
Calibration Standard GXR1	74	32	28	0,8	1,3	0,07	3	697	730	2,8	38,0	288	7,9	16,3	1,91	8,4	2,88	0,67	4,25	0,88	5,10	0,98	2,79	0,43	2,36	0,336
Certified GXR1	80	32	(38)	0,96	(0,8)	0,175	(14)	750	730	2,44	34,9	275	7,5	17		(18)	2,7	0,69	4,2	0,83	4,3		(0,43)	1,9	0,28	
Calibration Standard SY3	45	745	387	11,1	188	24,4	214	491	92	1 000	650	306	1 200	2230	223	723	121	19,5	126	22,7	138	29,6	88,3	13,8	71,7	9,14
Certified SY3	50	718*	320	9,70	148	30*	206*	450	133*	1003*	650*	302*	1340*	2230*	223*	670	109	17*	105*	18	118	29,5*	68	11,6*	(62)	
Calibration Standard STM1	-5	47,3	1 210	27,8	256	19,9	120	641	18	34,5	10,1	694	156	289	26,1	81,5	12,1	3,81	9,2	1,55	8,48	1,56	4,60	0,720	4,58	0,680
Certified STM1	(8,7)	46*	1210*	28*	268*	18,6*	118*	560*	17,7*	31*	9,06*	700*	150*	259*	19*	79*	12,6*	3,6*	9,5*	1,55*	8,1*	1,9	4,2*	0,69	4,4*	0,60
Calibration Standard IFG1	9	9,6	2	-0,1	-0,2	0,20	-1	3	-5	0,06	0,03	4	3,09	4,65	0,47	1,82	0,39	0,406	0,72	0,13	0,85	0,21	0,67	0,102	0,61	0,099
Certified IFG1	2	9*	1	0,04	0,1*	0,2	0,4	1,5	4	0,1	0,02	3	2,8*	4*	0,4*	0,2	0,4*	0,39*	0,74*	0,11*	0,8*	0,2*	0,63*	0,09*	0,6*	0,09*